# Effet élastocalorique dans le caoutchouc naturel

Zhong Jian Xie

N°d'ordre NNT : 2016LYSEI025

**THESE de DOCTORAT DE L'UNIVERSITE DE LYON**
préparée au sein de
**l'INSA LYON**

**Ecole Doctorale** ED160
**(Electronique, Electrotechnique, Automatique)**

**Spécialité de doctorat** :
**Discipline** : Génie Electrique

Soutenance prévue le 25/03/2016, par :
**Zhong jian XIE**

---

# Effet élastocalorique dans le caoutchouc naturel

---

Devant le jury composé de :

| | | | |
|---|---|---|---|
| Lebouc, Afef | Directrice de Recherches, | G2ElAb, Grenoble INP | Présidente |
| Remiens, Denis | Professeur des Universités | IEMN, Univ. Valenciennes | Rapporteur |
| Chenal, Jean-Marc | Maître de conférences | MATEIS, INSA-Lyon | Examinateur |
| Garnier, Bertrand | Chargé de Recherches HDR | LTN, Univ. Nantes | Examinateur |
| Guyomar, Daniel | Professeur des Universités | LGEF, INSA-Lyon | Directeur de thèse |
| Sebald, Gaël | Maître de conférences HDR | LGEF, INSA-Lyon | Co-directeur de thèse |

## Département FEDORA – INSA Lyon - Ecoles Doctorales – Quinquennal 2016-2020

| SIGLE | ECOLE DOCTORALE | NOM ET COORDONNEES DU RESPONSABLE |
|---|---|---|
| CHIMIE | **CHIMIE DE LYON**<br>**http://www.edchimie-lyon.fr**<br><br>Sec :Renée EL MELHEM<br>Bat Blaise Pascal 3* etage<br>Insa : R. GOURDON | M. Stéphane DANIELE<br>Institut de Recherches sur la Catalyse et l'Environnement de Lyon<br>IRCELYON-UMR 5256<br>Équipe CDFA<br>2 avenue Albert Einstein<br>69626 Villeurbanne cedex<br>directeur@edchimie-lyon.fr |
| E.E.A. | **ELECTRONIQUE, ELECTROTECHNIQUE, AUTOMATIQUE**<br>**http://edeea.ec-lyon.fr**<br><br>Sec : M.C. HAVGOUDOUKIAN<br>Ecole-Doctorale.eea@ec-lyon.fr | M. Gérard SCORLETTI<br>Ecole Centrale de Lyon<br>36 avenue Guy de Collongue<br>69134 ECULLY<br>Tél : 04.72.18 60.97 Fax : 04 78 43 37 17<br>Gerard.scorletti@ec-lyon.fr |
| E2M2 | **EVOLUTION, ECOSYSTEME, MICROBIOLOGIE, MODELISATION**<br>**http://e2m2.universite-lyon.fr**<br><br>Sec : Safia AIT CHALAL<br>Bat Darwin - UCB Lyon 1<br>04.72.43.28.91<br>Insa : H. CHARLES<br>Safia.ait-chalal@univ-lyon1.fr | Mme Gudrun BORNETTE<br>CNRS UMR 5023 LEHNA<br>Université Claude Bernard Lyon 1<br>Bât Forel<br>43 bd du 11 novembre 1918<br>69622 VILLEURBANNE Cédex<br>Tél : 06.07.53.89.13<br>e2m2@ univ-lyon1.fr |
| EDISS | **INTERDISCIPLINAIRE SCIENCESSANTE**<br>**http://www.ediss-lyon.fr**<br><br>Sec : Safia AIT CHALAL<br>Hôpital Louis Pradel - Bron<br>04 72 68 49 09<br>Insa : M. LAGARDE<br>Safia.ait-chalal@univ-lyon1.fr | Mme Emmanuelle CANET-SOULAS<br>INSERM U1060, CarMeN lab, Univ. Lyon 1<br>Bâtiment IMBL<br>11 avenue Jean Capelle INSA de Lyon<br>696621 Villeurbanne<br>Tél : 04.72.68.49.09 Fax :04 72 68 49 16<br>Emmanuelle.canet@univ-lyon1.fr |
| INFOMATHS | **INFORMATIQUE ET MATHEMATIQUES**<br>**http://infomaths.univ-lyon1.fr**<br><br>Sec :Renée EL MELHEM<br>Bat Blaise Pascal<br>3e etage<br>infomaths@univ-lyon1.fr | Mme Sylvie CALABRETTO<br>LIRIS – INSA de Lyon<br>Bat Blaise Pascal<br>7 avenue Jean Capelle<br>69622 VILLEURBANNE Cedex<br>Tél : 04.72. 43. 80. 46 Fax 04 72 43 16 87<br>Sylvie.calabretto@insa-lyon.fr |
| Matériaux | **MATERIAUX DE LYON**<br>**http://ed34.universite-lyon.fr**<br><br>Sec : M. LABOUNE<br>PM : 71.70 –Fax : 87.12<br>Bat. Saint Exupéry<br>Ed.materiaux@insa-lyon.fr | M. Jean-Yves BUFFIERE<br>INSA de Lyon<br>MATEIS<br>Bâtiment Saint Exupéry<br>7 avenue Jean Capelle<br>69621 VILLEURBANNE Cedex<br>Tél : 04.72.43 71.70 Fax 04 72 43 85 28<br>Ed.materiaux@insa-lyon.fr |
| MEGA | **MECANIQUE, ENERGETIQUE, GENIE CIVIL, ACOUSTIQUE**<br>**http://mega.universite-lyon.fr**<br>Sec : M. LABOUNE<br>PM : 71.70 –Fax : 87.12<br>Bat. Saint Exupéry<br>mega@insa-lyon.fr | M. Philippe BOISSE<br>INSA de Lyon<br>Laboratoire LAMCOS<br>Bâtiment Jacquard<br>25 bis avenue Jean Capelle<br>69621 VILLEURBANNE Cedex<br>Tél : 04.72 .43.71.70 Fax : 04 72 43 72 37<br>Philippe.boisse@insa-lyon.fr |
| ScSo | **ScSo***<br>**http://recherche.univ-lyon2.fr/scso/**<br>Sec : Viviane POLSINELLI<br>Brigitte DUBOIS<br>Insa : J.Y. TOUSSAINT<br>viviane.polsinelli@univ-lyon2.fr | Mme Isabelle VON BUELTZINGLOEWEN<br>Université Lyon 2<br>86 rue Pasteur<br>69365 LYON Cedex 07<br>Tél : 04.78.77.23.86 Fax : 04.37.28.04.48 |

*ScSo : Histoire, Géographie, Aménagement, Urbanisme, Archéologie, Science politique, Sociologie, Anthropologie

# Acknowledgements

The research conducted during my thesis would not have been possible without the support of many people. First and foremost, I wish to express my deep sense of gratitude to Laboratoire de Génie Electrique et Ferroélectricité (LGEF), for providing the opportunity to join the lab with a good environment and facilities to carry out my research. I would like also to convey thanks to the members of the administration helping me through all the procedures required for the completion of the thesis. My sincere thanks to China Scholarship Council (CSC) and my country for their cultivation and funding.

I sincerely thank to my thesis supervisors Daniel GUYOMAR and Gael SEBALD, for their patient guidance, enthusiastic encouragement, and for useful remarks and offering fascinating subject. My great appreciation goes to Gael SEBALD for his valuable and constructive suggestions. He is a very strict researcher. He taught me too much experimental skills and the basic requirements for being a researcher. I would like to gratefully thank Daniel GUYOMAR for giving me some ideas. Thank for our leader Laurent LEBRUN, who gave me too much tolerance when I made a mistake. That makes very warm in my heart.

I wish to extend my thanks for the support given by all the technicians in our laboratory. A warm thank goes to Frederic DEFROMERIE, Veronique PERRIN, Laurence SEVEYRAT and Evelyne DORIEUX for their help. Deepest gratitude goes to my colleagues, LI Yang, YIN Xunqian, BAO Bin, LIU Qing, Yukihiro YOSHIDA, Fouad BELHORA, and Alexandru CORNOGOLUB and all the colleagues in the lab for their kind help and encouragement.

Finally, I am forever indebted to my family and relatives for their understanding, endless patience and encouragement. I would like to express very great appreciation to my girlfriend ZHU Yao for her accompany, help and encouragement. I am grateful to all my friends in Lyon and in China for spending great times and their help.

# Abstract

Nowadays, the vapor compression technique takes up most of the refrigeration market. However, the use of hazardous gas from vapor compression technique has induced many environmental issues, like the ozone depletion and global warming. It's urgent to develop some sustainable cooling technologies as alternatives to vapor compression technique. Caloric effects refer to the isothermal entropy change or adiabatic temperature change on an external excitation, such as magnetic field, electric field, hydrostatic pressure and uniaxial stress, which are referred as magnetocaloric (MC), electrocaloric (EC), barocaloric (BC) and elastocaloric (eC) effect respectively. They are attracting more and more attention to be used for solid state cooling systems.

Natural rubber (NR) has been studied for a long time and is widely used as a mechanical part so far. Although the eC effect of NR is known from 19th century, its investigation and application remain limited. In this thesis, we aimed to study the eC effect of NR and to prove its potential to act as an eC material primarily. The method for improving the eC effect efficiency and fatigue life of NR were also proposed.

The eC effect of NR is characterized directly, and interpretation based on the theory of strain-induced crystallization/crystallite (SIC) is proposed. The eC adiabatic temperature change and isothermal entropy change of NR can be up to 9 K and 50 $kJ.m^{-3}.K^{-1}$ (56 $J.kg^{-1}.K^{-1}$), which are larger than most of caloric materials. Two coefficients, eC strain coefficient $\beta = -\partial s / \partial \varepsilon$ and eC stress coefficient $\gamma = \partial T / \partial \sigma_{stretching}$, are defined for evaluating the eC performance at different strains, where $s$ is the specific entropy, $\varepsilon$ is the engineering strain, $T$ is the temperature and $\sigma_{stretching}$ is the stretching stress. It's found that both coefficients are maximum for a strain around 4.5, indicating that the highest eC performance occurred at middle strain, which is attributed to the occurrence of SIC. To improve the eC performance, it is proposed to apply a pre-strain, so that the low strain regime where eC performance is low can be skipped. Moreover, the large needed deformation can be reduced by the pre-strain and thus the possibility of a compact cooling system designed based on NR is improved.

The directly measured eC temperature change $\Delta T$ was compared with indirect method, which is deduced from the Clausius-Clapeyron factor $(\partial \sigma / \partial T)_{\varepsilon}$, where $\sigma$ is the stress, $\varepsilon$ is the strain. The factor $(\partial \sigma / \partial T)_{\varepsilon}$ can be measured by two different methods. One is to measure the stress vs. strain behavior at different static temperatures. It is found that the $\Delta T$ deduction is underestimated or even of opposite sign compared to the directly measured one. These behaviors are different from eC effect of shape memory alloys (SMAs). The other characterization is to measure the stress vs. temperature at constant strain. It results in a prediction, which is in good quantitative agreement with the directly measured one. The stress appears then to be a non-state variable, thus questioning the ergodicity of the material. An interpretation based on SIC is proposed.

The two required quantities of eC effect, stress and eC temperature change, are simulated by a modified Flory's model based on SIC. It can almost predict the stress at different temperatures, which can't be predicted by the standard theory. For eC temperature change, the modified Flory's model can correspond to the experimental results at room temperature. It shows the capability of physical model based on SIC. Furthermore, the correspondence between the SIC model and results confirm that SIC is mainly responsible for the stress and temperature change of eC effect of NR.

The fatigue property of eC effect of NR is then investigated. The fatigue life at large deformation strain amplitudes (strain of 1-6) is about 800 cycles for the tested NR, which is too short to be used for a cooling system. Decreasing strain amplitude is necessary to extend fatigue life up to requirement of a cooling device. For the same small strain amplitude of 3, the fatigue property is compared at

amorphous strain regime (strain of 0-3), onset strain of melting (strain of 2-5) and high strain of SIC (strain of 4-7). It's found that a larger eC temperature change and a better fatigue property can be obtained at two SIC strain regimes (strain of 2-5 and 4-7) than amorphous strain regime. Especially, the fatigue property at the onset strain of melting (strain of 2-5) is better than that at high strain of SIC (strain of 4-7). A high-cycle fatigue was applied at the strain of 2-5 (most promising strain regime) up to $1.7\times10^5$ cycles. It was observed that there is no crack of the sample, as well as a degradation degree of 12% of the eC temperature change. Furthermore, the eC stress coefficient (4.4 K/MPa) at onset strain of melting is larger than that at high strain of SIC (1.6 K/MPa). As a result, the middle strain regime (onset strain regime of melting) can get a higher eC performance, larger temperature change, and better fatigue life, which should be chosen for eC cooling system.

In the above-mentioned work, the feasibility of NR acting as eC material is primarily proved. For a caloric material exhibiting time variation of temperature when excited by an external field, it is then necessary to convert the time variation into a spatial thermal gradient in order to obtain a cooling capability. In the last part of this manuscript, a model for a regenerative cooling system based on NR material is developed. It consists of combining a motion of the active layer relatively to a passive layer, which constitutes local heat storage necessary for the regenerative process. Based on the eC temperature change of 4 K at strain of 2-5, the maximal thermal gradient is calculated to be 0.5 K/cm with a motion of 3 cm at 1 Hz. Moreover, the cooling power and thermal gradient dependence on eC temperature change, heat capacity, thermal conductivity of eC material are simulated. It shows that the larger eC temperature change, heat capacity and thermal conductivity can result in a larger thermal gradient and cooling power. It establishes some guidelines for choosing eC materials.

# Résumé

De nos jours, le marché de la réfrigération est dominé par des systèmes à compression de fluide (fluides frigorifiques). Cependant, l'utilisation de ces fluides entraîne de nombreux problèmes environnementaux, comme l'appauvrissement de la couche d'ozone et la contribution au réchauffement climatique. Il est important de développer des technologies de refroidissement durables comme alternatives aux techniques de compression de fluide frigorifiques. Les effets caloriques représentent la capacité d'un matériau à voir son entropie varier en condition isotherme (ou sa température évoluer en condition adiabatique) sous l'effet d'une sollicitation externe telle que le champ magnétique, le champ électrique, la pression hydrostatique ou la contrainte uniaxiale, et sont désignés comme les effets magnétocalorique, électrocalorique, barocalorique et l'effet élastocalorique respectivement. Ils attirent de plus en plus l'attention des chercheurs pour être utilisés dans des systèmes de refroidissement à l'état solide.

Le caoutchouc naturel, étudié de longue date, est largement utilisé pour ses propriétés mécaniques. Bien que l'effet élastocalorique (eC) du caoutchouc naturel soit connu depuis le 19ème siècle, les recherches sur cet effet et son application restent limitées. Dans cette thèse, nous avons cherché à étudier l'effet élastocalorique du caoutchouc naturel et à démontrer la possibilité de l'utiliser comme matériau actif de systèmes de réfrigération. En outre, les effets de fatigue de ce matériau ont été caractérisés ainsi que les moyens pour l'améliorer.

Les propriétés élastocaloriques du caoutchouc naturel ont été caractérisées directement, et les résultats ont interprétés à partir de la notion de cristallisation induite par la déformation (« Strain induced crystalization / crystal » ou SIC). Le changement de température adiabatique élastocalorique et la variation d'entropie associée atteignent 9 K et 50 $kJ.m^{-3}.K^{-1}$ (56 $J.kg^{-1}.K^{-1}$), ce qui est très important comparé aux autres matériaux caloriques. Deux coefficients, $\beta = -\partial s / \partial \varepsilon$ (coefficient élastocalorique en déformation) et $\gamma = \partial T / \partial \sigma_{stretching}$ (coefficient élastocalorique en contrainte), sont définis pour évaluer la performance des matériaux élastocaloriques pour différentes déformations, où $s$ est l'entropie spécifique, $\varepsilon$ la déformation nominale, $T$ la température et $\sigma_{stretching}$ la contrainte lors de l'étirement. Il a été montré que ces deux coefficients qui représentent la performance élastocalorique sont maximum pour une déformation voisine de 4,5. Pour améliorer les performances élastocaloriques, il est proposé d'appliquer une pré-déformation, de sorte que la zone de faible déformation où la performance élastocalorique est faible peut être évitée. En outre, les grandes déformations nécessaires peuvent être réduites par la précontrainte et ouvre donc la possibilité d'un système de refroidissement compact à base de caoutchouc naturel.

La variation de température de l'effet élastocalorique mesurée directement a été comparée à une méthode indirecte, qui est déduite du facteur de Clapeyron $(\partial \sigma / \partial T)_{\varepsilon}$, où $\sigma$ est la contrainte, $\varepsilon$ la déformation. Le facteur de Clapeyron $(\partial \sigma / \partial T)_{\varepsilon}$ peut être mesuré de deux façons différentes. La première consiste à mesurer le comportement contrainte-déformation à différentes températures statiques. Il est montré que la déduction de la variation de température adiabatique élastocalorique est sous-estimée voire même de signe opposé par rapport à celle mesurée directement. Ce constat différencie l'effet élastocalorique du caoutchouc naturel par rapport à celui observé dans les alliages à mémoire de forme. L'autre caractérisation consiste à mesurer l'évolution de la contrainte directement lors d'un cycle de chauffe en fonction de la température (à déformation constante). Elle se traduit par une prédiction en excellent accord quantitatif avec la mesure directe. Il apparaît donc que la contrainte n'est pas une grandeur d'état, ce qui remet en question le comportement ergodique du matériau. Une interprétation fondée sur la SIC est proposée.

Les deux grandeurs contrainte et température élastocalorique sont simulées par un modèle de Flory modifié sur la base de la SIC. Il est possible de prédire le comportement contrainte-déformation à différentes températures, ce que ne permet pas la théorie standard. Ce modèle de Flory modifié permet en outre de prévoir les variations de température élastocaloriques à température ambiante. Cela démontre les capacités d'un modèle physique basé sur la cristallisation induite par la déformation. En outre, la correspondance entre ce modèle et les résultats expérimentaux montre que l'effet élastocalorique dans le caoutchouc naturel est étroitement lié à la cristallisation.

Les effets de la fatigue sur l'effet élastocalorique du caoutchouc naturel sont ensuite étudiés. La résistance à la fatigue pour de grandes amplitudes de déformation (déformation de 1 à 6) est d'environ 800 cycles pour le caoutchouc testé, ce qui est beaucoup trop faible pour être utilisé pour un système de refroidissement. La diminution de l'amplitude de la déformation est nécessaire de prolonger la durée de vie et atteindre les exigences d'un dispositif de refroidissement. Les effets de la fatigue sur la variation de température élastocalorique sont comparées pour le régime de déformation amorphe (déformation 0-3), au début de la fusion des SIC (déformation 2-5) et dans la zone de saturation du SIC (déformation 4-7). Il a été observé qu'une plus grande variation de température élastocalorique et une meilleure résistance à la rupture peuvent être obtenus pour les deux régimes de déformation SIC (déformation 2-5 et 4-7) que pour le régime de déformation amorphe. Plus particulièrement, l'effet de fatigue pour le régime de déformation 2-5 est meilleur que pour le régime de déformation 4-7. Enfin, un grand nombre de cycles de fatigue ($1,7\times10^5$ cycles) au régime de déformation 2-5 a été appliqué, démontrant une dégradation modérée de l'effet élastocalorique (12%) et l'absence de fissures ou de rupture de l'échantillon. En outre, le coefficient élastocalorique en contrainte pour le régime de déformation 2-5 (4,4 K / MPa) est supérieur à celui obtenu pour le régime de déformation 4-7 (1,6 K / MPa). En conséquence, le régime intermédiaire (correspondant à la déformation de début de fusion du SIC), permettant d'obtenir la plus grande performance élastocalorique (à travers la variation de température élastocalorique notamment) et une meilleure résistance à la fatigue, devrait être choisi pour des systèmes de refroidissement élastocalorique.

Dans le travail mentionné ci-dessus, le potentiel du caoutchouc naturel comme matériau élastocalorique est a priori démontré. Un matériau calorique présente des variations temporelles de température lorsqu'il est excité par la grandeur physique appropriée. Il est donc nécessaire de convertir ensuite ces variations temporelles en un gradient de température spatial pour obtenir une capacité de réfrigération. Dans la dernière partie de ce manuscrit, un modèle de système régénératif de refroidissement à base de matériaux caloriques est développé. Il est basé sur un mouvement de la couche active (source de température réversible) par rapport à une couche passive (qui constitue un accumulateur local de chaleur, nécessaire pour le fonctionnement régénératif). Basé sur le changement de température élastocalorique de 4 K pour une déformation de 2-5 obtenu précédemment, le gradient thermique maximal obtenu en simulation est de 0,5K/cm avec un mouvement relatif de 3 cm à 1 Hz. En outre, l'effet des propriétés élastocaloriques, de la chaleur spécifique et de la conductivité thermique sur la puissance de réfrigération et le gradient thermique sont simulés. Il est montré que les performances augmentent avec l'augmentation de l'effet élastocalorique, de la capacité thermique du matériau actif et de sa conductivité thermique. Ce travail de modélisation permet d'établir des lignes directrices pour le choix des matériaux élastocaloriques.

# Contents

# List of figures

# List of variables

| | |
|---|---|
| $\sigma$ | stress |
| $\sigma_{stretching}$ | stress in extension |
| $\sigma_{retraction}$ | stress in retraction |
| $\varepsilon$ | strain |
| $\varepsilon_r = \frac{\varepsilon_m}{1+\varepsilon_{pre}}$ | relative strain of sample with the pre-strain |
| $\varepsilon_{pre}$ | pre-strain |
| $\varepsilon_m$ | the strain the NR material really experiences |
| $N$ | network chain density |
| k | Boltzmann constant |
| T | temperature |
| $T_0$ | room temperature |
| $\lambda$ | elongation |
| C | heat capacity |
| $c = 1.8\times10^6\, J\cdot K^{-1}\cdot m^{-3}$ | specific heat of NR |
| $\tau$ | thermal time constant |
| $h$ | heat transfer coefficient |
| $\alpha = \frac{CI_{growth}}{CI_{nucleation}}$ | SIC growth degree |
| $CI_{nucleation}$ | crystallinity index of the SIC nucleation |
| $CI_{growth}$ | crystallinity index of the SIC growth |
| $\alpha_T = \frac{\Delta T_{relaxed}}{\Delta T_{stretching}}$ | temperature change ratio, $\Delta T_{relaxed} = \lvert\Delta T_{retraction}\rvert - \lvert\Delta T_{stretching}\rvert$ |
| $\Delta T_{retraction}$ | temperature decrease in retraction |
| $\Delta T_{stretching}$ | temperature increase in extension |
| $\alpha_\sigma = \frac{\sigma_{relaxed}}{\sigma_{stretching}}$ | stress relaxation ratio, $\sigma_{relaxed} = \sigma_{stretching} - \sigma_{retraction}$ |
| $A$ | Helmholtz free energy |
| $U$ | internal energy |
| $W$ | work |
| Q | heat |
| $S$ | entropy |
| $s$ | specific entropy |
| $f$ | force |
| $l$ | length of sample |
| $\beta = -\left(\frac{\partial s}{\partial \varepsilon}\right)_T$ | eC strain coefficient |

| | |
|---|---|
| $\beta = \left( \frac{\partial \sigma}{\partial T} \right)_{\varepsilon}$ | Clausius-Clapeyron factor |
| $\gamma = \frac{\partial T}{\partial \sigma_{stretching}}$ | eC stress coefficient |
| $\Delta G_m$ | melting Gibbs free energy |
| $\Delta H_m$ | the enthalpy of the chains |
| $\Delta S_{m,\lambda}$ | the entropy of the chains at the elongation $\lambda$ |
| $\Delta S_{undeformed}$ | the entropy change from deformed state of the chains at the elongation $\lambda$ to un-deformed state |
| $\Delta S_{m,1}$ | entropy of fusion of the crystalline phase in an stretched chain |
| $T_m^0$ | incipient crystallization temperature |
| $n$ | number of segments per chain |
| $v$ | crosslink density |
| $v_s$ | density of sulfur bridges |
| $v_{crystal}$ | density of crystallites |
| $N_c = 1 + \frac{\xi}{\psi}$ | new short chain number caused by crystallites in each chain |
| $\xi$ | number of crystalline links per chain |
| $\psi$ | number of links traversing the crystallite crosslink in one chain |
| $N_t = N_s \cdot N_c$ | total network chain density after crystallization |
| $N_s$ | chemical network chain density |
| $n_s$ | the number of equivalent random links per chain before crystallization |
| $n_t$ | total number of equivalent random links per chain after crystallization |
| $M_c$ | average molecular weight |
| $d_T$ | degradation degree of temperature change |
| $d_\sigma$ | degradation degree of stress |
| $\vec{v}(x,t)$ | motion of active material along the x axis |
| $S_a$, $\lambda_a$, $T_a(t)$ | the entropy, thermal conductivity and temperature of the active material |
| $S_p$, $\lambda_p$, $T_p(t)$ | the entropy, thermal conductivity and temperature of the passive material |
| $\delta$ | thickness of the thermal boundary layer |
| $P_{actif}$ | cooling power per unit area |
| $P_0$ | active heat flux which is cause by both the caloric effect and the motion of the active layer |
| $\lambda_{eq}$ | thermal conductivity induced by the eC effect and movement |

# Chapter 1 Introduction

As the industry develops and the living standards increase, the refrigeration market is large and remains growing. Vapor-compression has been the dominant technology for all cooling applications during the past 100 years. Although the performance of cooling technology is improving, it still results in many environmental problems. While ozone depletion and its damage to the world are being addressed, the battle against global warming is just beginning. Global warming effects include rising sea levels, changing precipitation, expansion of deserts in the subtropics, more frequent extreme weather events and species extinctions due to shifting temperature regimes. Even we are aware of the catastrophic global warming, but the global mean surface temperature always increase up to 0.7 K from 1960 due to human activity[1]. The global warming potential (GWP) of the conventional refrigerants used in vapor-compression equipment is as high as 1000 times that of $CO_2$. Hence, it is important and urgent to develop more sustainable and more efficient alternative cooling techniques.

The caloric effect is drawing more and more attention to be used for solid state cooling systems which can replace the vapor compression technique with hazardous gases. Among all the caloric materials, the elastocaloric (eC) effect of natural rubber (NR) (called the Gough-Joule effect) is the oldest known one, which was first observed by Gough and further investigated by Joule[2]. However, its research towards cooling application is rare and just beginning[3,4]. It shows a large temperature change of about 10 $^{o}$C at strain of 5[5–7]. NR is a soft material with Young modulus of several MPa, resulting in a low tensile stress. Furthermore, NR material is non-toxic, environmentally friendly and low cost[3]. At constant stress amplitude, increasing the mean stress was found to increase the fatigue life of NR up to $10^6$ cycles[8,9]. Moreover, the fatigue life can be up to $10^7$ cycles when strain amplitude is 200%[10]. The fatigue property of NR can also be optimized by adjusting the content of sulfur and filler (carbon black). It is an important property towards the development of the applicable NR material in an eC cooling device[11]. Furthermore, the fatigue damage of NR can be healed by a high temperature or a solvent exposure[12], which is inimitable compared with the inorganic materials. All these factors make NR material a potential candidate for solid-state-cooling systems.

In this chapter, the different caloric effects are firstly compared, then the potential of NR acting as eC material is discussed.

## 1.1. Comparison of different stimulus-caloric effect

The caloric effects mainly include four types: the magnetocaloric (MC), electrocaloric (EC), barocaloric (BC) and elastocaloric effects. They refer to the isothermal entropy change or adiabatic temperature change upon application or removal of magnetic field, electrical field, hydrostatic pressure and uniaxial stress, respectively. A solid-state cooling cycle based on these caloric effects is illustrated in Fig.1. 1.

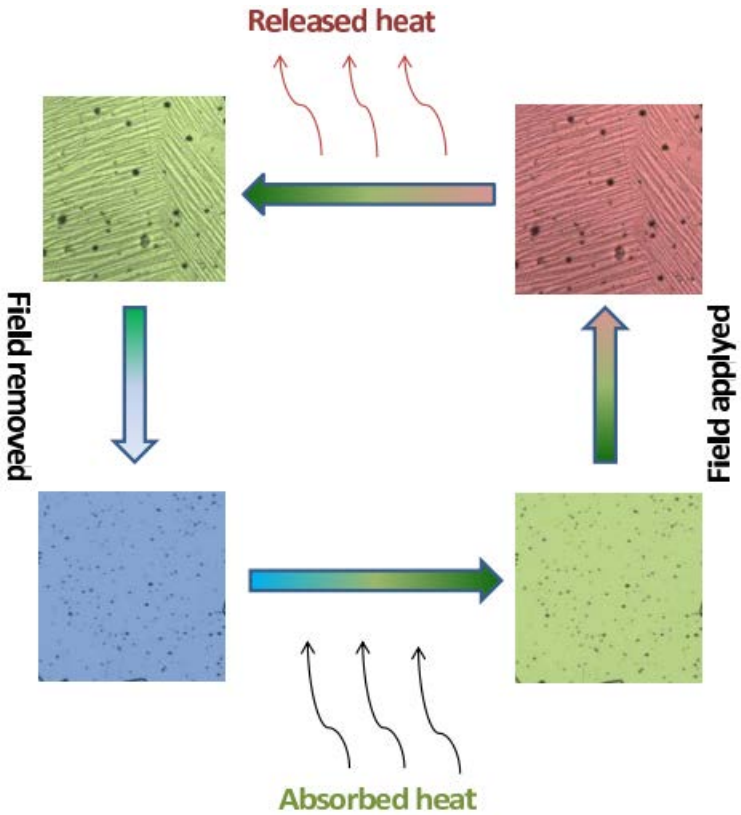


Fig.1. 1 Refrigerating cycle. Schematic diagram for a solid-state cooling cycle based on a caloric effect, which can be excited by a magnetic field, electric field, hysdrostatic pressure or uniaxial stress. In the first stage, a field is adiabatically applied resulting in a temperature increase of the material (a forward phase transition occurs). In the second stage, the heat of the material is transferred to a heat sink at constant field. In the third stage, the field is adiabatically removed and the material cools itself (the reverse phase transition occurs). In the fourth stage, the cool material absorbs heat from the cold sink[13].

In the last decade, MC refrigeration has attracted a large research interest, as it shows a significant potential as an alternative to the vapor-compression technology[14,15]. The recently reported temperature span produced by the MC devices can be close to or above 30 K, which is potential for a wide range of cooling applications[16]. However, the commercialization of MC refrigeration faces some problems. Firstly, the MC materials and the magnet arrays are expensive and based on rare-earth material, which is hardly sustainable. Secondly, a strong magnetic field is difficult to generate. At last, some MC materials like the As-based one could be toxic. The EC effect has been studied seriously only recently. Both the polymer film and oxide thin film can endure high electric field (larger than 100 MV/m). Thus, they can get a large temperature change (10 K). However, EC bulk materials are limited by their dielectric strength[17,18] and thin film may be only used. Thus, their application is limited to the small scale. The eC effect of shape memory alloys (SMAs) has recently attracted more and more attention due to the large available latent heat and large adiabatic temperature changes. It is an order of magnitude higher compared to the MC effect[11,19–21]. It appears some patents[22], some simulation papers of cooling device[11,23,24] and the fabrication of prototype based on the eC effect[25]. According to a report by the US Department of Energy[26], eC cooling shows the largest potential among all alternatives to vapor-compression technologies.

### 1.1.1. Magnetocaloric effect

#### *1.1.1.1. Magnetocaloric materials*

The MC effects of different materials for a magnetic field change of 2 T are summarized in Fig.1. 2[27]. It is apparent that, above room temperature, a few transition-metal-based alloys perform the best[27], which are mostly As-based alloys. Materials which do not include this element might be not adapted to near-room temperature cooling systems. Nevertheless this comparison shows that it is possible to control the temperature where this effect is maximum by adjusting the relative contents of the different elements.

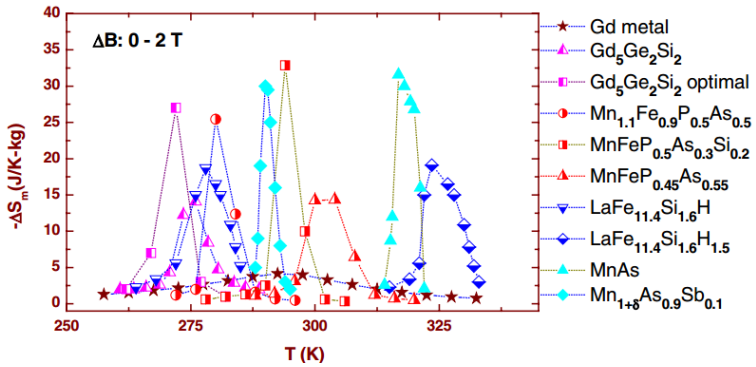

Fig.1. 2 Entropy change of different MC materials at magnetic field changes of 2 T[27].

#### *1.1.1.2. Magnetocaloric devices*

MC effects are still used for reaching ultralow temperatures, and have been suggested for the liquefaction of nitrogen and helium gases. The focus on MC cooling near room temperature has led to over 40 published prototype cooling devices[16]. Brown[28] firstly reported a near room temperature operating MC refrigerator. He achieved a much larger temperature span than the maximum observed MC effect: a 47 °C no-load temperature difference between the hot end (46 °C) and cold end (-1 °C). Following the work of Brown, the concept of active magnetic regenerator (AMR) was introduced by Steyert[29]. Subsequently, various MR units operating at different temperatures were brought to life. The AMR concept is briefly described below.

In the AMR cycle, a porous bed of a magnetic refrigerant material acts as both the refrigerant (coolant) and the regenerator for the heat transfer fluid. A schematic example of the working principle of AMR is shown in Fig.1. 3[15]. It is assumed that a porous bed of the magnetic refrigerant material is at a steady state with the hot heat exchanger at 24 °C and the cold one at 5 °C. The AMR cycle consists of four processes. The initial temperature profile (dashed line) for the bed without the application of a magnetic field is shown in Fig.1. 3 (a). The first step is to apply a magnetic field to the refrigerant. Each particle in the bed is magnetized and heated because of the MC effect to form the final magnetized bed temperature profile (solid line). Second, the 5 °C fluid flows through the bed from the cold end to the hot end (Fig.1. 3 (b)). The bed is thus cooled by the fluid (the dashed line to the solid line). The fluid absorbs heat from the bed and removes heat to the hot end (24 °C in this case) in the hot heat exchanger. Third, after the cold-to-hot fluid flow is stopped, the magnetic field is removed. Each particle in the bed is demagnetized and cooled (the dashed line to the solid line in Fig.1. 3 (c)). The last process is the hot-to-cold flow process (Fig.1. 3 (d)). With the magnetic field zero, the 24 °C fluid flows from the hot end to the cold end. The bed is thus heated (the dashed line to the solid

line). The fluid is cooled below 5 °C and absorbs heat from the cold end (5 °C in this case) in the cold heat exchanger.

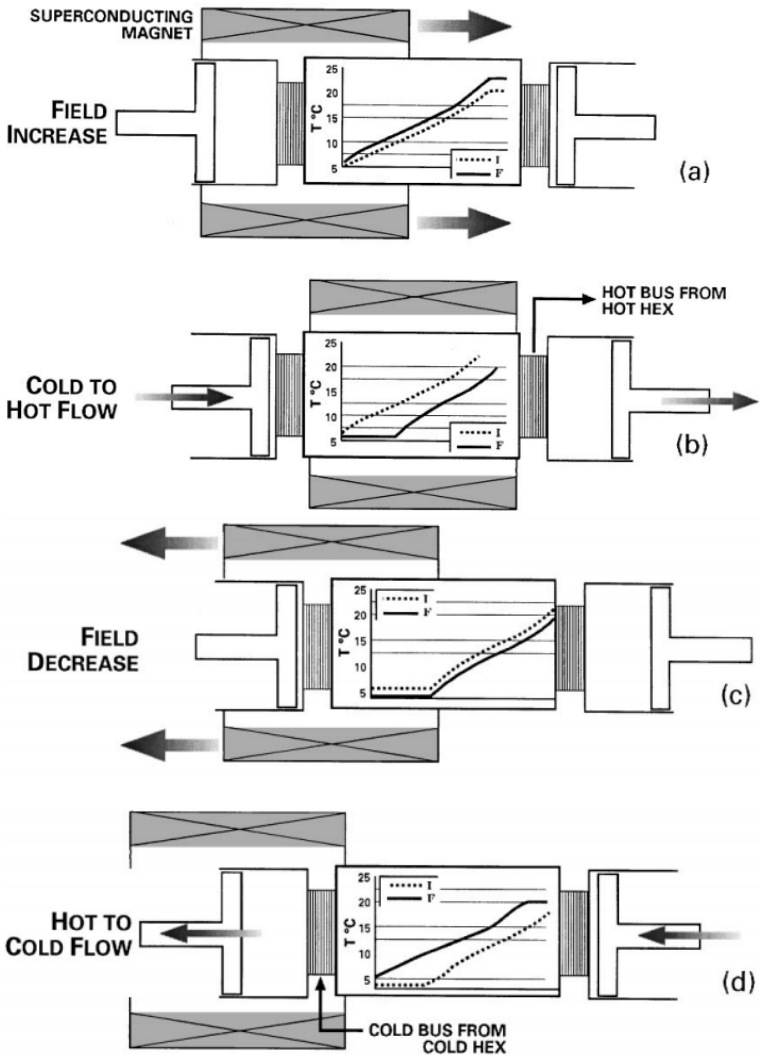


Fig.1. 3 The four steps of the active magnetic regenerator (AMR) cycle: magnetizing (a), heat transfer from cold to hot (b), demagnetizing (c), and heat transfer from hot to cold (d)[15].

The AMR cycle described above has several advantages useful for MC cooling devices. First, the temperature span of a single stage is determined by the MC effect of all the individual particles in the bed, thus it can greatly exceed that of the MC effect of the magnetic refrigerant. Second, the bed acts as its own regenerator and the heat is transferred in a single bed via the fluid flow between the hot and cold ends. A regenerative system seems to be the only way to use caloric materials in cooling devices, since it can convert the time variations of temperature of the caloric material into spatial gradients of temperature. Compared to other regenerative systems, AMR allows in addition compact devices.

### 1.1.2. Electrocaloric effect

**Bulk materials**

For the eC materials, one should notice the correlation between the EC effect, and the entropy and polarization change under an applied electric field. A large EC effect is usually associated to a large polarization change upon the application of an electric field, for example when working in the vicinity

of phase transitions. An EC temperature change of 2.3 K was reported for the highly ordered $PbSc_{1/2}Ta_{1/2}O_3$ ceramics in a temperature range of $T_c \pm 5$ K[30]. However, the temperature range is too narrow for a cooling cycle. Therefore, further research has focused on materials with a diffuse ferroelectric transition such as disordered crystals and especially relaxor ferroelectrics. A very large EC effect in bulk samples of the $Pb(Mg_{1/3}Nb_{2/3})O_3$–$PbTiO_3$ (PMN-PT) system has been reported by Chukka et al.[31]. They measured EC temperature changes of 2.7 K under an applied electric field of around 1.2MV/m for the single crystal. Moreover, this single crystal has a large temperature range, from 80 to 160 °C, as a result of a broad and diffuse ferroelectric transition.

Since the medium and large scale cooling applications requires a high refrigeration capacity, the quest for higher EC effects in bulk materials is increasing. It is unlikely to be achieved with any types of EC materials other than ceramics[17]. The problem concerning the bulk materials with high EC performance is the environmental sustainability. They all contain a large amount of lead, which is toxic and detrimental to the environment and human beings. The same with the current trends in piezoelectric technology, the research on EC materials should also focus on lead-free compounds.

**Thin films**

Research on EC thin films has been initiated by Mischenko et al.[32]. An EC temperature change of 0.48 K per volt was reported in 350-nm $PbZr_{0.95}Ti_{0.05}O_3$ thin films, which was termed the giant EC effect (12 K per 48 MV/m). The EC temperature change of thin films is significantly higher than that of the bulk materials. However, the applied electric fields are much higher because of the much higher dielectric strength of the films. Saranya et al.[33] reported a $\Delta T$ of 31 K ($\Delta E$ □ 75 MV/m) for a PMN-PT thin film. This material shows the highest $\Delta T / \Delta E$ in all the oxide thin films.

**Polymer**

All the EC studies of polymers have so far been conducted on polyvinylidene-fluoride-based polymers. A large entropy change of 56 J/(kg.K) has been reported by Neese et al.[34] in P(VDF-TrFE) films at the temperatures around the ferroelectric transition. It is much higher than that of oxide films (lower than 10 J/(kg.K))[32] and even higher than that of MC materials. However, such a large entropy change has been achieved with an extremely high electric field of 209 MV/m, which is five times stronger than that applied on oxide films. When we consider the EC effect efficiency which is indicated by the ratio of the temperature change to the electric field ($\Delta T / \Delta E$), it is very low for polymers compared to the oxides.

Another important parameter correlating with the EC effect of polymers is the crystallinity of the polymer. It has been indicated that defects in the chain order and the presence of an amorphous phase fix the domain motion under high electric fields[35].

In Fig.1. 4 (taken from [17]), the temperature change $\Delta T$ for bulk materials, thick films, thin films of ceramics and polymers were summarized. The correlation between the sample type, the applied field and the EC performance is shown apparently. High EC temperature change can be obtained for bulk samples and thick films with moderate applied electric field. For oxide and polymer thin films, extremely high fields should be applied to obtain higher $\Delta T$.

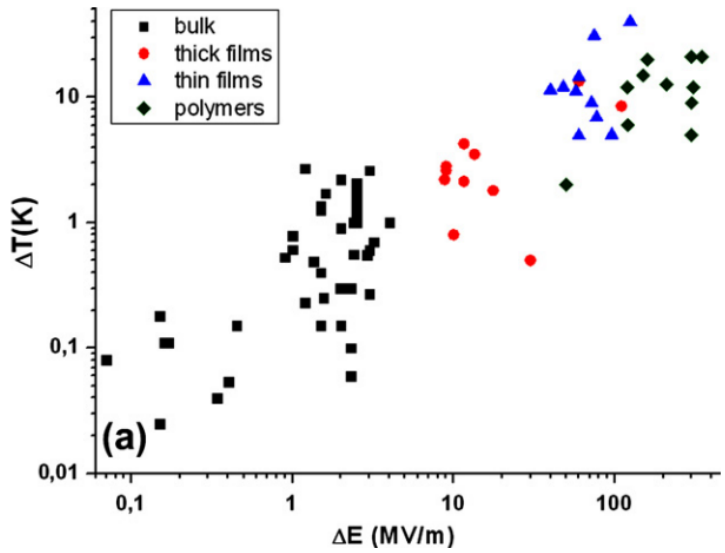

Fig.1. 4 (a) EC temperature change $\Delta T$ for different materials[17].

### 1.1.3. Barocaloric materials

In 1998, K. Alex Müller and his co-workers reported a small inverse BC effect in the polycrystalline nickelate $Pr_{0.66}La_{0.34}NiO_3$ at 350 K, near a structural transition. Its temperature change is about 0.2 K under a pressure of 0.5 GPa[36]. Large BC effects have now been observed in a super-elastic magnetic alloy of $Ni_{49.26}Mn_{36.08}In_{14.66}$ near room temperature[37]. The absolute temperature change $|\Delta T|$ is about 4.5 K under a pressure of 0.26 GPa. The transition indicates that the conventional BC effect also supports an inverse MC effect[37], whereas some BC materials show different BC and MC behaviors, like intermetallic $LaFe_{11.33}Co_{0.47}Si_{1.2}$ showing inverse BC effects and conventional MC effects[38], the giant MC material $Gd_5Si_2Ge_2$ showing conventional MC effects and conventional BC effects[39]. Therefore, as expected, giant MC materials represent promising BC materials as well. Cooling devices based on BC effect hasn't been however reported yet.

### 1.1.4. Elastocaloric effect

In many aspects, the eC technology is similar to the conventional vapor compression. They both use mechanical excitation (pressure or stress) to induce phase transformations. This may facilitate the technology transfer from vapor compression to eC technology.

The eC materials can be divided into shape memory alloys (SMAs) and elastomers. NR, one typical elastomer, can act as eC material, which will be discussed in detail in section 1.2. Recently, most of the eC research however focused on SMAs.

#### *1.1.4.1. Elastocaloric materials of SMAs*

The eC effect of SMAs is the mechanical analog of the MC effect. It involves a martensitic phase change process induced by stress change. There are mainly three types of SMAs: the copper based alloys, like the Cu-Zn-Al[19] and Cu-Al-Ni[40]; the Fe based alloys, including Fe-Pd[41] and the most promising SMA, Ni-Ti (nitinol), which was presented by Buehler *et al.*[42]. The most important parameter of SMAs is the adiabatic temperature change. Previous studies suggested that nitinol had adiabatic temperature change of 17-23 K[20,43], whereas the Cu-Zn-Al and Cu-Al-Ni had adiabatic temperature change of 11-19 K. The nitinol also has much better fatigue performance than copper

based alloys, since copper based alloys is brittle. The major drawback of nitinol compared to copper based SMAs is a higher hysteresis, although it is possible to reduce it by adding a small content of copper to the niticol alloy[44].

### *1.1.4.2. Elastocaloric device by using SMAs*

The AMR has been applied in all up-to-date magnetic refrigerators, since it is the most efficient way to utilize the MC effect so far[16]. Such a refrigerator system by using eC effect is proposed by Tusek et al[11]. The system configuration and its four operational steps are shown in Fig.1. 5. It consists of parallel eC plates, two heat exchangers, a heat-transfer fluid, a fluid pumping system, and an actuator to (un)load the material. First, the eC plates are loaded to perform the austenitic-martensitic transformation for heating them up. In the second step, the fluid is pumped through the heated plates (regenerator) to the hot heat exchanger (HHEX) where it expels heat to the surroundings. In the third step, the eC plates are unloaded and thus cooled down. In the final step, the fluid is pumped through the regenerator to the cold heat exchanger (CHEX). The fluid is thus cooled and can absorb heat from the CHEX. These four steps are continuously repeated, resulting in a temperature profile in the fluid flow direction. Therefore, a temperature span between HHEX and CHEX is established.

One main drawback for practical application of this technology is the large forces needed to perform the deformation. For example, the evaluated system (500 W of cooling power) requires an applied force of about 180 kN (stress of 900 MPa) for Ni-Ti alloy and about 50 kN (stress of 275 MPa) for Cu-Zn-Al[11]. The large force will easily cause the damage of the clamp after a large number of cycles. The large force will result in the decrease of the system stability and the increase of the cost. Tusek et al. proposed that the large force can be reduced by reducing the cross-section of the regenerator and increasing its length. If doing that, the system size will increase.

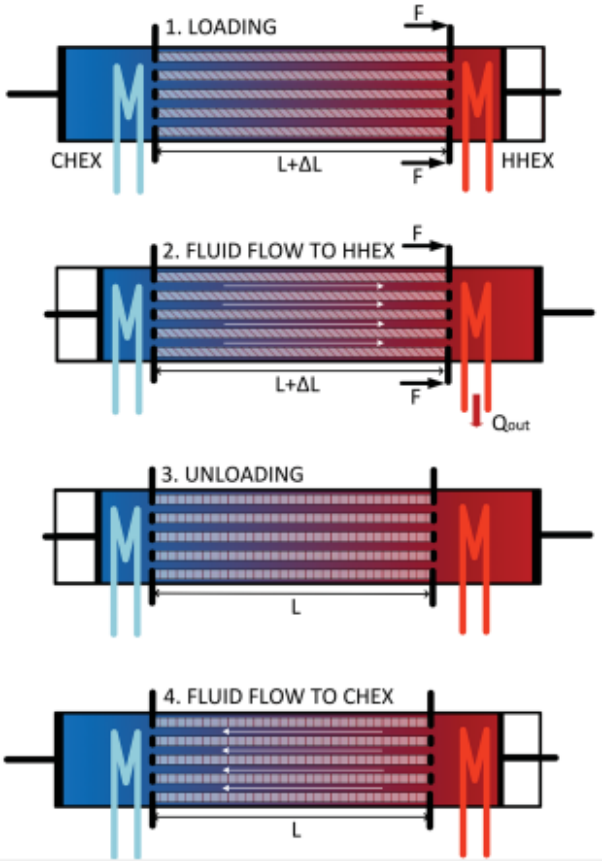


Fig.1. 5 Schematic presentation of the operation of the eC regenerator[11].

The problem concerning the large force has been highlighted by a real setup (Fig.1. 6)[25]. The authors used two linear motors to output a force of 2 kN. This large force only allows for loading SMA (NiTi) with a small cross section of 1.6 $mm^2$ (length=90 mm). Thus, the cooling power is low (only 9 J) in one cycle.

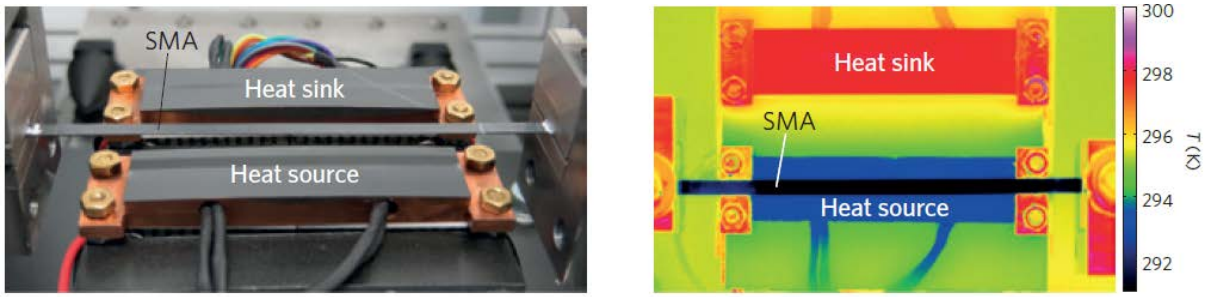


(a) (b)

Fig.1. 6 (a) Cooling device based on eC effect of a NiTi ribbon. (b)An infrared thermal image reveals the temperature change established by repeatedly using the SMA NiTi ribbon to absorb heat at the cold end and then dump it to the hot end[25].

Another similar AMR system by using the eC effect is proposed by Qian et al.[23]. Fig.1. 7 shows the schematic of a single SMA bed assembly using nitinol tubes. These tubes are used to produce cooling and heating capacity. Their holders are designed to sustain radial direction stress during their compression process, as well as to avoid bending. The two loading heads were originally designed to feed heat transfer fluid (HTF) into the nitinol tubes for heat transfer and transfer the compression force directly into the nitinol tubes.

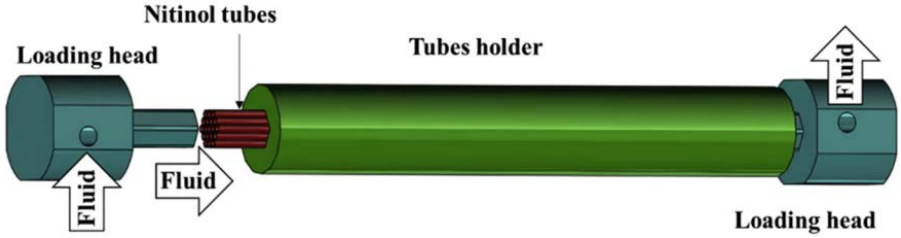


Fig.1. 7 Original design of the nitinol tubes bed for cooling.

## 1.2. An interesting eC material: natural rubber

NR is an interesting eC material but its eC effect is rarely studied up to now. It is a widely used material in elastomeric parts because it combines very large elastic strain and a remarkable crack growth resistance[45].

NR elasticity has been described in entropic elasticity. As an elastomeric material is stretched, the polymer chains become oriented and the degree of order increases, leading to the decrease of entropy (temperature increases in an adiabatic case). When the stretching stress is released, the material returns to its original disordered state and the entropy increases (temperature decreases in an adiabatic case). Thus, a molecular chain can be considered as an entropic spring[46]. The effect of mechanical excitation on the entropy of a polymer chain is illustrated in Fig.1. 8.

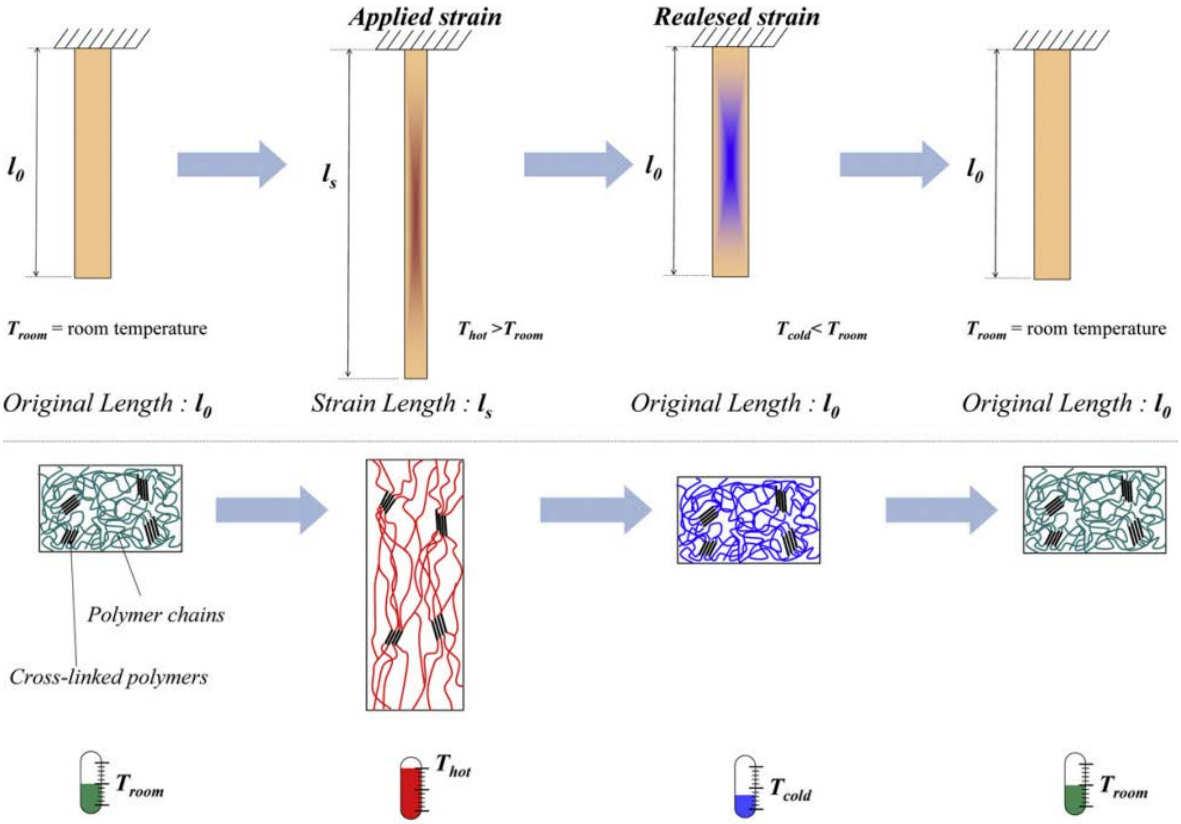


Fig.1. 8 Schematic representation of the molecular mechanism of the eC effect of polymer[3].

Strain-induced crystallization/crystallite (SIC) is widely believed to occur in the deformation process of NR[47]. The latent heat of SIC is believed to be responsible for the huge change in entropy of NR upon stretching. Moreover, the stress behavior of NR is mainly related to SIC[48]. Both the temperature change and stress are mainly influenced by SIC[45,49,50]. For eC effect, temperature change and stress (elasticity) are two necessary properties. Thus, the eC effect of NR mainly depends on the SIC and the SIC theory is important for understanding the eC behaviors of NR. The schematic model of network chains of SIC is shown in Fig.1. 9[51].

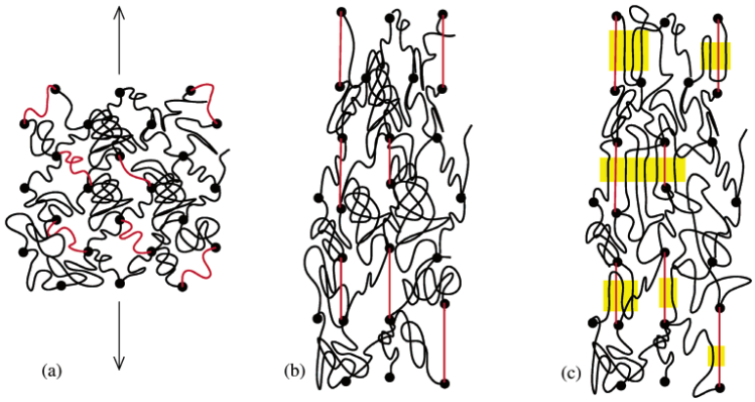


Fig.1. 9 SIC nucleation and growth in vulcanized NR. Shorter chains are drawn as red lines. Filled circles are the cross-links. (a) Before deformation, cross-links are homogeneous. (b) After deformation, shorter chains are fully elongated. The distribution of cross-links is no longer homogeneous. (c) The fully stretched chains act as nucleus of crystallites and bind more chains (yellow parts)[51].

SIC was discovered in 1925 by Katz[47,52], who was the first to show the X-ray diffraction pattern of a uniaxially stretched NR. Note that unstrained NR can also crystallize by cooling;

this phenomenon is called temperature-induced crystallization (TIC)[53]. After the discovery of Katz, SIC of NR has been widely studied. Many experimental investigations[51,54–66], theoretical descriptions[67–83] and reviews[47,84] are available.

### 1.2.1 Crystallographic structure

The crystal structure and the lattice parameters of SIC in NR can be deduced from the X-ray diffraction pattern. Fig.1. 10 gives a typical diffraction pattern that can be obtained when X-ray beam is perpendicular to the stretching direction of NR[51].

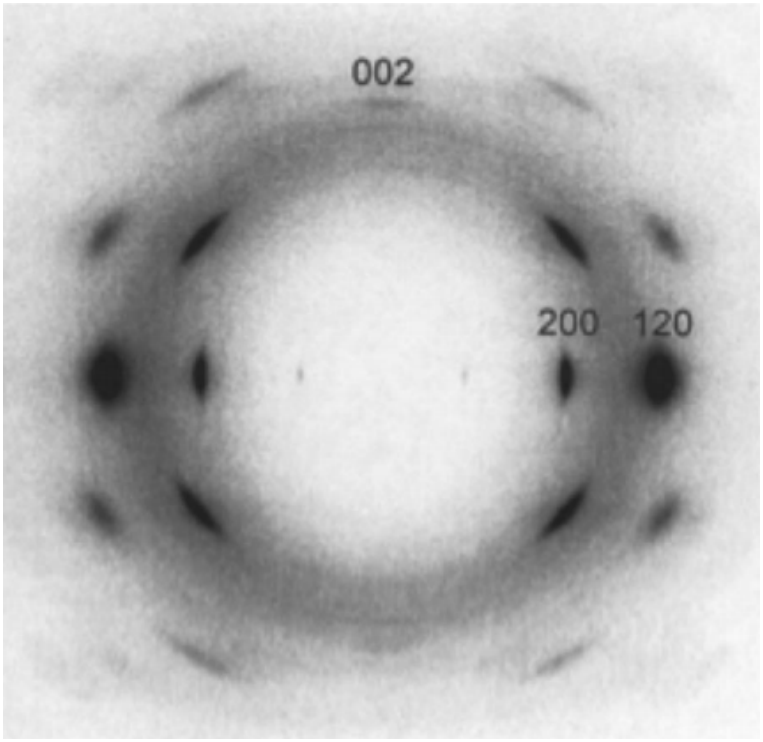


Fig.1. 10 Typical WAXD pattern of a vulcanized NR. The stretching direction is vertical[51].

Bunn[85] showed the monoclinic structure of NR with the following parameters: $a$ = 12.46 Å, $b$ = 8.89 Å, $c$ = 8.10 Å and $\beta$ = 92 °. As shown in Fig.1. 11, macromolecules are oriented along the $c$-axis of the crystal cell. Each cell contains four chains, corresponding to eight monomers. When SIC takes place in uniaxial tension, the active chemical bonds in the stretching direction (c-axis) are strong (covalent bonds) while the active bonds in the basal plane (001) are weaker (Van der Waals bonds). It leads to an anisotropy of the macromolecular structure. Such an alignment of the macromolecules in the stretching direction can strengthen the material, resulting in the excellent mechanical properties of NR.

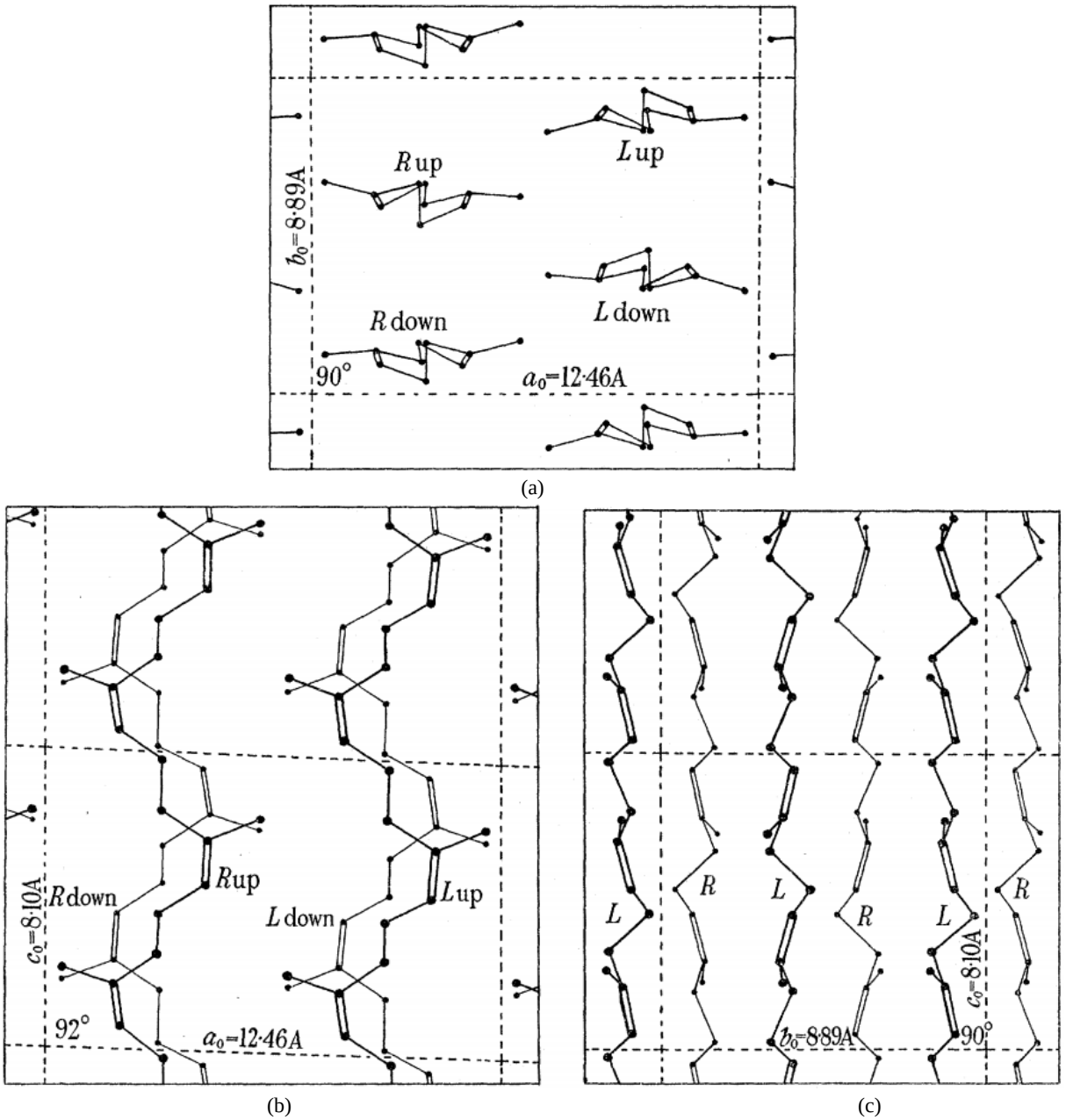


Fig.1. 11 The crystal structure in NR along: (a) *c*-axis, (b) *b*-axis, and (c) *a*-axis[85].

### 1.2.2 The occurence of SIC

The occurrence of SIC could be determined by the increase in melting temperature of crystallite upon deformation.

$$1/T_{m,\lambda} = 1/T_{m,1} - \Delta\Gamma_{def} / \Delta H_1 \quad (1.\ 1)$$

where $\lambda$ is the elongation, $T_{m,1}$ is the melting temperature of the un-deformed state, $T_{m,\lambda}$ is the melting temperature of the deformed state, $\Delta\Gamma_{def}$ is the entropy variation between the un-deformed and the deformed states, and $\Delta H_1$ is the latent heat of fusion.

According to Eq. (1.1), the melting temperature $T_{m,\lambda}$ increases with elongation as $\Delta\Gamma_{def}$ increases with elongation. As the melting temperature becomes higher than room temperature, the NR material enters into a super-cooling state, which will induce the SIC.

### 1.2.3 Stress and SIC

The relation between SIC and stress has been investigated by many researchers[47,50,57,75,86–88] . The pioneering work in this domain is that of Flory[70,89].

Flory proposed the two opposite views of the effect of SIC on stress:

1. **Stress relaxation effect.** The length of a chain in SIC is longer than the oriented amorphous one. The longer chain in SIC in the stretched direction makes the remaining amorphous chain relax. This mechanism can decrease the stress.

2. **Stress hardening effect.** SIC is a giant network point. The network chain density can be increased and thus the stress is increased.

The stress on the stretched NR can be reduced by the SIC. Albouy et al.[90,91] found that the local elongation of the amorphous chains get almost stablilized after SIC develops at any considered temperature (Fig.1. 12). This is consistent with the stress relaxation effect proposed by Flory, wherein partial incorporation of a polymer chain in a crystallite induces a relaxation of the remaining amorphous chain part.

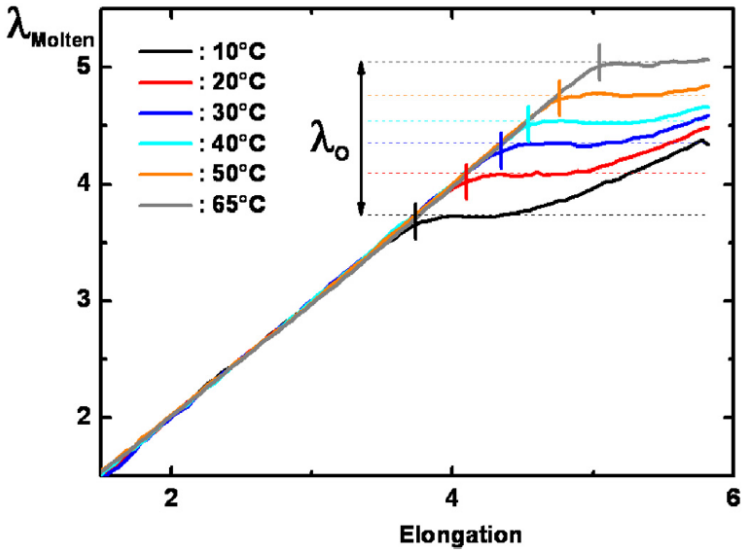


Fig.1. 12 The elongation of the amorphous fraction measured as a function of the macroscopic elongation and for different temperatures. The vertical segments point to the onset elongation of SIC[90,91].

The first thermodynamic treatment of stress relaxation of SIC was proposed by Flory[70,71]. He uses a Gaussian distribution function to model the partially crystallized polymer chains and assumes that the crystallized part of the chain is oriented in the stretching direction. Considering this model[70], Gent[74] was the first to extend the treatment of Avrami[81–83] to stretched NR and approximate the time functions governing SIC growth. The relaxed stress is found to be approximately proportional to the SIC degree.

Contrary to the stress relaxation effect of SIC, the lattice constants of the unit cell of SIC changed almost linearly with stress, which directly proved that the SIC is responsible for the increased stress upon strain[51]. This is consistent with the stress hardening effect proposed by Flory. Through the

stress variation responding to the constrained cooling and heating, results indicate that SIC is a new network structure, which reinforces the chemical network points[92]. Comparing the crystal unit cell lattice constants with the crystallite sizes[93,94], it can be concluded that SIC constitutes a big network point to bind many chains and divides the original long chain into short ones, which increases the network chain density and reduces the limit of chain extensibility[87]. This is the reason for stress hardening effect of SIC. Thus, the stress hardening effect of SIC is the mutual effect of increased network chain density and limited chain extensibility. As strain increases, the SIC develops and the stress hardening effect of SIC would become more and more prominent. This can be shown by the stress upturn at large strain (Fig.1. 13).

For the whole deformation cycle, the relations between stress and SIC at different strain regimes have been studied by many researchers[47,75,87,88,95]. Fig.1. 13 shows the corresponding stress-strain and crystallinity-strain curves. These curves were obtained at a low travel speed (strain rate ~ $5 \times 10^{-4}$ $s^{-1}$). The main observations are as follows:

1. At the onset of SIC of loading process, the stress relaxation effect of SIC is dominant. In Fig.1. 13(b), SIC starts at point A (around $\lambda = 4$). In Fig.1. 13(a), the stress-strain curve shows a plateau due to the stress relaxation effect of SIC;
2. At large strain in the loading process, the stress relaxation effect is weakened due to the restriction of network chains and the stress hardening effect becomes dominant.
3. In the unloading process, the stress relaxation effect of SIC becomes dominant again. For a given $\lambda$, the crystallinity during the unloading process is higher than the corresponding one in the loading process (Fig.1. 13 (b)). Due to the dominant stress relaxation effect of SIC, the stress during the unloading process is lower than the corresponding one in the loading process (Fig.1. 13 (a)).

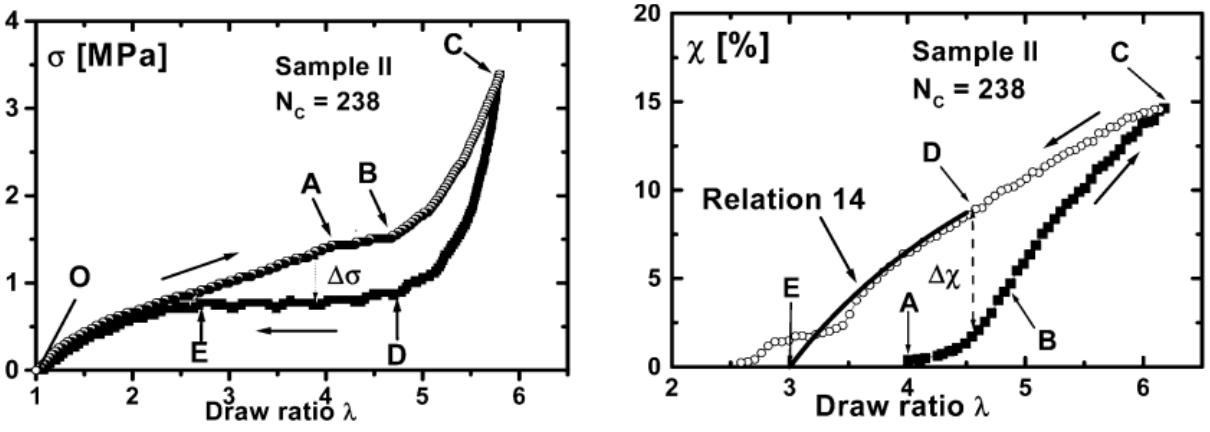


(a) (b)

Fig.1. 13 Simultaneous evolutions of: (a) stress and (b) crystallinity vs elongation during a deformation cycle (strain rate ~ $5 \times 10^{-4}$ $s^{-1}$) at 22 °C for a vulcanized NR[88].

According to these observations, it can be concluded that the mechanical hysteresis is mainly due to SIC. The occurrence of SIC is due to the super-cooling effect as well as the mechanical hysteresis[86,88,95,96].

This point is highlighted in Fig.1. 14 that shows the mechanical hysteresis *H* (the surface area between the two stress curves in the loading and unloading processes) obtained at different elongation $\lambda_{max}$ as a function of the maximum crystallinity $\chi_{max}$ reached for each $\lambda_{max}$ [47,88,97].

$$H = 0.1\chi_{max} \text{ J/cm}^3 \quad (1.\ 2)$$

Considering this relation, these authors considered the contribution of the viscoelastic properties on the mechanical hysteresis as negligible.

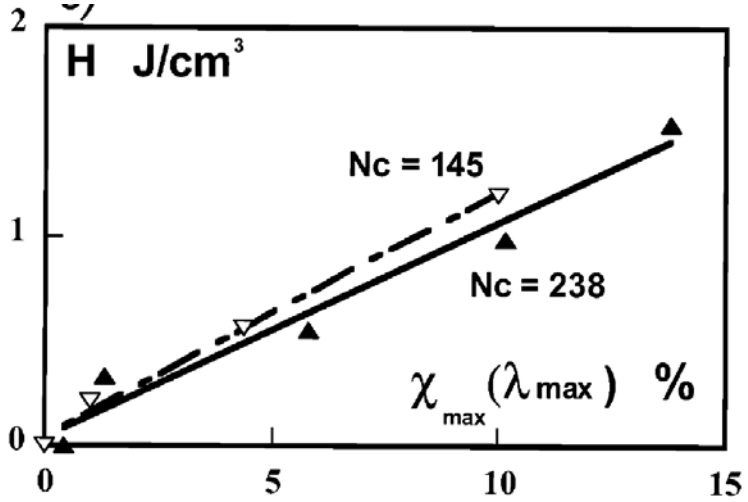


Fig.1. 14 Hysteresis as a function of the crystallinity for different NR samples[88].

Concerning the mechanical hysteresis and SIC hysteresis, Dargazany et al.[68,69,79] decomposed the NR matrix into five parallel networks, which were considered to be the origin of the purely elastic behavior, damage, hysteresis, and stress hardening of the SIC. By considering both the behavior of SIC and viscoelasticity of amorphous part, Kroon[76] adopted a full network model to predict stress–strain hysteresis and evolution of SIC degree. Very recently, Mistry et al.[78] modified the semi-crystallized chain model (Smith[80]) by using the non-affine microsphere model (Miehe et al.[77]). Guilie et al.[75] developed a micro-sphere 3D constitutive model. These models are thermodynamically consistent, and able to reproduce the main features, namely the stress relaxation, hardening and the hysteretic response in cyclic loadings.

### 1.2.4 Temperature change of eC effect and SIC

The temperature change of eC effect is mainly due to the SIC. There are relatively rare research work about the relation between temperature change and SIC. It's widely believed that the SIC occurs at a critical elongation (the onset elongation of SIC). For NR, the onset of SIC is around elongation of 3 [51,67,88,98]. For filler NR, the onset elongation of SIC is lower than NR[99].

The latent heat of SIC dominates the thermal effect in the region of high strains. This is apparent from Fig.1. 15, in which the temperature rise increases steeply in the region beyond strain of 3. The lack of reversibility between temperature change in extension and retraction is a further indication of SIC. These effects were not observed in the case of a rubber without exhibiting SIC, such as butadiene-acrylonitrile[100].

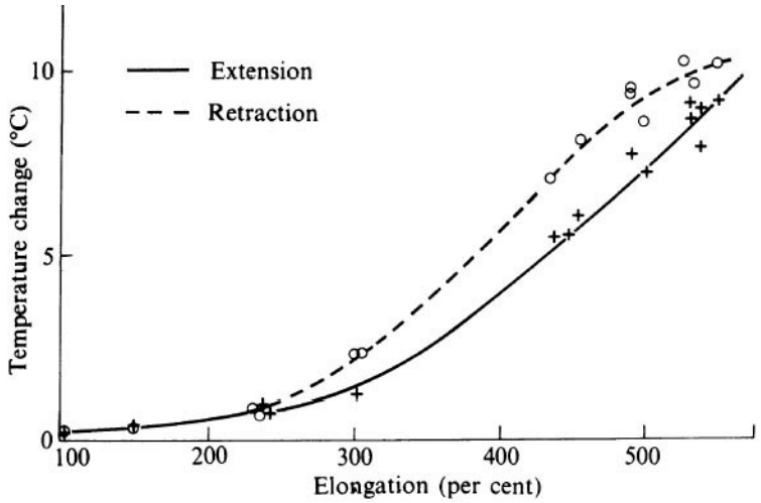

Fig.1. 15 Temperature changes vs. elongation in adiabatic extension and retraction[6].

Mitchell and Meier [7] defined an excess temperature rise, which is the temperature rise in excess of the heat converted by the work input in a stretched NR sample. The excess temperature rise may mainly be due to SIC. It was found that the excess temperature rise is dominant in the total temperature rise beyond elongation of 4, which indicated the dominant contribution of SIC compared with that from elastic entropy (Fig.1. 16).

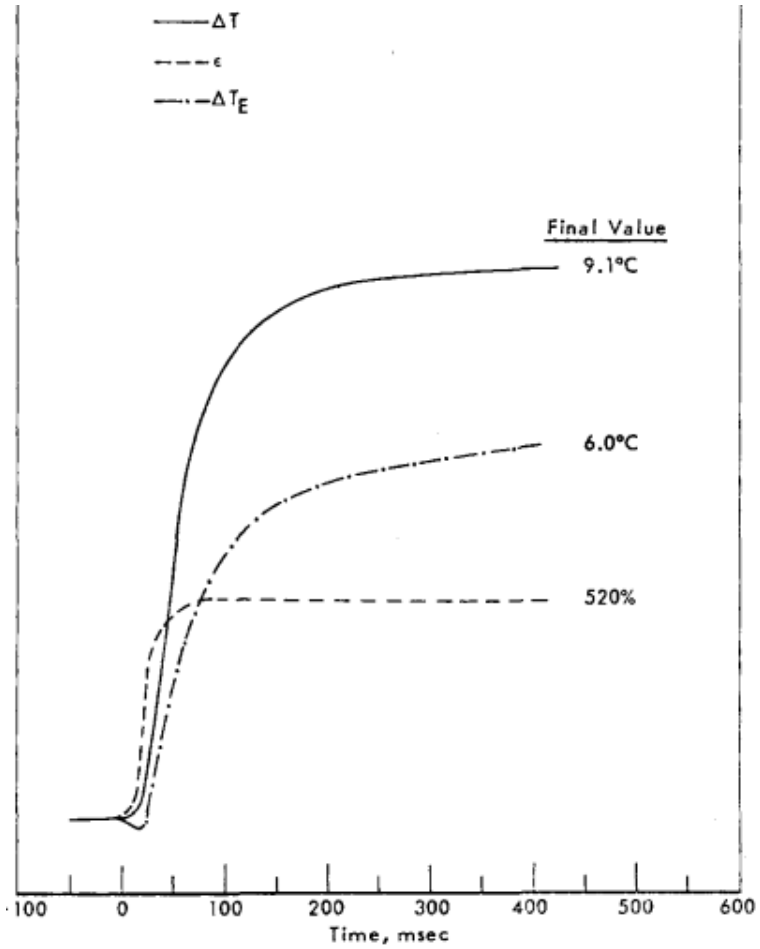

Fig.1. 16 The evolutions of temperature rise $\Delta T$ , excess temperature rise $\Delta T_e$, and elongation $\varepsilon$ with time for NR.

In the measurement of Sakata et al.[101], both the upturn of temperature change and the difference of the temperature changes in extension and retraction began at elongation of 4 (the onset of SIC), which indicates the occurrence of SIC (Fig.1. 17). The difference of the temperature changes in extension and retraction was explained by the different kinetic properties of crystallization and melting.

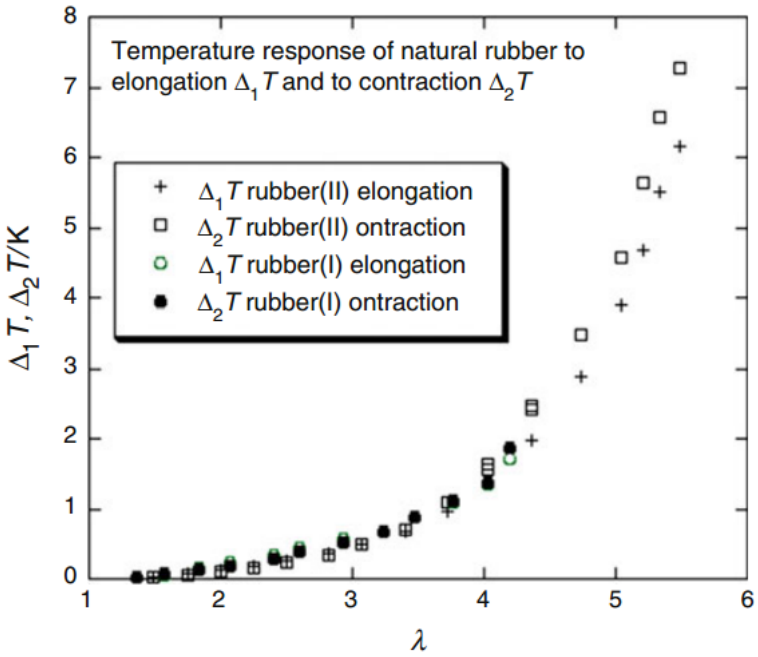


Fig.1. 17 eC effect of two kinds of NR. Hysteresis is evident at larger elongation [101].

Samaca Martinez et al.[102] observed that stress relaxed at constant elongation only if the elongation is higher than the onset of SIC in extension. Moreover, no significant stress variation at constant elongations was observed in retraction, which highlights the different kinetic of crystallization and melting. Furthermore, the creep of temperature increase was only observed when the elongation is higher than the onset of SIC. Contrary to the temperature increase, the temperature decrease is instantaneous with the retraction process. It further confirms the different kinetic properties of crystallization and melting.

In conclusion, all the phenomena tend to confirm that the temperature change mainly comes from the SIC. The observed thermal effects can be interpreted by the SIC theory. The first-order phase transition also contributes to the eC effect of shape memory alloys[20,103].

### 1.2.5 Fatigue property of eC effect and SIC

NR has been widely used as mechanical parts[104]. But there is relatively less research work about its eC effect[3,4] because polymer materials often exhibit large fatigue property upon repetitive deformation. However, there is a large improvement of the fatigue property for polymers exhibiting SIC. Among them, NR is a good candidate with good crack growth resistance[47,105–112] and excellent fatigue behavior[8–10,104,108,113–116].

The mechanical histories applied on NR are usually described by parameters such as minimum strain and strain amplitude (Fig.1. 18). In NRs that exhibit SIC, increasing the minimum strain has a significant beneficial effect for fatigue. This benefit was studied first in NR by Cadwell et al.[10]. Fielding[117] studied two synthetic rubbers. He found that Butyl-B exhibited the benefit, but styrene-butadiene rubber (SBR) did not. In NRs that do not exhibit SIC, non-zero minimum strain can have a deleterious effect[117]. Fielding identified SIC as the origin responsible for the fatigue life

improvement in NR and in Butyl-B. Comprehensive studies for fatigue crack growth were later reported by Lindley in crystallizing[118] and in non-crystallizing[119] rubbers. Under a static load, non-crystallizing rubbers can exhibit gradual crack growth, while crystallizing rubbers exhibit no crack growth. For cyclic load, the fatigue crack growth rate drops significantly for crystallizing rubbers which do not fully unload (non-zero minimum strain).

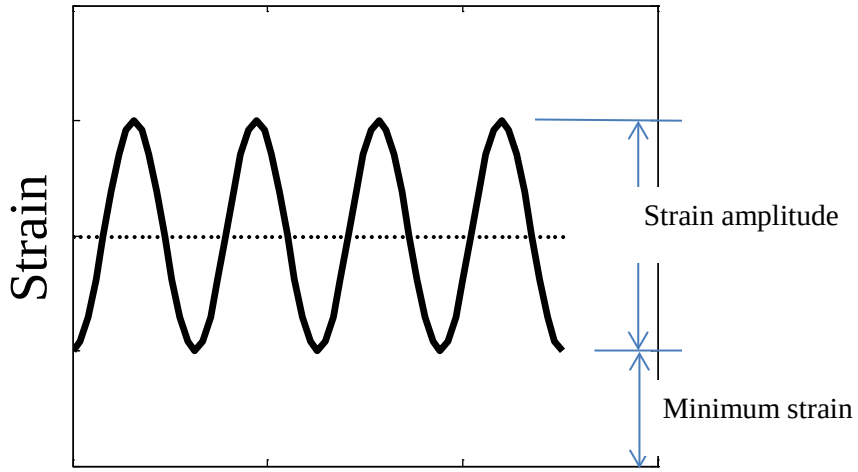


Fig.1. 18 Commonly used parameters for describing mechanical loading history.

One of the most important factors for the cooling application of eC effect of NR is the fatigue life. Due to the improvement of fatigue life on the non-zero minimum strain, it can be used for improving the fatigue life of cooling system based on eC effect of NR. Cadwell *et al.*[10] found that, for constant strain amplitude, the fatigue life of NR improved with increasing minimum strain, up to a moderately minimum strain level (200%). Beyond the moderately minimum strain, the fatigue life decreased with increasing minimum strain (Fig.1. 19). When the minimum strain is 200% and the strain amplitude is 200%, the fatigue life can be up to $10^7$ cycles [10].

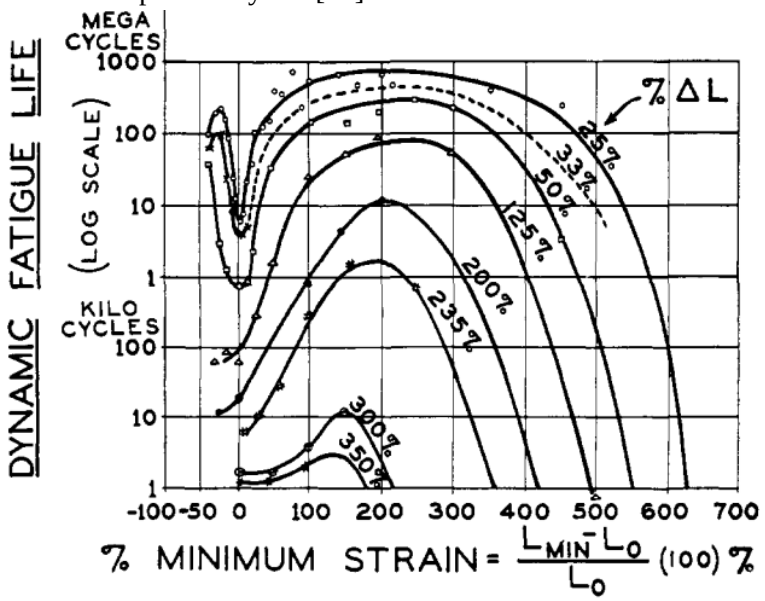


Fig.1. 19 The different fatigue life dependence on different minimum strains and strain amplitudes in biaxial stretching[10].

At constant stress amplitude, increasing the mean stress was found to increase the fatigue life up to $10^6$ cycles (Fig.1. 20)[8,9]. The longer fatigue life of NR proves its feasibility used for cooling system primarily.

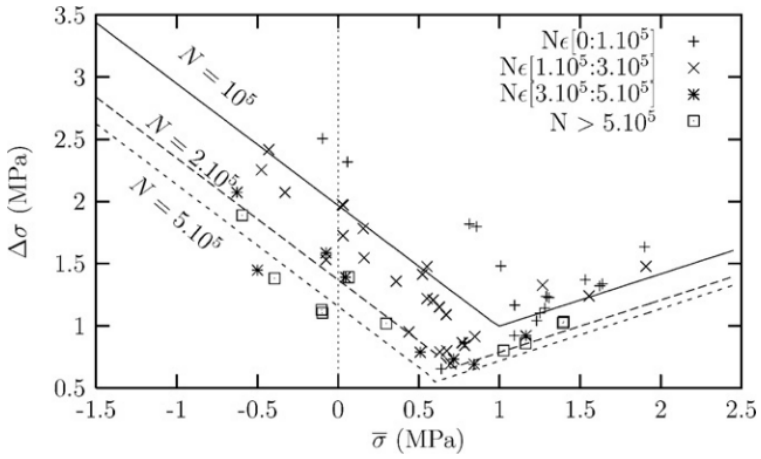


Fig.1. 20 The different fatigue life as a function of mean stress and stress amplitude in uniaxial stretching[8,9].

### 1.2.6 Other properties of SIC and eC effect

The other experimental investigations conducted have highlighted the kinetic nature of SIC [7,90,120–122] and its sensitivity to several parameters like temperature [48,88,123], network chain density [51,56,106], physical entanglements network [87,124,125], black carbon filler [99,126] and strain rate [121,123]. These properties of SIC may influence the eC performance of NR. These results can help to choose an applicable NR material for cooling application.

The existence of an optimal network chain density of vulcanized NR for the SIC was proposed to be $1.2 \times 10^4$ mol/cm$^3$ by Chenal *et al*.[56]. The NR with the optimal network chain density should lead to the largest temperature change. The influence of carbon black (CB) fillers on the mechanical behavior of NR is well known[127]. The stress is higher in filled rubber than in unfilled one[88]. The filler can increase the local strain of molecular chain and makes the nucleation easier (lower onset elongation in CB filled rubber) [88]. However, the crystallinity in filled rubber is lower.

As seen in Fig.1. 21, Albouy *et al*.[54] showed a regular decrease of SIC with temperature for an unfilled NR and noticed that SIC is almost inexistent at 80 °C. It indicates the existence of eC temperature change of can be up to 80 °C, and a regular decrease of the eC temperature change at temperature increases. They also showed that temperature affects the onset elongation of SIC, which increases with the temperature.

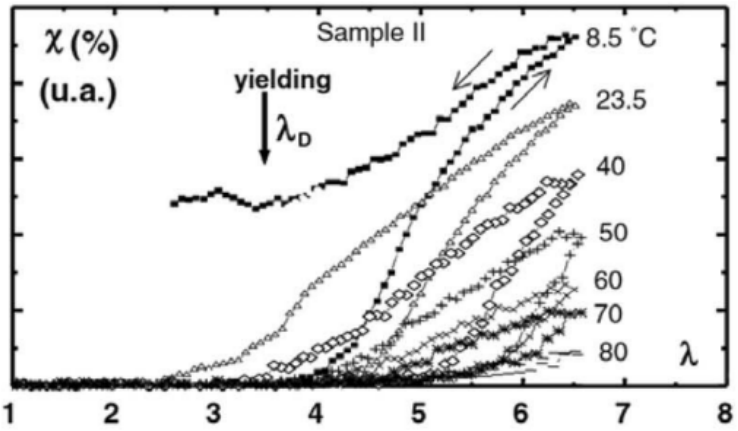


Fig.1. 21 Influence of temperature and elongation on crystallinity[54].

## 1.3. Comparison of eC effect of SMAs and NR

The eC properties of SMA and NR are compared. The SMAs are hard materials with Young modulus of several hundreds of MPa, whereas the NR is soft materials with Young modulus of several MPa. It results in a high tensile stress in SMAs while a low tensile stress in NR. Accordingly, the deformation of SMAs is only several percent of its original length, but the NR needs to be stretched several times of its original length. The lower stress of NR is good for the application, while the large deformation is a drawback for the compact cooling device. To overcome this drawback, a pre-strain can be applied[4].

The fatigue property of NR should be better than SMA. For SMA, the latest paper reported that the fatigue life of $Ti_{54}Ni_{34}Cu_{12}$ can be up to $10^7$ cycles at strain amplitude of 1.5%[128]. Seventy years before, the fatigue life of biaxial deformation of NR was proved to be up to $10^7$ cycles when the strain amplitude is 200%[10]. The uniaxial deformation of NR should get a higher fatigue life. Furthermore, the fatigue damage of NR can be healed[12]. It is an important property towards the development of the applicable NR material in an eC cooling device[103]. The comparisons of SMAs and NR are summarized in Table 1.

Table 1 Comparison of the eC material candidates

| | **shape memory alloys (SMAs)** | **Natural rubber (NR)** |
|---|---|---|
| **Cost** | 100 €/kg | 1.4 €/kg |
| **Fatigue life** | $10^7$ cycles in uniaxial stretching (at strain amplitude of 1.5%)[128] | $10^7$ cycles in biaxial stretching (at strain amplitude of 200%)[10] |
| **Stress** | Hundreds of Mpa | Several Mpa; |
| **Strain** | several percents; | several hundreds of percents; |
| **Thermal conductivity** | 18 $Wm^{-1}K^{-1}$[23] | 0.16 $Wm^{-1}K^{-1}$ |
| **Isothermal entropy change** | 32 $JK^{-1}kg^{-1}$ (NiTi)[21]<br>$2\times10^5$ $JK^{-1}m^{-3}$ | 80 $JK^{-1}kg^{-1}$[6]<br>$7\times10^4$ $JK^{-1}m^{-3}$ |
| **Adiabatic temperature change** | 17 K[21] | 12 K[6] |

The adiabatic temperature change and isothermal entropy change of SMAs and NR are larger than most of caloric materials[129]. Compared to SMAs as refrigerant, NR is more cost effective, has longer fatigue life and requires less critical stress. The drawback of NR is a lower thermal conductivity and large deformation.

## 1.4. Conclusions and perspectives

In the current technology, due to the large force of bulk SMA as eC material, and the low dielectric strength of bulk EC material, their film form is better choice, which is interesting for the small- and middle-scale cooling applications. For the large-scale applications, further improvements of dielectric strength of the bulk EC materials are needed, whereas the forces decrease for bulk SMA seems to be difficult. Elastomers, especially the NR, may be the best candidate for large-scale applications due to their low stretching force. The large necessary deformation may be reduced by applying a pre-strain as shown in this thesis.

The research of NR acting as an eC material is just beginning with a large margin for improvement. The eC effect of NR is mainly related to the SIC. SIC leads to a large temperature change and a good fatigue property of eC effect of NR. The research of SIC proves the potential of NR acting as eC material, showing for example that the SIC may be large for a wide temperature range. It

also helps to understand the eC effect of NR more deeply. Thus, the research of NR for eC cooling application should consider fully the SIC theory.

Considering the eC effect application of SMAs and NR, the fatigue property is an essential factor for cooling application. For the temperature change, a few Kelvin might be enough for refrigeration cycles. Further research on caloric materials with larger temperature change may be unnecessary, since one should not neglect other more important properties for cooling application, like the fatigue property.

AMR developed from MC technology can be used for other caloric effects, like the eC effect. The cooling device by using NR hasn't been investigated and similar AMR system can be used. Compared with the AMR system based on SMAs, that based on NR needs a motor with a small force but large displacement.

In this thesis, eC effect in NR is investigated, and considerations to SIC are provided. The characterization shows highly nonlinear behavior of both eC temperature change and stress. Modeling attempt is then proposed, where SIC is highlighted. As a preliminary step for cooling application, fatigue property is measured, both for eC temperature change and stress. Finally, a tentative model of regenerative system is proposed for determining the important parameters of eC effect based cooling device.

# Chapter 2 Experimental characterization of natural rubber

As referred in the Chapter 1, much research work is conducted on magnetocaloric, electrocaloric and other elastocaloric (eC) materials. For eC effect of NR, there is rare research work. The experimental characterization may be difficult. However, the physical interpretation of mechanical properties of natural rubber (NR) has been widely investigated, and is mainly related to the strain-induced crystallization (SIC). Thus, for the experimental characterization of eC effect of NR, two complementary expertises are necessary, one is the common characterization of other caloric material and the other is the SIC theory. This can help to understand the eC behavior of NR deeply and establish some guidelines for the characterization of eC effect of NR.

This chapter firstly shows some basic phenomena of eC effect of NR and discusses them by using SIC theory. Then, the eC performance is characterized through the definition of eC strain coefficient and eC stress coefficient. By using the method of pre-strain, the eC performance is improved and the necessary deformation for a given performance is reduced. Finally, an indirect measurement of eC effect is proved to agree with the direct measurement.

## 2.1. Experimental set-up presentation

Temperature change and stress are two required physical properties for eC effect. Meanwhile, they reveal the properties of SIC in mechanical field and thermal field. Thus, the study of eC effect must consider the SIC mechanism. Accordingly, the SIC mechanism of NR can be shown by the coupling of temperature change and stress.

SIC of NR has been widely studied since its discovery in 1925 by Katz[47,52]. SIC can be indirectly characterized by methods such as thermal measurements[7,102,130–134], birefringence[65], differential scanning calorimetry (DSC)[135], nuclear magnetic resonance[54,96,97], or stress relaxation[48,136]. Moreover, its morphological features can be studied by electron microscopy (TEM)[66,137,138] and wide-angle X-ray scattering (WAXS) experiments[51,56,88,91,122,139]. Nowadays, the possibilities offered by modern X-ray facilities (synchrotron radiation) allow an investigation of the growth at the very nanometric scale of the crystallites. In particular, it is possible to measure the crystallinity as well as the degree of molecular orientation during the deformation process[67,93,94].

In this part, the experimental setup and technique for studying the eC effect of NR were shown. The technique for studying SIC by means of the coupling of temperature change and stress was highlighted.

### 2.1.1. Experimental setup

In Fig.2. 1, the mechanical system consisted of tensile tests using an Ironless Linear Motor (XM-550, Newport, New-York) and the stress measurements using a force sensor (ELPF-T2M-250N, Measurement Specialities, Paris). The temperature measurements used an Infrared (IR) Camera (NEC G-120, Japan). The NR film was mounted in a sample holder composed of one fixed and one movable part.

A linear motor then produced the displacement, which caused the sample to become elongated[3]. In the measurement process, the sample was in an ambient environment. There were three possibilities

of heat loss: heat conduction, convection and thermal radiation. To diminish heat conduction, heat-insulating PVC plates were chosen for holding the rubber sample because of the low heat conductivity coefficient. The entire set-up was covered in order to prevent air flow and subsequent heat convection losses. The temperature was detected through a hole.

The calibration for the measured temperature showed an almost pure linear behavior with a temperature correction factor of 0.86 (corrected sample emissivity). Infrared (IR) images were recorded at a frame rate of 10 Hz and the noise level of the temperature information from the IR camera was $\pm 0.1^{\circ}$C[140].

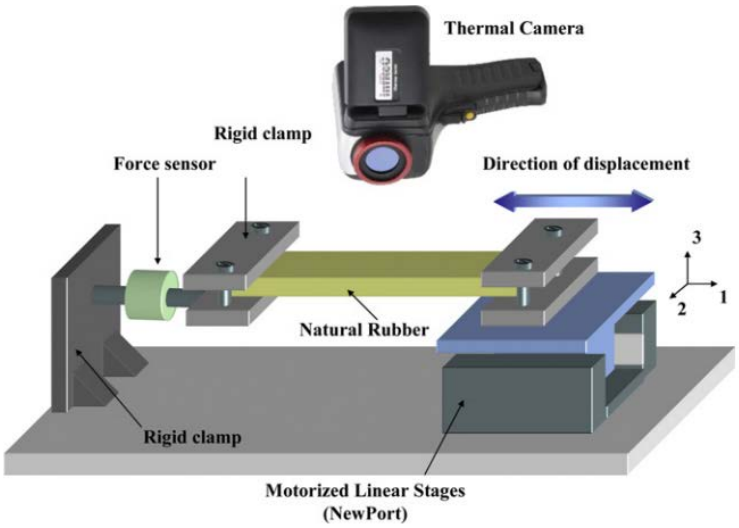


Fig.2. 1 Experimental setup[3].

### 2.1.2. The measuring technique of temperature change by using IR camera

When sufficiently rapid stretching is applied on NR, the measurement by using IR camera can be considered as an adiabatic process[3,4]. This is a simple and straightforward measurement. However, this method is rarely used for eC effect and EC effect[17]. Its important advantage is that it can be used for measurements of thin films; especially when the giant caloric effect is expected. They can provide much more reliable measurement than the indirect methods[17], since it is precise enough. Sebald et al.[140] compared the EC effect of P(VDF-TrFE-CFE) terpolymer measured by differential scanning calorimetry (DSC) and IR camera, whose results were consistent. IR thermal imaging offers furthermore the advantage of a higher frequency bandwidth capability compared to DSC technique.

For the eC effect measurement of NR, the IR thermal technique appears to be especially important, since it appears almost impossible to measure eC effect by using DSC.

### 2.1.3. SIC mechanism shown by the coupling of temperature change and stress

The thermal measurement by using IR camera is highlighted in this work. IR camera has been widely used in thermoelastic stress analysis (TSA), which is a well-established experimental technique for measuring the surface stress field of a dynamically loaded component. The IR camera is used to measure the small reversible temperature change associated with the thermo-elastic effect. The temperature change is related to the changes in the sum of the principal stresses on the surface of the material. The technique is non-destructive and non-contacting for damage assessment[141,142]. This

technique has been widely applied to the deformation of metal with small strain, but rarely to the deformation of polymer with large strain[130,134].

The temperature change measured at the macroscopic scale can exhibit the change in the microstructure (mainly the SIC). As discussed in 1.2.4, the upturn of temperature change and the hysteresis of temperature change in extension and retraction can show the SIC behavior. Besides the thermal behavior of SIC, SIC can be shown by mechanical behavior. For instance, the SIC can be shown by stress relaxation [106] and stress hardening [139] (more details in 1.2.3). Furthermore, the temperature change can couple with stress to show the mechanism of SIC more precisely. For the same SIC process, the variation of temperature change is not always corresponding to the stress. For example, the hysteresis direction of temperature change-strain curve[100,101] are anticlockwise, which is the same with crystallinity-strain curve[51,91], while the stress-strain curve is clockwise[143]. This experimental technique is economical and high-efficient.

There is rare research work about the eC effect of NR and SIC by using IR thermal technique. Both the research work of eC application and the SIC research will be beneficial from the IR thermal technique because it's simple, straightforward and precise. The two researches are complementary, since SIC research can help to understand the eC effect deeply.

## 2.2. Mechanism of elastocaloric effect

In this part, the eC characterizations including mechanical and thermal behaviors are presented. The experimental variables are defined and the tested material is described. Then, a typical temperature change upon strain is presented and discussed, considering both thermal conditions of the experiment and the SIC mechanism.

### 2.2.1. Experimental variables

The mechanical variables in deformation process are strain, elongation and stress.

Strain can be the engineering strain and true strain. The engineering strain $\varepsilon_{en} = (l - l_0)/l_0$ is defined as the ratio of the deformation length $l - l_0$ of the sample to the initial length $l_0$. The elongation is defined as $\lambda = \varepsilon_{en} + 1$. The true strain is defined as $\varepsilon_{tr} = \ln \lambda$.

Stress can be the engineering stress and true stress. When the NR material is stretched, the strain increases and the cross section decreases. The engineering stress $\sigma_{en} = F / A_0$ is the force $F$ divided by the original cross section $A_0$. The true stress $\sigma_{tr} = F / A$ is the force $F$ divided by the real cross section $A$. In the stretching process, the volume is kept constant. Thus, the relation between the original cross section and cross section at elongation of $\lambda$ is $A_0 = \lambda A$. The relation between true stress and engineering stress at elongation of $\lambda$ is $\sigma_{tr} = \lambda \sigma_{en}$.

### 2.2.2. Material

The NR material is bought from Xinyinte Rubber Products Co., Ltd. (China). It is a vulcanized NR. Two kinds of NR with different network chain density (N) are characterized, one is $1.3\times10^{-4} mol \cdot cm^{-3}$ and the other is $2.3\times10^{-4} mol \cdot cm^{-3}$. They are referred as the NR with "low N" and "high N", respectively.

An optimal network chain density (*N)* value of $1.2\times10^{-4} mol \cdot cm^{-3}$ for SIC was suggested by Chenal et al.[56]. The optimal SIC should lead to the optimal eC performance (high temperature

change, good fatigue property etc.). The NR with N of $1.3\times10^{-4} mol\cdot cm^{-3}$ may get the optimal eC performance.

Network chain density (N) was estimated according to Eq. (2.1) based on the standard theory of rubber elasticity [5].

$$\sigma = NkT(\lambda - \lambda^{-2}) \quad (2.1)$$

Where $\sigma$ is the stress, *N* is network chain density, *k* is the Boltzmann constant, *T* is the absolute temperature, and $\lambda$ is the elongation. The *N* is calculated from the initial region of stress-strain curve, which is of the same order of magnitude as published material[51].

The cross section area of the NR sample is 20mm x 100μm and the original length is 10mm. The stress-strain behavior of NR with low N and high N is shown in Fig.2. 2. The strain rate of 0.024 $s^{-1}$ and it shows a relatively stable hysteresis after 5 cycles. The mechanical hysteresis may be due to SIC[50,57,88]. The stress upturn during the stretching process is due to the stress hardening effect of SIC. Contrarily, the lower stress during the retraction process is due to the larger degree of SIC, indicating the stress relaxation effect of SIC dominates in this process.

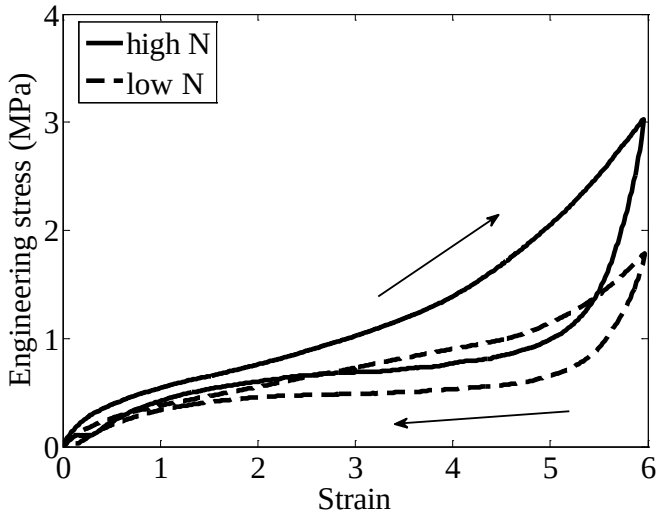


Fig.2. 2 Stress-strain curve of NR with low and high network chain density (N). It's a relative stable state after 5 cycles at strain rate of 0.024 $s^{-1}$.

The following characterization is mainly described in NR with low N. The characterization of NR with high N is summarized in section of 2.7.

### 2.2.3. Typical temperature change and stress

Fig.2. 3 displays a typical time profile of the temperature change of NR material upon deformation up to strain of 5. The strain rate in extension and retraction was 20 $s^{-1}$. The temperature increased abruptly when the NR is stretched to a strain and then decreased exponentially toward room temperature due to thermal heat exchange with the surrounding environment. The applied strain was kept constant for 20 s. Fig.2. 3 (a) showed the stress relaxation in the keeping time. When the applied strain was removed, the temperature decreased below room temperature and then increased exponentially back to room temperature.

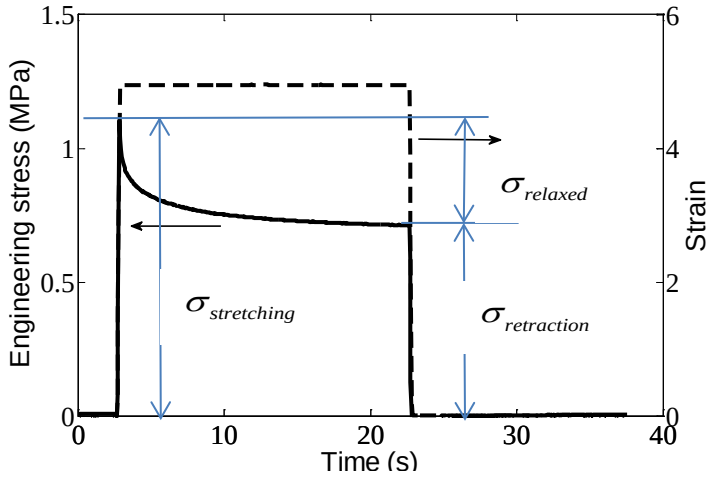


(a)

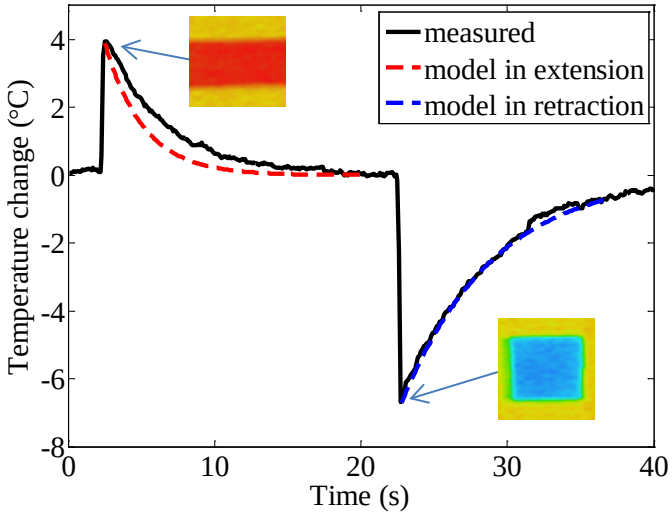


(b)

Fig.2. 3 Typical (a) stress – strain and (b) temperature change - time signal of NR at strain of 5 with the thermal images.

It's important to ensure that the measured temperature change corresponds to the eC activity and that it is not an experimental fault. In the following part, the temperature signal is interpreted in view of pseudo-adiabatic condition.

*2.2.3.1. Thermal conditions during eC characterization*

When stretching the sample in adiabatic condition (right after the strain step at $t = 0^+$), the temperature increases abruptly to $T(t = 0^+) = T_0 + \Delta T_0$, where $T_0$ is room temperature, T is the sample temperature and $\Delta T_0$ is the eC temperature change. Then, convective heat transfer allows the sample to cool down to $T_0$. From the heat balance of the sample, the convective heat transfer equals the heat loss:

$$\dot{Q} = -2Ah(T - T_0) = cAe\frac{\partial T}{\partial t} \qquad (2.\ 2)$$

where $h$ is the heat transfer coefficient, $A$ is the sample area, $e$ is the sample thickness, and $c = 1.8 \times 10^6\ J \cdot K^{-1} \cdot m^{-3}$ is an estimation of specific heat of NR[144], and assumed to be independent of the elongation and temperature.

The Eq. (2.2) is transformed to

$$\frac{\partial T}{\partial t}+\frac{2h}{ce}(T-T_0)=0 \tag{2. 3}$$

Thus,

$$T=T_0+\Delta T_0 e^{-\frac{2h}{ce}\cdot t} \tag{2. 4}$$

where $\Delta T_0$ is the temperature change of eC effect.

The thermal time constant writes

$$\tau=\frac{ce}{2h} \tag{2. 5}$$

In retraction, the sample thickness is 100 μm. The heat transfer coefficient is estimated as $h$ =14 W.m$^{-2}$.K$^{-1}$. The thermal time constant $\tau_{re}$ in retraction

$$\tau_{re}=\frac{ce}{2h}=\frac{1.8\times10^6\times100\times10^{-6}}{2\times14}=6.4s$$

The peak of temperature decrease in retraction is 6.7 K. Thus, the evolution of temperature change due to convective heat transfer in the retraction state is

$$\Delta T_{re}=-6.7e^{-0.14\cdot t}$$

When NR sample is stretched to strain of 5, the thickness decreases to 40 μm. The thermal time constant $\tau_{ex}$ in extension

$$\tau_{ex}=\frac{ce}{2h}=\frac{1.8\times10^6\times40\times10^{-6}}{2\times14}=2.6s$$

The peak of temperature increase in extension is 3.8 K. Thus, the evolution of temperature change due to convective heat transfer in the extension state is

$$\Delta T_{ex}=-3.8e^{-0.38\cdot t}$$

The calculated temperature change is compared with the measured counterpart (Fig.2. 3). It's shown the calculated temperature change can correspond to the measured counterpart in retraction, whereas it's lower than the measured counterpart in extension. This is due to the SIC growth in the stretched state which can further increase the temperature (more details in 2.2.4).

*2.2.3.2. Estimation of the adiabatic limit in harmonic regime*

The adiabatic limit corresponds to the characteristic time of heat exchange with outer medium. The angular frequency $\omega_0$ of adiabatic limit is

$$\omega_0=\frac{1}{\tau}=\frac{2h}{ce} \tag{2. 6}$$

Thus, frequency $f_0$

$$f_0=\frac{\omega_0}{2\pi}=\frac{h}{\pi ce} \tag{2. 7}$$

Thus, the frequency of adiabatic limit in extension is

$$f_0=\frac{h}{\pi ce}=\frac{14}{3.14\times1.8\times10^6\times40\times10^{-6}}=0.062Hz$$

To be sure to have an adiabatic condition, the frequency of adiabatic limit can be estimated

$$f_0=10\,f_0=0.62Hz$$

2.2.4. Larger temperature decrease in retraction and smaller temperature increase in extension

In Fig.2. 4, the temperature decrease and the temperature increase at different strains are compared. Before strain of 3.5, they are almost the same. After strain of 3.5, their difference becomes larger. It has been extensively evidenced that the SIC of NR occurs at around strain of 3 at 25ºC[51,67,88,98]. Thus, SIC might be the reason of that difference.

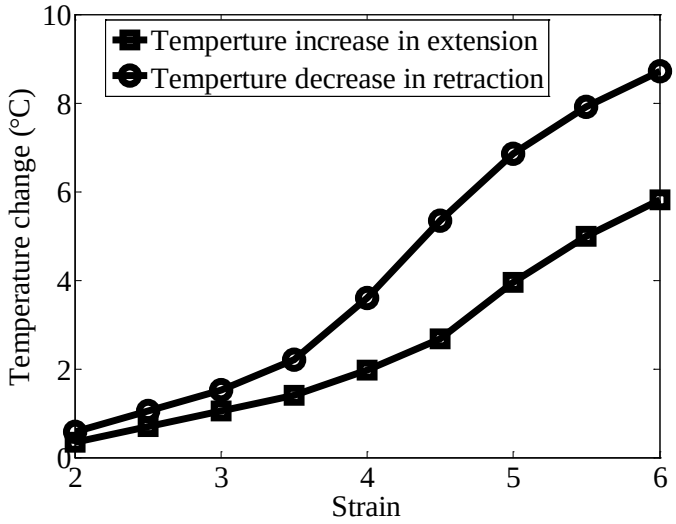


Fig.2. 4 The temperature increase in the stretching process and the temperature decrease in the retraction process.

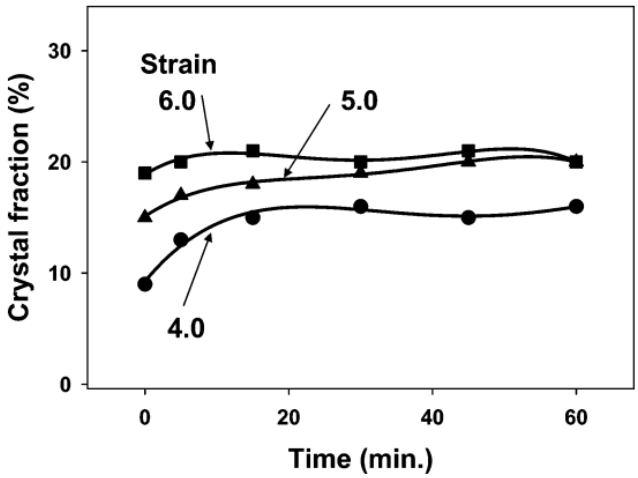


Fig.2. 5 The change of the crystal fraction with time during stress relaxation at strains 4.0, 5.0, and 6.0 for synthetic rubber at 30 °C[92].

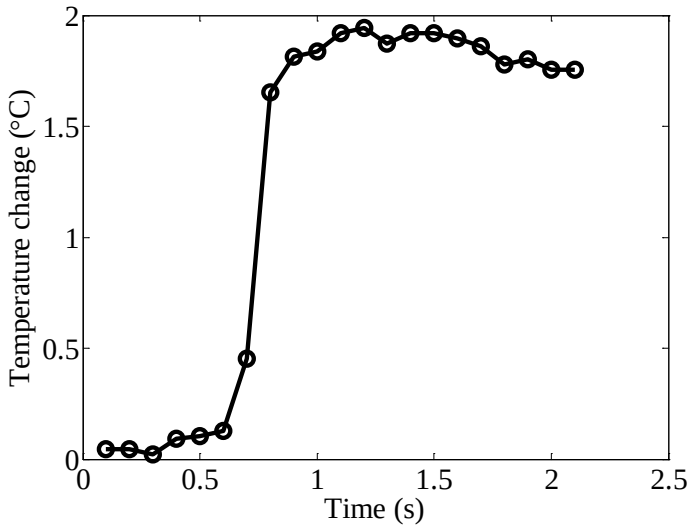

Fig.2. 6 The creep of temperature increase at pre-strain of 4.

This reason is two-fold. One is the different kinetic properties of SIC and melting[88,102,121]. SIC is a two-step process, first nucleation and then growth[121]. SIC requires time to be completed. In the fast stretching process, nucleation is the main SIC[121]. After the fast stretching process, SIC begins to grow in the keeping time of the stretched state[106]. This can be shown by the continuous increase of crystal fraction during stress relaxation process (Fig.2. 5) [92]. The SIC growth time is longer than the adiabatic limit (the adiabatic limit corresponds to the characteristic time of heat exchange with outer medium, see 2.2.3.1). This is clearly illustrated by the temperature signal right after the stretching (Fig.2. 6). Let's recall that the thermal heat exchange time constant is around 2 seconds, but it is observed that the temperature continue to increase despite the quick heat exchange. Consequently, part of the temperature increase due to the SIC growth can't be measured due to the heat loss with outer medium. Before the retraction process, the crystallinity is larger than that in the stretching process because it includes the SIC occurring in the stretching process and in the keeping time. In the retraction process, the melting is much faster than SIC[88]. So, nearly all the SIC will melt during the retraction process and contributing to the temperature decrease. Thus, the temperature decrease is larger than temperature increase.

The other reason is the different physical constraint of SIC chain in the stretching process and retraction process. Even in the slow deformation rate (0.033 $min^{-1}$), the crystallinity in the retraction process is larger than the stretching process[67,88]. It may be due to the different deformation histories. When the material is stretched, some network chains can't orient with the nucleation chains[78,80,88] due to the constraint from surrounding chains[76,77,145,146]. Thus, they can't become the SIC chains due to the SIC growth. In the retraction process, all the chains are relaxed. The constraint from surrounding chains is reduced and the network chains can adjust them to align with the nucleation chain. Thus, the further SIC growth occurs resulting in a larger crystallinity even the whole trend is the melting in the retraction process. This can be shown in Fig.2. 7. In Fig.2. 7 (a), the crystallinity shown by X-ray intensity increases in first stage of retraction (B-C stage). This is due to the transformation of crystallite morphology to secondary crystallites proposed by Toki et al[139]. The first increase of lateral crystallite size also proves this point (Fig.2. 7 (b))[51].

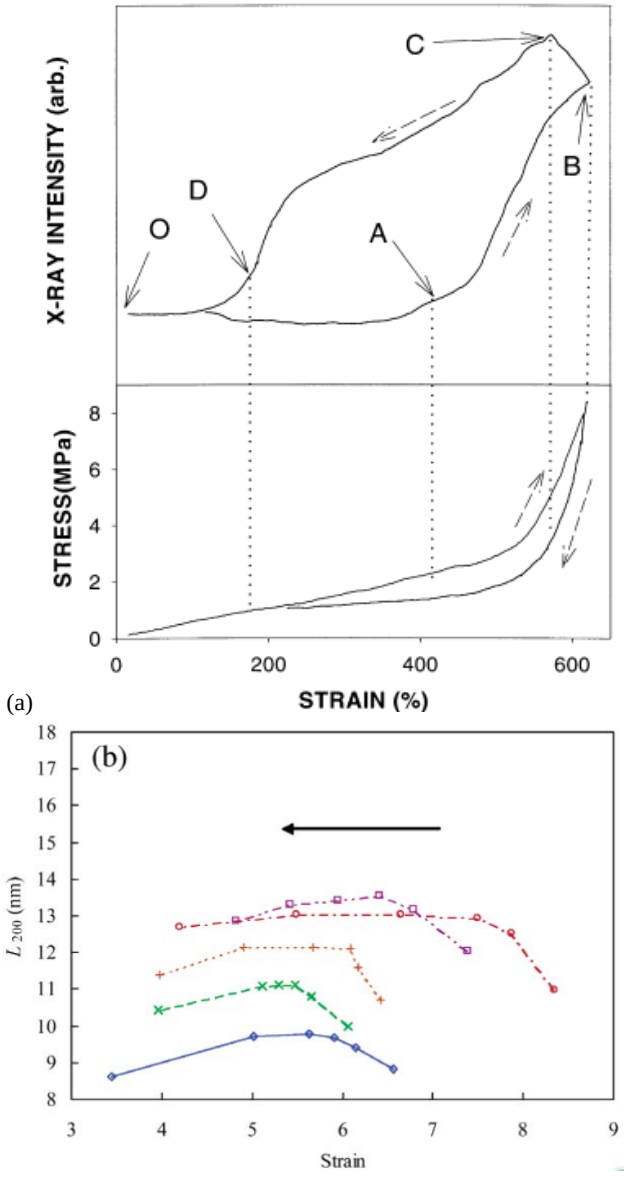


(b)

Fig.2. 7 (a) X-ray intensity and stress in extension and retraction[139] (b) Variation of lateral crystallite size with strain: $L_{200}$ in retraction[51].

As a result, the temperature increase mainly occurs in the stretching process and comes from the nucleation. The temperature decrease comes from both the nucleation and growth. Thus, the temperature decrease is larger than the temperature increase. This result was also observed by Sakata et al. at large strains[101].

### 2.2.5. Discussion on SIC growth degree

The temperature decrease is close to the thermodynamic equilibrium state and its variation trend is analyzed. Fig.2. 4 shows the temperature change vs. strain. It can be divided into two strain regimes, before and after the onset strain of SIC (strain of 3). Before the onset strain of SIC, temperature change increased slowly with strain. The entropy variation may be attributed mainly to the elastic entropy. At SIC strain regime, the temperature change can be further divided into three strain regimes:

it increased slowly at the onset strain of SIC (strain of 3-4), fast at middle strain of SIC (strain of 4-5.5), and a saturation phenomenon was observed at high strains (from strain of 5.5).

*2.2.5.1 Definition of SIC growth degree*

This variation trend of temperature change can be interpreted by SIC growth. The SIC growth is the process that the nucleation chain binds its surrounding chains. The amount of the surrounding chains bound by one nucleation chain in the SIC growth process can be referred as SIC growth degree $\alpha$, which is defined as

$$\alpha = \frac{CI_{growth}}{CI_{nucleation}} \tag{2. 8}$$

where $CI_{nucleation}$ is the crystallinity index of the SIC nucleation, $CI_{growth}$ is the crystallinity index of the SIC growth.

SIC nucleation mainly occurs in stretching process and SIC growth mainly occurs after the stretching. Thus, SIC growth degree can be estimated by the ratio of crystallinity in stretching process to the crystallinity after stretching. Toki measured the evolution of crystallinity after stretching (Fig.2. 5)[92]. The beginning points of the curves are the crystallinity occurred in stretching process. The SIC growth degree can be estimated from these curves, which are 0.67, 0.4 and 0.1 at strain of 4, 5 and 6 respectively. It means the SIC growth degree decreases as strain increases.

Furthermore, the SIC growth degree can be shown by the temperature change and stress. As interpreted in Fig.2. 4, the difference of temperature decrease and temperature increase is due to the SIC growth. Temperature increase mainly comes from the nucleation. Thus, the SIC growth degree can be estimated by a temperature change ratio,

$$\alpha_T = \frac{\Delta T_{relaxed}}{\Delta T_{stretching}} \tag{2. 9}$$

where $\Delta T_{relaxed} = \left|\Delta T_{retraction}\right| - \left|\Delta T_{stretching}\right|$ is the difference of the temperature decrease $\Delta T_{retraction}$ in the retraction process and the temperature increase $\Delta T_{stretching}$ in the stretching process.

This analysis considers that SIC nucleation is instantaneous and that SIC growth occurs slowly and is not measured because of the adiabatic limit in extension. In the retraction process, all SIC melts instantaneous and can be measured.

In view of stress, the stretching stress comes from the coil-stretch and nucleation transition[121,147]. The stress relaxation effect comes from the SIC growth [106]. Thus, the SIC growth degree can be estimated by a stress relaxation ratio,

$$\alpha_\sigma = \frac{\sigma_{relaxed}}{\sigma_{stretching}} \tag{2. 10}$$

where $\sigma_{relaxed} = \sigma_{stretching} - \sigma_{retraction}$ is the difference of the stretching stress and the retraction stress (an example shown in Fig.2. 3 (a)). The stretching stress can show the stress hardening effect of SIC. Thus, this ratio can also mean the ratio of the SIC contributing to the stress relaxation to the SIC contributing to the stress hardening.

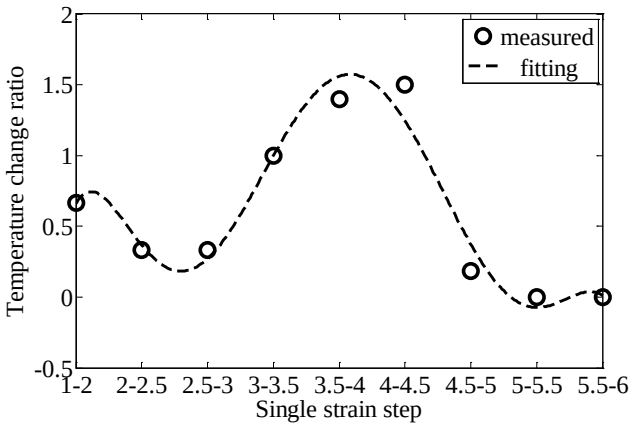


(a)

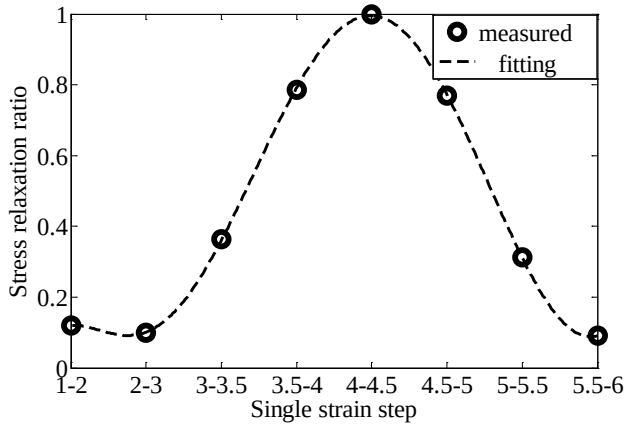


(b)

Fig.2. 8 The SIC growth degree can be estimated by the (a) temperature change ratio $\alpha_T = (\Delta T_{retraction} - \Delta T_{stretching}) / \Delta T_{stretching}$ and (b) the stress relaxation ratio $\alpha_\sigma = (\sigma_{stretching} - \sigma_{retraction}) / \sigma_{stretching}$. Both the ratios obtain the maximum at the same strain step of 4-4.5, where they show the highest SIC growth degree.

The two ratios at single strain step are calculated and compared. In Fig.2. 8, the temperature change ratio firstly increases from strain step of 3-3.5, reaching the maximum at strain step of 4-4.5, and then decreases. It means that one nucleation chain can bind the most surrounding chains in the strain step of 4-4.5, i.e. the highest SIC growth degree. This shows the different SIC growth degrees at different strains. In Fig.2. 8 (b), the stress relaxation ratio shows the same variation trend. It indicates that the proportion of SIC contributing to the stress relaxation, i.e. the SIC growth, first increases and then decreases as strain increases. The SIC growth degree can also be represented by the slope of the crystallinity-strain curve (Fig.2. 9) [51]: the gentle slope due to the lower SIC growth degree at the onset strain of SIC, sharp slope due to the highest growth degree at the middle strain of SIC and the gentle slope again due to the lower growth degree at the high strain of SIC.

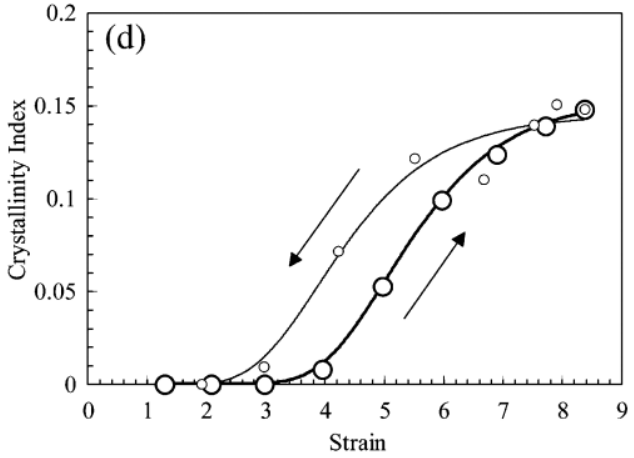

Fig.2. 9 Variation of crystallinity index with strain[51].

From strain of 4, the SIC growth degree estimated from temperature change ratio and stress relaxation ratio show the same trend as Toki's work. However, our calculated value (temperature change ratio or stress relaxation ratio) at around strain of 4 is larger than that from Toki. It's due to the long stretching time (around 600 s) of Toki, whereas our stretching time is around 0.2 s. Thus, in Toki's work, more SIC growth occurs in stretching process and less SIC growth occurs after stretching, resulting in a lower SIC growth degree.

*2.2.5.2 Interpretation of three regimes of SIC growth degree*

The three strain regimes of temperature change at SIC strain regimes can be interpreted by the SIC growth degree. The gentle slope at the onset strain of SIC, sharp slope at the middle strain of SIC and gentle slope at high strain of SIC for temperature change-strain curve (Fig.2. 4) are attributed to the lower, highest and lower SIC growth degree respectively. There is a best environment for the SIC growth at middle strain of SIC. SIC is a process that the SIC nucleation chains bind the surrounding chains and divide the original long chain into short ones[93]. Then, the network chain density will increase. Thus, more and more network chains can align with the nucleation chain and the SIC growth degree increases to the highest at strain of 4.5, which is about strain of 1 larger than the onset strain of SIC. As SIC evolves continuously, there is no room to crystallize and saturation of SIC occurs[148]. The saturation of SIC should be firstly the saturation of SIC growth and then the saturation of the nucleation because the SIC growth needs more space. It results in the decrease of the SIC growth degree at high strain.

The maximum temperature change ratio $\alpha_T$ is 1.5, which is slightly larger than the maximum stress relaxation ratio $\alpha_\sigma$ of 1. It may be interpreted as follows. The $\Delta T_{stretching}$ corresponds to the $\sigma_{stretching}$. Whereas the $\Delta T_{relaxed}$ doesn't correspond to the $\sigma_{relaxed}$. The $\Delta T_{relaxed}$ includes two parts. One is from the SIC growth in the keeping time of the stretched state. The other is the further SIC growth in the retraction process due to the reduced physical constraint of SIC chain (see details in 2.2.4). Whereas the $\sigma_{relaxed}$ is only from the SIC growth in the keeping time of the stretched state. Thus, the SIC growth degree estimated by temperature change ratio is larger than the estimation of stress relaxation ratio.

## 2.3. Thermodynamic analysis

A thermodynamic writing of constitutive equations is used for defining eC coefficients.

The Helmholtz free energy $A$,

$$A = U - TS \tag{2. 11}$$

where $U$ is the internal energy, $T$ is the temperature, $S$ is the entropy.

Writing Eq. 2.11 in differential form,

$$dA = dU - TdS - SdT \tag{2. 12}$$

According to the first law of thermodynamics, the change in internal energy $dU$ in any process is given by

$$dU = dQ + dW \tag{2. 13}$$

where $dQ$ and $dW$ are the heat absorbed by the system and the work done on it by the external forces, respectively. The second law defines the entropy change $dS$ in a reversible process by the relation

$$dQ = TdS \tag{2. 14}$$

A tensile force $f$ applied on a specimen of length $l$, the work done in a small displacement is

$$dW = fdl \tag{2. 15}$$

From Eq. 2.13, 2.14, 2.15,

$$dU = TdS + fdl \tag{2. 16}$$

Combining Eq. 2.12 and Eq. 2.16, Eq. 2.12 can be written as

$$dA = fdl - SdT \tag{2. 17}$$

Hence, by partial differentiation,

$$f = \left(\frac{\partial A}{\partial l}\right)_T \; ; \; S = -\left(\frac{\partial A}{\partial T}\right)_l \tag{2. 18}$$

Maxwell relation writes,

$$\frac{\partial}{\partial l}\left(\frac{\partial A}{\partial T}\right)_l = \frac{\partial}{\partial T}\left(\frac{\partial A}{\partial l}\right)_T \tag{2. 19}$$

And hence,

$$-\left(\frac{\partial S}{\partial l}\right)_T = \left(\frac{\partial f}{\partial T}\right)_l \tag{2. 20}$$

The $df$ and $dS$ are expressed as,

$$\begin{cases} df = \dfrac{\partial f}{\partial l}\Big|_T \cdot dl + \dfrac{\partial f}{\partial T}\Big|_l \cdot dT \\ dS = \dfrac{\partial S}{\partial l}\Big|_T \cdot dl + \dfrac{\partial S}{\partial T}\Big|_l \cdot dT \end{cases} \tag{2. 21}$$

where $(\partial f / \partial l)_T$ can be defined as the stiffness $k$ and $(\partial S / \partial T)_l$ as the heat capacity ($C$) divided by the temperature ($T$). Thus, Eq. (2.21) can be rewritten as,

$$\begin{cases} df = k \cdot dl + \beta_0 \cdot dT \\ dS = -\beta_0 \cdot dl + \dfrac{C}{T} \cdot dT \end{cases} \tag{2. 22}$$

where $\beta_0 = -\frac{\partial S}{\partial l}\Big|_T = \frac{\partial f}{\partial T}\Big|_l$ .

In the adiabatic extension, $dQ = T \cdot dS = 0$ . So,

$$T \cdot dS = -T \cdot \beta \cdot dl + C \cdot dT = 0 \tag{2. 23}$$

The temperature change is obtained by integration,

$$\Delta T = -\frac{T}{C}\int_{l_0}^{l}\left(\frac{\partial S}{\partial l}\right)_T dl = \frac{T}{C}\int_{l_0}^{l}\left(\frac{\partial f}{\partial T}\right)_l dl \tag{2. 24}$$

In the above deduction, the extensive variables *C*, *S* and *f* are used in view of the system. To show the material property, they are transformed into intensive variables. The differential form of tensile stress $d\sigma$ and the specific entropy $ds$ are expressed as[3],

$$\begin{cases} d\sigma = \frac{\partial \sigma}{\partial \varepsilon}\Big|_T \cdot d\varepsilon + \frac{\partial \sigma}{\partial T}\Big|_\varepsilon \cdot dT \\ ds = \frac{\partial s}{\partial \varepsilon}\Big|_T \cdot d\varepsilon + \frac{\partial s}{\partial T}\Big|_\varepsilon \cdot dT \end{cases} \tag{2. 25}$$

where $\sigma$ is the engineering stress, $\varepsilon$ is the engineering strain, $(\partial\sigma/\partial\varepsilon)_T$ can be defined as the Young modulus *E* and $(\partial s/\partial T)_\varepsilon$ is related to the specific heat capacity (*c*) as a function of the temperature (*T*). The Maxwell relation between cross derivatives imply

$$\beta = \left(\frac{\partial \sigma}{\partial T}\right)_\varepsilon = \frac{\partial}{\partial T}\left(\frac{\partial A}{\partial \varepsilon}\right)_T = \frac{\partial}{\partial \varepsilon}\left(\frac{\partial A}{\partial T}\right)_\varepsilon = -\left(\frac{\partial s}{\partial \varepsilon}\right)_T \tag{2. 26}$$

where $\beta = -\left(\frac{\partial s}{\partial \varepsilon}\right)_T$ is referred as the eC strain coefficient[4], $\beta = \left(\frac{\partial \sigma}{\partial T}\right)_\varepsilon$ is the Clausius-Clapeyron factor[13].

Thus, Eq. (2.25) can be rewritten as,

$$\begin{cases} d\sigma = E \cdot d\varepsilon + \beta \cdot dT \\ ds = -\beta \cdot d\varepsilon + \frac{c}{T} \cdot dT \end{cases} \tag{2. 27}$$

The adiabatic temperature change upon deformation is deduced by

$$\Delta T = -\frac{T_0}{c}\int_0^{\varepsilon}\left(\frac{\partial s}{\partial \varepsilon}\right)_T d\varepsilon = \frac{T_0}{c}\int_0^{\varepsilon}\left(\frac{\partial \sigma}{\partial T}\right)_\varepsilon d\varepsilon \tag{2. 28}$$

Eq. (2.28) connects the elastocaloric effect and the thermo-mechanical coefficient. The knowledge of $(\partial\sigma/\partial T)_\varepsilon$ is used for calculating eC effect, which constitutes the indirect method.

The Maxwell relation is based on the assumption that the thermodynamic system is ergodic[149]. In an ergodic system, the stress is a state variable. Thus, whatever the thermo-mechanical coefficient characterization (different applied sequences of the deformation and the temperature variation), the thermo-mechanical coefficient $(\partial\sigma/\partial T)_\varepsilon$ should be the same.

## 2.4. Characterization of elastocaloric effect in NR

The temperature change ratio in the thermal field and the stress relaxation ratio in the mechanical field show the different SIC growth degree at different strains, which must lead to the different eC performance at different strains. To evaluate the eC performance at different strains, two eC effect

coefficients coupling the mechanical and thermal behavior are established: eC strain coefficient and eC stress coefficient.

### 2.4.1. Elastocaloric strain coefficient

The adiabatic temperature variation $\Delta T$ is proportional to the isothermal elastocaloric entropy variation $\Delta s$ ,

$$T_0 \times \Delta s\Big|_{T=T_0} = -c \times \Delta T\Big|_{s=s_0} \tag{2. 29}$$

where $T_0 = 295K$ is the temperature at which the elastocaloric effect is observed, $s_0$ is the specific entropy when undergoing an adiabatic measurement, and $c = 1.8\times10^6 J\cdot K^{-1}\cdot m^{-3}$ is an estimation of specific heat of NR[144], and assumed to be independent of the elongation and temperature. So,

$$\Delta s = -\frac{c}{T_0}\Delta T \tag{2. 30}$$

The eC strain coefficient $\beta = -\partial s/\partial\varepsilon$ was used to evaluate the eC effect conversion effectiveness of eC materials. It can be calculated by deriving $\Delta T$ versus $\varepsilon$ function

$$\beta = \frac{c}{T_0}\cdot\frac{\partial T}{\partial\varepsilon} \tag{2. 31}$$

In Fig.2. 10, the eC strain coefficient with strain is shown. It increases fast from strain of 3 to 4.5, then reaches the highest at strain of 4.5, and decreases from strain of 4.5 to 6. The different eC strain coefficients at different strains are due to different SIC growth degrees at different strains (more details in 2.2.5).

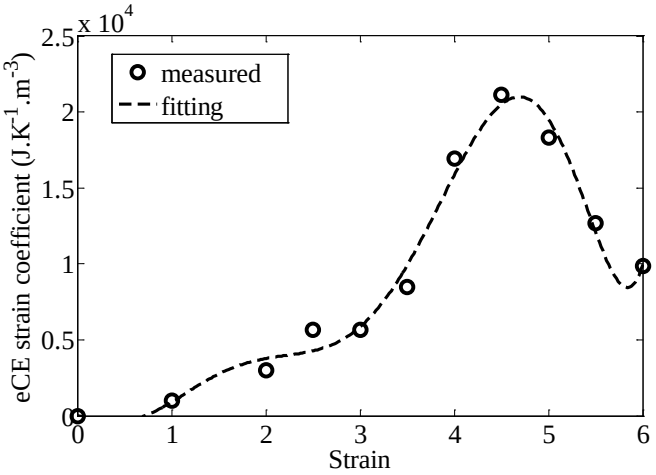


Fig.2. 10 The different eC strain coefficients at different strains.

### 2.4.2. Elastocaloric stress coefficient

The eC effect performance is evaluated by an eC stress coefficient $\gamma$ , which is defined as

$$\gamma = \frac{\partial T}{\partial\sigma_{stretching}} \tag{2. 32}$$

This is similar to the characterization of electrocaloric effect (ECE), where the temperature change is normalized by the electric field[17]. It can enable insight into the intrinsic properties of the eC materials.

As the temperature decrease in the retraction process is close to the thermodynamic equilibrium state and can represent the capability of temperature change (including SIC nucleation and growth),

the eC effect coefficient is defined as the ratio of temperature decrease $\Delta T_{retraction}$ to the stretching stress $\sigma_{stretching}$ (defined in Fig.2. 3),

$$\gamma = \frac{\partial T_{retraction}}{\partial \sigma_{stretching}} \tag{2. 33}$$

It shows that the temperature change induced by one unit of stretching stress, which can represent the eC effect effectiveness. The higher the eC effect coefficient is, the higher the eC effect effectiveness should be.

The eC effect coefficient is also calculated in local strain step. In Fig.2. 11, the eC effect coefficients at different strains are different. It shows almost the same variation trend with the temperature change ratio $\alpha_T$ and stress relaxation ratio $\alpha_\sigma$. The maximum is obtained at strain of 4.5. It indicates that the highest SIC growth degree (more details in 2.2.5) leads to the highest eC effect coefficient and the eC effect efficiency.

All the SIC including SIC nucleation and growth contributes to the temperature decrease. However for stress, the SIC nucleation mainly contributes to the stress hardening and the SIC growth contributes to the stress relaxation. The different stress relaxation ratios $\alpha_\sigma$ at different strains indicate that the proportions of SIC contributing to the stress relaxation and the stress hardening are different at different strains. From strain of 3 to 4.5, more and more SIC comes from the SIC growth and contributes to stress relaxation (Fig.2. 8 (b)). Thus, the eC stress coefficient increases from strain of 3 to 4.5. From strain of 4.5 to 6, the SIC growth degree decreases and the stress hardening effect of SIC becomes dominant (Fig.2. 8 (b)). Thus, the eC stress coefficient decreases from strain of 4.5 to 6.

The same variation trend of stress relaxation ratio and eC effect coefficient demonstrates that to get a higher eC effect efficiency, there should be more SIC contributing to the stress relaxation and less SIC contributing to the stress hardening.

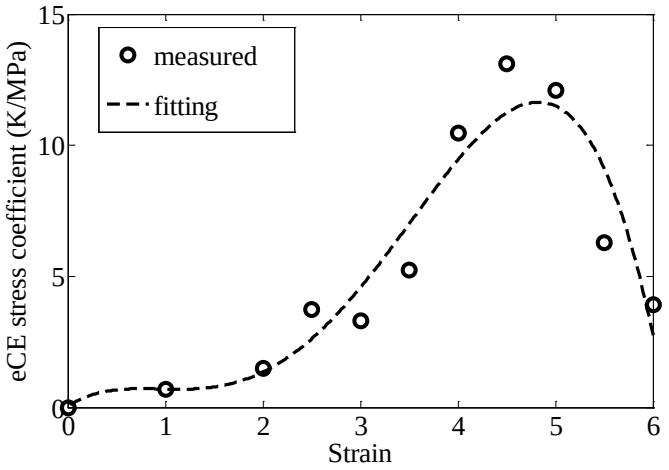


Fig.2. 11 The elastocaloric coefficient $\gamma = \Delta T_{retraction} / \sigma_{stretching}$ defined as the ratio of temperature decrease $\Delta T_{retraction}$ in the retraction process to the stretching stress $\sigma_{stretching}$. It shows the highest eC effect efficiency occurs at around strain of 4.5.

Both the eC strain coefficient and the eC stress coefficient exhibit that the high eC performance occurs at middle strain of SIC (around strain of 4.5 or 5), which should be chosen as the deformation regime of eC effect.

Compared to eC strain coefficients for SMAs, it is found that NR exhibits an eC strain coefficient two orders of magnitude lower than that of SMAs, but a stress coefficient two orders of magnitude larger thanks to its low Young modulus[150].

## 2.5. Comparison of direct and indirect measurement of the elastocaloric effect in NR

The Maxwell relation can transform some hardly measurable variables into easier measured variables. Moreover, the usage of Maxwell relation constitutes an indirect measurement, which can verify the direct measurement. The deduction of eC temperature change by using Eq. (2.28) constitutes the indirect method for quantifying caloric effect. The indirect measurement of eC effect has been widely studied in shape memory alloys (SMAs)[13,19,151,152]. In this part, the direct and indirect characterization of eC effect in NR is compared, and the underlying SIC mechanism is discussed.

The Maxwell relation is based on the assumption that the thermodynamic system is ergodic[149]. In an ergodic system, the Clausius-Clapeyron factor $(\partial\sigma/\partial T)_\varepsilon$ experimental determination should not depend on the characterization technique (different applied sequences of the deformation and the temperature variation). The factor $(\partial\sigma/\partial T)_\varepsilon$ is measured using two different methods in this work. The first characterization technique consists of measuring the stress-strain behavior for different static temperatures, and comparing the obtained stress for different temperatures at a given strain value. It is referred thereafter as "increasing static temperature for stress-strain behavior". In this technique, we may consider that the sequence of solicitation of the material is first to modify the temperature and then to increase the strain. The second characterization technique consists of measuring the stress dependence on temperature variation at constant strain. It is referred thereafter as "increasing temperature at constant strain". The corresponding solicitation sequence may then be considered as applying first a static strain, and then increasing the temperature.

Due to the occurrence of SIC, the mechanical behavior of NR exhibits stress relaxation and stress hardening effects[70,87,96,139]. It is believed that this paradoxical situation can further lead to the paradoxical situation in the thermo-mechanical characterization: when increasing temperature at constant strain, the stress increases, $(\partial\sigma/\partial T)_\varepsilon > 0$ [92]. On the contrary, when increasing static temperature for stress-strain behavior in extension, the stress decreases, $(\partial\sigma/\partial T)_\varepsilon < 0$ [87]. This phenomenon is in contradiction with the standard theory of the rubber elasticity,[87] which considers only entropic elasticity without SIC. Then, how to measure the $(\partial\sigma/\partial T)_\varepsilon$ for the deduction of eC effect through Maxwell relation?

### 2.5.1. First indirect measurement

For the indirect characterization, the first attempt to evaluate the Clausius-Clapeyron factor $(\partial\sigma/\partial T)_\varepsilon$ is to measure stress-strain behavior at different static temperatures: 5 ºC, 15 ºC, 23 ºC and 35 ºC (Fig.2. 12). The experimental setup was then adapted in order to able to place the sample inside a temperature controlled oven; while leaving actuators and force sensor outside of the oven in order to avoid any disturbance.

In extension, the stress increases linearly with the strain up to 4.5, and shows little dependence on the temperature. From strain of 4.5, a nonlinear stress increase occurs, especially for the lower temperatures. In extension, the stress is larger for the lower temperatures. In retraction, a stress plateau occurs when the strain decreases below 5. At the stress plateau, the stress is larger for the higher temperature, which is opposite to the trend in extension, as observed also by Rault[96].

For the mechanical behavior of SIC, Flory proposed two opposite views of SIC effect on stress: stress hardening effect and stress relaxation effect[70]. SIC is a giant network point[93,94], which can increase the network chain density[87] and stiffen the material, leading to the nonlinear increase of the stress when increasing the strain. This is referred as the stress hardening effect of SIC. The length of a chain in SIC is longer than the oriented amorphous one. The longer chain in SIC in the stretched direction makes the remaining amorphous chain relax. This mechanism tends to decrease the stress and is referred as the stress relaxation effect of SIC[90,91]. The mechanical behavior can be coupled with the thermal behavior of SIC. Crystallinity decreases when increasing temperature (melting)[54], which is the case both for extension and retraction.

In extension, SIC consists of two steps: first the SIC nucleation and then the SIC growth[121]. The origin of the stress hardening comes from the nucleation chain density. In extension of "increasing static temperature for stress-strain behavior", the temperature is first increased and then the strain is increased. In this case, the density of nucleation chain must be lower resulting in lower network chain density and thus lower stress as observed in Fig.2. 12. It appears to behave like different NR material with different network chain density. The crystallinity is higher and the stress is larger at lower temperatures, which is consistent with the dominant stress hardening effect of SIC in extension. In retraction, the crystallinity is higher and the stress is smaller at lower temperatures, which indicates that the stress relaxation effect of SIC is dominant.

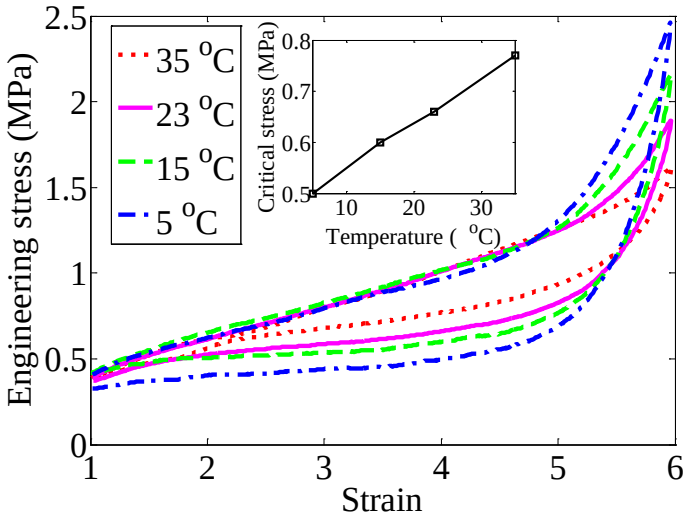


Fig.2. 12 The NR sample was stretched and retracted at different static temperatures. The strain rate was 0.02 $s^{-1}$. It exhibits the opposite trend of stress with temperature in extension and in retraction. The inset shows the critical stress at the stress plateau in retraction increases with temperature linearly.

In case of SMAs, this indirect characterization leads to an overestimation of the eC temperature change[151,152], but a reliable estimation of the entropy change[13,19]. In this case, a stress plateau is usually observed both in extension and retraction, and is used for evaluating the factor $(\partial\sigma/\partial T)_\varepsilon$, which is always positive. The stress plateau is attributed to the transformation between austenitic and martensitic phase[20]. In case of NR, there is no stress plateau in extension. In addition, it is observed that the stress-strain behavior is almost temperature independent (leading to an estimation $(\partial\sigma/\partial T)_\varepsilon \approx 0$) before a strain around 4.5. For larger strain, the factor $(\partial\sigma/\partial T)_\varepsilon$ appears to be negative. As a consequence, the deduction using Eq. (4) from $(\partial\sigma/\partial T)_\varepsilon < 0$ will get $\Delta T < 0$ in extension, which is of opposite sign to the direct characterization of eC effect.

In retraction of NR, there is a clear stress plateau, consistent with a phase transition leading to a constant stress at which the crystallites melt into amorphous phase. At the stress plateau, it is observed

that $(\partial\sigma/\partial T)_\varepsilon > 0$, which is the same sign as for SMAs. Pursuing the analogy with SMAs, this stress value may be defined as the "critical" stress. The inset of Fig.2. 12 shows that the critical stress at the stress plateau in retraction increases with temperature linearly, with a slope $(\partial\sigma/\partial T)_\varepsilon = 8.9\times10^3$ Pa/K. Considering a strain variation from a strain of 2 (corresponding to the end of the melting of SIC[153]) to the final stretching strain of 6 ($\Delta\varepsilon = 4$**),** the eC temperature change can be estimated as $\Delta T = \frac{T_0}{c}\left(\frac{\partial\sigma}{\partial T}\right)_\varepsilon \Delta\varepsilon = 5.9$ K. This deduction is smaller than the experimental eC temperature change (8 K for the same strain variation). As a conclusion, from this characterization, the stress-strain behavior exhibits hysteresis, most probably due to the SIC, and it remains difficult to estimate the stress dependence on temperature. The absence of a clear stress plateau in extension limits considerably the applicability of this indirect measurement. In other words, the stress is not a state variable since its value depends on the history of the material and the deduction is far from accurate.

### 2.5.2. Second indirect measurement

The second characterization technique ("increasing temperature at constant strain") is conducted from strain of 3 to 6. Using the same experimental setup as for the first indirect measurement, a ramp of temperature increase was applied to the sample at constant strain. Fig.2. 13 shows the stress-temperature relation at different strains. In the inset is illustrated the experimental procedure. The NR material was stretched up to a given strain at the strain rate of 0.02 $s^{-1}$ at room temperature. The stretched state was kept about 150 s for completing SIC[153]. Then, the temperature was increased at this constant strain. In this case, it is observed that the stress increases with the temperature, i.e. $(\partial\sigma/\partial T)_\varepsilon > 0$. The coefficient $(\partial\sigma/\partial T)_\varepsilon$ is estimated by calculating the measn slope of the curve $\sigma = f(T)$ (example of curves are shown in Fig.2. 13). The local derivative is not used because of uncertainty of the sample temperature, i.e. difference in temperature increase of the sample, and the measurement thermocouple. When the SIC contributing to stress relaxation melts, it would result in a reversed stress effect, i.e. stress increase. The largest slope $(\partial\sigma/\partial T)_\varepsilon$ of stress-temperature curve occurs at strain of 5. It should be noted that strain of 6 is close to the ultimate strain of NR and the material easily degrades when increasing temperature. Strain of 6 is then not appropriate for cooling applications.

"Increasing temperature at constant strain" indicates that the strain is increased first and then the temperature is increased. The SIC including SIC nucleation and SIC growth occurs completely before the increasing temperature. The thermal-mechanical behaviors of SIC nucleation and SIC growth are further discussed.

The SIC nucleation is formed from the firstly oriented chains and the SIC growth from the later oriented chain. So, the local strain of SIC nucleation chain is larger than the SIC growth chain resulting in a better orientation degree. The melting temperature increases with the SIC orientation degree[56,88]. Thus, the melting temperature of SIC nucleation is higher than that of the SIC growth. The SIC growth melts first and then the SIC nucleation as temperature increases. The different parts of SIC induce the different stress effects upon temperature. The local strain of the SIC growth chain is smaller than the SIC nucleation chain. Thus, the SIC growth chain is more likely to be relaxed as SIC develops than the SIC nucleation chain and contributes to the stress relaxation. Accordingly, the SIC nucleation is more likely to contribute to the stress hardening.

These properties can be proved by the observation of Toki. et al. on a similar NR that the stress increased at constant strain when the temperature increased from 30 °C to about 80 °C and then decreased from about 80 °C (Fig.2. 14)[92]. When increasing temperature at constant strain, the SIC

growth, contributing to the stress relaxation, melts first as temperature increases (below 80 °C) and thus lead to the increase of stress (Fig.2. 13). The SIC nucleation, contributing to the stress hardening, melts at higher temperature (above 80 °C) and should thus lead to the decrease of stress.

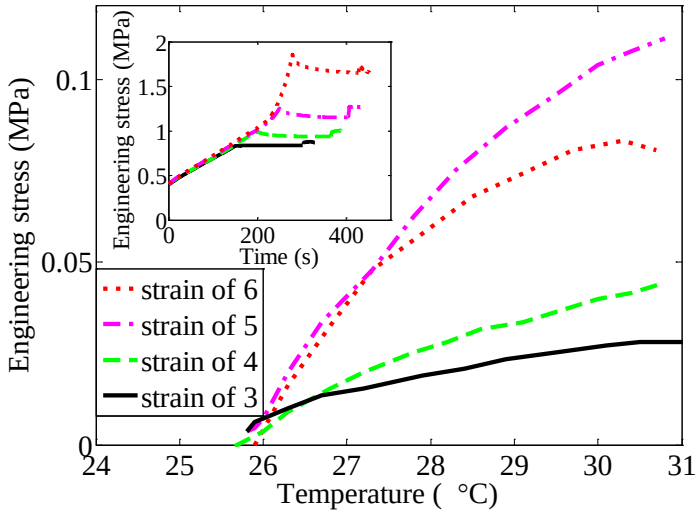


Fig.2. 13 The stress-temperature behaviors at different constant strains. The inset shows the experimental procedure. The NR sample was stretched to a given strain and was kept 150 s before increasing temperature. Then, the temperature was increased at this constant strain.

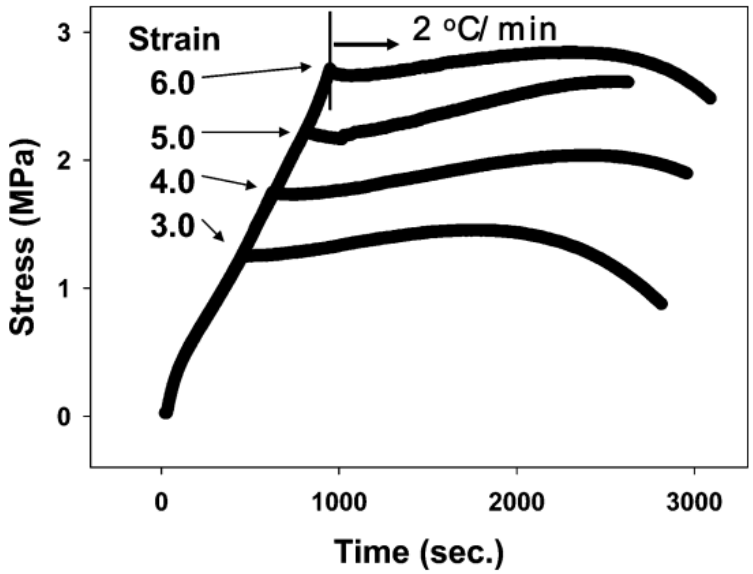


Fig.2. 14 Stress changes during stretching at 30 °C and subsequent constrained heating (at a rate of 2 °C/min) at strains 3.0, 4.0, 5.0, and 6.0[92].

According to the measured factor $(\partial\sigma/\partial T)_{\varepsilon}$ from the second characterization consisting of increasing temperature at constant strain (the inset of Fig.2. 15), the deduced eC effect is calculated by using Eq. (4) at 25°C. In Fig.2. 15, it is compared with the direct measurement. In the direct characterization of eC effect, as discussed in 2.1.3, the temperature decrease is larger than temperature increase and is closer to the thermodynamic equilibrium state since it is related to crystallite melting[88]. In the Clausius-Clapeyron factor measurement, the increase of the temperature induces crystallite melting, which is on the other hand the same origin for the entropy variation measured

during eC effect direct characterization, and also close to the thermodynamic equilibrium state. Consequently, the deduction from the Clausius-Clapeyron factor agrees well to the temperature decrease. Considering the good agreement between direct and indirect measurement, the NR material behavior is thus consistent with ergodic behavior assumption under certain circumstances.

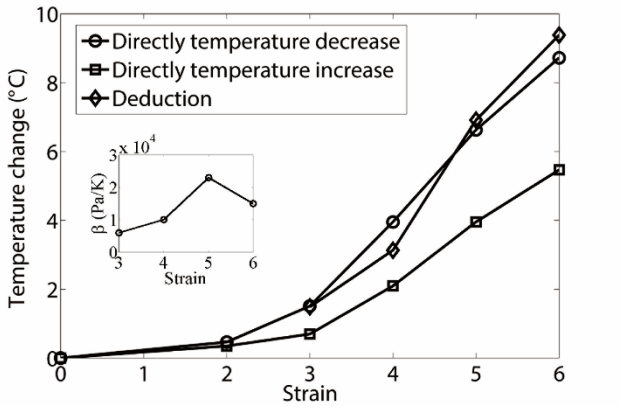


Fig.2. 15 The comparison between direct characterization and indirect characterization. The inset shows the Clausius-Clapeyron factor at different strains.

### 2.5.3. Discussion

The origin of this discrepancy in two Clausius-Clapeyron factor $(\partial\sigma/\partial T)_\varepsilon$ measurements might be the influence of the applied sequence of strain and temperature variation on the SIC (melt first or crystallization first). SIC consists of two steps: first the SIC nucleation and then the SIC growth[121]. SIC nucleation mainly contributes to stress hardening[121] and SIC growth mainly contributes to stress relaxation[106]. The SIC melt will result in the reverse stress variation to SIC. In the two different indirect measurements, the melting SIC parts are different as temperature increases and thus the corresponding stress variations are different. In the extension of the first indirect measurement, the temperature is first increased and then the strain is increased. The SIC nucleation part is prohibited, which can be considered as "melt first", and thus the SIC can't be formed. Thus, the stress hardening effect of SIC nucleation, which is responsible for the stress increase, is prohibited, resulting in $(\partial\sigma/\partial T)_\varepsilon < 0$. The further deduced $\Delta T$ is thus of the opposite to the direct measured one. In retraction of the first indirect measurement and the second indirect measurement, the strain is first increased and then the temperature is increased, which indicates that the SIC can occur completely first (including SIC nucleation and SIC growth) and then the melt occurs. It is opposite to the "melt first" in the extension of the first indirect measurement. The melting point of SIC growth part is lower than SIC nucleation part[56,88]. Thus, in this process, the first melting SIC is the SIC growth part. Then, the stress variation $(\partial\sigma/\partial T)_\varepsilon > 0$ induced by the melt of SIC growth part is obtained (reverse to the stress relaxation effect of SIC growth). The further deduced $\Delta T$ is thus of the same sign to the direct measured one. Regarding to the underestimation in retraction of the first indirect method and the accurate estimation of the second indirect method, the different mechanisms would need to be further investigated.

## 2.6. Pre-strain effect of NR with low network chain density

Both the eC strain coefficient (Fig.2. 10) and eC stress coefficient (Fig.2. 11) first increases and then decreases as strain increases, which indicate there is a best eC performance in the middle strain regimes. The eC performance may be improved by a method of pre-strain. The small strain regime with low eC performance can be skipped and go directly into the high eC performance region.
To obtain large temperature variations, the NR needs to be stretched to several times its initial length. Moreover, like in active magnetic regenerator (AMR), where a porous bed of magnetic refrigerant material is used to transfer heat efficiently[15], to transfer heat efficiently in the eC cooling cycle, the eC material should have enough area in the extension and retraction state. When the retraction state is assured to have an enough area, the extension state of NR material would be too large. These factors make NR impractical in the design of compact cooling device. Furthermore, the pre-strain can improve the fatigue property, which is proved in Chapter 4. Considering the eC performance, the requirement of compact cooling device and better fatigue property, the eC effect of NR when applying a pre-strain is investigated.

For the engineering stretching of NR with pre-strain, the strain doesn't include the pre-strain. Moreover, the length of NR sample after pre-strain can be considered as the initial length for the further stretching. Thus, the further strain for the NR with pre-strain should be relative to this initial length. A relative strain from the point of engineering stretching (doesn't include the pre-strain) for the NR with pre-strain is defined as

$$\Delta\varepsilon_r = \frac{\Delta l}{l_{pre}} = \frac{\Delta l}{l_0 \cdot (1+\varepsilon_{pre})} = \frac{\Delta\varepsilon_m}{1+\varepsilon_{pre}} \tag{2. 34}$$

where $\Delta l$ is the further elongated length when a pre-strain is first applied (between pre-strain and final strain), $l_0$ is the initial length without pre-strain, $l_{pre}$ is the initial length with pre-strain, $\varepsilon_{pre}$ is the pre-strain, $\Delta\varepsilon_m = \varepsilon_{\max} - \varepsilon_{pre}$ is the strain variation that the NR material really experiences. For the NR without pre-strain, the relative strain is equal to its strain.

For example, consider a pre-strain $\varepsilon_{pre} = 2$, and a final strain of $\varepsilon_{\max} = 5$.The strain variation is then $\Delta\varepsilon_m = 3$, and the $\Delta\varepsilon_r = 1$, which is consistent with the fact that the length of the sample changes from $3l_0$ to $6l_0$.

Eq. (2.34) shows the relation between relative strain $\Delta\varepsilon_r$ and strain $\Delta\varepsilon_m$. The pre-strain effect is discussed in two perspectives. One is from point of engineering stretching and the relative strain $\Delta\varepsilon_r$ is used. The other is from the point of material and the strain $\Delta\varepsilon_m$ is used.

### 2.6.1. Experimental procedure

The eC effect measurements were conducted in the conditions of pre-strain and no pre-strain. For the condition of no pre-strain, the applied strain was changed from strain of 0 to 6 by a strain step of 0.5 or 1. For the condition of pre-strain, a pre-strain of 1, 2, 3, 4 and 5 were applied. The further stretching was applied by a strain step of 0.5 or 1. Considering the stretching limit of NR material, the final strains were the same strain of 6 for all the stretching in conditions of pre-strain and no pre-strain. The strain rates in extension and retraction were 20 $s^{-1}$. The adiabatic temperature change and stress were measured for all the conditions.

### 2.6.2. Elastocaloric strain coefficient dependence on pre-strain

Upon the stretching of NR, irreversible entropy variation may occur due to the rupturing of network chains[154]. In this work, only the temperature decrease upon unloading was presented in order to avoid any irreversible effect as well as ensuring a reliable adiabatic condition as discussed in 2.2.4.

The temperature changes with relative strain at different pre-strains and no pre-strain are shown in Fig.2. 16 (a). It is obviously shown that the slope of the curve of temperature change-strain is enhanced by pre-strain. There is a large decrease of relative strain needed for the same temperature change when pre-strain is applied. For example, for the same temperature change of 4 °C, the relative strain of 4 is needed for NR without pre-strain, whereas only relative strain of 1 is needed for NR with pre-strain of 2.

The eC effect in conditions of different pre-strains are compared. The slope of the curve of temperature change-strain increases as pre-strain increases. Thus, the relative strain needed for the same temperature change decreases as pre-strain increases, which is the advantage of increasing pre-strain. It's also observed that temperature change decreases due to the decreased strain amplitude as the pre-strain increases, which is the disadvantage of pre-strain. The maximum temperature change at pre-strain of 4 and 5 are 2.3 °C and 1.2 °C respectively, which can't be used for a cooling system[17]. The temperature change at no pre-strain, pre-strain of 1, 2, 3 are 8.6 °C, 8.1 °C, 6 °C and 3.8 °C respectively, which may be used for a cooling system.

Thus, considering the objectives of reducing applied strain and the enough maximum temperature change for a cooling system, the pre-strain of 1, 2 and 3 may be chosen.

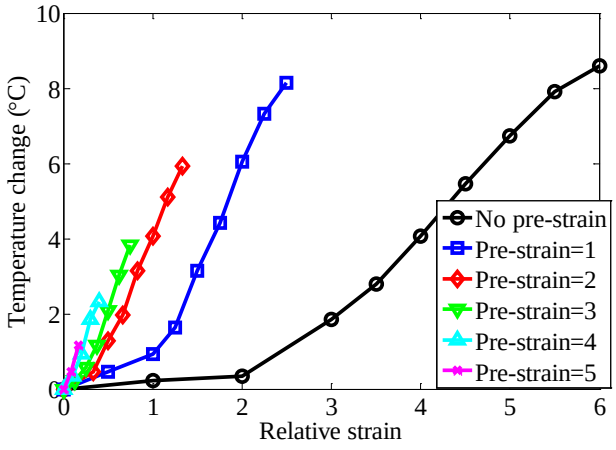


(a)

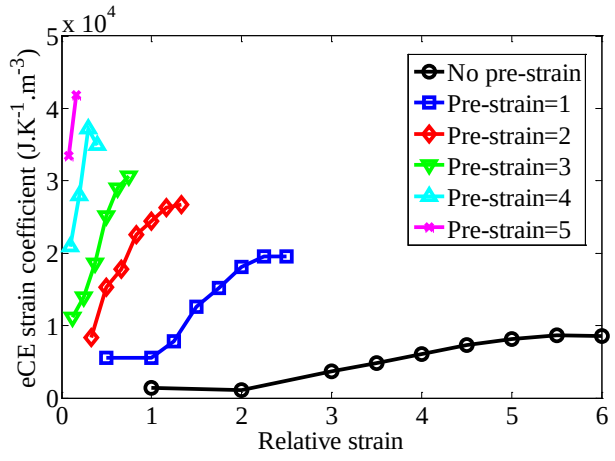


(b)

Fig.2. 16 Comparisons of eC effect at different pre-strains and no pre-strain: (a) temperature change as a function of relative strain, (b) eC strain coefficient as a function of relative strain.

The eC strain coefficient $\beta = \frac{c}{T_0} \cdot \frac{\partial T}{\partial \varepsilon}$ defined in section 2.4 is used to evaluate the eC performance of in condition of pre-strain. It's calculated from $\beta = \frac{c}{T_0} \cdot \frac{\Delta T}{\Delta \varepsilon_r}$ in whole strain range for every stretching, which is practical for the application. The eC strain coefficients with relative strain at different pre-strains and no pre-strain are shown in Fig.2. 16. (b). In all the conditions of pre-strain, the eC strain coefficients are larger than no pre-strain. As the pre-strain increases, the eC strain coefficient increases in the overall level.

Thus, when pre-strain increases, the applied strain decreases and eC strain coefficient increases, whereas the maximum temperature change decreases. Through balancing these three factors, pre-strain of 2 and 3 can be chosen.

### 2.6.3. Elastocaloric stress coefficient dependence on pre-strain

The eC performances at different pre-strains are further compared through eC stress coefficient. As the calculation of eC strain coefficient, the eC stress coefficient is also calculated in whole strain range for every stretching by using $\gamma = \frac{\Delta T_{retraction}}{\Delta \sigma_{stretching}}$.

In Fig.2. 17, the stretching stresses and eC stress coefficients at different pre-strains and no pre-strain are shown. The stress at pre-strain is suppressed. The slope of stress becomes larger as pre-strain increases (Fig.2. 17 (a)). It's due to the stress hardening effect of SIC. When the pre-strain is larger than the onset strain of SIC, SIC occurs in the keeping time of the pre-strain (shown by the creep of temperature increase in Fig.2. 6), which increases the network chain density. Thus, the stress curve becomes steeper in the further stretching than no pre-strain. Moreover, the stress curve becomes steeper and steeper as pre-strain increases. It indicates that more and more SIC occurs in the keeping time of pre-strain as pre-strain increases.

The maximum stress at strain of 6 firstly increases and then decreases as pre-strain increases (the strain amplitude between pre-strain and the same final strain of 6 decreases). For pre-strain of 1 and 2, the strain amplitudes are 5 (from strain of 1 to 6) and 4 (from strain of 2 to 6) respectively. For pre-strain of 3 and 4, their strain amplitudes are 3 (from strain of 3 to 6) and 2 (from strain of 4 to 6), which are smaller than pre-strain of 1 and 2, whereas their maximum stresses are larger than pre-strain of 1 and 2. It shows the stress is not proportional to the strain amplitude. However, the maximum temperature change (Fig.2. 16 (a)) decreases as pre-strain increases, which is proportional to the strain amplitude. For example, the maximum stresses at pre-strain of 3 and 4 are larger than pre-strain of 1 and 2, whereas their maximum temperature changes are smaller than pre-strain of 1 and 2. The opposite tendency of stress and temperature change indicates that: the entropy change upon deformation is mainly due to the latent heat of SIC, and the contribution from elastic entropy is secondary.

In Fig.2. 17 (b), it's found that there is a large decrease of eC stress coefficient at pre-strain of 3 for all tested amplitudes. It's due to the stress hardening effect of SIC occurred in the keeping time of pre-strain, which results in the decrease of eC stress coefficient.

In all the conditions of pre-strain (except pre-strain of 5), the eC stress coefficient first increases to around strain of 5 and then decreases. It's due to the evolution of SIC and its influence on stress, which is descripted in 2.4.

In conclusion, considering maximum temperature change, the applied strain, eC strain coefficient and stress coefficient, pre-strain of 2 should be chosen, i.e. right before the onset strain of SIC. For

pre-strain of 2, the further relative strain of 1 can get temperature change of 4 °C, eC strain coefficient of 2.4 × $10^4$ J.$K^{-1}$.$m^{-3}$, and eC stress coefficient of 6 K/MPa.

Furthermore, the fatigue properties at different pre-strains are investigated in the chapter 4.

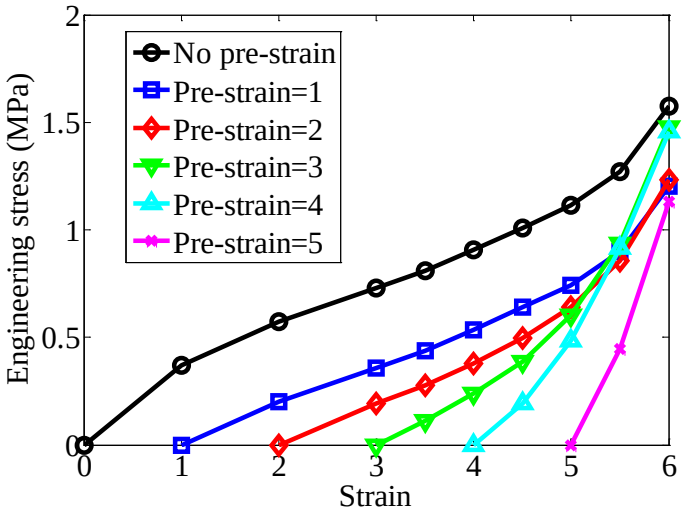


(a)

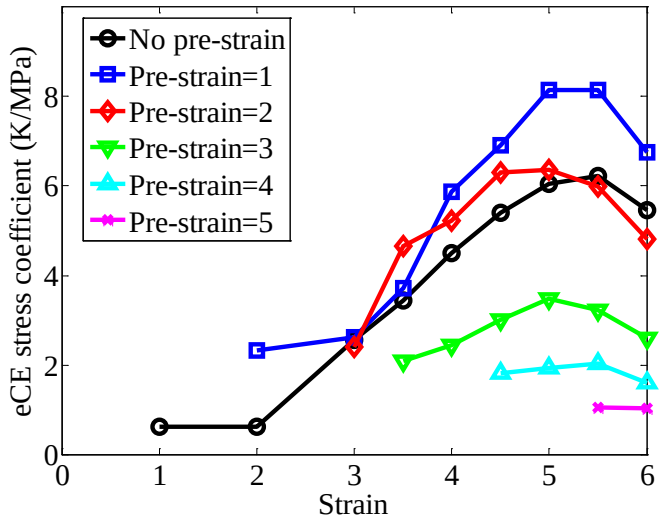


(b)

Fig.2. 17 Comparisons of eC effect at different pre-strains and no pre-strain: (a) stress as a function of strain, (b) eC stress coefficient as a function of strain.

### 2.6.4. Discussion in view of material science

In view of the strain that NR material really experiences, the eC effect of NR material with pre-strain as a function of strain is shown, when using the eC effect of NR without pre-strain as a reference. For example at no prestrain, we observe a temperature change of 2K for a strain of 3. Then, when plotting the curve for a prestrain of 3, the curve is translated so that the value for strain of 3 is 2K.

In Fig.2. 18 (a), all the temperature changes in condition of pre-strain are lower than the condition of no pre-strain. When the pre-strain is lower than the onset strain of SIC, it's due to the more chain slip occurring in the keeping time of the pre-strain, which reduces the potential SIC chains in the further deformation and thus the temperature change is reduced. When the pre-strain is higher than the onset strain of SIC, it's due to the further SIC in the keeping time of pre-strain, which also reduces the

potential SIC chains in the further deformation. This can be further proved by the corresponding stress in Fig.2. 18 (b), plotted similalry as for temperature change. The stress curve for a given prestrain is translated so that the value for a strain of corresponds to the stretching stress obtained at no prestrain. When the pre-strain is larger than the onset strain of SIC (pre-strain of 3, 4 and 5), there is larger stress upturn in the condition of pre-strain compared with the condition of no pre-strain. It's due to the stress hardening effect of further SIC occurring in the keeping time of pre-strain. In conclusion, the SIC occurring in the keeping time of pre-strain leads to the different variation trend of temperature change and stress. It further proves that the entropy change upon deformation is mainly due to the latent heat of SIC, and the contribution from entropic elasticity is secondary.

Another difference between the variation trend of temperature change and stress is the saturation of temperature change and the upturn of stress at final strain. Both are due to the saturation of SIC (more details in 2.4).

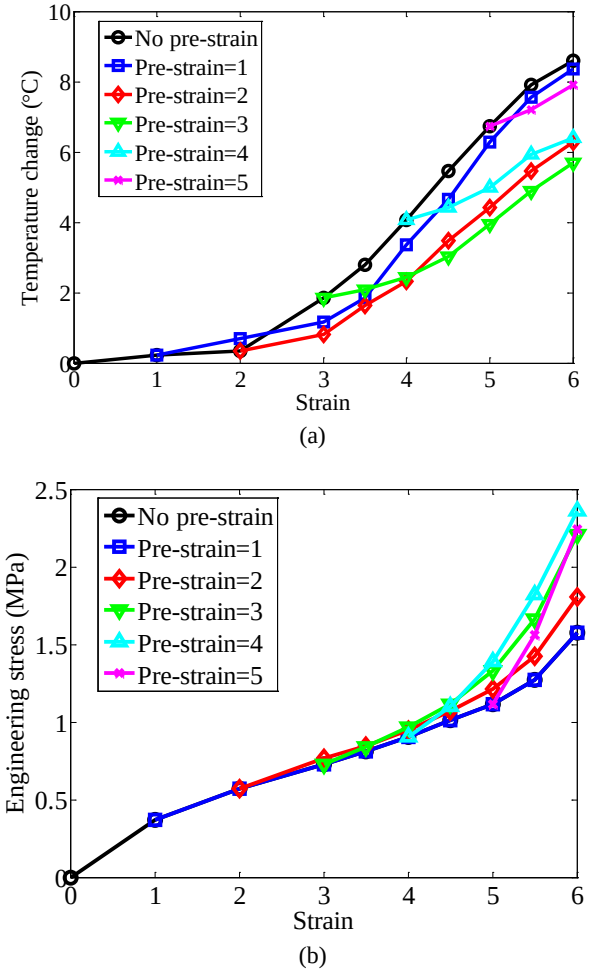


Fig.2. 18 Opposite variation trend of (a) temperature change and (b) stress in the NR with pre-strain using the NR without pre-strain as a reference.

## 2.7. The characterization of NR with high network chain density

The experimental process and characterization of NR with high N are the same as the NR with low N. Compared with the NR with low N, some similar properties and different eC performances are observed.

The temperature change and eC strain coefficient are shown in Fig.2. 19. They show some similar phenomena as the NR with low N. The slope of the curve of temperature change-relative strain increases as pre-strain increases. The maximum temperature change decreases as pre-strain increases.

The eC strain coefficient increases as pre-strain increases. The difference of NR with low N and high N is the lower temperature change, earlier saturation of temperature change and lower eC strain coefficient for the NR with high N.

The stress and eC stress coefficient are shown in Fig.2. 20. Similar phenomena are shown as the NR with low N. The slope of the curve of stress-strain increases as pre-strain increases (Fig.2. 20 (a)). The eC stress coefficients in all the conditions of pre-strain (except pre-strain of 5) and no pre-strain first increase to around strain of 4.5 and then decrease as strain increases (Fig.2. 20 (b)). The eC stress coefficient decreases dramatically in condition of pre-strain of 3. The difference of NR with low N and high N is larger stress, earlier stress upturn, lower eC stress coefficient and earlier peak of eC stress coefficient for the NR with high N.

In Fig.2. 21, the temperature change and stress in condition of pre-strain exhibit an opposite variation trend when using the condition of no pre-strain as a reference. All the temperature changes in condition of pre-strain are lower than the condition of no pre-strain. Whereas for stress, when the pre-strain is larger than the onset strain of SIC (pre-strain of 3, 4 and 5), there is larger stress upturn in the condition of pre-strain compared with the condition of no pre-strain.

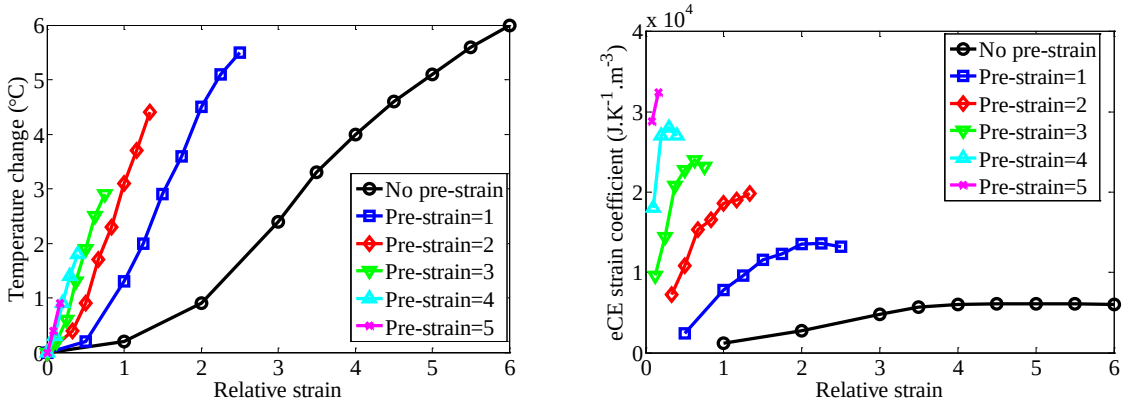


Fig.2. 19 Comparisons of eC effect at different pre-strains and no pre-strain: (a) temperature change as a function of relative strain, (b) eC strain coefficient as a function of relative strain.

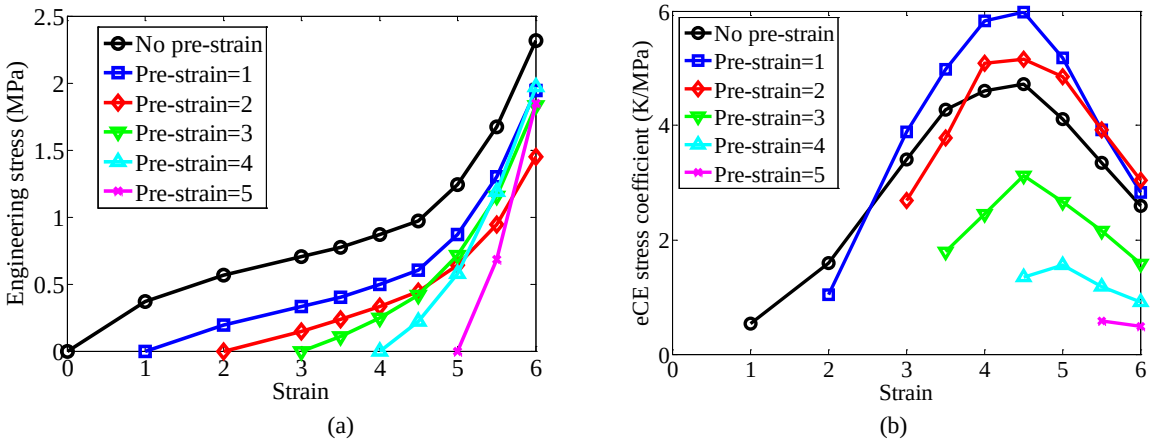


Fig.2. 20 Comparisons of eC effect at different pre-strains and no pre-strain: (a) stress as a function of strain, (b) eC stress coefficient as a function of strain.

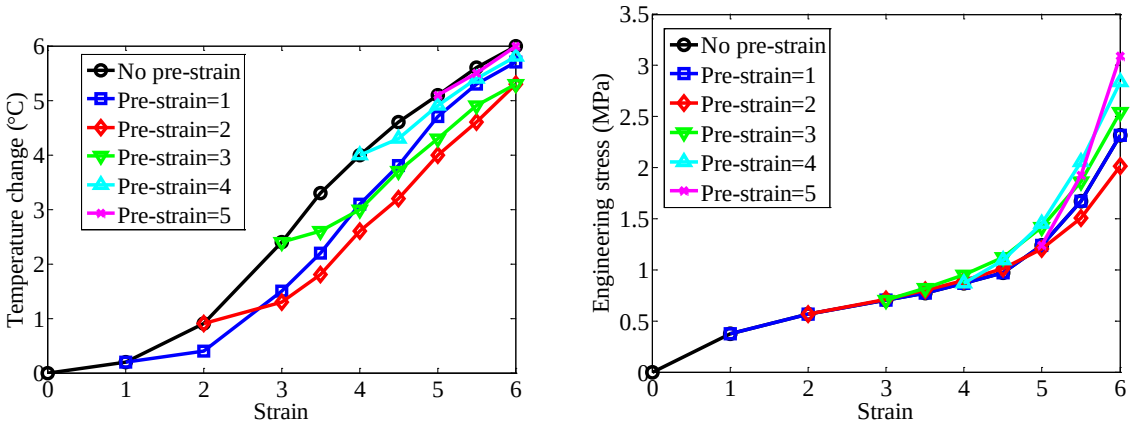


Fig.2. 21 Opposite variation trend of (a) temperature change and (b) stress in the NR with pre-strain using the NR without pre-strain as a reference.

## 2.8. Conclusions

In this chapter, the elastocaloric (eC) effect of NR is characterized.

Some basic eC phenomena are characterized and understood by the SIC theory. It's found the temperature increase in stretching $\Delta T_{stretching}$ is smaller than temperature decrease in retraction $\Delta T_{retraction}$, which is due to the different kinetics of crystallization in stretching and melting in retraction.

The eC performance dependence on strain is characterized by using eC strain coefficient and eC stress coefficient, which is defined as $\beta = -\partial s / \partial \varepsilon$ and $\gamma = \partial T / \partial \sigma_{stretching}$ respectively, where $s$ is the specific entropy change, $\varepsilon$ is the engineering strain, $T$ is the eC adiabatic temperature and $\sigma_{stretching}$ is the stretching stress. Both the eC strain coefficient and the eC stress coefficient exhibit the highest eC performance at middle SIC strain (around strain of 4.5 or 5), which should be chosen as the deformation regime of eC effect. These are due to the highest SIC growth degree at middle SIC strain. The SIC growth degree can be estimated by a temperature change ratio and a stress relaxation ratio. The temperature change ratio is defined as $\alpha_T = \Delta T_{relaxed} / \Delta T_{stretching}$, where $\Delta T_{relaxed} = \Delta T_{retraction} - \Delta T_{stretching}$. The stress relaxation ratio is defined as $\alpha_\sigma = \sigma_{relaxed} / \sigma_{stretching}$, where $\sigma_{relaxed} = \sigma_{stretching} - \sigma_{retraction}$ is the difference of the stretching stress and the retraction stress. Both the temperature change ratio and stress relaxation ratio show similar trend as eC strain coefficient and eC stress coefficient, indicating the highest eC performance is induced by the highest SIC growth degree.

To improve the eC performance, a pre-strain is applied. Considering the required temperature change for a cooling cycle, the reduced applied strain for a compact cooling device, higher eC strain coefficient and higher eC stress coefficient, pre-strain of 2 should be chosen, i.e. right before the onset strain of SIC. The fatigue life can also be improved by the pre-strain, which is investigated in Chapter 4. Moreover, the NR with high network chain density (N) exhibits a lower temperature change (Fig.2. 19 (a)), lower eC strain coefficient (Fig.2. 19 (b)) and lower stress coefficient (Fig.2. 20 (b)), but larger stress (Fig.2. 20 (a)). Thus, the NR with low N ($1.3\times10^{-4} mol \cdot cm^{-3}$) is a better eC material.

The eC effect in NR is directly measured and compared to indirect method using Maxwell relation. The validity of this relation is challenged using two different characterizations for Clausius-

Clapeyron factor determination, $(\partial\sigma/\partial T)_\varepsilon$, where $\sigma$ is the stress, $\varepsilon$ is the strain, respectively. The first characterization is "increasing static temperature for stress-strain behavior". The second characterization is "increasing temperature at constant strain". The first characterization technique reveals that the stress dependence on temperature is difficult to evaluate, because of the complex stress effects of SIC and melting (stress relaxation and stress hardening). Thus, the deduction from $(\partial\sigma/\partial T)_\varepsilon$ is either underestimated or even of the wrong sign. On the contrary, the second characterization (increasing temperature at constant strain) allows an accurate prediction of the eC activity. From this result, it is confirmed that the Maxwell relation $\left(\partial\sigma/\partial T\right)_\varepsilon = -\left(\partial s/\partial\varepsilon\right)_T$ is valid. The importance of this validity is highlighted in appendix 2 where it is proved that it is a consequence of the conservation of energy. The observed complex stress effects highlight that the stress is not a state variable, thus challenging the ergodic behavior NR material. It is noticeable that non-ergodic behavior is also observed for electrocaloric effect (ECE) of terpolymer.[149] Non-ergodic behavior might then be a common phenomenon in the stimulus-caloric effect of polymers, which might be related to the stimulus-induced crystallite. Compared with eC effect of shape memory alloys, it is shown in this work that the evaluation of $(\partial\sigma/\partial T)_\varepsilon$ is more difficult in natural rubber. The difference may rely in the nature of the phase transition in natural rubber, which is probably different from a first-order transition.

# Chapter 3 Physical model of elastocaloric effect of natural rubber

## 3.1. Introduction

For elastocaloric (eC) effect of natural rubber (NR), temperature change and stress are two required properties. Stress represents the elasticity of NR material. Elasticity should be primary factor for the eC effect. Both the temperature change and stress are mainly related to the strain-induced crystallization (SIC) (more details in Chapters 1 and 2). SIC can be influenced by temperature, which in turn influences the variations of temperature change and stress of eC effect.

The superior physical properties of NR would be due to the occurrence of SIC. Flory proposed a paradoxical situation on SIC: stress relaxation effect and stress hardening effect[70]. The clue to the resolution of this "paradox" may be found in the limitation of thermos-dynamical theories to states of equilibrium[70]. When NR is stretched, the SIC equilibrium state where the theory applies will not be reached. The standard theory of rubber elasticity suggests that the stress varies with temperature linearly[5]. The stress variation trend coincides with this theory at static condition[92]. While at dynamic condition, the stress at higher temperatures is lower than the stress at lower temperatures [5]. Is this phenomenon against the classic theory of rubber elasticity? The theory of rubber elasticity proposed by Flory[70], and which included SIC, eems to be correct under equilibrium conditions (at constant elongation).

These two paradoxes are both interpreted by the non-equilibrium conditions. However, even for the equilibrium conditions, the classical theory of rubber elasticity can't predict the experimental data precisely. At cooling condition of constant elongation, the stress decrease is significantly larger than the prediction of classical theory of rubber elasticity. The deviate can be mainly attributed to the behavior of SIC[155]. As a result, whatever the equilibrium and the non-equilibrium conditions, standard theory of rubber elasticity (i.e. entropic elasticity) is invalid without considering occurrence of SIC.

In this chapter, the SIC model of Flory is modified to predict the stress behavior at different temperatures and the temperature change at room temperature. Further experiments were conducted and are presented in this chapter, and were done on the low-N rubber sample.

## 3.2. Modified Flory's model

### 3.2.1. Flory's model

A theory of oriented crystallite in elongated polymers having network structures (e.g., in vulcanized rubber) is developed through the application of statistical mechanical procedures by Flory[70].

The free energy of crystallization is the energy needed for the transition from the un-deformed state of polymer chain to the deformed state and further crystallized state. The melting free energy is the opposite.

The melting Gibbs free energy $\Delta G_m$, which at a given stretching state and temperature $T$, can be written as follows[70,72,73,76,78,80],

$$\Delta G_m = \Delta H_m - T\Delta S_{m,\lambda} \quad (3.\ 1)$$

$\Delta H_m$ is the enthalpy and $\Delta S_{m,\lambda}$ is the entropy of the chains at the elongation $\lambda$ and is written,

$$\Delta S_{m,\lambda} = \Delta S_{m,1} + \Delta S_{undeformed} \quad (3.\ 2)$$

where $\Delta S_{m,1}$ is the entropy of fusion of the crystalline phase in an stretched chain and $\Delta S_{undeformed}$ is the entropy change from deformed state of the chains at the elongation $\lambda$ to un-deformed state.

$\Delta S_{m,1}$ is obtained from the equilibrium state between crystallized and melted chain in the deformed state,

$$\Delta S_{m,1} = \frac{\Delta H_m}{T_m^0} \quad (3.\ 3)$$

where $T_m^0$ is incipient crystallization temperature.

Finally, the melting Gibbs free energy is

$$\Delta G_m = \Delta H_m (\frac{T_m^0 - T}{T_m^0}) - T \cdot \Delta S_{undeformed} \quad (3.\ 4)$$

Thus, the Gibbs free energy of crystallization is

$$\Delta G_c = \Gamma_s - \Delta G_m = \Gamma_s - \Delta H_m (\frac{T_m^0 - T}{T_m^0}) + T \cdot \Delta S_{undeformed} \quad (3.\ 5)$$

where $\Gamma_s$ is the is the surface energy required for the formation of the interface between the crystallite and the surrounding amorphous phase[76]. The calculation of $\Delta S_{undeformed}$ is using the Gaussian function.

The condition for equilibrium with respect to the degree of longitudinal growth of the crystallite can be stated as

$$(\frac{\partial G_c}{\partial C_e})_\lambda = 0 \quad (3.\ 6)$$

where $C_e$ is the crystallinity.

Solving the above equation for the equilibrium value of crystallinity, in addition to considering additional thermodynamics calculations[70],

$$C_e = 1 - \{[\frac{3}{2} - \varphi(\lambda)] / (\frac{3}{2} - \theta)\}^{1/2} \quad (3.\ 7)$$

where $\varphi(\lambda) = (6/\pi)^{1/2} \lambda / n^{1/2} - (\lambda^2/2 + 1/\lambda)/n$, the incipient crystallization temperature for the undeformed chain $\theta = 600(1/250 - 1/T)$, $n$ is the number of rigid equivalent random links between crosslinks.

### 3.2.2. The contradiction of Flory's model with experimental results

Thus, the engineering stress $\sigma$ in terms of the crystallinity $C_e$,

$$\sigma = \frac{\partial G_c}{\partial \lambda} = \frac{NkT}{1 - C_{e1}} (\lambda - 1/\lambda^2) - \frac{NkT}{1 - C_{e2}} (6n/\pi)^{1/2} C_{e2} \quad (3.\ 8)$$

where the suffix $e$ denotes an equilibrium condition for the degree of SIC. $N$ is network chain density, $k$ is the Boltzmann constant, $\lambda$ is the elongation and $T$ the absolute temperature. $C_{e1}$ and $C_{e2}$ are the same value, while their contributions to stress are different.

The different stress effect of SIC can be represented by the stress model,

1. When $C_{e1}$ increases, the stress $\sigma$ increases, i.e. $C_{e1} \uparrow \Rightarrow \sigma \uparrow$. Thus, $C_{e1}$ is responsible for the hardening part of SIC;
2. When $C_{e2}$ increases, the stress $\sigma$ decreases, $C_{e2} \uparrow \Rightarrow \sigma \downarrow$. Thus, $C_{e2}$ is responsible for the relaxing part of SIC.

In Fig.3. 1 (a), the crystallinity at 25 °C and 50 °C is calculated by using Eq. 3.7. In Fig.3. 1 (b), the stress-elongation relation without SIC and with SIC at 25 °C and 50 °C are compared. Qualitatively, the discrepancies between Flory's model and experimental data are as follows,

1. Stress-elongation relation. The NR with SIC has a lower stress than the one without SIC (Gaussian), which is opposite to the experimental result[5]. This is because of the Flory's assumption: SIC completely occurs after stretching. It indicates all SIC contribute to stress relaxation in Flory's model. Actually, the SIC incubation time in on the order of 10 ms-100ms[153]. It mainly occurs in the stretching process (before the final elongation is reached) and contribute to stress hardening. Thus, in Flory's model, the stress hardening effect of SIC, i.e. the function of $C_{e1}$, needs to be strengthened and the stress relaxation effect, i.e. the function of $C_{e2}$, needs to be weakened.
2. Stress-elongation relation at different temperatures. The crystallinity at 50 °C is lower than at 25 °C (Fig.3. 1 (a)). The stress at 50 °C is then larger than that at 25 °C (Fig.3. 1 (b)), which is in contradiction with experimental result[87]. It's due to the only stress relaxation effect of SIC and thus the lower crystallinity induces the larger stress in Flory's model. Thus, the contribution of $C_{e1}$ on stress in Flory's model need to be strengthened and the contribution of $C_{e2}$ on stress need to be weakened when considering the thermal-mechanical behavior.

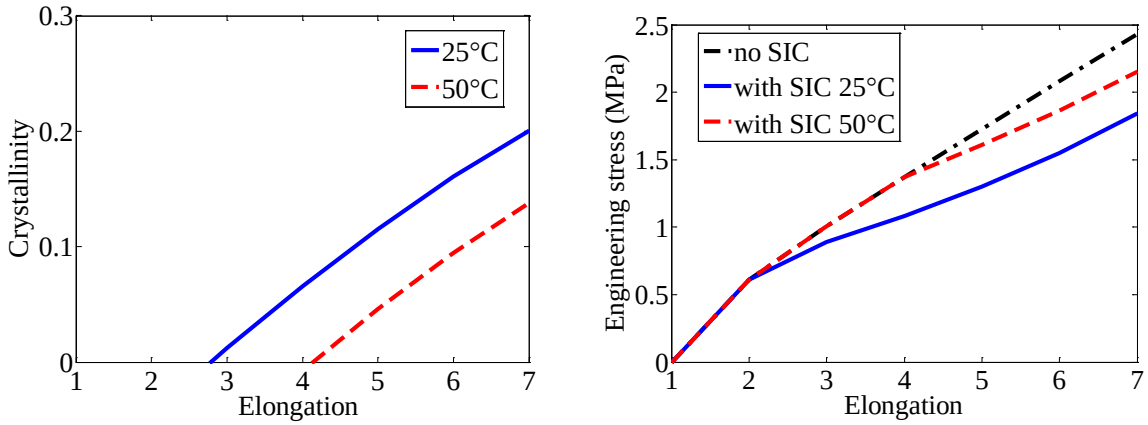


Fig.3. 1 (a) Crystallinity-elongation curves and (b) stress-elongation curves without crystallization and with equilibrium crystallization at the two temperatures indicated respectively. Network chain density $N = 1.3 \times 10^{-4} mol \cdot cm^{-3}$ and equivalent random links $n$=75.

As a result, the two discrepancies between Flory's model and experimental result comes from the incorrect degree of the contributions of the stress hardening part ($C_{e1}$) and relaxing part ($C_{e2}$) of SIC. This can be revised through the related parameters, network chain density $N$ of $C_{e1}$ and equivalent random links $n$ of $C_{e2}$. To strengthen the stress hardening part of SIC, i.e. the function of $C_{e1}$, $N$ should be increased. To weaken the stress relaxing part of SIC, i.e. the function of $C_{e2}$, $n$ should be

increased. This is the postulate of mathematical assumption. Then, how the parameters $N$ and $n$ change with elongation and temperature physically?

SIC may function as additional network points of larger sizes[70]. Following this, the crosslink density is then the sum of the density of sulfur bridges $\nu_s$ and the density of crystallites $\nu_{crystal}$ [96]. As elongation increases, the crystallinity increases. The crosslink density is then

$$\nu = \nu_s + \nu_{crystal}$$

Crosslink density $\nu$ is related to network chain density *N*. Network chain density *N* will increase as crystallinity increases. The crystallite crosslinks divide the original long chain into short one. Then, *n* will decrease, which corresponds to the mathematical assumption. Temperature influences the formation of crystallite and thus influences *N* and *n.*

### 3.2.3. Modified Flory's model

In Flory's model, SIC completely occurs after stretching. *N* and *n* are kept constant neglecting the SIC network in the stretching process. Thus, the SIC can only contribute to stress relaxation and not to stress hardening. *N* and *n* need to be modified with elongation and temperature.

As crystallite can act as new crosslink (crystallite crosslink), so that the long chain formed by chemical crosslink is separated into short chain by crystallites. The new short chain number $N_c$ caused by crystallites in each chain is

$$N_c = 1 + \frac{\xi}{\psi} \tag{3. 9}$$

where $\xi$ is number of crystalline links per chain, $\psi$ is the number of equivalent random links traversing the crystallite crosslink in one chain.

Then, the total network chain density $N_t$ after crystallization is,

$$N_t = N_s \cdot N_c = N_s(1 + \frac{\xi}{\psi}) = N_s(1 + \frac{n_s \cdot C_e}{\psi}) \tag{3. 10}$$

$N_s$ and $n_s$ are chemical network chain density and the number of equivalent random links per chain respectively before crystallization; $C_e$ is crystallinity at equilibrium condition.

The total number of equivalent random links $n_t$ after crystallization is

$$n_t = \frac{n_s - \xi}{N_c} = \frac{\psi \cdot n_s \cdot (1 - C_e)}{n_s \cdot C_e + \psi} \tag{3. 11}$$

Substitute $N_t$ and $n_t$ into Flory's model,

$$\sigma = N_s(1 + \frac{n_s \cdot C_e}{\psi}) \cdot \frac{kT}{1 - C_e}[(\lambda - 1/\lambda^2) - [\frac{6\psi \cdot n_s \cdot (1 - C_e)}{\pi(n_s \cdot C_e + \psi)}]^{1/2} C_e] \tag{3. 12}$$

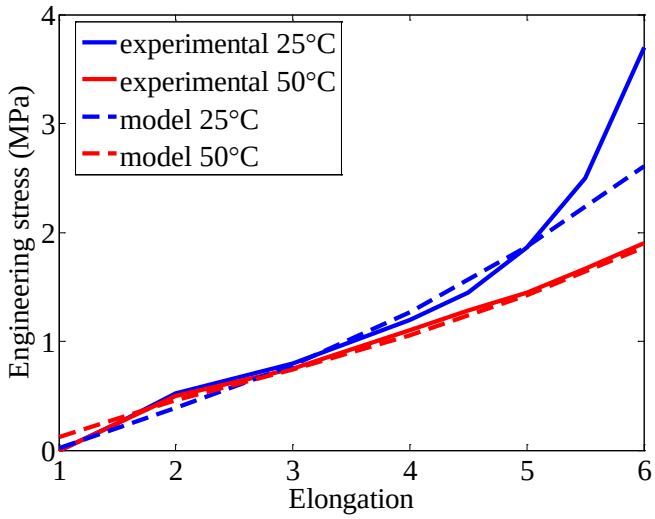


Fig.3. 2 The comparison of stress-strain relation at different temperatures with model. Results were calculated from Eq. (3.12). $N_s = 1.3\times10^{-4} mol\cdot cm^{-3}$, $n_s = 75$. The experimental data was taken from Toki[87] for the NR with same network chain density.

Eq. (3.12) is used for calculating stress vs. strain at different temperatures. The model is compared with the experimental result in Fig.3. 2. For the experimental result, it's shown that the lower stress is obtained for the higher temperature. It's due to the weaker stress hardening effect of SIC at high temperature. Some crystallite can't be formed at high temperature. Thus, the network chain density induced by crystallite crosslink is lower at higher temperature, resulting in the lower stress. In Fig.3. 2, when elongation is smaller than 5 ($\lambda < 5$), the modified Flory's model fits well with experimental data at different temperatures, which can't be predicted by the standard theory of rubber elasticity without considering SIC (lower stress for the lower temperature). When $\lambda > 5$, the model deviate from the experimental data at 25 °C. The SIC network chains may reach the limited extensibility. Thus, the model by using Gaussian distribution function can't predict the stress from elongation of 5. However for 50 °C, the model can predict the stress up to elongation of 6. It's due to the less crystallinity at 50 °C and thus the less stress hardening of SIC. It proves the stress hardening effect mainly comes from the SIC.

### 3.2.4. Contribution to stress from non-Gaussian chains and SIC network chain structure

In Treloar's book[5], it seems reasonable to interpret the main features of the experimental stress elongation curve in terms of the non-Gaussian statistical theory, and to regard the effects of crystallization as secondary, producing only minor modifications[100]. The quantitative applications of this non-Gaussian statistical theory to stress-elongation curves at high extensions have been hindered by inadequacies in methods of determining the network structure[156]. Mullins attempts to relate the physical properties of NR to their network structure by using Mooney-Rivlin plots[156–158]. However, he confirms that stress upturns at high elongations are due to limited extensibility of the network and not to crystallization[156]. The idea of Mullins is followed and developed, which is to relate the physical properties of NR to the new network structure composed of chemical network structure and SIC network structure.

The improvement of X-ray diffraction techniques since the last ten years allowed a renewal of the study of SIC in NR. Toki et al. suggest that the mechanical behavior of NR should be considered by combined theories of non-Gaussian deformed chains and the SIC[86,87]. However there is no exact

relation between non-Gaussian chains and SIC. It is difficult to distinguish between the contribution of the limited extensibility of chains and hardening effect of SIC.

Based on the modified Flory's model, the stress-elongation relation of NR can be divided into three regions,

1. Small elongation region before the onset elongation of SIC. The chemical network is responsible for stress-elongation behavior. The Gaussian distribution function can be used to describe this behavior;
2. Middle elongation region. The new network structure is composed of chemical network and SIC network. Stress hardening can be explained by the increase of network chain density of new network structure without considering the finite extensibility of the chains[88]. On the other hand, the network chains can be relaxed by SIC and thus avoid to reach the limited extensibility. Consequently, Gaussian distribution function is still valid for this new network structure;
3. Large elongation region. SIC begin to saturate. Part of the network chains can't be relaxed by SIC. Thus, the limited extensibility of new network chains need to be considered by using non-Gaussian distribution function.

### 3.2.5. Difference between chemical network structure and SIC network structure: difference between network chain density and crosslink density

From the values of the parameters *N* and *n* required to fit the experimental force-extension curve in Fig.3. 2, it is possible to estimate the number of isoprene units in the equivalent random link. The average molecular weight $M_c$ between crosslink corresponds to network chain density $N_s$ caused by vulcanization,

$$M_c = \frac{\rho}{N_s} = \frac{920 kg \cdot m^{-3}}{1.3\times10^{-4} mol \cdot m^{-3}} = 7077 g \cdot mol^{-1}$$

Since this is equivalent to 75 random links from the fitting for experimental data, it follows that the 'molecular weight' of the equivalent random link is $94 g \cdot mol^{-1}$, which is equal to 1.4 isoprene units.

When $n_s = 75$, $\psi = 15$, this model is in agreement with experimental data. That is to say, there are 15 random links, ie. 21 isoprene units, traversing the SIC crosslink in each chain.

In paper[67], the average molecular weight of $M_c = 6800 g \cdot mol^{-1}$, is similar to our case. So, the crystallites size should be similar to our material. To set the order of magnitude of the size of crystallites, $L_{002}$ corresponds to 22−23 isoprene units (the stretching direction). The maximal values for $L_{200}$ and $L_{120}$ correspond to 14 chains in the "a" direction and 5 chains in the "b" direction. Comparing with 21 isoprene units in one chain traversing one SIC crosslink, we get a conclusion: SIC is a big network points which bind about 70 chains. While chemical network points only connect two chains or four chains[87]. So, the SIC crosslink density is much lower than the SIC network chain density, while the chemical crosslink density and chemical network chain density are the same order of magnitude. We can go back the assumption of Trabelsi[88], it may be not correct to combine density of crystallites and chemical crosslink density directly. As a result, it's better to use the network chain density of SIC network structure for mechanics model.

### 3.2.6. Future work of the modified model

The drawbacks and improvements of this modified Flory's model:

1. All the relations in Flory's model are derived for uniaxial loading using an affine deformation assumption, which is known to result in inaccurate predictions for large deformations[78]. When a polymer chain is stretched so that it approaches its maximum extensibility, it will deform less than the macroscopic stretch and will thus not deform affinely[76].
2. The interaction with surrounding polymer chains is neglected; like the tube constraint[159];
3. This model uses a Gaussian distribution function. There is no consideration of the limited extensibility of chain. So, there is no obvious stress upturn at large elongations (Fig.3. 4). In the further work, the non-Gaussian distribution function need to be used for the SIC network chains.

Though the numerous drawbacks, this modified Flory' model can give a qualitative agreement with the experimental data, which can't be predicted by the standard theory of rubber elasticity[87]. It points out a way to modify the standard theory of rubber elasticity. It highlights the function of real network structure induced by SIC on thermo-mechanical behavior of NR.

## 3.3. Temperature change deduced from Flory's model

As described in the stress model of Flory, the deviation between model and experimental results should come from the Flory's assumption: SIC completely occurs after stretching. Thus, the stress hardening effect of SIC hasn't been considered and only the stress relaxation of SIC is considered. In the following part, the assumption of Flory is checked if it can influence the crystallinity and thus the temperature change at a given strain.

### 3.3.1. Experimental procedure

Upon the stretching of NR, irreversible entropy variation may occur due to the rupturing of network chains[154]. In this work, only the temperature decrease in retraction process was presented in order to avoid the entropy influenced by chain rupture.

NR sample was stretched at different elongation rates (from 0.009 $s^{-1}$ to 70 $s^{-1}$) and retracted at the same elongation rate of 20 $s^{-1}$ for recording the adiabatic temperature decrease. In Fig.3. 3 was shown the stress and temperature decrease at elongation rates of 0.07 $s^{-1}$ and 14 $s^{-1}$.

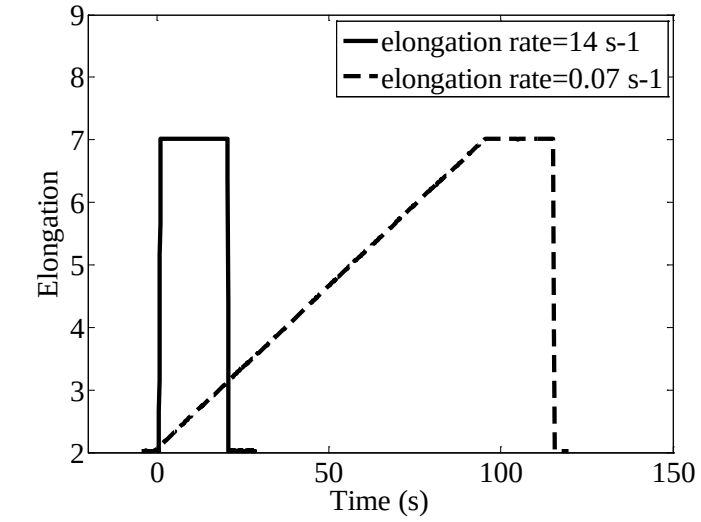


(a)

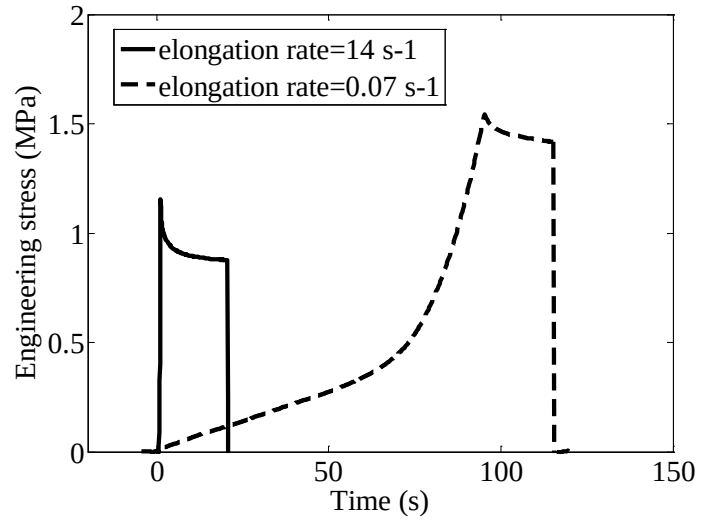


(b)

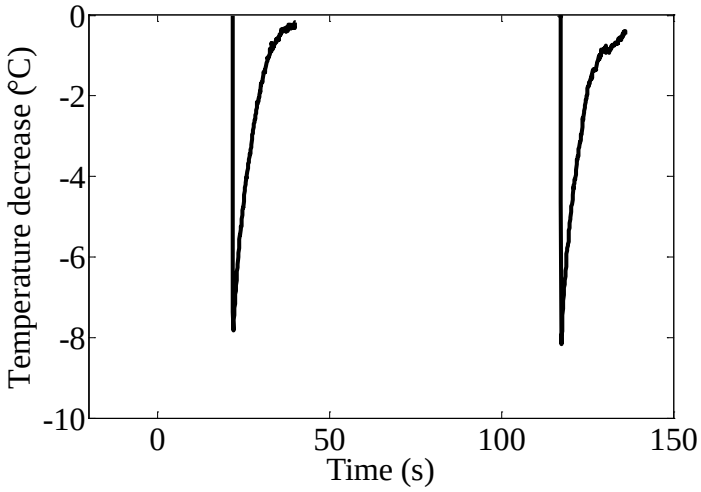


(c)

Fig.3. 3 NR sample is stretched at elongation rate of 14 $s^{-1}$ and 0.07 $s^{-1}$ and retracted at the same fast elongation rate to measure the adiabatic temperature decrease: (a) the elongation-time; (b) the stress-time; (c) the temperature decrease-time.

### 3.3.2. Results and discussion

In Fig.3. 3 was shown that the smaller elongation rate ($0.07s^{-1}$) results in the larger stretching stress but small relaxed stress, whereas the smaller elongation rate ($14s^{-1}$) results in the smaller stretching stress but larger relaxed stress.

The comprehensive property of SIC can be shown by the thermal behavior. Both the SIC contributing to stress relaxation and the SIC contributing to stress hardening will contribute to the same variation trend of enthalpic entropy. Fig.3. 4 was shown the comparison of stress and temperature decrease at different elongation rates. The stress decreased from 1.7 MPa to 1 Mpa when the elongation rate increased from 0.009 $s^{-1}$ to 70 $s^{-1}$ (Fig.3. 4 (a)). However, the temperature change was almost the same at different elongation rates (Fig.3. 4 (b)). SIC requires time to be completed. In the fast stretching process, SIC mainly occurs after the stretching resulting in the stress relaxation. Whereas in the slow stretching process, SIC mainly occurs in the stretching process resulting in the stress hardening. In other word, the effect of SIC is transformed from stress relaxation effect to stress hardening effect when the elongation rate decreases. However, whatever the elongation rate, the total SIC (including the SIC occurred in stretching process and after stretching) only depends on the elongation, resulting in the same temperature change. The SIC contributing to the opposite stress effects exhibits the same thermal variation. The temperature change $\Delta T$ is an indication of entropy change $\Delta s = c \cdot \Delta T / T_0$ (Eq. 2.30). Thus, the entropy change is only a function of elongation, not depending on its history, whereas stress depends strongly on the loading history.

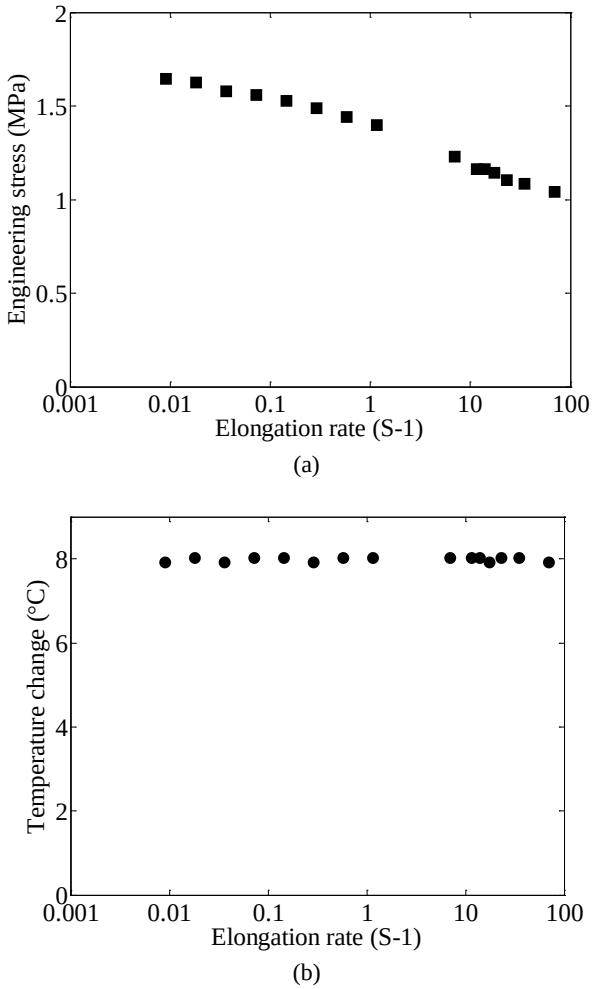


Fig.3. 4 (a) The comparison of stress and the (b) temperature decrease at the same elongation of 6 when different elongation rates were applied.

In Flory's assumption, SIC occurs after stretching, which can be regarded as the fast stretching process where SIC can't occur in the stretching process. Even though this assumption can't predict the mechanical behavior correctly, the predicted crystallinity may be right because the crystallinity doesn't depend on the loading history. Thus, the temperature change is calculated by using the crystallinity (Eq. (3.7)) in Flory's model. The temperature change $\Delta T_c$ from the contribution of SIC can be written as,

$$\Delta T_c = C_e \cdot \frac{h_f}{c} \tag{3. 13}$$

where $c = 1.8\times10^6 J\cdot K^{-1}\cdot m^{-3} = 2J\cdot K^{-1}\cdot g^{-1}$ is an estimation of specific heat of NR[144], and $h_f = 64J\cdot g^{-1}$ is the latent heat of fusion. $C_e$ is crystallinity calculated from Eq. (3.7).

The directly measured temperature change is taken from the previous characterization (presented in Chapter 2). The melting is much faster than crystallization. Thus, temperature decrease in retraction process is much closer to the thermodynamic equilibrium than temperature increase in stretching process (more details in 2.2.4). The crystallinity calculated in Flory's model is an equilibrium state. Thus, the temperature change calculated from Eq. (3.14) is compared with the direct measured temperature decrease. In Fig.3. 5, it's shown the temperature change from SIC dominates in the total temperature change. The difference may be due to the entropy variation of coil-stretch transition (elastic entropy or entropy from purely elastomeric behavior).

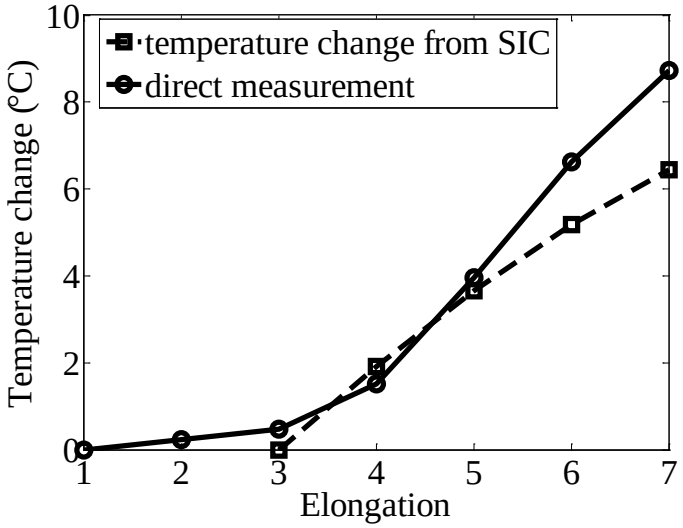


Fig.3. 5 The comparison between directly measured temperature change and deduction from the contribution of SIC.

The entropy variation caused by the coil-stretch transition can be described by the entropy elasticity model. If the rubber chain length does not approach its fully extended length, the specific entropy variation $\Delta s_e$ is[160],

$$\Delta s_e = -\frac{1}{2}Nk(\lambda_x^2+\lambda_y^2+\lambda_z^2-3) \tag{3. 14}$$

For the uniaxial stretching, $\lambda_y = \lambda_z = \sqrt{1/\lambda_x}$ ,

$$\Delta s_e = -\frac{1}{2}Nk(\lambda_x^2+\frac{2}{\lambda_x}-3) \tag{3. 15}$$

where $k$ is Boltzmann's constant, $\lambda_x, \lambda_y, \lambda_z$ are the elongation ratios in three dimensions, $N = \frac{\rho N_A}{\overline{Mc}}$ is the network chain density, $\rho$ is the density of NR, $N_A$ is Avogadro's constant and $\overline{Mc}$ is the average molecular mass of a polymer chain.

The adiabatic temperature variation $\Delta T_e$ is proportional to the isothermal elastocaloric entropy variation $\Delta s$ ,

$$T_0 \times \Delta s_e \Big|_{T=T_0} = -c \times \Delta T_e \Big|_{s=s_0} \tag{3. 16}$$

where $T_0 = 298K$ is the temperature at which the elastocaloric effect is observed, $s_0$ is the entropy when undergoing an adiabatic measurement, and $c = 1.8 \times 10^6 J \cdot K^{-1} \cdot m^{-3}$ is the specific heat capacity. So, entropy variation caused by the coin-stretch transition,

$$\left|\Delta T_e\right| = \frac{T_0}{c} \Delta s = \frac{T_0 Nk}{2c} (\lambda_x^2 + \frac{2}{\lambda_x} - 3) \tag{3. 17}$$

Finally, the deduction of temperature change from both the contributions of SIC and entropy elasticity can be written,

$$\Delta T = \Delta T_c + \left|\Delta T_e\right| = C_e \cdot \frac{h_f}{c} + \frac{T_0 Nk}{2c} (\lambda_x^2 + \frac{2}{\lambda_x} - 3) \tag{3. 18}$$

In Fig.3. 6, the direct measured temperature change is almost in agreement with the deduction from the contribution of SIC and entropy elasticity. The crystallinity used for the deduction of temperature change is from the Flory's model (Eq. (3.7)). Thus, the calculated crystallinity may be correct even Flory assumes that SIC occurs after the stretching. This assumption corresponds also to a very fast stretching where the SIC can't occur immediately in the stretching process. It proves that the crystallinity doesn't depend on the loading history. It indicates that both the SIC contributing to stress relaxation and the SIC contributing to stress hardening would contribute to the same variation trend of enthalpic entropy.

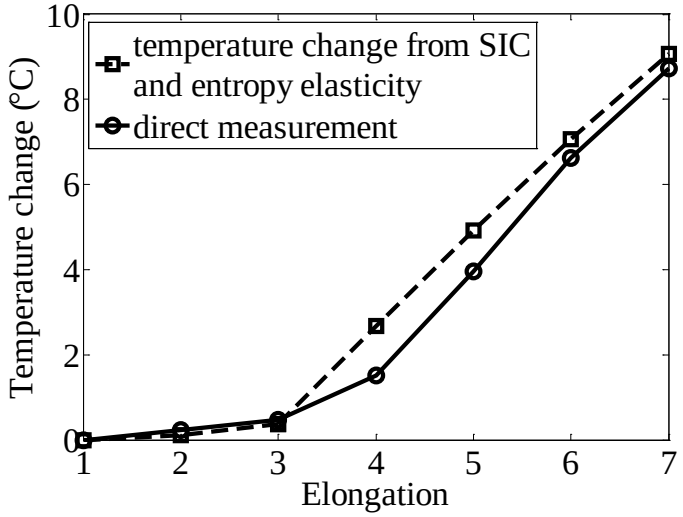


Fig.3. 6 The comparison between directly measured temperature change and deduced one from both the contributions of SIC and entropy elasticity.

## 3.4. Conclusions

Stress and temperature change are two required quantities for eC effect. The eC effect (including stress and temperature change) dependent on temperature is an important property for eC application. The SIC model of Flory is modified to describe both the stress and temperature change of eC effect. The stress model can correspond to the experimental results at different temperatures, which can't predicted by the standard model. The temperature change model can correspond to the experimental results at room temperature. This highlights the capability of a SIC model To further prove this SIC model and the potential of NR acting as eC material, the eC temperature change dependence on temperature needs to be further measured and modeled.

The SIC is mainly responsible for the thermal-mechanical behavior of NR. The SIC is mainly responsible for the thermal-mechanical behavior of NR, which cannot be predicted by the standard theory of rubber elasticity (see appendix 2 for entropic elasticity model and utilization). Finally, the model should be further developed through considering the multi-physics coupling as well as considering SIC.

The Maxwell relation $\left(\frac{\partial \sigma}{\partial T}\right)_{\varepsilon} = -\left(\frac{\partial s}{\partial \varepsilon}\right)_{T}$, is however not verified by this model (opposite sign). This means that the model can be used to simulate simple characterizations, like $\sigma = f(\varepsilon)$ or $\Delta T = f(\varepsilon)$ only. It cannot be used for thermodynamic cycles (as shown in appendix 2 since it would contradict the 1st principle). The writing of unified model verifying both Maxwell relation and experimental stress-strain behavior remains a challenge.

# Chapter 4 The fatigue of elastocaloric effect in natural rubber influenced by strain-induced crystallization

## 4.1. Introduction

As stated in Chapter 1, investigations on fatigue effect on eC properties are mandatory for further developments of NR based cooling applications. In NR sample stretched more than 3.8 times, the SIC, acting as reinforcing and toughening fillers, increases the crack resistance[107]. "Annealing" (increasing minimum strain) of an elastomer can result in significant changes of fatigue life and the ultimate tensile strength, which depends on the strain level of annealing[161]. For a constant strain amplitude, the fatigue life of NR improves with increasing minimum strain, up to a moderate minimum strain level[10,104]. At constant stress amplitude, increasing the mean stress from about 1MPa to 2MPa increases also the fatigue life[8,9]. These phenomena show the fatigue property dependence on strain regime.

In this chapter, the fatigue property of eC effect in NR with low N is tested. The fatigue property at different strain regimes is compared. The degradations of stress and temperature change are shown after cyclic deformation cycles up to $10^5$ cycles. The observed tendencies are interpreted in terms of crystallization properties. Finally, an optimal strain regime is identified for further working condition in case of eC cooling system.

## 4.2. Experimental procedure

Considering the eC application, two properties are needed. One is the elasticity, and the other is the temperature change. Elasticity should be the primary factor for eC application, which can be represented by stress. Thus, the evolutions of temperature change and stress are characterized with the number of deformation cycles, which may show the fatigue property of eC effect.

To evaluate the influence of the strain amplitude on the fatigue property of eC effect, the fatigue test was conducted at a large strain amplitude of 5 (strain regime of 1-6) and small strain amplitude. For fatigue test at small strain amplitude, to evaluate the fatigue property at different strain regimes, the strain regime of 0-3, 2-5 and 4-7 with the same strain amplitude of 3 was chosen, respectively.

For the fatigue test, two kinds of experimental processes were conducted. One was a large number of deformation cycles for inducing fatigue, which can be referred as the "fatigue cycles". The other was a step deformation for measuring the fatigued state (including measuring the eC temperature change and stress). The step deformation ensures a quasi-adiabatic condition for eC temperature change measurement. For strain amplitude of 1-6, the specific loading history is as follows. Firstly, the adiabatic temperature change and stress were measured from strain of 1 to 6 with a step of 1 or 0.5 (an example is shown in Fig.4. 1). The strain rate in extension and retraction processes was 20 $s^{-1}$, which was larger than the adiabatic limit (the adiabatic limit corresponds to the characteristic time of heat exchange with outer medium). Then, a number of deformation cycles stimulated by sine wave with a frequency of 2 Hz were applied (Fig.4. 2). The number of cycles was divided into different periods (10 cycles or 80 cycles at one time). This procedure allows a follow-up of the properties of NR with gradual fatigue. At last, after every period of deformation cycles, the temperature change and stress were measured as for the first time.

Fig.4. 1 displays a typical time profile of the temperature change of NR material upon a step deformation. The temperature increased abruptly when the NR is stretched to a given strain and then decreased exponentially towards room temperature due to the thermal heat exchange with the surrounding environment. The applied strain was kept constant for 20 s. Fig.4. 1 (a) showed the stress relaxation during the keeping time. When the applied strain was removed, the temperature decreased below room temperature and then increased exponentially back to room temperature. The temperature decrease is larger than the temperature increase (see 2.2.4). Further characterizations of eC effect always utilize the decreasing temperature peak in order to measure a reliable value.

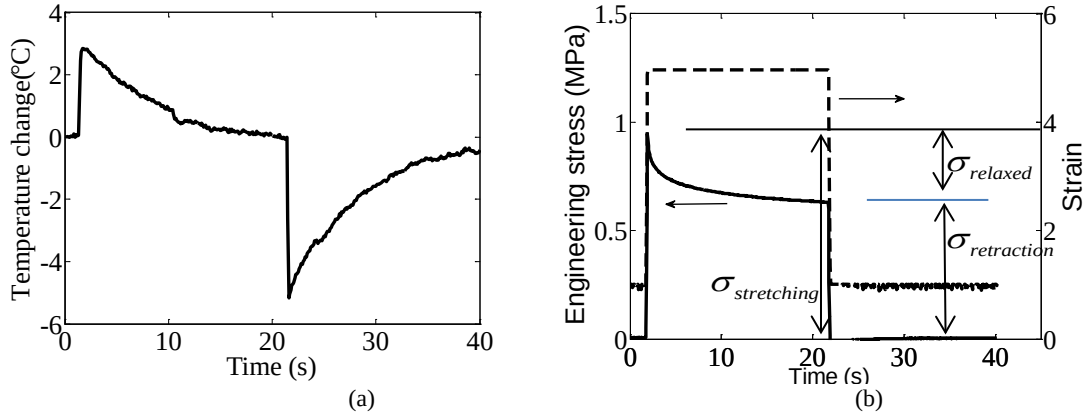


(a) (b)

Fig.4. 1 (a) eC temperature change - time signal and (b) stress – strain behavior of NR from strain varying from an initial value of 1 up to a maximum value of 5.

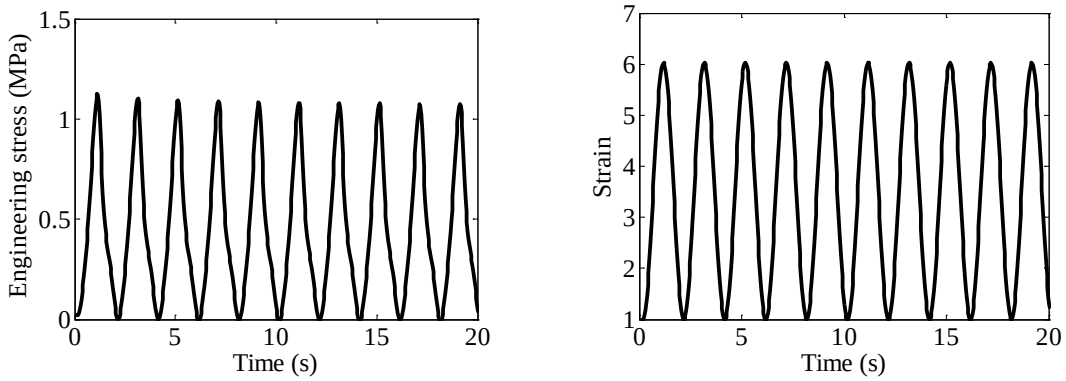


(a) (b)

Fig.4. 2 The deformation cycles stimulated by sine wave with a frequency of 2 Hz; (a) Engineering stress versus time; (b) Strain versus time.

For the fatigue test at the small strain amplitude, the basic experimental procedure was the same as for the strain regime of 1-6. The difference was the different periods of the fatigue cycles. The eC temperature change and stress were only measured at the same strain amplitude as fatigue cycles.

One of the origins of fatigue of eC effect comes from the breakage of network chains. The stretching stress is related to the number of network chains, which is used as an indicator of fatigue property of eC effect. When stretching NR, irreversible entropy variation may occur due to the breakage of network chains[154]. Thus, for eC characterization, only the temperature decrease in the retraction process was presented in order to avoid any irreversible effect, and, as stated above, for ensuring an adiabatic temperature measurement.

## 4.3. Results and discussion

In order to show the degradation of eC temperature change and stress quantitatively in a specific period of fatigue cycles, a degradation degree of temperature change is defined as

$$d_T = \frac{\Delta T_1 - \Delta T_2}{\Delta T_1} \quad (4.\ 1)$$

and a degradation degree of stress is defined as

$$d_\sigma = \frac{\sigma_1 - \sigma_2}{\sigma_1} \quad (4.\ 2)$$

where $\Delta T_1$, $\sigma_1$ are the temperature change and stress before a specific range of fatigue cycles, and $\Delta T_2$, $\sigma_2$ are the temperature change and stress after a specific range of fatigue cycles.

### 4.3.1. Fatigue test for large strain amplitude

In Fig.4. 3, the evolution of eC temperature change and stress at strain regime of 1-6 from the first cycle to 650 cycles were compared. From the first cycle to 10 cycles, the eC temperature change is almost constant with a slight degradation before strain of 3.5 and no degradation from strain of 3.5 (Fig.4. 3 (a)). Meanwhile, there is an upturn of eC temperature change from strain of 3. On the contrary, for stress, there was a large degradation at all tested strain levels (Fig.4. 3 (b)) and from the first cycle. As an example, at strain of 6, the stress decreased from 1.5 MPa to 1.1 MPa (degradation degree of stress of 27%) when comparing the first characterization and after 10 cycles (Fig.4. 4).

From 10 cycles to 650 cycles, the degradation of eC temperature change becomes larger and the degradation increases as strain increases (Fig.4. 3 (a)). In Fig.4. 3 (b), the degradation of stress shows the same tendency after 650 cycles. At strain of 6, eC temperature change decreased from 7 K to 5.3 K (degradation degree of 24%). The stress decreased from 1.1 MPa to 0.87 MPa for a strain level of 6 (degradation degree of stress of 21%).

It is worth to notice that the degradation degree of eC temperature change is much lower than stress degradation degree from the first cycle to 10 cycles, whereas it is similar from 10 cycles to 650 cycles (24% and 21% for degradation degree of eC temperature change and stress respectively). Moreover, the degradation degree of stress (27%) from the first cycle to the 10 cycle is larger than that (21%) from 10 cycles to the 650 cycles, which is not proportional to the number of fatigue cycles.

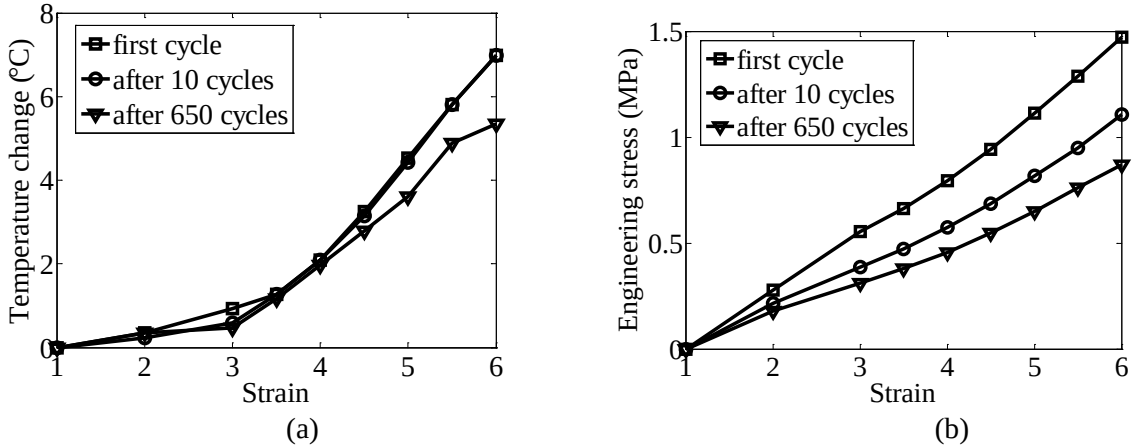


Fig.4. 3 The degradation of (a) the temperature change and (b) the stress from the first cycle to 10 cycles.

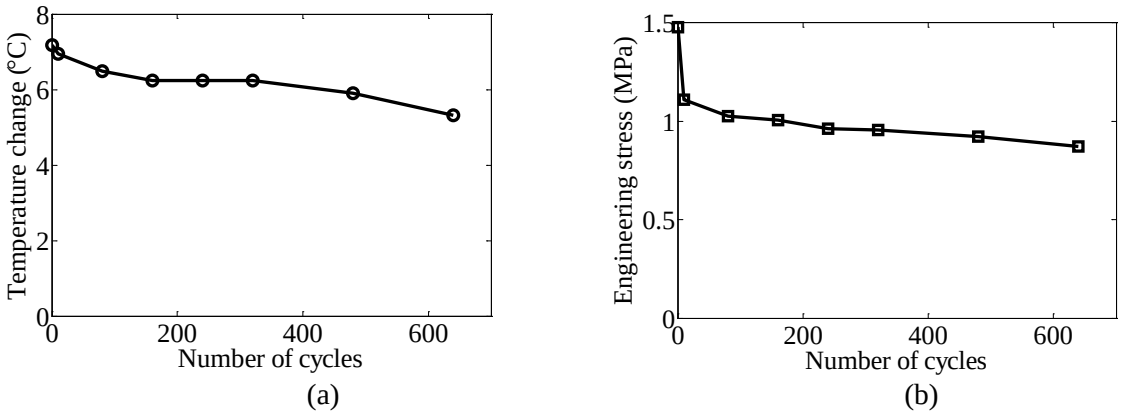


Fig.4. 4 The degradation of (a) eC temperature change and (b) stress represented as a function of the fatigue cycles. The presented results correspond to strain of 6.

In the following, an explanation based on the mechanism of SIC growth is proposed in order to interpret the observed difference between degradations of eC temperature change and stress from the first cycle to 10 cycles. It has been extensively evidenced that the SIC of NR occurs at around strain of 3 at 25ºC[51,67,88,98], which indicates that the upturn of eC temperature change is attributed to the enthalpy of SIC.

The SIC growth is a process where the nucleation chain binds its surrounding chains. The amount of the surrounding chains bound by one nucleation chain in the SIC growth process can be referred as SIC growth degree. In the stretching process, the short chains are first stretched and become the nucleation chains [51,121,147]. The nucleation chains should interact with the surrounding chains. Thus, the stretching stress comes from two parts. One is the entropy elasticity of coil-stretch transition of nucleation chains, and the other is the constraint from the surrounding chains of nucleation chains[76,77,145,146]. Accordingly, the degradation of stress can be caused by the chain breakage and the inertia effect of SIC chains. Due to the chain mobility, the surrounding chains can align with the nucleation chains in the stretching process and can become the SIC chains in the SIC growth process. The alignment of surrounding chains is kept even after the retraction, which can be referred as the inertia effect of SIC chains. Thus the constraint of nucleation chain from the surrounding chains is reduced by the inertia effect of SIC after 10 cycles, which results in the large stress degradation. This is similar to the memory effect: if the macromolecules have not totally relaxed during the retraction, re-nucleation can be eased[67,162]. It can be further concluded that it's the SIC growth in one deformation cycle induces the inertia effect of SIC chains in different deformation cycles. The SIC growth can induce the stress relaxation[106]. The inertia effect of SIC chains can induce the stress degradation. Thus, the stress relaxation in one deformation cycle should be responsible for the stress degradation in different deformation cycles.

The exact chain transition needs to be further proved by the evolution of eC temperature change. The eC temperature change comes from the entropy of coil-stretch transition and mainly the enthalpic entropy (SIC transition of network chains)[4,7]. The breakage of network chains can decrease the temperature change. The inertia effect of SIC chains may decrease the entropy induced by coil-stretch transition, but doesn't influence the enthalpic entropy so much. Thus, the inertia effect of SIC chains wouldn't influence the temperature change so much. From the result of large degradation of stress and small degradation of temperature change after 10 cycles, it can be concluded that the chain transition should mainly be the inertia effect of SIC chains rather than chain breakage.

The increased degradations of eC temperature change and stress as strain increases ("horn" shape of the degradations of temperature change and stress in Fig.4. 3) may be due to the stress effect of SIC.

As SIC binds more and more chains as strain increases, the SIC network is built resulting in increased network chain density and stress, which is referred as the stress hardening effect of SIC. The chain mobility is reduced by the SIC network. Some network chains can't align with the nucleation chain and the potential SIC growth chains decreases as SIC network develops with strain. This is the self-hindering effect of SIC chains. Consequently, the stress relaxation effect induced by SIC growth[106] is reduced and the stress hardening effect of SIC becomes dominant as strain increases. This would easier lead to the breakage of network chain after large number of fatigue cycles and thus lead to a degradation of the eC temperature change and stress. Besides the chain breakage, the residual SIC may also occur after fatigue cycles. The influence of the chain breakage and residual SIC on eC temperature change and stress is further investigated by the self-recovery of NR.

The self-recovery experiment is conducted after 650 fatigue cycles. It consists of two measurements, one was conducted right after the fatigue cycles, called "instant measurement", and the other was conducted after 10 hours, called "rest measurement". In both measurements, the eC temperature change and stress at different strains were measured. The comparison of these two measurements is shown in Fig.4. 5. It exhibits the self-recovery mechanism of NR material. In Fig.4. 5 (a), the temperature change of the "rest measurement" is larger than that of the "instant measurement" from strain of 3.5 to 6. In Fig.4. 5 (b), the stress is on the contrary almost the same in the two measurements. This shows again that eC temperature change and stress are governed by different mechanisms. Interestingly, the difference of the temperature change in two measurements begins at the strain of 3.5, which indicates the recovery of temperature change may be due to the SIC. After 650 deformation cycles, residual SIC may exist. In the "instant measurement", the residual SIC chains wouldn't contribute to temperature change. After 10 hours, the residual SIC melts and these residual SIC chains can further crystallize and contribute to the eC temperature change (which is relative to the enthalpy of crystallization). The residual SIC may be the further development of the inertia effect of SIC chains. It should be noted that the temperature change (6 K) after recovery hasn't reached the temperature change (7 K) in the first characterization. It may be due to irreversible chain transition of the chain breakage. The residual SIC may be related to the SIC growth part. The fast stretching stress is mainly related to the SIC nucleation part. Thus, the melting of the residual SIC shouldn't influence the stress extensively. The degradation of stress from 10 cycles to 650 cycles may thus mainly come from the chain breakage.

An advantage of NR, acting as eC material, is the capability of self-recovery, which can heal the fatigue damage of deformation. To further improve the recovery capability and shorten the recovery time of NR, it can be exposed in a high temperature or a solvent, which can induce a complete recovery[12].

In conclusion, from the first cycle to 10 cycles, the main chain transition is the inertia effect of SIC chains, which results in the large degradation of stress and almost no degradation of temperature change. From 10 cycles to 650 cycles, the degradation of stress is due to the chain breakage. For degradation of the temperature change, one part may be due to the residual SIC and the other part may be due to the chain breakage. Moreover, it's proved that the Mullins effect in the first 10 cycles mainly comes from the inertia effect of SIC chains rather than the chain breakage. After a large number of cycles, the Mullins effect mainly comes from the chain breakage. After about 800 deformation cycles, the NR sample appears a large number of white points and begins to crack. The white point may be the residual SIC network point.

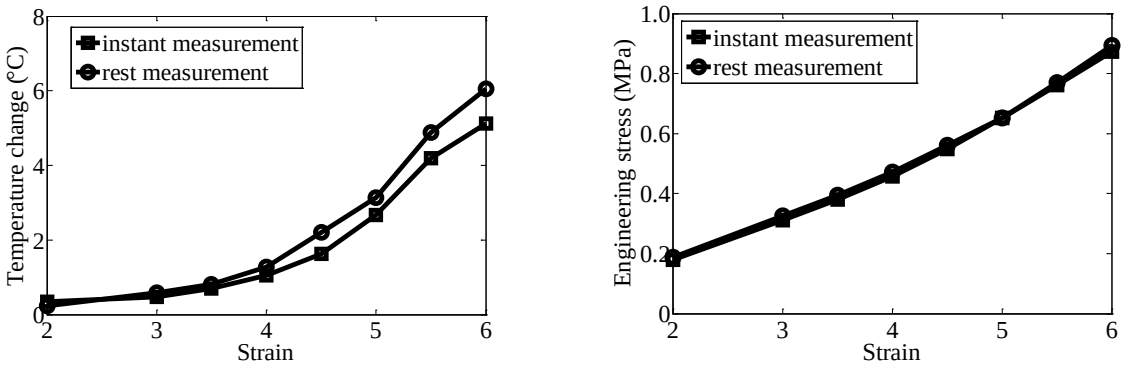


Fig.4. 5 After 8*80 deformation cycles, (a) the temperature change and (b) the stress were measured instantly and after 10 hours, which exhibits the self-recovery mechanism of eC effect of NR.

As a conclusion, although presenting a very large eC temperature change, large strain amplitude (from strain of 1 to strain of 6) are associated to large degradation of both eC temperature change and stress, and material crack for a small number of cycles (a few hundreds). This observation demonstrates that such a small number of cycles before crack at this strain regime is inadequate for eC cooling system. Thus, in order to increase the fatigue life and get an adequate number of cycles used for cooling systems, a decrease of the strain amplitude is tested, since it was already demonstrated that this could increase largely the fatigue life[8–10]. The question is which strain regime is better for eC application.

4.3.2. The fatigue test at small strain amplitudes

The choice of strain regime with small strain amplitude should be related to the occurrence of SIC. SIC occurs at around strain of 3. When SIC occurs in extension in a deformation cycle, its melting strain in retraction is lower than the onset strain of SIC due to the SIC-strain hysteresis, which is around strain of 2[67]. The fatigue property of NR can be improved by SIC[88,107], and the strain regime should be chosen according to both onset strain of SIC and the melting strain[108,163].

Keeping the same strain amplitude of 3, the degradations of both eC temperature change and stress were measured for three different strain regimes, before the onset of SIC (strain of 0-3), at the onset strain of melting (strain of 2-5), and high strain of SIC (strain of 4-7). Strain of 0-3 is referred as amorphous strain regime and strain of 2-5, 4-7 are referred as SIC strain regimes. When studying fatigue at a different strain regime, a virgin sample was systematically used.

The fatigue property of eC effect for a strain of 0-3 was tested first. In Fig.4. 6 (a), it is shown that the eC temperature change was almost stable during the 2200 cycles whereas stress decreases continuously with the logarithm of the number of fatigue cycles. After 2200 cycles, the degradation of stress is found to be around 10% (Fig.4. 6 (b)). When reaching 2000 cycles, some cracks appeared. From 2200 cycles, numerous cracks of 1-3 mm size appeared indicating irreversible damage of the sample and indicating a very short fatigue life.

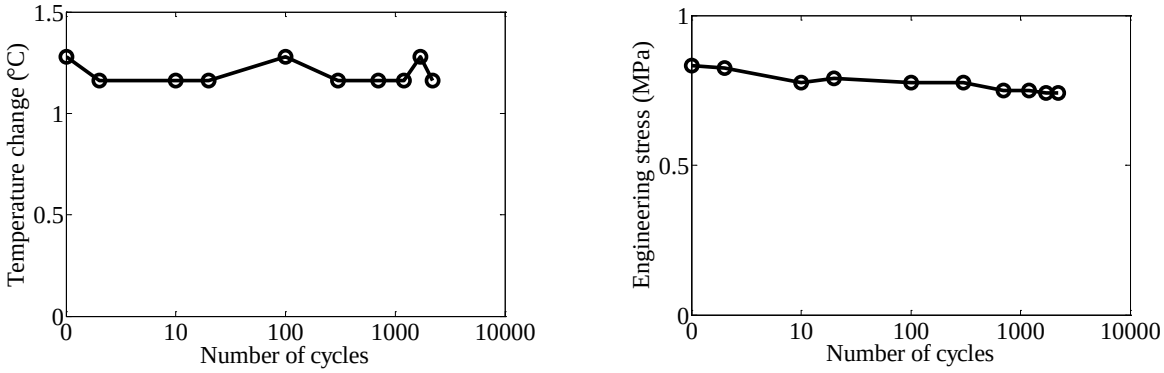


(a) (b)

Fig.4. 6 (a) Degradation of the eC temperature change, and (b) degradation of the stress versus the number of fatigue cycles at amorphous strain regime (strain of 0-3).

In case of the second tested strain regime (strain from 2 to 5), it is observed that no cracks appeared and the sample remain undamaged whatever the number of cycles tested (>3000 cycles). When comparing this observation to the previous case of strain regime of 0-3, the protection mechanism of SIC is evidenced. The degradations of eC temperature change and stress are shown in Fig.4. 7. From first cycle to 100 cycles, there is a clear decrease of the eC temperature change from 4 K to 3.3 K, representing a degradation degree of 17%. For stress, it degrades from 1.16 MPa to 0.83 MPa (degradation degree of 28%), which is larger than the degradation degree of eC temperature change. As described in section 3.1, it is attributed to the inertia effect of SIC chains, which is kind of memory effect of polymer chains. From 100 cycles to 3000 cycles, both the eC temperature change and stress are observed to be stable, showing that the internal structure of the material recovers its initial state from one cycle to another cycle. Moreover, it indicates the absence of irreversible processes, such as chain breakage.

The fatigue property can be associated to the ability of crack growth resistance[9]. SIC can freeze the network chains, making them avoid the coil-stretch transition and thus avoid the occurrence of fatigue. Furthermore, SIC can bind many chains forming a SIC network, which can effectively prevent cracks formation and growth[88,107]. Thus, the material remains intact after 3000 deformation cycles at strain of 2-5. On the contrary for strain amplitude of 0-3, no freezing effect of SIC avoids the occurrence of fatigue of network chain and no SIC network resists to crack formation and growth.

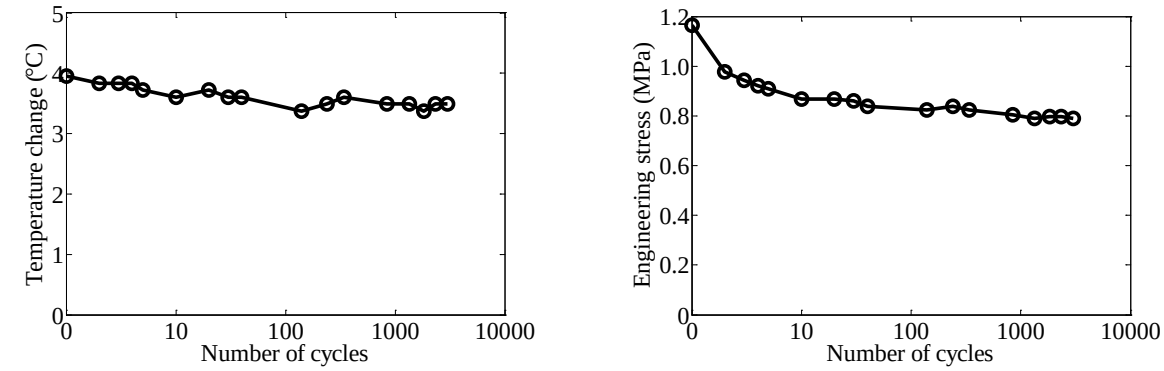


(a) (b)

Fig.4. 7 (a) The degradation of the eC temperature change, and (b) degradation of the stress versus the number of fatigue cycles at SIC strain regime (strain of 2-5).

The fatigue property of eC effect for strain of 4-7 was finally tested. After 3000 deformation cycles, no cracks were observed, which exhibits the same protection mechanism of SIC as for strain

amplitude of 2-5. In Fig.4. 8, the degradations of eC temperature change and stress are displayed. From first cycle to 500 cycles, the eC temperature change remains constant, whereas the stress continuously decreases. For 500 cycles, the degradation degree of eC temperature change is measured to be 7%, whereas the stress degradation degree is 28%. Similarly to the case of strain of 1-6 and strain of 2-5, where a small degradation degree of eC temperature change but a large degradation degree of stress is observed, which may be attributed to the inertia effect of SIC chains. From 500 cycles to 3000 cycles, the eC temperature change becomes stable, whereas the stress always continuously decrease in the logarithmic scale of the number of cycles up to 3000 cycles. The trend is however different from the stable stress state after 100 fatigue cycles at strain regime of 2-5 (Fig.4. 7 (b)). It should be noted that a linear scale for the number of fatigue cycles leads to a stabilization of the stress versus the number of cycles.

In order to provide a selection criterion for further eC cooling application, the results are summarized and compared for the three tested strain regimes. The eC effect is reported in terms of adiabatic temperature change or isothermal entropy change[11,19,20]. For the same strain amplitude, the stable eC temperature changes after large number of cycles at the three strain regimes are compared. The eC temperature change at the strain of 0-3, 2-5 and 4-7 are 1.2 K, 3.5 K and 4.2 K, respectively. It indicates that the eC temperature changes at SIC strain regimes (strain of 2-5 and 4-7) are much larger than that of amorphous strain regime (strain of 0-3) due to the latent heat of SIC. It confirms that SIC strain regime must be chosen for eC application. Similarly, in a previous paper[4], it was demonstrated that the best eC performances for pre-strained conditions were also obtained at the onset of SIC for a similar NR.

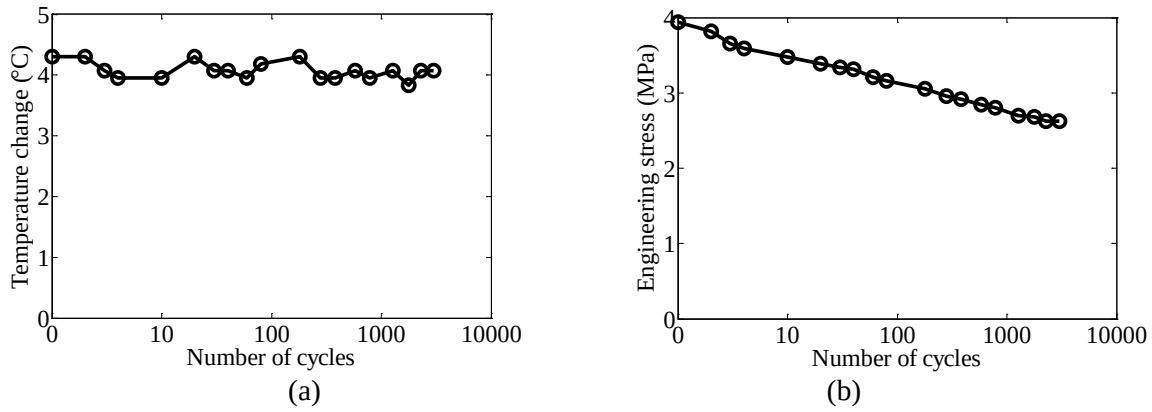


Fig.4. 8 (a) The degradation of the temperature change; (b) The degradation of the stress in logarithmic time scale during the 3000 deformation cycles at strain of 4-7.

It was observed the longer fatigue life at SIC strain regimes (strain of 2-5, 4-7) than amorphous strain regime (strain of 0-3), which further proves that the SIC strain regime should be chosen for eC application. Moreover, in an attempt of comparing the experimental results, the fatigue property is illustrated by the degradation degree of stress. In Fig.4. 9, the degradation degrees of stress at strain regimes of 0-3, 2-5 and 4-7 are compared. Reaching 2000 cycles, the degradation degree is measured to be 10%, 32% and 33% at strain regimes of 0-3, 2-5 and 4-7 respectively. The degradation degrees of stress at SIC strain regimes are larger than amorphous strain regime, which was attributed to the inertia effect of SIC chains. Meanwhile, the larger degradation degree observed is also associated to a much better crack growth resistance of SIC and longer fatigue life. It might be concluded that the larger degradation degree of stress induces a better crack resistance, although inducing larger degradation degree of stress.

In this work, the limited number of fatigue cycles at strain regimes of 2-5 and 4-7 may be not relevant to a fatigue damage situation. However, reaching 3000 cycles already reveals strong

differences between the different strain regimes. In Fig.4. 9, it's worth noting that the degradation degree of strain of 4-7 is always lower than that of strain 2-5, but the tendency show a continuous degradation of stress. On the contrary, for strain 2-5, the degradation degree increases from the first cycles but stabilizes rapidly to a value around 30%. If these tendencies are kept identical for further increase of the number of cycles, one might easily foresee that the degradation degree for strain regime of 2-5 will increase a little whereas the degradation degree for strain regime of 4-7 will still increase.

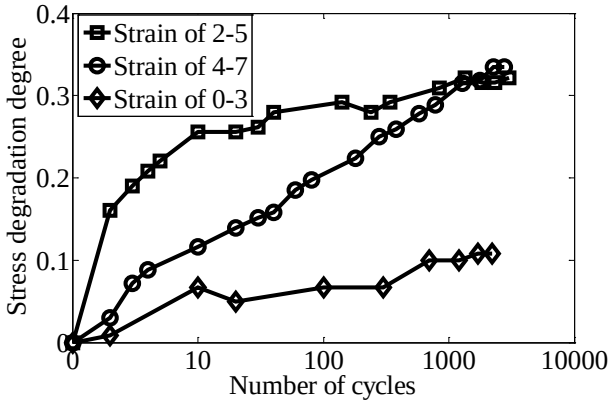


Fig.4. 9 Comparison of the stress degradation degrees at SIC strain regimes (strain of 2-5 and 4-7) and amorphous strain regime (strain of 0-3).

In order to interpret the stress degradation phenomenon after large number of cycles for the three strain regimes, the stress relaxation effect for a single deformation cycle can be used. The stretching stress comes from the coil-stretch and nucleation transition[121,147], while the stress relaxation is induced by SIC growth[106]. SIC growth degree can be estimated qualitatively by a stress relaxation ratio,

$$\alpha_\sigma = \frac{\sigma_{relaxed}}{\sigma_{stretching}} \tag{4. 3}$$

where $\sigma_{relaxed} = \sigma_{stretching} - \sigma_{retraction}$ is the difference of the stretching stress and the retraction stress (the definition of the different stresses are illustrated in Fig.4. 1 (b)), i.e. the relaxed stress at the applied strain.

In Fig.4. 10, the stress relaxation ratios at strain regimes of 0-3, 2-5 and 4-7 are shown. The stress relaxation ratio at strain regime of 2-5 is larger than at strain regime of 4-7, which indicates a larger SIC growth degree. It is interpreted that a larger SIC growth degree should be associated to a larger inertia effect of SIC chains and a larger stress degradation (more details in 3.1). Thus, the larger stress relaxation at strain of 2-5 is correlated with the rapidly obtained stable stress degradation degree at strain of 2-5 than at strain of 4-7.

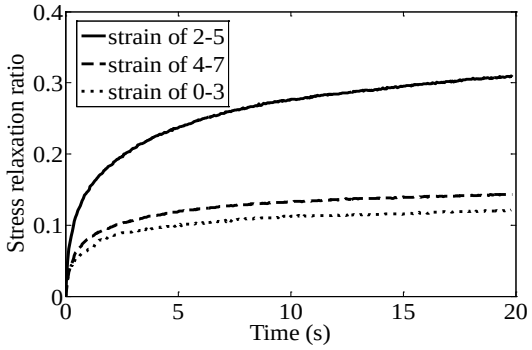


Fig.4. 10 The stress relaxation ratios at strain of 0-3, 2-5 and 4-7. The onset strain of melting (strain of 2-5) exhibit a higher relaxation than amorphous strain regime (strain of 0-3) and high strain of SIC (strain of 4-7).

In Fig.4. 3, the “horn” shape of the degradations of temperature change and stress may indicate the good fatigue property at middle strain and bad fatigue property at high strain (the fatigue property at SIC strain regime is only considered). Similar result can be obtained in Fig.4. 9 and Fig.4. 10. The small stress relaxation ratio indicates the dominant stress hardening effect of SIC at strain of 4-7 and the related SIC mechanism has been discussed in Fig.4. 3. The tendency of continuous stress degradation after 3000 cycles at strain of 4-7 may indicate the bad fatigue property. On the contrary, the larger stress relaxation in the keeping time of applied strain and the rapidly obtained stable stress in less number of cycles at strain of 2-5 may indicate the good fatigue property. This can be further proved by the result of Cadwell et al.[10]. They tested the fatigue life dependence on the minimum stretching strain and strain amplitude. For constant strain amplitude, the fatigue life of NR improves with increasing minimum strain up to a moderately minimum strain level, beyond which fatigue life decreases with increasing minimum strain. It indicates that the moderately minimum strain with the longer fatigue life should be the onset strain of SIC, which may correspond to our tested strain regime of 2-5, and the shorter fatigue life should occur at the high strain of SIC, which may correspond to our tested strain regime of 4-7.

The eC performances at the two SIC strain regimes, onset strain of melting (strain of 2-5) and high strain of SIC (strain of 4-7) are finally compared. Considering another caloric effect, such as electrocaloric effect, and in order to evaluate performance of different materials, the reported electrocaloric temperature changes are often normalized per unit of the applied electric field[17]. Thus, in order to evaluate the eC performance and enable insight into the intrinsic properties of eC effect of NR at different strain regimes, the temperature changes at different strain regimes should be normalized by the corresponding stretching stress,

$$\gamma = \frac{\Delta T}{\sigma_{stretching}} \tag{4. 4}$$

This is referred as eC stress coefficient. Considering the stable state after 3000 cycles, the eC stress coefficient at onset strain of melting (strain of 2-5) and high strain of SIC (strain of 4-7) are $\gamma_{2-5} = 4.4K/MPa$ and $\gamma_{4-7} = 1.6K/MPa$, respectively. It should be noted that in both cases, the strain amplitude is $\Delta\varepsilon = 3$. The lower value of the coefficient for strain regime of 4-7 is a consequence of working in the upturn of the stress-strain behavior, which is a consequence of the stress hardening effect of SIC, so that the same strain amplitude requires a much larger stress. Thus, the higher eC performance is obtained at the onset strain of melting. Consequently, considering the longer fatigue life and higher eC performance at the onset strain of melting (strain of 2-5), this strain regime should be chosen for eC cooling applications.

At strain of 2-5, a fatigue test of high cycles (up to $1.7 \times 10^5$) was conducted. To do so, a specific equipement was developed using a rotating motor for imposing the cyclic deformations. As a consequence, the measurment of both eC effect and stress were not obtained at the same strain rate as usual, explaining the very small discrepencies compared to the previous results. After $1.7 \times 10^5$ cycles, there was no crack, thus indicating the excellent fatigue life of the NR material. In Fig.4. 11, the degradations of eC temperature change and stress were shown up to $1.7 \times 10^5$ cycles. The eC temperature change degraded from 4.2 K to 3.7 K with the degradation degree of 12%. The stress degraded from 1.3 MPa to 0.7 MPa with a degradation degree of 46%, which is much larger than the degradation degree of eC temperature change. The eC temperature change and stress were almost stable after $1.7 \times 10^5$ cycles. It proves the feasibility of NR applicable for high cycles cooling application.

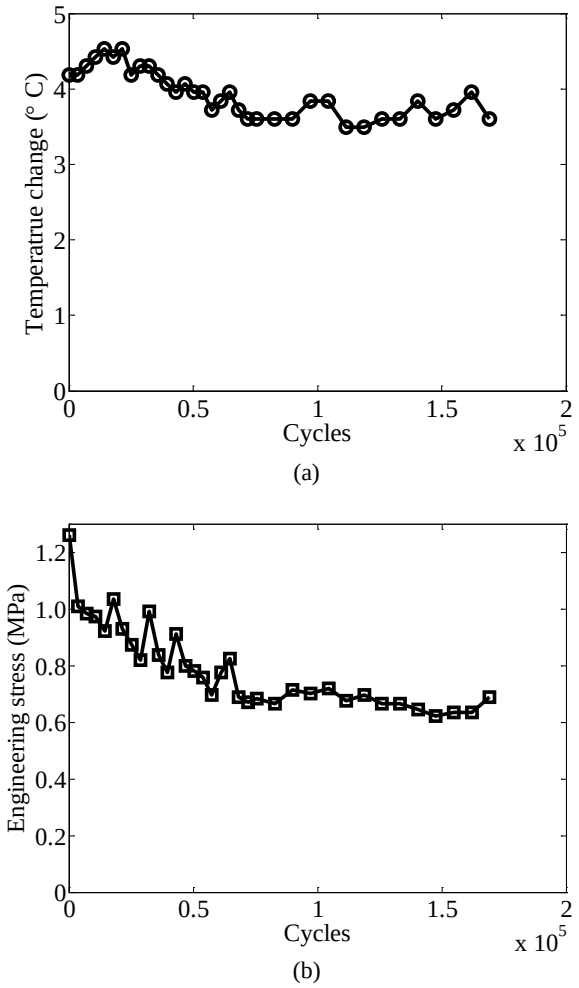


Fig.4. 11 The degradations of (a) eC temperature change and (b) stress during $1.7 \times 10^5$ cycles.

## 4.4. Conclusion

The fatigue of elastocaloric (eC) effect in natural rubber (NR) was investigated. Using deformation cycles at strain regime of 1 to 6, NR cracks from a limited number of cycles (~800 cycles) showing a very short fatigue life. This limited number makes the material totally inadequate for cooling applications where a very large number of cycles would be necessary. Thus, in order to increase the fatigue life and get an adequate number of cycles for cooling systems, the method of decreasing strain amplitude can be utilized.

The fatigue of eC effect was investigated for three strain regimes with a same strain amplitude of 3 (strain of 0-3, 2-5 and 4-7). Strain of 0-3 is the amorphous strain regime and strain of 2-5, 4-7 are the SIC strain regimes. It is observed that the fatigue life of eC effect of NR is improved and temperature change is higher when working at SIC strain regimes (strain of 2-5 and 4-7) rather than amorphous strain regime (strain of 0-3). Moreover, the stress degradation at SIC strain regime (strain of 2-5 and 4-7) are larger than amorphous strain regime (strain of 0-3).

For both SIC strain regime (strain of 2-5 and 4-7), there is a large stress degradation but a slight temperature change degradation. At strain regime of 2-5, there is a quicker stabilization of the stress than strain regime of 4-7. The stress at strain regime of 4-7 keeps decreasing up to 3000 cycles. This may be related to the larger stress relaxation in the keeping time of the applied strain of 2-5 than strain of 4-7. It is concluded that working at the onset of SIC melting (strain of 2-5) induces a better fatigue

life and smaller degradation of stress than when working at high strain of SIC (strain of 4-7). Furthermore, to compare the eC performances at onset of SIC and high strain of SIC, an eC stress coefficient $\gamma = \Delta T / \sigma_{stretching}$ is defined. The eC stress coefficient at strain of 2-5 $\gamma_{2-5} = 4.4K / MPa$ is larger than strain of 4-7 $\gamma_{4-7} = 1.6K / MPa$, which shows that the highest performance is obtained at the onset of melting (strain of 2-5).

Although the 3000 cycles in SIC strain regimes are still far from realistic working conditions of eC effect based cooling systems, it is determined that the SIC strain regime is promising whereas other strain regimes are not satisfactory. This proves the fatigue life can be improved through decreasing strain amplitude and choosing the SIC strain regimes.

The high-cycle fatigue test is finally applied at strain of 2-5. It's found that no crack occurs after $1.7 \times 10^5$ cycles. The eC temperature change was 3.7 K and kept stable after $4 \times 10^4$ cycles. The order of $10^5$ cycles is closer to the requirement ($10^6$-$10^7$ cycles) for a cooling device. It proves the feasibility of NR applicable for high-cycle cooling application. This work constitutes a first step toward the application of eC effect of NR. Further fatigue test on higher cycles ($10^7$) is needed, as well as checking the influence of combined stress and temperature cycles, typical to those encountered in heat engines.

# Chapter 5 The application of elastocaloric effect

## 5.1 Introduction

Elastocaloric materials, when driven with cyclic strain, exhibit time variations of their temperature. For cooling systems, it is necessary to design a thermal/mechanical system for transforming the temporal variation into spatial thermal gradients. A simple and intuitive way is to move cyclically the eC material from the cold and hot sources synchronously with the strain. An example of the performance using a Carnot cycle is given in Appendix 2. However, doing so, the system might me quite complicated on the one hand, and the maximal temperature gradient that may be achieved is limited by the adiabatic temperature change of the eC material.

Regenerative systems are a promising way to enhance the overall temperature gradient, while at the same time solving the problem of temporal variation into gradient transformation. For MC effect, the active magnetic regenerator (AMR) was shown to be so far the most efficient way in all up-to-date magnetic refrigerators[16]. It consists of using a magnetocaloric bed on which a fluid flowing along the cooling axis synchronously to the magnetic field application as described in Chapter 1. A similar AMR system by using eC effect is proposed by Tusek et al.[11]. They showed in particular that the eC cooling can significantly exceed the performance of a magnetic refrigerator (with Gd) with comparable or even higher efficiency at high temperature spans.

Numerical models for simulating the operation and performance of an AMR in magnetic refrigerator were already well-developed[164], and they can be also used for the eC refrigerating systems. Earlier 1D models assume that the fluid flow and the thermal conduction occur only in the downstream fluid direction[165]. Moreover, the intra-particle thermal conduction is neglected and a heat-transfer coefficient between the fluid and the solid matrix is required. Recently, a 2D model of the AMR was developed[166]. It takes into account the 2D velocity field and thermal conduction, which is established both in the downstream direction of the fluid flow and one transverse direction. Equations for the fluid and the solid matrix in 2D models are not directly coupled through an arbitrary heat-transfer coefficient, but consider an additional boundary condition that defines the thermal contact between the fluid and the solid, which is physically more appropriate than the use of the heat transfer coefficient. However, 2D models can only be applied for AMRs with ordered structures (flat parallel plates, square channel, etc.). In general, a fully developed 3D model could be applied to any geometry. The first attempt of the 3D AMR model is presented in Bouchard et al.[167].

In the previous chapters, the different properties of eC effect of NR were measured. Adiabatic temperature variation upon strain is comparable to the best other caloric materials. Moreover, the fatigue properties were quantified for a few thousands of cycles, and it is believed that a much larger number of cycles is feasible as shown in other studies. It proves preliminary the feasibility of NR acting as eC material for cooling application. For further development of eC effect based cooling systems, it is of primary importance to determine the relevant properties. Does the highest eC effect lead to the highest performance? What other parameters influences the device performances? In order to start answering to these questions, a theoretical model was developed for a regenerative system. In this chapter, a 2D model for AMR of eC effect is developed. The assumptions, necessary to converge towards analytical solutions, are limiting the applicability and the accuracy of the model, but it is believed that the main tendencies will be kept the same. After the presentation of the model, several simulation results are presented and a tentative prototype

design is proposed including the quantification of the cooling power and temperature difference that may be achieved.

In this part, the first objective is to show a regenerative cooling effect along one axis. On the other hand, the different properties (like thermal conductivity) are varied in order to search for the best performance.

## 5.2 Model presentation

The model developed here follows a decomposition of the 2D problem into two successive 1D problems considering the different time and length scales between both directions. It follows a modeling strategy already used in case of thermo-acoustic devices. Relevant theoretical investigations devoted to thermo-acoustic devices were published in thesis of G. Poignant[168] and related publications[169–171].

### 5.2.1 Presentation of the problem

The cooling device is composed of an active material sandwiched between two passive materials (Fig.5. 1). The materials are plate-shaped in the xOy plane, with large lateral dimensions compared to their thickness. The infinite dimension along y axis and the absence of motion along y axis leads to the assumption of invariance of all variables along y axis.

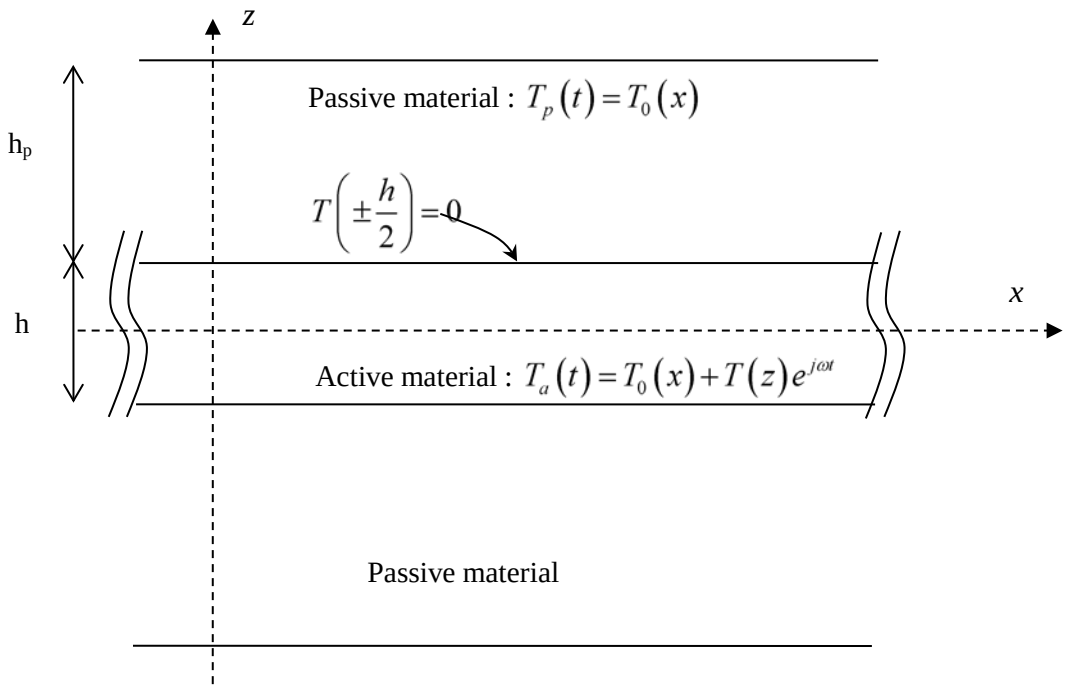


Fig.5. 1 The schematic diagram of the cooling device.

The active material moves along the x axis with a sinusoidal motion.

$$\vec{v}(x,t) = v(x,t)\overrightarrow{u_x} = \underline{v_0}(x)e^{j\omega t}\overrightarrow{u_x} = v_0 e^{j\varphi}e^{j\omega t}\overrightarrow{u_x} \quad (5.\ 1)$$

Phase $\varphi$ is the phase shift between the speed of the active layer and the caloric effect.

The active material is a caloric material. At this stage of the model definition, we don't consider the exact nature of the caloric effect. It may be MC, EC or eC effect. When driven by the relevant excitation, the active material is subjected to an internal heating given by

$$Q(t) = q_0 e^{j\omega t} \tag{5. 2}$$

In the case of a eC effect,

$$q_0 = T_0 \beta \varepsilon_0 \tag{5. 3}$$

where $\varepsilon_0$ is the applied strain and $\beta$ is eC strain coefficient as defined in Chapter 2.

The passive material plays the role of both a heat transfer and heat storage medium. In should be noted that some fluids could be used, such as water, oil, etc. In this case, we could consider a static non-moving active material and moving passive materials. Since the only relative motion is responsible for the cooling capability of the device, this model could be further extended to any situation of passive and active layers, moving or not.

For the sake of simplicity, for this first model development, it was chosen static passive layers and one moving active layer.

### 5.2.2 Thermal equation of active material

#### *5.2.2.1 Assumptions*

The passive material is assumed to exhibit a thermal conductivity and heat capacity far superior to those of the active material. As a consequence, its temperature variation with time is neglected compared to those of the active material. In other words, it acts as a boundary with a static temperature gradient. As earlier assumed, only the temperature gradient along x axis is considered. Thus the temperature of the passive material is written

$$T_p(t) = T_0(x) \tag{5. 4}$$

- The edge effects along y axis are neglected.

- In the equation of heat diffusion of the active material, variations along z are assumed to exhibit very large variations compared to variations along x. In addition, the temperature at the contact points between two adjacent materials (z = + / - h / 2) are identical. Given these assumptions, the temperature of the active material is written

$$T_a(t) = T_0(x) + T(z)e^{j\omega t} \text{ and } T\left(\pm\frac{h}{2}\right) = 0 \tag{5. 5}$$

#### 5.2.2.2 *Heat diffusion in the active material*

The general equation of heat transfer[172] is*:*

$$T_a(\mathrm{x},t)\left(\frac{\partial S_a(\mathrm{x},t)}{\partial t} + \overrightarrow{v(\mathrm{x},t)}.\overrightarrow{grad}\left(S_a(\mathrm{x},t)\right)\right) = div\left(\lambda_a.\overrightarrow{grad}\left(T_a(\mathrm{x},t)\right)\right) \tag{5. 6}$$

where, $S_a$, $\lambda_a$ are the entropy and heat conductivity of the active material, respectively. The entropy change of the active material is written

$$T_a dS_a = dQ + c_a dT_a \tag{5. 7}$$

Note that in this case, the term dQ correspond to the internal heat source related to the caloric coupling. It does not refer directly to the heat exchange with outer medium which is given by TdS. Thus,

$$\frac{\partial S_a(x,t)}{\partial t} = \frac{1}{T_a(x,t)}\left(\frac{\partial Q(x,t)}{\partial t} + c_a \frac{\partial T_a(x,t)}{\partial t}\right) \tag{5. 8}$$

where $c_a$, $dQ(x,t)$ are the specific heat capacity and the eC heat of active material.

Assuming that the thermal conductivity is homogeneous and isotropic, and eC heat is uniform throughout the active material,

$$div\left(\lambda_a . \overrightarrow{grad}\left(T(x,t)\right)\right) = \lambda_a div\left(\overrightarrow{grad}\left(T(x,t)\right)\right) = \lambda_a \nabla T(x,t)$$

$$\overrightarrow{grad}\left(S_a(x,t)\right) = \frac{c_a}{T_a(x,t)} \overrightarrow{grad}\left(T_a(x,t)\right)$$

The speed of the active material is only along x, the thermal equation is

$$c_a\left(\frac{\partial T_a(x,t)}{\partial t} + v\frac{\partial T_a(x,t)}{\partial x}\right) + \frac{\partial Q(x,t)}{\partial t} = \lambda_a \nabla T_a(x,t) \tag{5. 9}$$

Considering that the heat transfers are neglected along x axis compared with z axis, and keeping only harmonic terms ($e^{j\omega t}$),

$$c_a\left(j\omega T + \underline{v_0}\frac{\partial T_0}{\partial x}\right) + j\omega q_0 = \lambda_a \frac{\partial^2 T}{\partial z^2} \tag{5. 10}$$

*5.2.2.3 Solution for the temperature variation T*

Eq. (5.10) is rewritten as

$$\frac{\partial^2 T}{\partial z^2} - \frac{j\omega c_a}{\lambda_a} T = \frac{c_a}{\lambda_a}\underline{v_0}\frac{\partial T_0}{\partial x} + \frac{j\omega q_0}{\lambda_a} \tag{5. 11}$$

The general solution of Eq. (5.11) is

$$T = A\cos kz + B\sin kz + \frac{1}{k^2}\left(\frac{c_a}{\lambda_a}\underline{v_0}\frac{\partial T_0}{\partial x} + \frac{j\omega q_0}{\lambda_a}\right) \tag{5. 12}$$

where $k = \sqrt{-\frac{j\omega c_a}{\lambda_a}} = \pm\frac{1-j}{\delta}$ and $\delta = \sqrt{\frac{2\lambda_a}{\omega c_a}}$ is the thickness of the thermal boundary layer[168].

By applying the boundary condition $T\left(\pm\frac{h}{2}\right) = 0$, $T$ is obtained

$$T = \left(j\frac{v_0}{\omega}\frac{\partial T_0}{\partial x} - \frac{q_0}{c_a}\right)\left(1 - \frac{\cos kz}{\cos\frac{kh}{2}}\right) \tag{5. 13}$$

*5.2.2.4 Heat flux of the active material*

The flow of instant heat that passes through the unit area per unit time in the x direction is written

$$\frac{dQ_a}{dt}(x,t) = T_0 S_a(x,t) v(x,t) \tag{5. 14}$$

The time average heat flux is given by

$$p_a = \left\langle \frac{dQ_a}{dt} \right\rangle = \frac{1}{2}\mathrm{Re}\left\{ T_0 \underline{S_0 v_0}^* \right\} \tag{5. 15}$$

where

$$\underline{S_0} = \frac{q_0 + c_a \underline{T}}{T_0} \tag{5. 16}$$

The total heat flux through the section of the active material is given by

$$P_a = l \int_{-\frac{h}{2}}^{\frac{h}{2}} p_a dz \tag{5. 17}$$

where $l$ is the width of active material along y axis.

$$P_a = \frac{l}{2} \int_{-\frac{h}{2}}^{\frac{h}{2}} \mathrm{Re}\left\{ T_0 \underline{S_0 v_0}^* \right\} dz$$

$$P_a = \frac{l}{2} \int_{-\frac{h}{2}}^{\frac{h}{2}} \mathrm{Re}\left\{ \left( q_0 + c_a \left( j \frac{\underline{v_0}}{\omega} \frac{\partial T_0}{\partial x} - \frac{q_0}{c_a} \right) \left( 1 - \frac{\cos kz}{\cos \frac{kh}{2}} \right) \right) \underline{v_0}^* \right\} dz$$

$$P_a = \frac{l}{2} \int_{-\frac{h}{2}}^{\frac{h}{2}} \mathrm{Re}\left\{ \left( j \frac{c_a \underline{v_0}}{\omega} \frac{\partial T_0}{\partial x} + \left( j \frac{c_a \underline{v_0}}{\omega} \frac{\partial T_0}{\partial x} - q_0 \right) \left( - \frac{\cos kz}{\cos \frac{kh}{2}} \right) \right) \underline{v_0}^* \right\} dz$$

After calculation, we obtain:

$$P_a = \frac{l}{2}\mathrm{Re}\left\{ \left[ j \frac{c_a {v_0}^2}{\omega} \frac{\partial T_0}{\partial x} h + \left( -j \frac{c_a {v_0}^2}{\omega} \frac{\partial T_0}{\partial x} + q_0 \underline{v_0}^* \right) \frac{2}{k} \tan \frac{kh}{2} \right] \right\} \tag{5. 18}$$

The first term is imaginary, its contribution to the real part is zero.

We write $\frac{2}{k}\tan\frac{kh}{2} = \delta \frac{\sin\xi + \sinh\xi}{\cos\xi + \cosh\xi} + j\delta \frac{\sin\xi - \sinh\xi}{\cos\xi + \cosh\xi}$, with $\xi = \frac{h}{\delta}$.

We assume in addition that the motion of the active material is in phase with the caloric effect. Since the speed of the active material is the time derivative of its displacement, the speed writes

$$v(x,t) = j v_0 e^{j(\omega t)} \tag{5. 19}$$

Then $\underline{v_0}^* = -j v_0$,

$$P_a = \frac{l}{2}\mathrm{Re}\left\{ \left[ \left( \delta \frac{\sin\xi + \sinh\xi}{\cos\xi + \cosh\xi} + j\delta \frac{\sin\xi - \sinh\xi}{\cos\xi + \cosh\xi} \right) \left( -j \frac{c_a {v_0}^2}{\omega} \frac{\partial T_0}{\partial x} + q_0 \underline{v_0}^* \right) \right] \right\}$$

$$P_a = -\delta_{eff}\frac{l}{2}\frac{c_a v_0^{\,2}}{\omega}\frac{\partial T_0}{\partial x} - \delta_{eff}\frac{l}{2}q_0 v_0$$

where $\delta_{eff} = -\delta\dfrac{\sin\xi - \sinh\xi}{\cos\xi + \cosh\xi}$

The cooling power per unit area is calculated as (the previous result is divided by *hl*)

$$P_{actif} = P_0 - \lambda_{eq}\frac{\partial T_0}{\partial x} \tag{5. 20}$$

In this equation, $P_0 = -\dfrac{q_0\delta_{eff}v_0}{2h}$ corresponds to an active heat flux which is cause by both the caloric effect and the motion of the active layer, $\lambda_{eq} = c_a\dfrac{\delta_{eff}}{h}\dfrac{v_0^{\,2}}{2\omega}$ corresponds to a thermal conductivity induced by the movement.

*5.2.2.5 Maximum temperature*

We can estimate the maximum temperature gradient that can generate the system considering the passive heat flow from hot side to cold side as being equal to the active heat flow from cold side to the hot side:

$$-\left(\lambda_a hl + 2\lambda_p h_p l\right)\frac{\partial T_0}{\partial x} - lh\lambda_{eq}\frac{\partial T_0}{\partial x} + lhP_0 = 0 \tag{5. 21}$$

The maximum temperature gradient is given by

$$\left.\frac{\partial T_0}{\partial x}\right|_{MAX} = \frac{P_0}{\lambda_a + 2\lambda_p\dfrac{h_p}{h} + \lambda_{eq}}$$

## 5.3 Simulation results

### 5.3.1 One example of elastocaloric device

In the following example, we consider an active layer made of natural rubber and a passive layer made of aluminum. The simulation parameters are displayed in Table 1. We obtain the following results:

Thermal boundary layer thickness of $\delta = 1.6\times10^{-4}$ m;

Maximal thermal gradient $\left.\dfrac{\partial T_0}{\partial x}\right|_{MAX} = 0.5$ K/cm;

Maximum cooling power $P_0 = 8\times10^3$ W.m$^{-2}$ and the cooling power of 0.4 W for the designed dimension (cross-sectional area of the whole device 7mm x 1cm).

Table 5. 1. The simulation conditions.

| **Active layer (NR)** | |
|---|---|
| **Thickness [mm]** | 5 |
| **Width [mm]** | 10 |
| **Heat capacity [$J.m^{-3}.K^{-1}$]** | $1.8\times10^{6}$ |
| **Thermal conductivity [$W.m^{-1}.K^{-1}$]** | 0.18 |
| **Adiabatic temperature change [K]** | 4 |
| **Active heat source $q_0$ [$J.m^{-3}$]** | $3.6\times10^{6}$ |
| **Displacement along x-axis [mm]** | 20 |
| **Stretching frequency [Hz]** | 1 |

| **Passive layer (aluminum)** | |
|---|---|
| **Thickness [mm]** | 1 |
| **Width [mm]** | 10 |
| **Heat capacity [$J.m^{-3}.K^{-1}$]** | $2.5\times10^{6}$ |
| **Thermal conductivity [$W.m^{-1}.K^{-1}$]** | 200 |

In the following simulations, the conditions are almost the same with Table 5. 1. For each simulation, one parameter is varied in order to check its influence on the device performances.

### 5.3.2 Limit case

The limit of this model is at the high frequency. In experiment, when the frequency is around 1 Hz, the eC heat can't be released, which results in no temperature decrease. Thus, the cooling power should decrease when the frequency is higher than one value. In Tusek's model, for shape memory alloys (SMAs), when the frequency is above 1 Hz, the cooling power begins to decrease. Whereas in our model (Fig.5. 2), the cooling power and thermal gradient always increase with the increased frequency. This should be due to the assumption of the boundary of a static temperature gradient between active material and passive material.

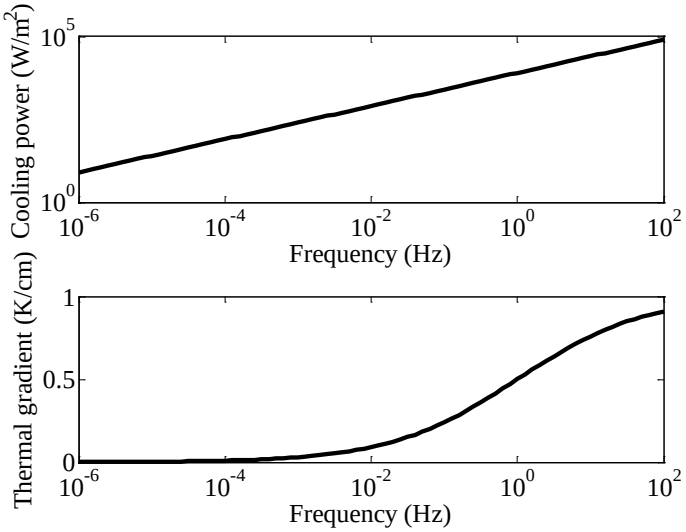


Fig.5. 2 The limit case of the model at high frequency.

### 5.3.3 Thermal boundary layer

The thermal boundary layer indicates the efficiency of heat transfer: the thinner thermal boundary layer and the better heat transfer. The thickness of thermal boundary layer as a function of frequency, heat capacity and thermal conductivity is shown in Fig.5. 3. In Fig.5. 3 (a), the thickness of thermal boundary layer decreases as frequency increases. It may be due to the large convective heat transfer induced by the high speed of active material.

As heat capacity and thermal conductivity increases, the thickness of thermal boundary layer decreases. It indicates the larger heat capacity and smaller thermal conductivity are better for the heat transfer.

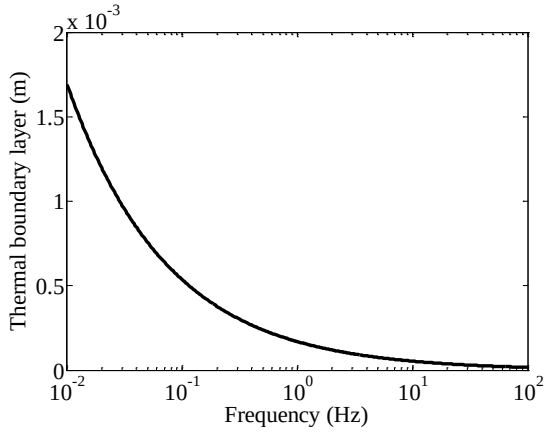


(a)

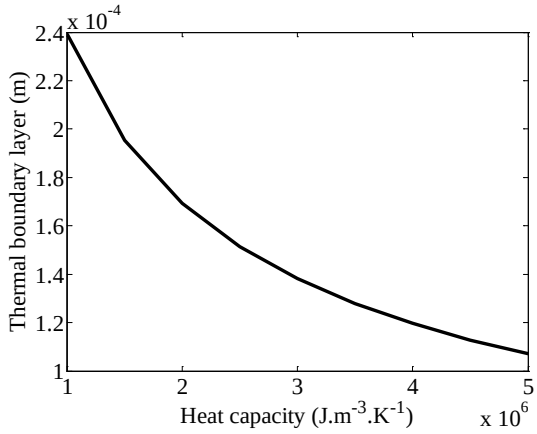


(b)

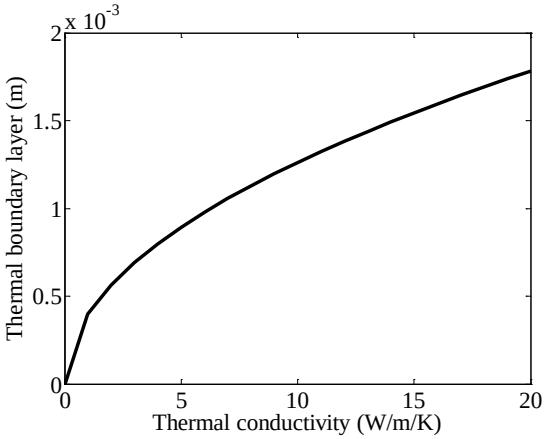


(c)

Fig.5. 3 The thermal boundary layer as a function of (a) frequency, (b) heat capacity, (c) thermal conductivity. For other parameters, refer to the table 5.1

### 5.3.4 Influence of the motion of active layer

The cooling power and thermal gradient denpendence on motion of active layer is shown in Fig.5. 4. As the motion of active layer increases, the cooling power gradually increases. However, thermal gradient first inceases and then decreases with motion of active layer. It indicates there is an optimum motion for the thermal gradient. In this case, the optimum motion of active layer is 0.02 m.

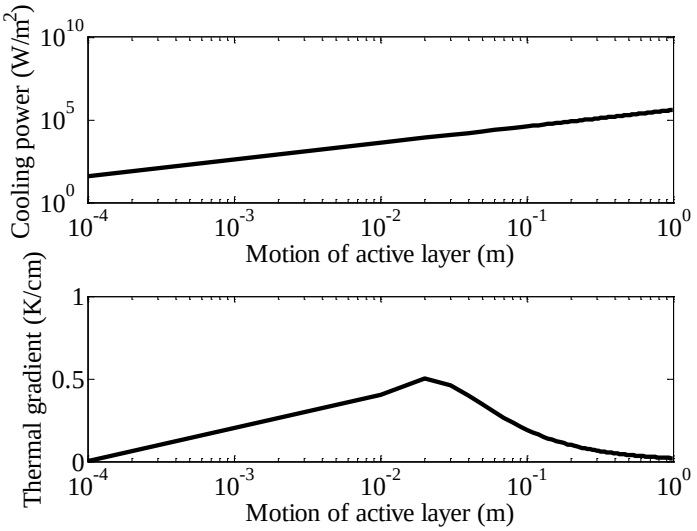


Fig.5. 4 The influence of motion on cooling power and thermal gradient. For other parameters, refer to the table 5.1.

### 5.3.5 Influence of the parameters

The strain amplitude determines the fatigue life[10]. As discussed in Chapter 4, decreasing strain amplitude can increase the fatigue life but decrease the temperature change. Thus, to get a large fatigue life, the temperature change is decreased. We evaluate the eC performance at different temperature changes by using cooling power and thermal gradient. For NR, the temperature change ranges from 1 K to 12 K. In Fig.5. 5, both the cooling power and thermal gradient increase linearly with the temperature change. The larger temperature change shows the obvious advantage for improving the eC performance.

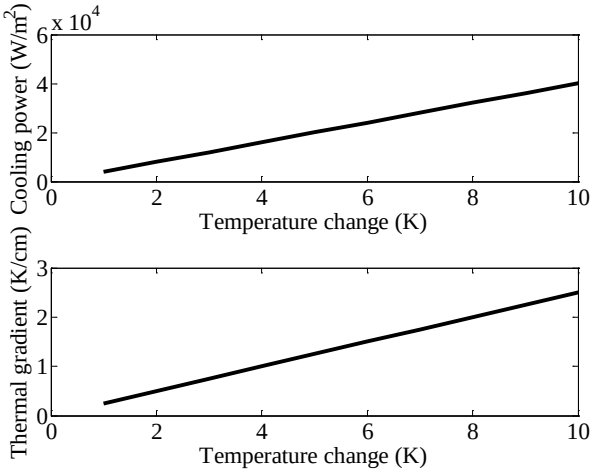


Fig.5. 5 The influence of temperature change on cooling power and thermal gradient. For other parameters, refer to the table 5.1.

The cooling power and thermal gradient as a function of thermal conductivity of active material are shown in Fig.5. 6. The performance of AMR for different MC materials at different thermal conductivities has been investigated by Legait *et al.*[173]. As thermal conductivity increases, both the cooling power and thermal gradient increase. Thus, it's better to choose the eC material with a larger thermal conductivity. Considering this parameter, the shape memory alloys (SMAs) acting as eC materials are better than NR.

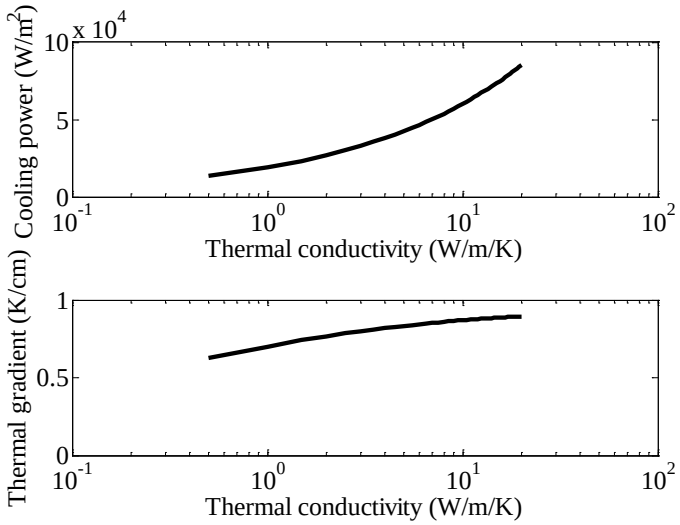


Fig.5. 6 The influence of thermal conductivity on cooling power and thermal gradient. For other parameters, refer the the table 5.1

The cooling power and thermal gradient are compared at different heat capacities of active material. As heat capacity increases, the cooling power increases much, whereas the thermal gradient increases a little (Fig.5. 7). Thus, the eC material with larger volumetric heat capacity can get a higher eC performance.

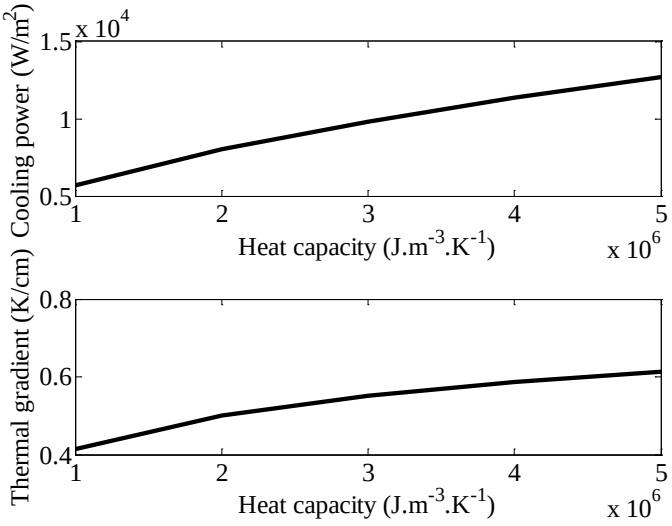


Fig.5. 7 The influence of heat capacity on cooling power and thermal gradient. For other parameters, refer the the table 5.1

## 5.4 Conclusions

Compared to numerical models, the results obtained from this analytical model is less time-consuming and show some principles for choosing the eC materials.

In this model, the eC performance is evaluated in parameters of temperature change, thermal conductivity and heat capacity. For all the parameters, their increase will lead to the increase of the cooling power and almost increase of the thermal gradient. Thus, the eC material with a larger temperature change, larger thermal conductivity and larger heat capacity can obtain a high eC performance.

Considering the conditions of eC effect of NR: strain of 2-5, temperature change of 4 K (experimental results in Chapter 4), thickness of 5 mm and width of 10 mm, then the temperature gradient along the cooling device is predicted to be 0.5 K/cm and cooling power is 0.4 W.

In the further work, some strong assumption of the model need to be removed and a more precise model can be obtained. Considering the requirement of a cooling device towards large-scale application, a multi-layer model needs to be established. Moreover, some experiments need to be conducted for proving this model effectiveness.

# General Conclusion

In the framework of solid-state cooling, the potential of natural rubber (NR) acting as elastocaloric (eC) material is investigated and proved primarily, and constitutes a promising candidate among other caloric materials. Although NR application to cooling device may be seen as uncommon at this stage, some important characterizations were conducted in this thesis. Compared to other caloric materials, such as electrocaloric or magnetocaloric materials, NR exhibits numerous advantages: large effect, good fatigue life; low-cost and environment friendly.

The eC effect of NR is firstly characterized directly by a thermal measurement and interpreted in the view of the strain induced crystallization (SIC). The eC effect dependence on strain is characterized by defining eC strain coefficient and eC stress coefficient, which are defined as $\beta = -\partial s / \partial \varepsilon$ and $\gamma = \partial T / \partial \sigma_{stretching}$ respectively, where $s$ is the specific entropy, $\varepsilon$ is the engineering strain, $T$ is the temperature and $\sigma_{stretching}$ is the stretching stress. Both the eC strain coefficient and the eC stress coefficient exhibit the highest eC efficiency at middle SIC strain (around strain of 4.5). These are attributed to the highest degree of SIC growth at middle SIC strain. Due to the high eC effect at middle SIC strain, a pre-strain of 2 (onset of SIC melting) should be chosen because reduced applied strain is necessary for a compact cooling device on the one hand, and a higher eC efficiency (represented by eC strain coefficient and eC stress coefficient) is observed on the other hand.

The eC effects direct and indirect characterizations are then compared. The indirect measurement is based on the Maxwell relation $\left(\frac{\partial \sigma}{\partial T}\right)_{\varepsilon} = -\left(\frac{\partial s}{\partial \varepsilon}\right)_{T}$ and the deduction of eC temperature change is given by $\Delta T = \frac{T_0}{c}\int_0^{\varepsilon}\left(\frac{\partial \sigma}{\partial T}\right)_{\varepsilon} d\varepsilon$, where $\sigma$ is the engineering stress, $T_0$ is the temperature, and $c$ is volumetric specific heat. The indirect measurement is conducted in two methods. One is to measure the stress-strain behavior at different static temperatures. The other is to measure the stress-temperature behavior at constant strain. It is found that the deduction of temperature change is underestimated or even of opposite sign to the directly measured one in the former method while it is in good quantitative agreement in the latter method. The observed complex stress effects highlight that the stress is not a state variable, thus questioning the ergodic behavior of NR. It is proposed that these behaviors are due to the inhomogeneous property of SIC; different contribution to stress and melting point of SIC nucleation and SIC growth.

Stress and temperature change are two required quantities for eC effect. The eC effect (including stress and temperature change) dependence on temperature is an important property for eC application. The SIC model of Flory is modified to describe both the stress and temperature change of eC effect. The stress model can correspond to the experimental results at different temperatures. The temperature change model can correspond to the experimental results at room temperature. To further prove this SIC model and the potential of NR acting as eC material, the eC temperature change dependence on temperature needs to be further measured. The SIC is mainly responsible for the thermal-mechanical behavior of NR, which cannot be predicted by the standard theory of rubber elasticity. Finally, the

model should be further developed through considering the multi-physics coupling as well as considering SIC.

When the eC temperature change is large enough for a cooling cycle, the fatigue property becomes the most important property for eC cooling device. The fatigue property of eC effect of NR is characterized. At large strain amplitude regime of 1-6, NR cracks after 800 cycles. Such a small number of cycles can't be used for the cooling system. Thus, to decrease the fatigue damage and to get an adequate number of cycles used for the cooling system, the strain amplitude must be decreased. The fatigue property and eC performance at three small strain amplitudes (strain of 0-3, 2-5 and 4-7) are measured and compared. Strain of 0-3 is the amorphous strain regime and strain of 2-5, 4-7 are the SIC strain regimes where SIC occurs. The eC effect at SIC strain regimes (strain of 2-5 and 4-7) has a better fatigue property and higher temperature change than that at the amorphous strain regime (strain of 0-3). It is observed that the larger stress relaxation is correlated to a faster stabilization of the stress state after a large number of cycles, especially for the strain regime at the onset of melting (strain of 2-5). It may have furthermore a better fatigue property. The eC performances at the onset of melting and high strain of SIC are compared by using the eC stress coefficient $\gamma = \Delta T / \sigma_{stretching}$. They are 4.4 K/MPa at strain of 2-5 and 1.6 K/MPa at strain of 4-7, which exhibits a better eC performance at the onset of melting (strain of 2-5). Thus, the onset of melting should be chosen for the eC application.

A stable eC performance (stress and temperature change) after 3000 cycles is observed at the onset strain of melting. It proves that the fatigue property can be improved through decreasing strain amplitude and choosing the appropriate SIC strain regimes. A high cycle fatigue test was conducted at strain regime 2-5. No rupture was observed up to 1.7 $10^5$ cycles and the degradation of eC effect was limited to 12% and stable after 3000 cycles. It's a first step towards the applicability of eC effect of NR in cooling device. In the further work, the fatigue property of eC effect needs to be further characterized in order to obtain statistics of the rupture, as well as fatigue life dependence on temperature.

Finally, considering the feasibility of NR acting as eC material, a simplified analytical model for a regenerative cooling system by using NR material is developed. It can evaluate the eC performance through cooling power and thermal gradient. It exhibits that the higher eC performance can be obtained by the eC material with a larger temperature change, larger thermal conductivity and larger heat capacity. In the further work, some strong assumptions of the model need to be removed and experiments need to be conducted for determining the prediction capability of this model.

To conclude this work, it was experimentally established that using a soft NR at strain regime of 2-5 results in an optimum eC activity, with a temperature change of 4 K and little fatigue dependence up to $10^5$ cycles. Finally, such eC effect might lead to a cooling device using a regenerative system, exhibiting a temperature gradient up to 0.5 K/cm and a cooling power of 0.4 W for a cross-sectional area of 50 $mm^2$. Some of the most important features of NR were highlighted in a comprehensive investigation of its properties and application. Further work should deal with complementary and more complete characterization of NR material and investigation of a cooling device. Research on soft eC materials should be based on SIC in elastomers. For the characterization of NR, the eC effect dependence on temperature and high-cycle fatigue test towards a realistic cooling device is necessary. Based on the simulation results, demonstrators have to be built using regenerative systems.

# Appendix 1 Some other attempts for cooling effects

Some high-risk, but high potential impact research towards some new cooling methods were attempted during this PhD.

## A1.1. Electrorheological (ER) fluid

Electrorheological (ER) fluids are a class of materials whose rheological characteristics are controllable through the application of an electric field[174].

These ER fluids show a phase transition from the liquid state to a weak solid state with a solid-like behavior by forming a chain-like structure within milliseconds when an electric field is applied. The structured ER fluids then return to a liquid-like state as soon as the applied electric field is removed. It is known that these characteristics of ER fluids are a consequence of the fibrillation of particles aligned along the electric field, and this structure formation is known to be induced by the mismatch of the dielectric constants between suspended particles and the non-conducting medium. When a strain is applied perpendicular to the electric field, it distorts and destroys the fibril structures of particles aligned between the electrodes. The viscosity increment under the shear field results from the energy spent to break the chain-like or columnar structure of the particles[175].

It is proposed that the entropy may change in the ER effect as the particles alignment is similar to a phase transition. On the other, another possibility was to considering that it is also an electrical conductor, and that it may also exhibit Seebeck / Peltier effect. Finaly, tntropy of the formation of crystal-like structure ER fluid is also calculated for explaining the failure of this attempt.

### A1.1.1. Fabrication of ER fluid

Two kinds of ER fluids were fabricated. One is using zeolite particles and the other is using Ag particles.

ER fluid is composed of zeolite particles (a kind of CRC NaY zeolite particle, density 1.85 g cm$^{-3}$, average diameter 1 $\mu$m) and silicone oil (a viscosity 10 mPa s at room temperature 20$^{o}$C, a density 0.93 g cm$^{-3}$, and a dielectric constant 2.56) with a particle volume fraction 28% and a zero-field viscosity of 6.5 Pa s at room temperature. This one has a relatively strong ER performance[175,176].

The zeolite particles were washed with de-ionized water several times and then dried in a microwave oven. A mixture of 1: 9 glycerin/ethanol was then combined with the dry zeolite particle to obtain a weight ratio of 1% glycerin to zeolite particles, which results in a thin coating of glycerin on the zeolite particles. Silicone oil was used as received. Zeolite particles were mixed with silicone oil in a four-roll miller to obtain a uniform ER suspension[177].

The other ER fluid is fabricated by silicon oil and Ag particles coated by polymer. The weight ratio of Ag particles is 17%.

### A1.1.2. Results and discussion

#### *A1.1.2.1. Basic measurement*

To get the ER effects, the testing equipments are shown in Fig.A1. 1. The ER effect was tested between two electrode plates with the distance of 5 mm. The temperature change is measured by a thermocouple.

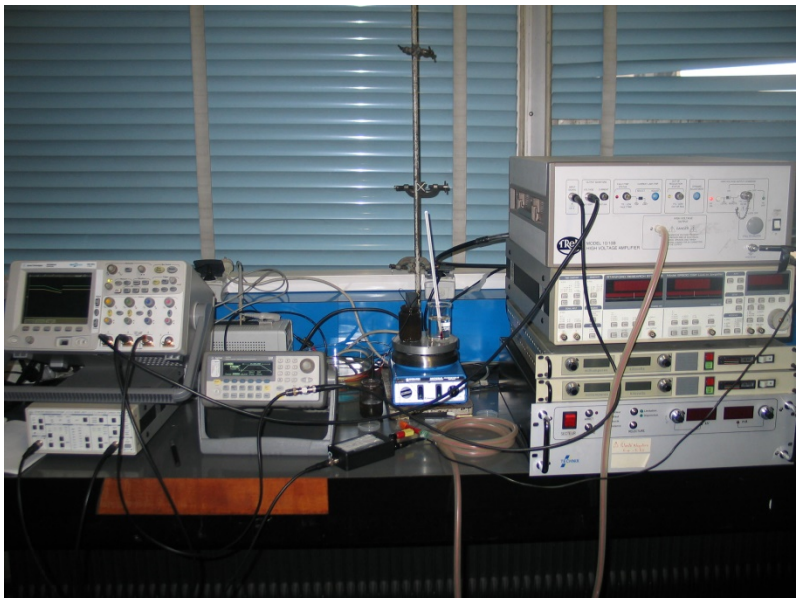

Fig.A1. 1 Testing equipments.

For the ER fluid of zeolite particles, when a rectangular wave with the voltage of 2 kV was applied, the ER effect occurred (Fig.A1. 2) showing a compact and solid volume of ER fluid sandwiched betweent the electrodes. When decreasing the electric fields down to zero, the fluid flows again, out of the electrodes. The smallest electric field for ER effect was 400 V/mm. However, the temperature change between two electrodes plates is only about 1 ºC during the formation of the compact structure

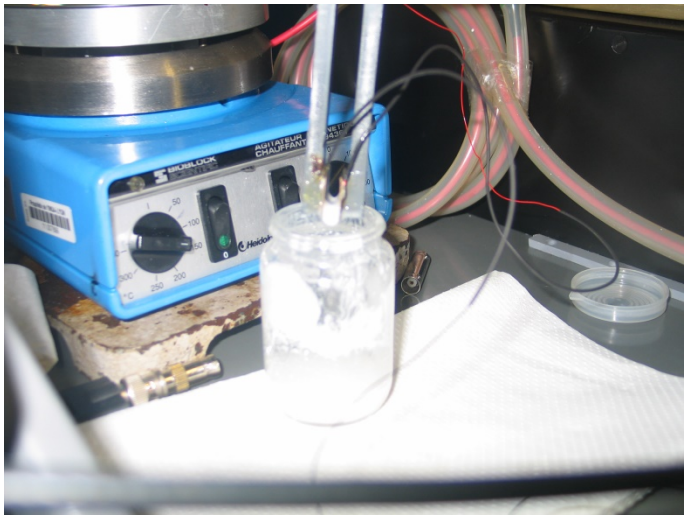

Fig.A1. 2 ER effect based zeolite particles.

For the ER fluid of Ag particles, the ER effect occurs (Fig.A1. 3). However, as the ER fluid of zeolite particles, the temperature change between two electrodes plates is also only about 1 ºC. Though there is a temperature difference between two sides of the device, both the temperatures of the two sides increase, which is attributed to the joule heating effect.

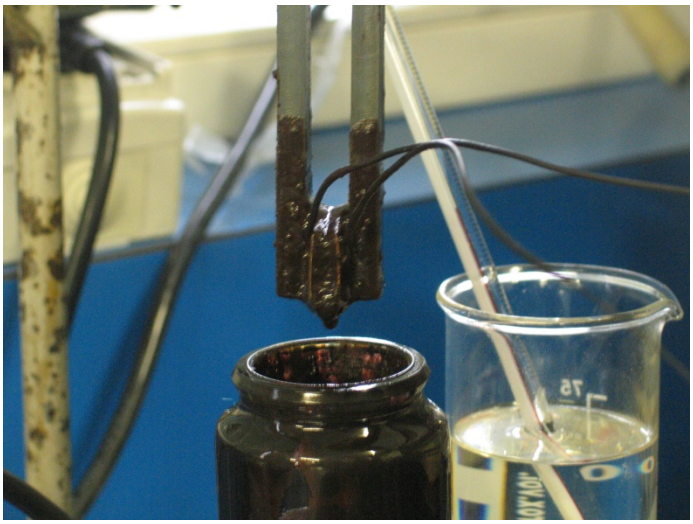

Fig.A1. 3 ER effect based Ag particles.

Conversely to Peltier effect, a thermoelectric device creates voltage when there is a different temperature on each side, which is the Seebeck effect. To test the existence of peltier effect of ER fluid, a method of measurement of Seebeck effect of ER fluid was experimented. If the Seebeck effect of ER fluid is proved, the Peltier effect can be proved.

The device to prove the Seebeck effect of ER fluid is shown in Fig.A1. 4. The experiment composed of two steps. The first step, one side of the ER fluid was heated and the other side was cooled at the same time by using the Peltier element. When the temperature difference between two sides reached about 10 degree, the voltage applied on Peltier element was disconnected to avoid any corona effect. Then, the temperature difference between two sides decreased. The second step, a electric field was applied on ER fluid. The applied electric field is sine wave with peak value of 7 kV and frequency of 1Hz. The current was measured. If the Seebeck effect existed, the current should decrease with the decreased temperature difference between two sides. The heat side and cold side were fixed, whereas the voltage was applied in two opposite phases (phase=0$^{o}$ and 180$^{o}$) respectively.

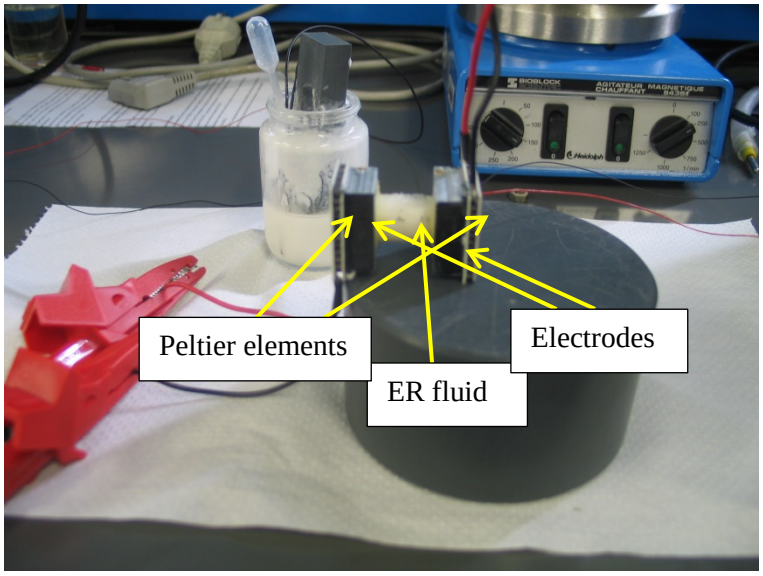


Fig.A1. 4 The device to prove the Seebeck effect of ER fluid.

In both tests, the current increases and the temperature at both sides of the ER fluid increases. It indicates there is no or weak Seebeck effect of ER fluid and the Joule heating effect is dominant. Accordingly, there is no or weak Peltier effect. Thus, the ER fluid can't be used for cooling.

Facing the failure in finding any thermally coupled phenomenon, we tried to understand the reason of the absence of entropy variation.

When subjected to an excitation, particles agglomerates in thin lines, which makes a "demixing" between particles and liquid. In order to estimate the entropy of such "demixing", we consider that there is no bonding energy between the particles (such as chemical bonding). Simply, the particles being aligned by the external field, the well mixed liquid becomes sorted with 100% particles zones, and 0% particles zones. Upon the removal of the external field, the particles becomes mixed again thanks to the thermal agitation. In the following calculation, two limit cases are considered. The first state consider that the particles are packed in cylinders with no fluid molecules inside the cylinder. All the fluid is pushed outside the cylinder when the particles are getting packed.

Entropy of mixing well separated particles and fluid is given by:

$$\Delta S = k \ln(\Omega) = k \ln(\frac{N!}{N_1! N_2!}) \quad \text{(A1. 1)}$$

where $\Omega = N!/(N_1! N_2!)$ is the number of possible states of the system, k is the Boltzmann constant, $N_1$ is the number of particles, $N_2$ is the number of liquid molecules. $N = N_1 + N_2$ is the quantity of available space for the particles is N=N1+N2. "!" denotes factorial of the number

Using simple mathematical rewriting, and using Stirling formula, the entropy may also be written as

$$\Delta S = -k(N_1 \ln \frac{N_1}{N} + N_2 \ln \frac{N_2}{N})$$

Now let make a numerical example. The fluid is water, and the total quantity of molecules in a unit volume filled with 100% water (=1 cubic meter) is $n_2$=56000 moles.

The volume fraction of particule is written $\chi$ .Then the total number of molecules $N_2$ is

$N_2 = (1-\chi) n_2 N_a$ where $N_a$ is the Avogadro number.

Now we consider spherical solid particles of diameter *d* and a volume $d^3$.

In a unit volume of ER fluid, the total volume of the particules is $\chi$ . Since each particle have a volume of $d^3$, the total number of particles is

$$N_1 = \frac{\chi}{d^3}$$

Then the entropy is calculated for different particles volume fraction, and for size ranging from 0.1nm to 1µm, and for volume fraction of 0.1, 0.5 and 0.9.

From the heat capacity of the fluid, we estimate the adiabatic temperature using

$$\Delta T = T_0 \frac{\Delta S}{c}$$

Where $T_0$ is the room temperature of 300 K and *c* is the total heat capacity of a unit volume of fluid (= 4.18 x $10^6$ $J \cdot m^{-3} \cdot K^{-1}$ in case of water).

The results are shown in Fig.A1. 5.

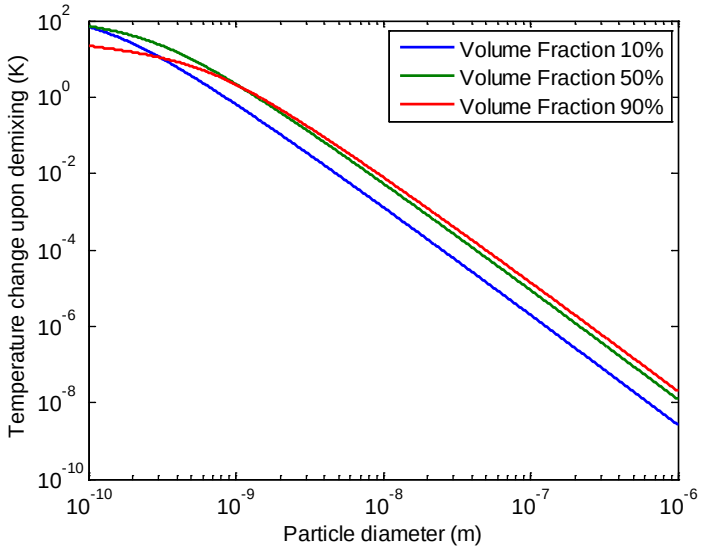


Fig.A1. 5 The relation of temperature change and particle diameter.

The results show that the volume fraction has little influence on the adiabatic temperature change. Moreover, the temperature change only exceeds 1K when the particle size becomes lower than 1nm. The average diameter of zeolite particle used for ER fluid is 1 μm. Thus, there is no temperature change.

## A1.2. Electrocaloric effect and elastocaloric effect of terpolymer

As a part of the study of elastocaloric effect, coupled caloric effect was studied. For electrocaloric effect of polymer, the entropy change comes from the latent heat of the field-induced phase transition and dipole alignment[17]. For elastocaloric effect, the entropy change comes from the alignment of polymer chain[3]. It is the different mechanism. Both the electrocaloric effect and elastocaloric effect were observed on P(VDF-TrFE-CTFE). The idea is that combining the two mechanisms by applying both electric field and mechanical field on P(VDF-TrFE-CTFE) may give a larger entropy change than the single mechanism.

The polymer film was fabricated using a solution-cast method by dissolving P(VDF-TrFE-CTFE) powders in methyl ethyl ketone(MEK) solvent. Then, the polymer solution was cast onto clean glass plates. The terpolymer solution coated glass plates were dried at 70 °C for 2 h in an oven and then the terpolymer films were peeled off from the plates and annealed at 110 °C for more than 3 h to increase the crystallinity and further remove the residual solvent.

The experiment was conducted on a non-stretched sample. The sample thickness is 40μm. The applied strain is 5%. The applied electric field is sine wave with peak value of 25MV/m and frequency of 1Hz. In Fig.A1. 6, the temperature change is measured by using Infrared Camera (NEC G-120, Japan). At 3-13s, the electric field and strain were applied in-phase. At 13-27s, only the electric field is applied. It’s shown that there is no difference of the temperature change between the two conditions.

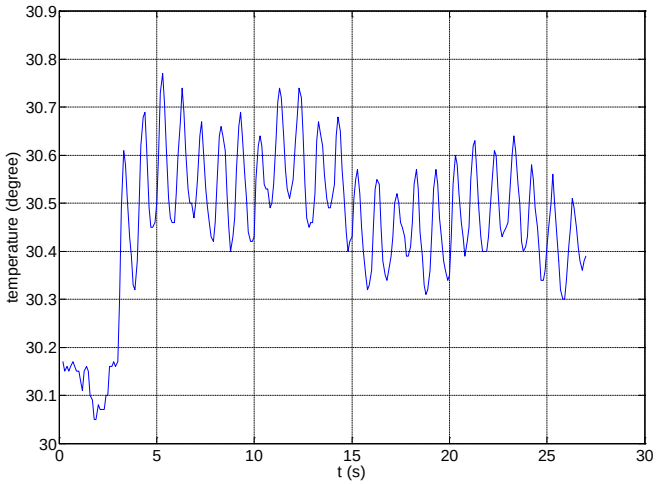


Fig.A1. 6 The electrocaloric effect accompanying the deformation of terpolymer film.

The result is not obvious, probably because the strain level too low. Some stretching process is possible to enlarge elastocaloric activity, but will result in a very low dielctric strength making impossible any electrocaloric attempt. Although much promising of combining electric field and strain excitation for increasing the entropy variation, it is not successful. The reduced dielectric strength is the main reason of this failure.

# Appendix 2 Thermodynamic cycles for an entropic elastomer

## A2.1 Constitutive equations

Internal energy density variation $dU$ writes as follows:

$$dU = TdS + \sigma d\varepsilon \quad \text{(A2. 1)}$$

where $T$, $S$, $\sigma$ and $\varepsilon$ are temperature, specific entropy, stress and strain respectively.

Helmholtz energy writes as follows:

$$A = U - TS, \quad \text{(A2. 2)}$$

$$dA = dU - TdS - SdT = -SdT + \sigma d\varepsilon$$

Then, it is found that $S = -\frac{\partial A}{\partial T}$ and $\sigma = \frac{\partial A}{\partial \varepsilon}$.

According to the classical stress-strain relationship given by Treloar, the constitutive mechanical writes

$$\sigma = NkT\left(\lambda - \frac{1}{\lambda^2}\right) \quad \text{(A2. 3)}$$

where $\sigma$, $\lambda$, $k$, $T$ and $N$ are the stress, elongation, Boltzmann constant, temperature and the crosslink density respectively.

Elongation and strain are both expressed as a function of the length variation $l$ as $\lambda = \frac{l}{l_0}$, where $l_0$ is the initial length of the material. $\varepsilon = \frac{l - l_0}{l_0} = \frac{l}{l_0} - 1 = \lambda - 1$ is the engineering strain.

Then, the Helmholtz energy is calculated by integrating the stress expression (since $d\varepsilon = d\lambda$):

$$A = NkT\left(\frac{\lambda^2}{2} + \frac{1}{\lambda}\right) + f(T) \quad \text{(A2. 4)}$$

And the thermal equation writes as:

$$S = -\frac{\partial A}{\partial T}, \quad \text{(A2. 5)}$$

$$S = -Nk\left(\frac{\lambda^2}{2} + \frac{1}{\lambda} - \frac{3}{2}\right) + c\ln(T)$$

where $S$ and $c$ are specific heat and heat capacity respectively.

$$c\ln\left(\frac{T}{T_{ref}}\right)-\frac{3}{2}NkT=-\frac{\partial}{\partial T}\left(f(T)\right) \tag{A2. 6}$$

where the term $\frac{3}{2}NkT$ references the entropy to be zero for a null elongation.

## A2.2 Thermodynamic cycle

We recall here the two constitutive equations of an elastomer:

$$\sigma=NkT\left(\lambda-\frac{1}{\lambda^2}\right) \quad \text{and} \quad S=-Nk\left(\frac{\lambda^2}{2}+\frac{1}{\lambda}-\frac{3}{2}\right)+c\ln\left(\frac{T}{T_{ref}}\right)$$

For small strain, i.e. elongation not far from 1 (recalling that $\varepsilon=\lambda-1$ and $d\varepsilon=d\lambda$), we simplify the expressions

$$\sigma=NkT\left((1+\varepsilon)-\frac{1}{(1+\varepsilon)^2}\right)=NkT\left((1+\varepsilon)-(1-2\varepsilon)\right)=3NkT\varepsilon \tag{A2. 7}$$

For the expression of the entropy, a second order approximation is necessary. Writing

$$(1+\varepsilon)^n=1+n\varepsilon+\frac{n(n-1)}{2}\varepsilon^2,$$

$$\frac{\lambda^2}{2}+\frac{1}{\lambda}-\frac{3}{2}=\frac{(1+\varepsilon)^2}{2}+\frac{1}{(1+\varepsilon)}-\frac{3}{2}=\frac{1}{2}(1+\varepsilon)^2+(1+\varepsilon)^{-1}-\frac{3}{2}=$$

$$\frac{1}{2}(1+2\varepsilon+\varepsilon^2)+(1-\varepsilon+\varepsilon^2)-\frac{3}{2}=\frac{1}{2}(1+2\varepsilon+\varepsilon^2)+(1-\varepsilon+\varepsilon^2)-\frac{3}{2}=\frac{3}{2}\varepsilon^2$$

Then, the entropy writes

$$S=-Nk\left(\frac{\lambda^2}{2}+\frac{1}{\lambda}-\frac{3}{2}\right)+c\ln\left(\frac{T}{T_{ref}}\right)\approx-\frac{3}{2}Nk\varepsilon^2+c\ln\left(\frac{T}{T_{ref}}\right) \tag{A2. 8}$$

We consider in the following part a Carnot cycle in order to highlight the relevant parameters for enhancing energy conversion. In a cooling system, we consider two heat reservoirs at temperatures $T_1$ and $T_2$. It will be connected to the elastomer at different times and elongation states in order to transfer heat from the cold reservoir to the hot reservoir.

### 1. Carnot cycle

We consider first the idealized Carnot cycle consisting of two isothermal and adiabatic thermal conditions and cyclic stretching.

The different states of the cycles are:

| State | Temperature | Strain | Stress | Entropy |
|---|---|---|---|---|
| A | $T_1$ | $\varepsilon_A$ | $\sigma_A$ | $S_A$ |
| B | $T_2$ | $\varepsilon_B$ | $\sigma_B$ | $S_B$ |
| C | $T_2$ | $\varepsilon_C$ | $\sigma_C$ | $S_C$ |
| D | $T_1$ | $\varepsilon_D$ | $\sigma_D$ | $S_D$ |

From state A to B, the sample is in adiabatic condition, and we consider that the adiabatic temperature change upon strain variation from $\varepsilon_A$ to $\varepsilon_B$ is identical to $T_2$-$T_1$. From state B to C, the sample is in contact to the reservoir at temperature $T_2$ and the sample is stretched from $\varepsilon_B$ to $\varepsilon_C$. During this step, heat is transferred to the hot reservoir. Upon retraction from state C to D (strain decreasing from $\varepsilon_C$ down to $\varepsilon_D$), temperature decreases to $T_1$ in adiabatic condition. From state D back to state A, the sample is in contact with the cold reservoir at $T_1$, and upon further retraction from $\varepsilon_D$ to $\varepsilon_A$, heat is absorbed from the cold reservoir.

The stress and entropy of the different states is then calculated. For state A (initial state), the temperature is $T_1$, strain $\varepsilon_A$ and stress $\sigma_A$ and the entropy is set to 0 arbitrarily (i.e. $T_{ref}=T_1$).

From state A to B, the sample is in adiabatic condition. Therefore dS=0 and $S_B=S_A=0$. Besides

$$\varepsilon_B^{\,2}-\varepsilon_A^{\,2}=\frac{2c}{3Nk}\ln\left(\frac{T_2}{T_1}\right),\ \text{and}\ \sigma_A=3NkT_1\varepsilon_A\ \text{and}\ \sigma_B=3NkT_2\varepsilon_B \qquad \text{(A2. 9)}$$

From state B to C, the sample is in isothermal condition at temperature $T_2$. The variation of entropy is:

$$S_C-S_B=S_C=-\frac{3}{2}Nk\left(\varepsilon_C^{\,2}-\varepsilon_B^{\,2}\right)\ ,\ \text{and the stress is}\ \sigma_C=3NkT_2\varepsilon_C \qquad \text{(A2. 10)}$$

From state C to D, the sample is in adiabatic condition. Therefore $S_D=S_C=-\frac{3}{2}Nk\left(\varepsilon_C^{\,2}-\varepsilon_B^{\,2}\right)$. Besides

$$\varepsilon_D^{\,2}-\varepsilon_C^{\,2}=\frac{2c}{3Nk}\ln\left(\frac{T_1}{T_2}\right),\ \text{and}\ \sigma_D=3NkT_1\varepsilon_D \qquad \text{(A2. 11)}$$

The thermodynamic cycle is displayed in Fig.A2. 1.

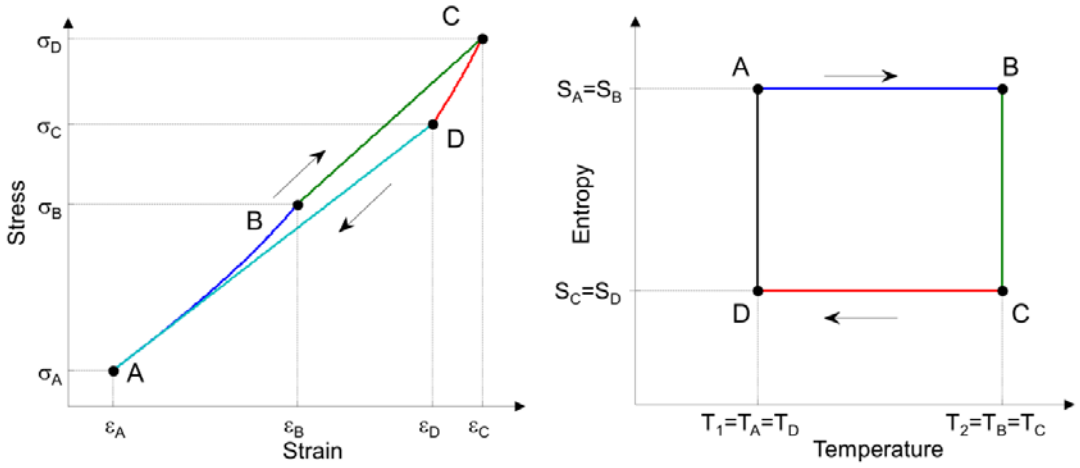


Fig.A2. 1 Thermodynamic cycle.

**Heat received from the hot reservoir** at temperature $T_2$ can writes as:

$$Q_h = Q_{BC} = T_2\left(S_C - S_B\right) = -\frac{3}{2}NkT_2\left(\varepsilon_C{}^2 - \varepsilon_B{}^2\right) \tag{A2. 12}$$

Replacing $\varepsilon_B{}^2$ yields

$$Q_h = Q_{BC} = -\frac{3}{2}NkT_2\left(\varepsilon_C{}^2 - \varepsilon_A{}^2\right) - T_2\,\mathrm{c}\ln\left(\frac{T_2}{T_1}\right) \tag{A2. 13}$$

**Heat received from the cold reservoir** at temperature T1 writes

$$Q_c = Q_{DA} = T_1\left(S_A - S_D\right) = -T_1S_D = \frac{3}{2}NkT_1\left(\varepsilon_C{}^2 - \varepsilon_B{}^2\right) \tag{A2. 14}$$

Replacing $\varepsilon_B{}^2$ yields

$$Q_c = Q_{DA} = \frac{3}{2}NkT_1\left(\varepsilon_C{}^2 - \varepsilon_A{}^2\right) + T_1\,\mathrm{c}\ln\left(\frac{T_2}{T_1}\right) \tag{A2. 15}$$

Mechanical work is calculated through the conservation of energy

$$Q_c + Q_h + W = 0\,,\ W = \left(T_2 - T_1\right)\left(\frac{3}{2}Nk\left(\varepsilon_C{}^2 - \varepsilon_A{}^2\right) + \mathrm{c}\ln\left(\frac{T_2}{T_1}\right)\right) \tag{A2. 16}$$

**The coefficient of performance then writes as:**

$$COP = \frac{Q_c}{W} = \frac{\frac{3}{2}NkT_1\left(\varepsilon_C{}^2 - \varepsilon_A{}^2\right) + T_1\,\mathrm{c}\ln\left(\frac{T_2}{T_1}\right)}{\left(T_2 - T_1\right)\left(\frac{3}{2}Nk\left(\varepsilon_C{}^2 - \varepsilon_A{}^2\right) + \mathrm{c}\ln\left(\frac{T_2}{T_1}\right)\right)} = \frac{T_1}{T_2 - T_1} \tag{A2. 17}$$

2. **Effect of a different coefficient between $\left(\frac{\partial \sigma}{\partial T}\right)_{\varepsilon}$ and $\left(\frac{\partial s}{\partial \varepsilon}\right)_{T}$**

In this part, for the sake of simplicity, linear equations are chosen. If the relation $\left|\left(\frac{\partial \sigma}{\partial T}\right)_{\varepsilon}\right| \neq \left|\left(\frac{\partial s}{\partial \varepsilon}\right)_{T}\right|$ is physically possible in Carnot cycle?

Let consider an example

$$\begin{cases} d\sigma = E \cdot d\varepsilon + \beta_1 \cdot dT \\ ds = -\beta_2 \cdot d\varepsilon + \frac{c}{T_0} \cdot dT \end{cases} \quad \text{(A2. 18)}$$

Where $E, \beta_1 > 0$, $\beta_2 > 0$ and $c$ do not depend on $\varepsilon$ or $T$

For a cycle of Carnot, there are 4 states and 2 heat reservoirs at $T_1$ and $T_2$.

- Adiabatic: state A→B

From state A to B, it's the adiabatic situation. Thus, $ds = 0$ and

$$dT = \frac{T_0 \beta_2}{c} d\varepsilon \quad \text{(A2. 19)}$$

Thus, the strain $\varepsilon_B$ in state B is

$$\varepsilon_B = \frac{c(T_2 - T_1)}{T_0 \beta_2} \quad \text{(A2. 20)}$$

$\varepsilon_B$ is the necessary strain for bring the sample from $T_1$ to $T_2$.

From $d\sigma = E \cdot d\varepsilon + \beta_1 \cdot dT$,

$$d\sigma = E \cdot d\varepsilon + \beta_1 \cdot \frac{T_0 \beta_2}{c} d\varepsilon = (E + \beta_1 \cdot \frac{T_0 \beta_2}{c}) d\varepsilon \quad \text{(A2. 21)}$$

The stress in state A is zero. Thus, the stress in state B is

$$\sigma_B = (E + \beta_1 \cdot \frac{T_0 \beta_2}{c}) \varepsilon_B \quad \text{(A2. 22)}$$

$$\sigma_B = (E + T_0 \cdot \frac{\beta_1 \beta_2}{c}) \frac{c(T_2 - T_1)}{T_0 \beta_2}$$

Thus, in the adiabatic situation,

$$\begin{cases} Q_1 = 0 \\ W_1 = \int_A^B \sigma d\varepsilon = \frac{1}{2}(E + \beta_1 \cdot \frac{T_0 \beta_2}{c})\varepsilon_B^2 \end{cases}$$

- Isothermal: state B→C

From state B to C, it's the isothermal process in contact with the hot reservoir. Further increase of strain is from $\varepsilon_B$ to $\varepsilon_C$ (arbitrary final strain).

As dT=0, thus Eq. (A2.18) becomes

$$\begin{cases} d\sigma = E \cdot d\varepsilon \\ ds = -\beta_2 \cdot d\varepsilon \end{cases} \quad \text{(A2. 23)}$$

and

$$\sigma_C = E \cdot (\varepsilon_C - \varepsilon_B) + \sigma_B \quad \text{(A2. 24)}$$

Thus, the input work is

$$W_2 = \int_B^C \sigma d\varepsilon = \frac{1}{2} E(\varepsilon_C - \varepsilon_B)^2 + \sigma_B(\varepsilon_C - \varepsilon_B) \quad \text{(A2. 25)}$$

The entropy variation $ds = -\beta_2 \cdot d\varepsilon$ can be written as

$$s_C - s_B = -\beta_2(\varepsilon_C - \varepsilon_B) \quad \text{(A2. 26)}$$

Writing $s_A = s_B = 0$ (arbitrary), then

$$s_C = -\beta_2(\varepsilon_C - \varepsilon_B) \quad \text{(A2. 27)}$$

$$Q_2 = \int_B^C Tds = T_2 s_C = -\beta_2 T_2(\varepsilon_C - \varepsilon_B) \quad \text{(A2. 28)}$$

- Adiabatic: state C→D

From Eq. (A2.19),

$$T_1 - T_2 = \frac{T_0 \beta_2}{c}(\varepsilon_D - \varepsilon_C)$$

$$\varepsilon_D = \frac{c(T_1 - T_2)}{T_0 \beta_2} + \varepsilon_C = \varepsilon_C - \varepsilon_B \quad \text{(A2. 29)}$$

From Eq. (A2.21),

$$\sigma_D - \sigma_C = (E + \frac{T_0 \beta_1 \beta_2}{c})(\varepsilon_D - \varepsilon_C) = (E + \frac{T_0 \beta_1 \beta_2}{c})(-\varepsilon_B) = -\sigma_B$$

$$\sigma_D = \sigma_C - \sigma_B = E(\varepsilon_C - \varepsilon_B) \quad \text{(A2. 30)}$$

Finally, for the adiabatic process from C to D,

$$\begin{cases} Q_3 = 0 \\ W_3 = \int_C^D \sigma d\varepsilon = -\frac{1}{2}(E + \frac{T_0\beta_1\beta_2}{c})(\varepsilon_D - \varepsilon_C)^2 + \sigma_D(\varepsilon_D - \varepsilon_C) \end{cases} \quad \text{(A2. 31)}$$

- Isothermal: state C→D

$$\begin{cases} W_4 = \frac{1}{2}E(\varepsilon_A^2 - \varepsilon_D^2) = -\frac{1}{2}E\varepsilon_D^2 \\ Q_4 = T_1(s_A - s_D) = -T_1 s_D = -T_1 s_C = \beta_2 T_1(\varepsilon_C - \varepsilon_B) \end{cases} \quad \text{(A2. 32)}$$

In summary,

| state | T (°C) | $\varepsilon$ | $\sigma$ | $s$ |
|---|---|---|---|---|
| A | $T_1$ | 0 | 0 | 0 |
| A→B | $W_1 = \frac{1}{2}(E + \beta_1 \cdot \frac{T_0\beta_2}{c})\varepsilon_B^2$ | | $Q_1 = 0$ | |
| B | $T_2$ | $\varepsilon_B = \frac{c(T_2 - T_1)}{T_0\beta_2}$ | $\sigma_B = (E + \beta_1 \cdot \frac{T_0\beta_2}{c})\varepsilon_B$ | 0 |
| B→C | $W_2 = \frac{1}{2}E(\varepsilon_C - \varepsilon_B)^2 + \sigma_B(\varepsilon_C - \varepsilon_B)$ | | $Q_2 = -\beta_2 T_2(\varepsilon_C - \varepsilon_B)$ | |
| C | $T_2$ | $\varepsilon_C$ | $\sigma_C = E \cdot (\varepsilon_C - \varepsilon_B) + \sigma_B$ | $s_C = -\beta_2(\varepsilon_C - \varepsilon_B)$ |
| C→D | $W_3 = -\frac{1}{2}(E + \frac{T_0\beta_1\beta_2}{c})(\varepsilon_D - \varepsilon_C)^2 + \sigma_D(\varepsilon_D - \varepsilon_C)$ | | $Q_3 = 0$ | |
| D | $T_1$ | $\varepsilon_D = \varepsilon_C - \varepsilon_B$ | $\sigma_D = \sigma_C - \sigma_B$ | $s_D = s_C$ |
| D→A | $W_4 = \frac{1}{2}E(\varepsilon_A^2 - \varepsilon_D^2) = -\frac{1}{2}E\varepsilon_D^2$ | | $Q_4 = \beta_2 T_1(\varepsilon_C - \varepsilon_B)$ | |

The heat received from hot reservoir is

$$Q_h = Q_2 = -\beta_2 T_2(\varepsilon_C - \varepsilon_B) \quad \text{(A2. 33)}$$

The heat received from cold reservoir is

$$Q_c = Q_4 = \beta_2 T_1(\varepsilon_C - \varepsilon_B) \quad \text{(A2. 34)}$$

The work received from actuator,

$$W = W_1 + W_2 + W_3 + W_4$$
$$= \frac{1}{2}(E + \beta_1 \cdot \frac{T_0\beta_2}{c})\varepsilon_B^2 + \frac{1}{2}E(\varepsilon_C - \varepsilon_B)^2 + \sigma_B(\varepsilon_C - \varepsilon_B)$$
$$-\frac{1}{2}(E + \frac{T_0\beta_1\beta_2}{c})(\varepsilon_D - \varepsilon_C)^2 + \sigma_D(\varepsilon_D - \varepsilon_C) - \frac{1}{2}E\varepsilon_D^2$$
$$= \frac{1}{2}(E + \beta_1 \cdot \frac{T_0\beta_2}{c})[\varepsilon_B^2 - (\varepsilon_D - \varepsilon_C)^2] + \frac{1}{2}E[(\varepsilon_C - \varepsilon_B)^2 - \varepsilon_D^2] + \sigma_B(\varepsilon_C - \varepsilon_B) + \sigma_D(\varepsilon_D - \varepsilon_C)$$

As $\varepsilon_D = \varepsilon_C - \varepsilon_B$, thus

$$W = \sigma_B(\varepsilon_C - \varepsilon_B) - \sigma_D\varepsilon_B = (E + \beta_1 \cdot \frac{T_0\beta_2}{c})\varepsilon_B(\varepsilon_C - \varepsilon_B) - E(\varepsilon_C - \varepsilon_B)\varepsilon_B = T_0 \cdot \frac{\beta_1\beta_2}{c}\varepsilon_B(\varepsilon_C - \varepsilon_B)$$

From $\varepsilon_B = \frac{c(T_2 - T_1)}{T_0\beta_2}$,

$$W = \beta_1(T_2 - T_1)(\varepsilon_C - \varepsilon_B) \quad \text{(A2. 35)}$$

Application of the conservation of energy,

$$Q_h + Q_c + W = 0 \quad \text{(A2. 36)}$$

Thus,

$$-\beta_2 T_2(\varepsilon_C - \varepsilon_B) + \beta_2 T_1(\varepsilon_C - \varepsilon_B) + \beta_1(T_2 - T_1)(\varepsilon_C - \varepsilon_B) = 0$$

$$(T_2 - T_1)(\varepsilon_C - \varepsilon_B)(\beta_1 - \beta_2) = 0$$

Thus,

$$\beta_1 = \beta_2 \quad \text{(A2. 37)}$$

In conclusion of this calculation, two different coefficients are observed (or even a different sign) during the indirect characterization. It violates the first principle by applying a Carnot cycle. This brings us to think about how to ensure both the experimental results and thermodynamics laws.

# Synthèse de la thèse en français

## 1 Introduction

Les dispositifs à fluide frigorifique représentent la technologie dominante de réfrigération, et bien que leurs performances s'améliorent, ils s'accompagnent de problèmes environnementaux. Par exemple, les fluides frigorifiques sont des gaz à effets de serre présentant un impact 1000 fois supérieur à celui du $CO_2$.

Les effets caloriques représentent une solution attractive en remplacement des systèmes conventionnels. De tous ces effets, l'effet élastocalorique du caoutchouc naturel (appelé effet Gough-Joule) est le plus ancien connu [2]. Pour autant, les recherches sur cet effet restent rares et à leurs débuts [3,4]. Cet effet permet un changement de température de 10°C pour une déformation de 500%.[5–7] Le caoutchouc naturel est un matériau souple (module d'Young de l'ordre du MPa) permettant une faible contrainte mécanique. En outre, ce matériau est non-toxique, et bon marché [3]. Pour une amplitude de contrainte constante, l'augmentation de la contrainte moyenne permet d'augmenter la durée de vie en fatigue jusqu'à $10^6$ cycles[8,9], et même $10^7$ cycles pour une déformation de 200%[10].

Les propriétés de fatigue du caoutchouc naturel peuvent être optimisées en ajustant la proportion de souffre et de charges (comme le carbon black). Cela constitue une étape importante vers l'application du caoutchouc naturel pour le refroidissement[103]. De plus, les dommages liés à la fatigue peuvent être réparés par un traitement thermique ou une exposition à un solvant[12] ce qui est unique comparé aux matériaux inorganiques. Tous ces facteurs font du caoutchouc naturel un candidat potentiel pour des applications de refroidissement.

Dans cette introduction, les différents effets caloriques sont comparés, puis le potentiel du caoutchouc naturel est discuté.

### 1.1 Comparaison de différents effets caloriques

Les effets caloriques sont principalement de 4 types : magnétocalorique (MC), électrocalorique (EC), barocalorique (BC) et élastocalorique (eC). Ils correspondent à une dépendance de l'entropie avec le champ magnétique, le champ électrique, la pression hydrostatique et la traction uniaxiale respectivement. Un exemple de cycle de réfrigération à l'aide d'un matériau de ce type est illustré sur la Fig.FR 1.

De tous les effets caloriques, la réfrigération magnétocalorique est la plus aboutie, et constitue aujourd'hui une alternative crédible aux dispositifs traditionnels, avec des refroidissements pouvant atteindre 30K[14,15][16]. Toutefois, la réfrigération magnétocalorique utilise des matériaux à base de terres rares, voire toxiques (As) tout en nécessitant de très forts champs magnétiques difficiles à générer. Les matériaux électrocaloriques, dans le but d'avoir des effets importants, sont opérés à très fort champ électrique et sont limités par leur rigidité diélectrique [17,18]. L'effet élastocalorique dans les alliages à mémoire de forme (SMAs) a fait l'objet de recherches très actuelles en raison du très fort effet élastocalorique associé[11,19,20,43], de quelques brevets d'invention (par exemple voir [22]), de simulations de systèmes de refroidissement [11,23,24], et enfin de prototypes de système de refroidissement, (par exemple voir [25]). L'intérêt de ce couplage est d'ailleurs corroboré par un rapport de l'US Department of Energy[26].

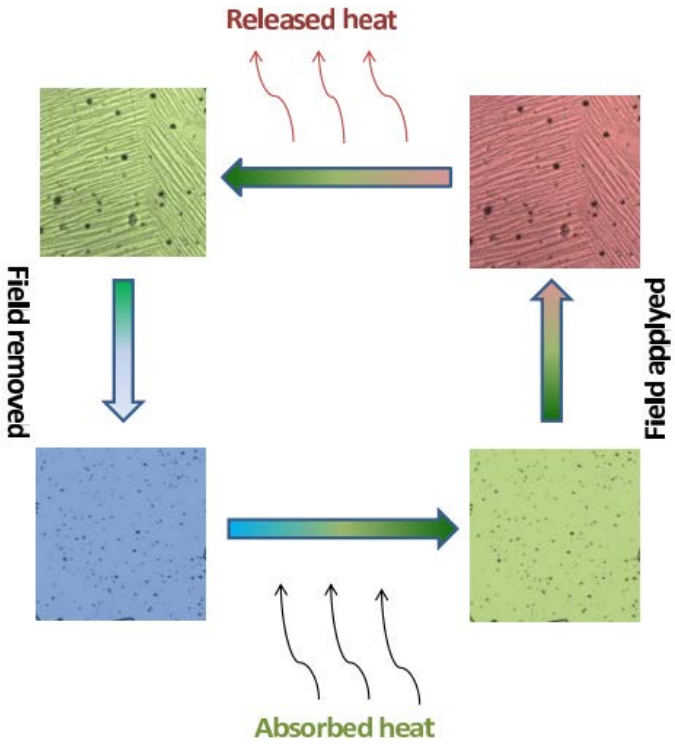


Fig.FR 1 Cycle de réfrigération avec un matériau calorique: 1ère étape : le champ extérieur est appliqué en condition adiabatique, 2ème étape : le matériau refroidit au contact avec la source chaude (chaleur allant du matériau vers la source chaude), 3ème étape, le champ est réduit en condition adiabatique, 4ème étape, le matériau s'échauffe au contact de la source froide (chaleur allant de la source froide vers le matériau). Le champ peut être aussi bien le champ magnétique, le champ électrique, la pression hydrostatique ou la traction uniaxiale suivant le matériau calorique considéré[13].

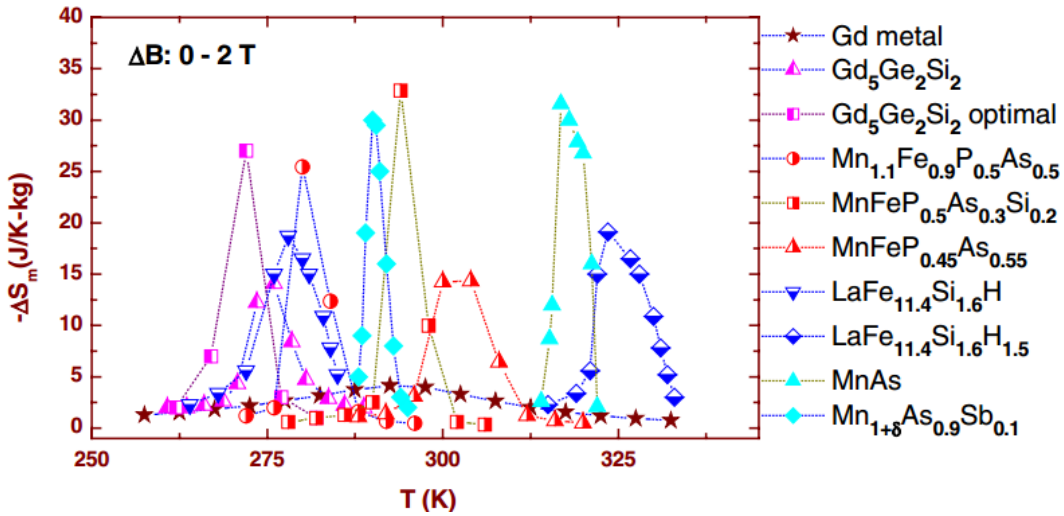


Fig.FR 2 Variation d'entropie induite par un champ magnétique de 2T pour différents matériaux magnétocaloriques [27].

**Effet magnétocalorique**

L'effet magnétocalorique (MC) sous un champ magnétique de 2T est donné pour différents matériaux sur la Fig.FR 2. Pour l'ensemble des matériaux rassemblés ici, l'effet est de l'ordre de 10 à 30 J/(K.kg), les valeurs les plus hautes étant obtenues avec des alliages à base d'arsenic. Si l'effet MC est utilisé principalement pour atteindre de très basses températures en complément des dispositifs usuels, son application autour de la température ambiante est plus récente et de nombreux prototypes

ont maintenant été publiés [16]. Le matériau doit être intégré à un système régénératif permettant de démultiplier le gradient thermique. Ainsi la différence de température entre les deux extrémités du systèmes est bien plus importante que la variation de température adiabatique induite lors de l'application du champ magnétique[28,29]. Un système régénératif comprend par exemple un matériau MC poreux à travers lequel circule un fluide caloporteur.

Lorsque le champ magnétique est appliqué, par l'utilisation d'une pompe, le fluide est amené à circuler vers la droite, tandis que quand le champ magnétique revient à zéro, le fluide est pompé vers la gauche. A la suite de plusieurs cycles de fonctionnement, un gradient thermique spatial apparaît dans la ligne de refroidissement. Chaque particule active voit donc sa température moyenne évoluer. Un tel système présente l'avantage de permettre un échange thermique entre les différentes parties du matériau MC est de démultiplier le gradient thermique global comparé au principe décrit Fig.FR 1.

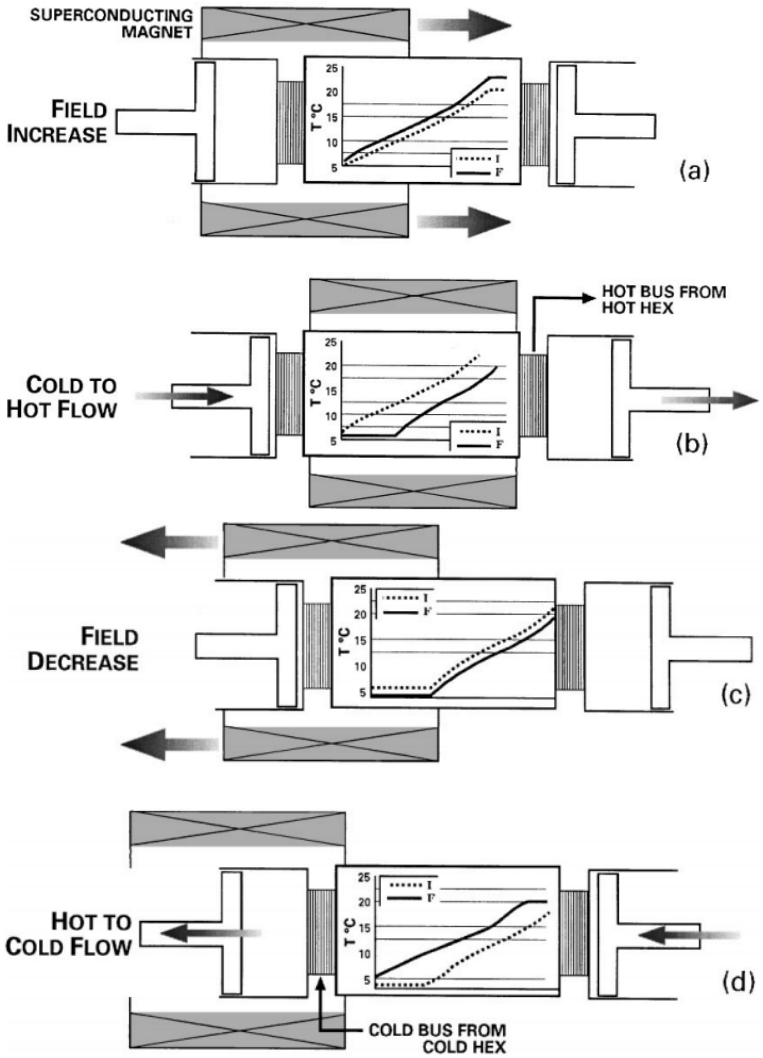


Fig.FR 3 Les quatre « temps » d'un système régénératif magnétocalorique. Magnétisation (a), fluide circulant du côté chaud vers le côté froid(b), démagnétisation (c), et fluide circulant du côté chaud vers le côté froid (d)[15].

**Effet électrocalorique**

Les effets électrocaloriques importants sont obtenus dans les matériaux dont la polarisation varie fortement en température, comme à proximité de la transition de Curie (Tc). Par exemple, dans les céramiques $PbSc_{1/2}Ta_{1/2}O_3$ c, on peut obtenir des variations de 2.3K autour d'une température à $T_c \pm 5$ K[30]. Toutefois, cette plage de température pour laquelle l'effet EC est important est trop étroite pour des systèmes de refroidissement. D'autres classes de matériaux permettent de répondre à cette problématique, comme par exemple la famille du $Pb(Mg_{1/3}Nb_{2/3})O_3–PbTiO_3$ (PMN-PT)[31]. Des variations de température adiabatique jusqu'à 2.7 K ont été obtenus par l'application d'un champ électrique de 2MV/m sur des monocristaux. La plage de température pour laquelle l'effet est important est de 80 à 160 ºC, grâce à fait que la transition est diffuse.

Les systèmes de refroidissement nécessitent des puissances et des énergies que seuls des matériaux massifs peuvent produire, ce qui amène à considérer que les céramiques massives sont les meilleurs candidats pour les applications[17].

Les couches minces ferroélectriques permettent d'appliquer des champs électriques très importants. Mischenko et al.[32] a ainsi montré que l'on pouvait obtenir une variation de température de 0.48 K par volt appliqué sur des couches minces de 350nm de $PbZr_{0.95}Ti_{0.05}O_3$, (12 K pour 48 MV/m). L'avantage de la couche mince est l'augmentation considérable de la rigidité diélectrique par rapport à un matériau massif. Sur des couches minces de PMN-PT, Saranya et al.[33] a annoncé une variation de température $\Delta T$ de 31 K ( $\Delta E$ □ 75 MV/m).

D'autres études traitent des polymères électrocaloriques, à base de polyvinylidene-fluoride. Des variations d'entropie de 56 J/(kg.K) ont été rapportées par Neese et al.[178] sur des films de P(VDF-TrFE) autour de la température de transition ferroélectrique. Il est à noter que cette valeur est bien plus importante que les meilleurs matériaux magnétocaloriques. En revanche, cet effet est obtenu pour des champs électriques très important (209 MV/m). Si les matériaux polymères présentent les effets électrocaloriques les plus importants, leur efficacité $\Delta T / \Delta E$ est pourtant la plus faible.

**Effet barocalorique**

En 1998, un faible effet barocalorique (~0.2K) dans un polycristal de Pr0.66La0.34NiO3 à 350 K près d'une transition structurelle sous une pression de 0.5GPa a été rapporté[36]. Un effet bien plus large a été obtenu sur un alliage magnétique super élastique de Ni49.26Mn36.08In14.66 à température ambiante[37](4.5K pour une pression 0.26 GPa). De manière générale, les matériaux magnétocaloriques présentent souvent une activité barocalorique.[39]. Toutefois, aucun démonstrateur exploitant cet effet n'a été présenté à ce jour.

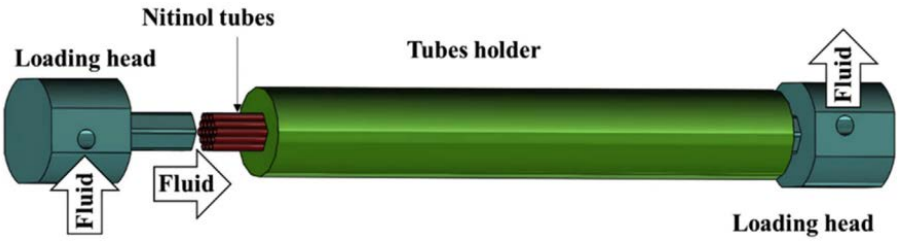


Fig.FR 4 Schéma d'un système régénératif dans lequel des tubes de niticol sont traversés par un fluide.

**Effet élastocalorique**

Par bien des aspects, l'effet élastocalorique est similaire à la compression d'un fluide frigorifique. Les deux utilisent une excitation mécanique (pression ou contrainte) pour induire une transition de phase. Cette similitude pourrait aider au développement de systèmes de refroidissement exploitant cet effet. Les matériaux élastocaloriques se répartissent entre les alliages à mémoire de forme (Shape Memory Alloys ou SMA) et les élastomères. Récemment, beaucoup d'efforts de recherche se sont concentrés sur les SMAs.

L'effet élastocalorique sur un SMA est l'équivalent mécanique de l'effet magnétocalorique. Il fait intervenir une transition de phase martensitique induite par la contrainte mécanique. Parmi ces matériaux, on trouve des alliages à base de cuivre Cu-Zn-Al[19] et Cu-Al-Ni[40]; des alliages à base de fer comme le Fe-Pd[41], et les alliages les plus prometteurs Ni-Ti (nitinol)[42].
Un paramètre important est la variation de température adiabatique induite par la contrainte. Le nitinol présente une variation de 17 K à 23 K[20,43], tandis que pour le Cu-Zn-Al et le Cu-Al-Ni les valeurs s'échelonnent entre 11 K et 19 K[44].

Les systèmes régénératifs ont été largement appliqués aux matériaux magnétocaloriques, et Tusek et al.[11] l'ont transposé au cas élastocalorique. Dans ce cas, la limitation principale est la très grande force nécessaire pour déformer le matériau. Par exemple, pour atteindre 500W de puissance de réfrigération, une force 180 kN (contrainte de 900 MPa) est nécessaire[11]. Un système régénératif comparable a été proposé par Qian et al.[23].(Fig.FR 4).

### 1.2 Un matériau élastocalorique intéressant: le caoutchouc naturel

Le caoutchouc naturel est un très intéressant matériau élastocalorique, mais cet effet couplé n'a fait l'objet que de peu d'études. Ce matériau est largement utilisé comme pièce mécanique élastomérique, en raison de sa grande déformation élastique et sa résistance remarquable à la rupture[45].

L'élasticité du caoutchouc a d'abord été décrite comme une élasticité entropique. Lorsqu'il est étiré, les chaînes de polymère s'orientent, entraînant une augmentation de l'ordre dans le matériau et une diminution de l'entropie (augmentation de température en condition adiabatique). Lorsque la contrainte est relâchée, le matériau retrouve son état originel et l'entropie augmente (diminution de la température en condition adiabatique). Ainsi, les chaînes moléculaires se comportent comme un ressort entropique[8]. Cet effet est illustré Fig.FR 5.

Lors de la déformation du caoutchouc, une cristallisation induite par la déformation apparaît. Elle est désigné par la « Strain-induced crystallization/crystallite » (SIC)[47]. La chaleur latente de cristallisation peut être alors considérée comme une source majeure de la variation d'entropie observée. En outre, les propriétés mécaniques sont largement influencées par la SIC[45,49,50]. Pour l'effet élastocalorique, aussi bien la variation de température adiabatique que la contrainte (élasticité) sont des propriétés importantes. Il est donc nécessaire de comprendre et de s'appuyer sur la théorie du SIC pour comprendre l'effet élastocalorique. Une vue schématique des chaînes de polymère et de la cristallisation est donné Fig.FR 6[51].

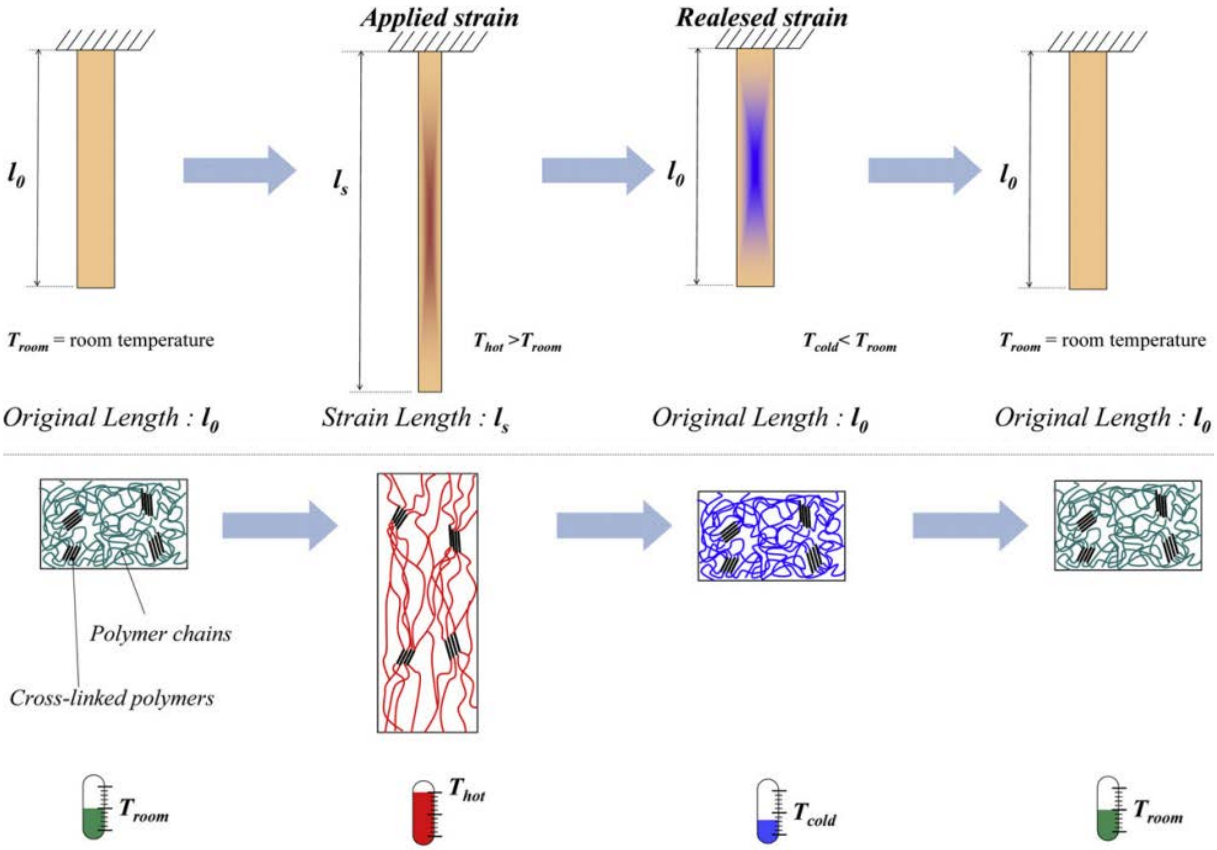


Fig.FR 5 Représentation schématique de la structure du polymère et du mécanisme responsable de l'effet élastocalorique [3].

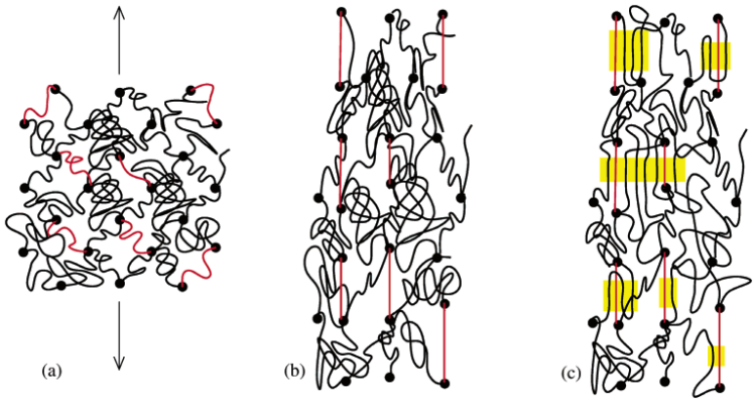


Fig.FR 6 Modèle de la nucléation et de la cristallisation dans du caoutchouc vulcanisé. Les chaînes courtes sont tracées en lignes rouges. Les cercles pleins sont les points de réticulation. (a) avant déformation : les points de réticulation sont distribués aléatoirement, (b) après déformation les chaînes courtes sont complètement étirées et (c) les chaines complètement étirées constituent les germes de la cristallisation (parties jaunes)[51].

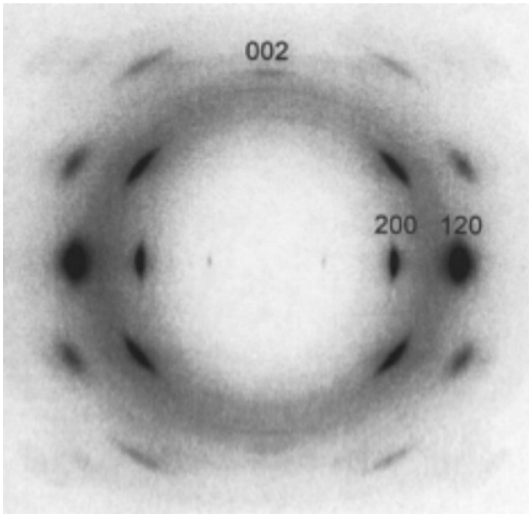

Fig.FR 7 Diffractogramme typique obtenu en WAXD sur un caoutchouc vulcanisé étiré 7.35 fois[51].

Depuis sa découverte au début du XXème siècle par Katz[47,52] par diffraction RX, la cristallisation induite par la déformation a été largement étudiée expérimentalement[51,54–66], théoriquement[67–83] et des articles de revues sont disponibles[47,84]. La structure du cristal et les paramètres de maille des cristallites peuvent être déterminés par l'analyse de diffractogrammes (voir Fig.FR 7)[51]. Bunn[85] a déterminé une structure monoclinique dont les paramètres de mailles sont $a$ = 12.46 Å, $b$ = 8.89 Å, $c$ = 8.10 Å and $\beta$ = 92 °.

L'apparition de la SIC peut être déterminée par l'augmentation de la température de fusion lors de l'étirement

$$1/T_{m,\lambda} = 1/T_{m,1} - \Delta\Gamma_{def} / \Delta H_1 \qquad \text{(Équation 1)}$$

où $\lambda$ est l'élongation, $T_{m,1}$ est la température de fusion dans l'état de repos, $T_{m,\lambda}$ est la température de fusion dans l'état déformé, $\Delta\Gamma_{def}$ est la variation d'entropie entre les états de repos et déformé, et $\Delta H_1$ est la chaleur latente de fusion.

Ainsi, la température de fusion augmente avec la déformation, dans la mesure où $\Delta\Gamma_{def}$ augmente avec la déformation. Lorsque cette température de fusion dépasse la température ambiante, le matériau se retrouve dans un état de surfusion et la cristallisation apparaît.

**Lien entre la contrainte et la SIC**

La relation entre la contrainte et la SIC a été largement étudiée[47,50,57,75,86–88], les résultats pionniers ayant été obtenus Flory[70,87,89,96].

Ce dernier a proposé deux interprétations opposées à l'effet de la SIC sur la contrainte:

**1. Effet de relaxation de la contrainte**. La longueur de la chaîne cristallisation étant plus grande que dans la phase amorphe, la partie restante de la chaîne non cristallisée se relâche et la contrainte diminue.

**2. Effet de durcissement.** Les cristallites agissent comme de nouveaux points de réticulation, et la contrainte est directement proportionnelle à la densité des points de réticulation.

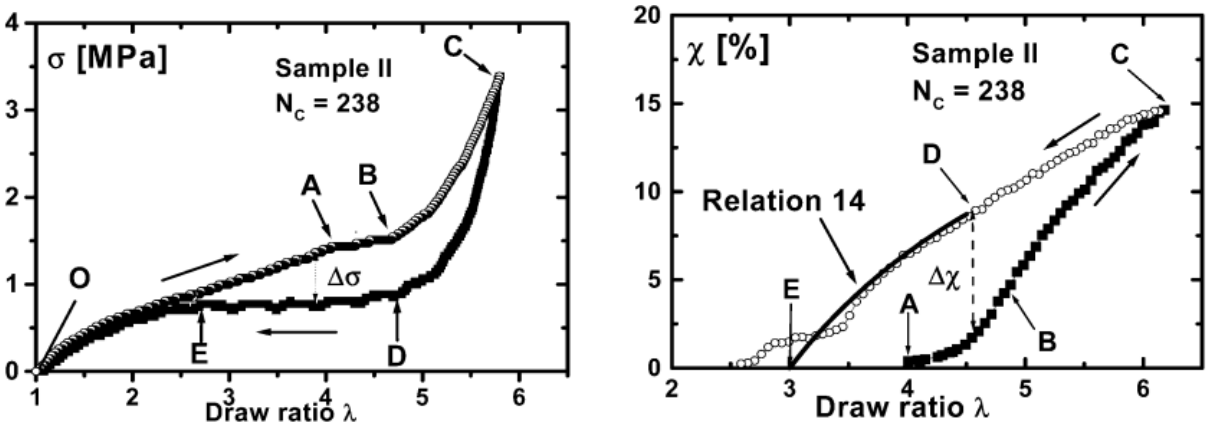


Fig.FR 8 Evolution comparée de (a) la contrainte et (b) le taux de cristallinité à 22°C dans un caoutchouc naturel vulcanisé[88].

Cette propriété apparemment paradoxale est illustrée Fig.FR 8, montrant la courbe contrainte - déformation à gauche et la courbe taux de cristallinité - déformation à droite. On observe principalement :

1. La cristallisation débute au point noté A sur la figure de droite (déformation de 4). Il en résulte un plateau sur la courbe contrainte-déformation jusqu'au point B. Dans cet intervalle, l'effet de relaxation est dominant.
2. Pour de plus grandes déformations, l'effet de relaxation est diminué et l'effet de durcissement devient prépondérant (du point B au point C).
3. Lors de la rétraction de l'échantillon, la contrainte commence par diminuer (du point C au point D) puis on observe un large plateau du point D au point E pour lequel l'effet de relaxation est à nouveau prépondérant.
4. On observe également un fort hystérésis sur la courbe cristallisation-déformation responsable du fort hystérésis sur la courbe contrainte-déformation.

Différents modèles ont été développés pour interpréter ou prévoir le comportement mécanique du caoutchouc : par une décomposition en 5 réseaux parallèles (comportement élastique pur, endommagement, hystérésis et effet de durcissement) [68,69,79], en considérant simultanément le comportement de la phase viscoélastique et le comportement de la SIC[76], ou encore des modèles basés sur des microsphères dans une phase amorphe [75,77,78].

**Variation de température élastocalorique et SIC**

On peut considérer que la variation de température adiabatique due à l'effet élastocalorique est principalement reliée à la SIC, même si on ne trouve que peu d'études établissant ce lien.

Pour le caoutchouc faiblement réticulé, la cristallisation débute autour d'une déformation de 3 et diminue avec le taux de réticulation [51,67,88,98,99].

La chaleur latente de transition étant le moteur principal de la variation d'entropie à grande déformation, il est naturel que la variation de température adiabatique se produise principalement à partir d'une déformation de 3. En outre, le manque de réversibilité entre la variation de température enregistrée lors de l'extension et lors de la rétraction est un indicateur fort de l'influence de la cristallisation, ces effets étant absents des matériaux ne cristallisant pas[100].

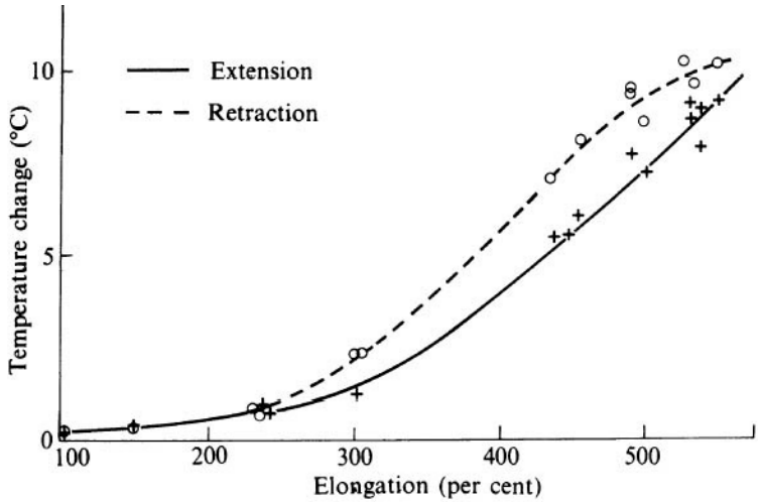

Fig.FR 9 Variation de température élastocalorique en extension et en rétraction[6].

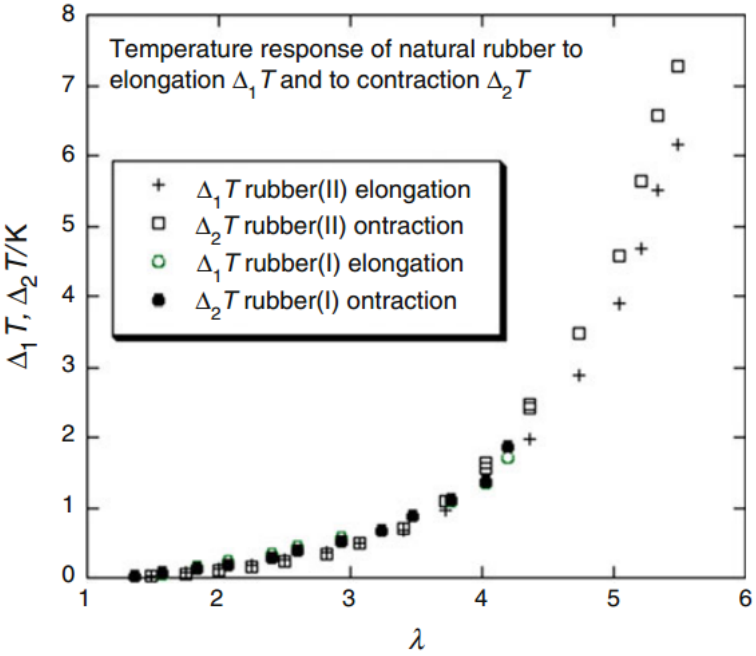

Fig.FR 10 Effet élastocalorique dans deux types de caoutchouc [101].

Dans les résultats expérimentaux obtenus par Sakata et al.[101], l'inflexion forte de la courbe température – déformation se produit autour d'une déformation de 4 (Fig.FR 10), aussi bien pour l'extension que pour la rétraction (déformation de début de la cristallisation). La différence observée toutefois sur la valeur de la variation de température est expliquée par des cinétiques différentes de cristallisation et de fusion. Ces cinétiques différentes ont été mises en évidence par Samaca Martinez et al.[102], notamment à travers l'observation du fluage mécanique (ne se produisant qu'à partir du moment où la SIC intervient) différent en extension et en rétraction.

En conclusion, il apparaît clairement que la cristallisation induite par la déformation est une donnée importante pour comprendre et améliorer l'effet élastocalorique dans le caoutchouc. Il est à noter que la transition est de nature différente de celle observée dans les alliages à mémoire de forme (généralement du 1$^{er}$ ordre)[20,103].

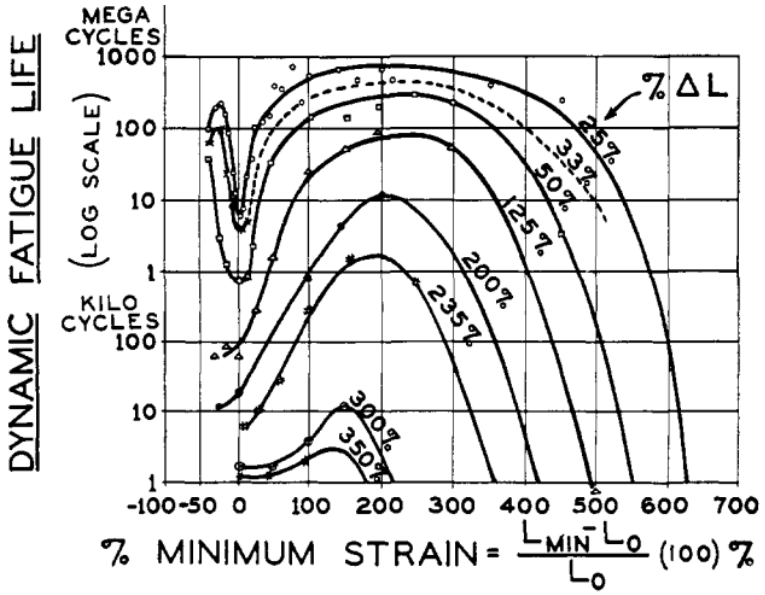


Fig.FR 11 Limite de résistance à la fatigue en fonction de la déformation moyenne et de son amplitude dynamique[10].

**Effets de la fatigue sur l'effet élastocalorique**

Le caoutchouc naturel a été peu étudié en tant que matériau élastocalorique, peut-être en raison des forts effets de fatigue apparaissant lors de cycles répétitifs à grandes déformations. Pourtant, ce matériau peut présenter une excellente résistance à la rupture lorsqu'il est utilisé dans une plage soigneusement choisie de déformation [47,105–112][8–10,104,108,113–116]. De manière étonnante, c'est dans les caoutchouc présentant de la cristallisation que la meilleure résistance à la fatigue est observée.[10][117][118][119].

Il est notamment possible d'augmenter considérablement la résistance à la fatigue en travaillant autour d'une déformation statique (Fig.FR 11), tel que démontré par Cadwell *et al.*[10] dans le cas d'une déformation biaxiale. Avec une déformation statique de 200% autour de laquelle on applique une déformation dynamique de 200%, le matériau résiste à des déformations cycliques jusqu'à $10^7$ cycles. En travaillant avec la contrainte uniaxiale comme grandeur d'excitation, des résultats similaires sont obtenus, où une précontrainte permet d'atteindre $10^6$ cycles[8,9].

**Comparaison entre les alliages à mémoire de forme et le caoutchouc naturel**

Il est intéressant de comparer les propriétés élastocaloriques des alliages à mémoire de forme (SMA) et du caoutchouc naturel. Le module d'Young est de l'ordre de quelques centaines de MPa pour les SMA tandis qu'il est de l'ordre de quelques MPa pour le caoutchouc. En revanche, pour obtenir un effet élastocalorique conséquent, le caoutchouc doit être déformé de plusieurs fois sa longueur initiale tandis que quelques pourcents suffisent pour les SMA. Les deux matériaux présentent la même résistance à la fatigue et permettent d'atteindre $10^7$ cycles, comme c'est le cas de l'alliage de $Ti_{54}Ni_{34}Cu_{12}$ à une déformation de 1.5%[128]. Ces données sont comparées dans le Tableau 1.

Tableau 1 : Comparaison entre deux matériaux élastocaloriques

| | **Alliages à mémoire de forme (SMAs)** | **Caoutchouc naturel (NR)** |
|---|---|---|
| **Coût** | 100 €/kg | 1.4 €/kg |
| **Résistance à la fatigue** | $10^7$ cycles @ 1.5% en contrainte uniaxiale [128] | $10^7$ cycles en étirement biaxial @ 200% de déformation [10] |
| **Contrainte** | Centaines de Mpa | Quelques Mpa; |
| **Déformation** | Quelques pourcents | Quelques centaines de pourcents; |
| **Conductivité thermique** | 18 $Wm^{-1}K^{-1}$[23] | 0.16 $Wm^{-1}K^{-1}$ |
| **Variation d'entropie isotherme** | 32 $JK^{-1}kg^{-1}$ (NiTi)[21]<br>$2\times10^5$ $JK^{-1}m^{-3}$ | 80 $JK^{-1}kg^{-1}$[6]<br>$7\times10^4$ $JK^{-1}m^{-3}$ |
| **Variation de température adiabatique** | 17 K[21] | 12 K[6] |

En résumé, les variations de température ou d'entropie des matériaux SMA et caoutchoucs sont plus importantes que dans les autres matériaux caloriques[129]. En comparaison aux SMA, le caoutchouc présente l'avantage d'être bon marché et souple, tandis qu'il nécessite des déformations importantes. En revanche, le caoutchouc est un isolant thermique, ce qui peut poser des problèmes d'échanges thermiques dans le cadre d'un système de réfrigération.

### 1.3 Conclusions et perspectives

En considérant l'ensemble des matériaux caloriques, les matériaux magnétocaloriques, bien que très performants utilisent des métaux rares (voire toxiques) tandis que les matériaux électrocaloriques sont toujours utilisés proches de leur rupture diélectrique.

Les matériaux élastocaloriques présentent un certain nombre d'avantages, et parmi les deux classes de matériaux prometteuses, le caoutchouc naturel apparait comme un très bon candidat : un fort effet élastocalorique, un matériau souple, bon marché, et pouvant malgré tout résister à la fatigue sous certaines conditions (pré déformation). Les recherches sur le caoutchouc naturel en tant que matériau élastocalorique sont rares, et la marge de progression est grande. En outre, les développements effectués pour la réfrigération magnétocalorique (systèmes régénératifs) peuvent certainement se transposer à d'autres effets caloriques, notamment élastocaloriques.

En considérant l'application de l'effet élastocalorique pour le refroidissement, la seule recherche du plus fort effet ne saurait être pertinente, si elle se fait au détriment de la résistance à la fatigue ou des propriétés élastiques ou de conduction thermique par exemple.

Dans le cadre de ce travail de thèse, l'effet élastocalorique du caoutchouc naturel a été étudié, en s'appuyant sur la cristallisation induite par la déformation. Le comportement est fortement nonlinéaire aussi bien sur l'effet élastocalorique que l'élasticité. Un modèle physique est proposé dans lequel l'importance de la cristallisation induite par la déformation est soulignée. Les effets de fatigue sont ensuite caractérisés. Enfin, un modèle analytique de système régénératif est proposé pour permettre une identification des paramètres clés et un dimensionnement du système.

## 2 Caractérisation expérimentale du caoutchouc naturel

Cette partie est consacrée à la caractérisation expérimentale de l'effet élastocalorique dans le caoutchouc.

### 2.1 Dispositif expérimental

Le banc expérimental comprend une table de translation (XM-550, Newport, New-York) permettant d'étirer l'échantillon associé avec un capteur de force pour mesurer la contrainte (ELPF-T2M-250N, Measurement Specialities, Paris). La mesure de température est réalisée à l'aide d'une caméra thermique (NEC G-120, Japan).

Les échanges thermiques de l'échantillon sont de plusieurs natures: conduction dans les mors de fixation de l'échantillon, convection avec l'air ambiant et rayonnement thermique. Afin de se rapprocher au maximum d'une condition adiabatique, des matériaux isolants thermiquement ont été utilisés pour tenir l'échantillon. La caméra thermique est ensuite calibrée sur l'échantillon pour corriger son émissivité (facteur de correction de 0,86). Les images thermiques ont été enregistrées à une fréquence de 10Hz et le bruit de mesure constaté est de $\pm 0.1^{\circ}$C[140].

Lorsque l'échantillon est étiré rapidement (échelon de déformation), la mesure peut être considérée comme adiabatique dans les premiers temps suivant l'échelon. C'est une méthode qui a montré sa pertinence dans le cas de l'effet électrocalorique[140]. Dans le cas de l'effet élastocalorique, une mesure de chaleur isotherme en calorimétrie différentielle paraît très compliquée à mettre en œuvre en raison de l'encombrement d'un système de traction.

Les grandeurs mécaniques utilisées dans ce travail sont

- la déformation nominale $\varepsilon_{en} = (l - l_0)/l_0$ avec $l - l_0$ variation de la longueur de l'échantillon par rapport à sa longueur initiale $l_0$. L'élongation $\lambda$ est alors définie comme $\lambda = 1 + \varepsilon_{en}$.
- La contrainte nominale $\sigma_{en} = F / A_0$, la force $F$ divisée par la section initiale avant étirement $A_0$.

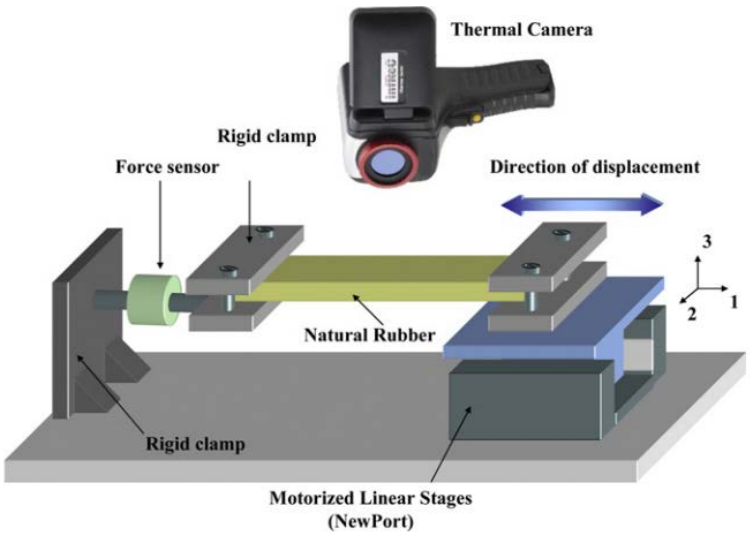


Fig.FR 12 Dispositif expérimental[3].

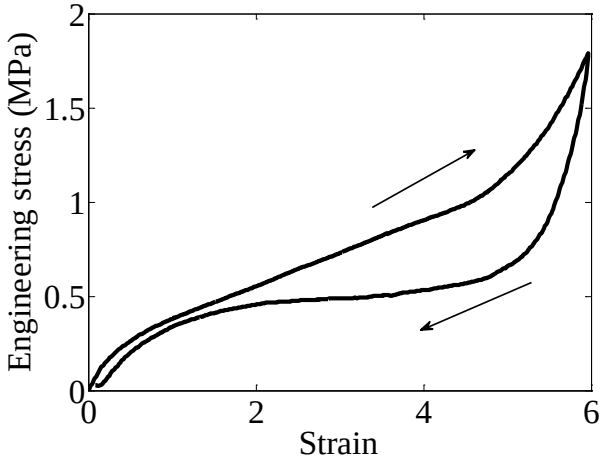


Fig.FR 13 Contrainte-déformation après 5 cycles identiques (stable) à la vitesse de déformation constante de 0.024 $s^{-1}$.

Le matériau choisi pour les caractérisations est un caoutchouc commercialisé par Xinyinte Rubber Products Co., Ltd. (China). La référence testée est faiblement réticulée et présente une densité de chaîne du réseau de $1.3\times10^{-4} mol\cdot cm^{-3}$. Il est à noter qu'il s'agit d'une valeur très proche de celle désignée par Chenal et al.[56] ($1.2\times10^{-4} mol\cdot cm^{-3}$) comme optimale pour favoriser la cristallisation induite par la déformation La valeur expérimentale de l'échantillon testé a été déterminée à bas niveau de déformation[51] en supposant que l'échantillon se comporte comme un élastomère pur[5]:

$$\sigma = NkT(\lambda - \lambda^{-2}) \qquad \text{(Équation 2)}$$

avec $\sigma$ la contrainte, *N* la densité de chaîne du réseau, *k* la constante de Boltzmann constant, *T* la température absolue et $\lambda$ l'élongation.

La section de l'échantillon est de 20mm x 100µm et la longueur initiale est de 10mm. Les mesures contrainte-déformation sont réalisées avec une rampe de déformation de 0.024 $s^{-1}$ (Fig.FR 13).

Lors de l'application d'un échelon de déformation, un résultat typique de contrainte et de température est donné Fig.FR 14. La rampe de montée et de descente de la déformation est de 20 $s^{-1}$ et l'amplitude de l'échelon est de 5.

On observe lors de la montée de la déformation que la température augmente brutalement avant de décroître de manière exponentielle jusqu'à la température ambiante en raison des échanges thermiques avec l'extérieur. La contrainte augmente aussi brutalement, avant de décroitre aussi pendant le plateau de déformation. Lorsque la déformation revient à zéro, la température décroît brutalement en dessous de la température ambiante et la contrainte revient à zéro. La décroissance de la contrainte lors du plateau de déformation est typique de la relaxation de la contrainte due à la cinétique de cristallisation induite par la déformation.

Comme dans toute caractérisation d'effet calorique, il est important de s'assurer que la température mesurée est bien caractéristique de l'effet couplé et non pas un biais expérimental. Pour cela, on s'assure que les constantes de temps thermiques lors de l'étirement et de la rétraction sont bien compatibles. Par un modèle d'échange thermique linéaire, il est possible de montrer que la constante de temps thermique $\tau$ est donnée par

$$\tau = \frac{ce}{2h} \qquad \text{(Équation 3)}$$

avec c, e et h chaleur spécifique (en $J.m^{-3}.K^{-1}$), épaisseur de l'échantillon et le coefficient d'échange thermique superficiel (en $W.m^{-2}.K^{-1}$) respectivement.

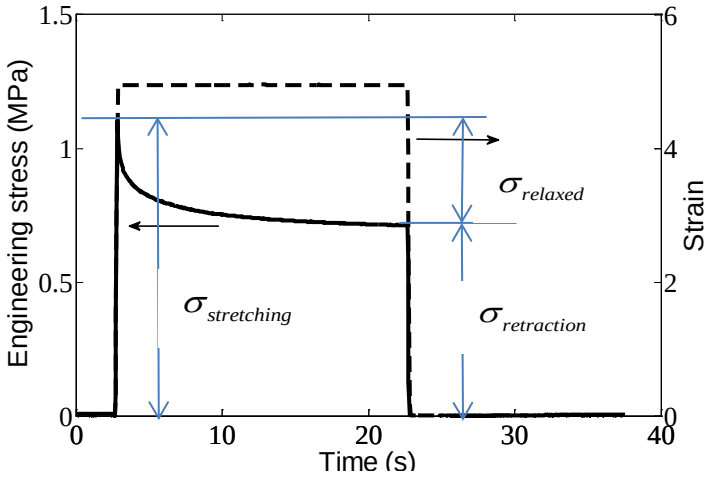


(a)

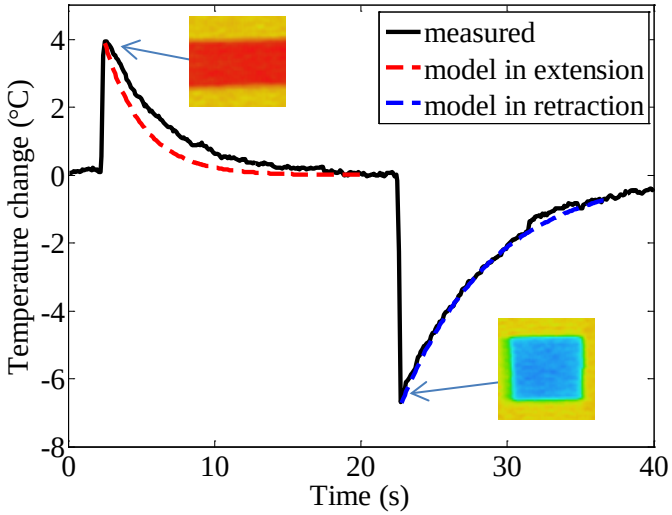


(b)

Fig.FR 14 Résultat typique contrainte-déformation (a) et température en fonction du temps (b) pour un échelon de déformation d'amplitude 5. Les images thermiques aux deux extremums de température sont données.

Compte-tenu de valeurs raisonnables pour *c* et *h*, ainsi que des épaisseurs de l'échantillon de 100µm au repos et de 40µm à l'état étiré, on obtient

$$\tau_{re} = \frac{ce}{2h} = \frac{1.8\times10^{6}\times100\times10^{-6}}{2\times14} = 6.4s$$

$$\tau_{ex} = \frac{ce}{2h} = \frac{1.8\times10^{6}\times40\times10^{-6}}{2\times14} = 2.6s$$

Les décroissances exponentielles associées sont représentées sur la Fig.FR 14. On remarque alors que si on ajuste le paramètre c/h pour simuler correctement le pic négatif de température, on surestime la décroissance de la température lors de l'étirement. Il apparaît donc que la température semble « durer » trop longtemps, et cela est significatif de la cinétique de la cristallisation induite par la déformation. La cristallisation et la fusion apparaissant lors d'un cycle de déformation sont différentes [88,102,121], notamment la cristallisation présente un fort fluage tandis que la fusion est rapide. Ceci est mis en évidence par des quantifications de taux de cristallinité déterminés sur des matériaux similaires (voir Fig.FR 16)[92]. Ainsi, la mesure lors de la rétraction est plus représentative de l'effet élastocalorique car d'une part la fusion est rapide et se termine dans un temps respectant la

condition pseudo-adiabatique, ceci étant facilité d'autre part par le fait que la constante de temps thermique est plus grande.

Si on compare les pics positifs et négatifs de température pour différentes amplitudes de déformation, on obtient le résultat présenté Fig.FR 16. Dans le temps de mesure où la condition adiabatique est respectée, la fraction ayant cristallisée peut dans certains cas être faible devant celle mise en jeu lors de la fusion, ce qui explique la différence entre les pics mesurés lors de l'étirement et de la rétraction. Il n'y a donc pas de violation d'un quelconque principe thermodynamique, simplement la mesure lors de l'étirement n'est pas suffisamment fiable en raison de la difficulté d'être en condition adiabatique « suffisamment longtemps » pour que la cristallisation induite par la déformation soit complète. Un résultat comparable a aussi été observé par Sakata et al. [101] à de grandes déformations.

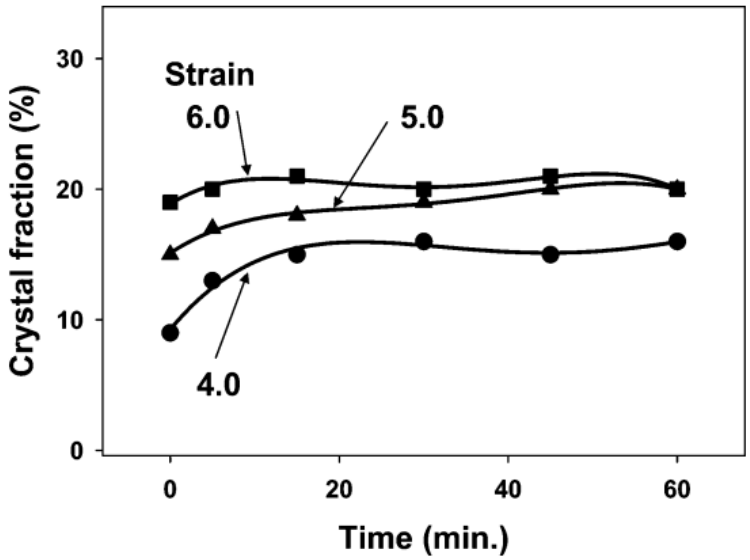


Fig.FR 15 Taux de cristallinité en fonction du temps pour différents échelons de déformation à 30°C sur un caoutchouc similaire à celui étudié ici [92].

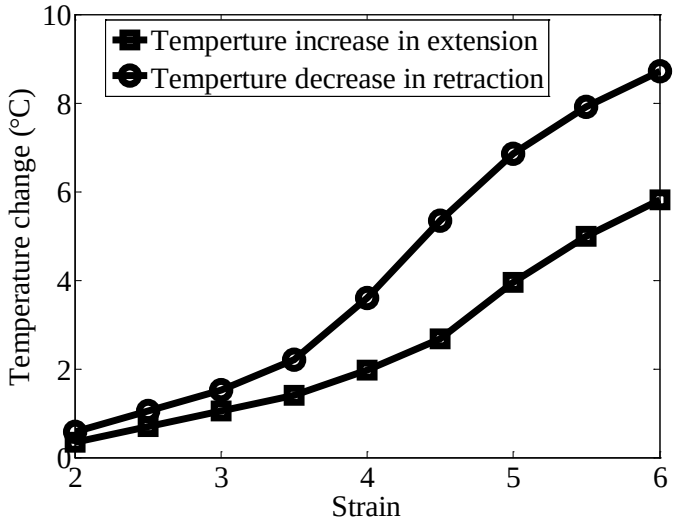


Fig.FR 16 Variations de température élastocaloriques à l'étirement et à la rétraction.

### 2.2 Analyse thermodynamique

Afin de quantifier l'effet élastocalorique à partir des mesures de températures adiabatiques, et de définir des coefficients élastocaloriques, une analyse thermodynamique des grandeurs constitutives est menée.

L'énergie libre d'Helmholtz $A$ s'écrit,

$$A = U - TS$$

avec $U$ l'énergie interne, $T$ la température, $S$ l'entropie.

En forme différentielle:

$$dA = dU - TdS - SdT$$

La conservation de l'énergie implique

$$dU = dQ + dW$$

avec $dQ = TdS$ et $dW = fdl$ chaleur et travail mécanique échangée avec l'extérieur, $f$ étant la force appliquée à l'échantillon de longueur $l$.

Par conséquent $dU = TdS + fdl$ et $dA = fdl - SdT$

Force et entropie sont donc données par

$$f = \left(\frac{\partial A}{\partial l}\right)_T \; ; \; S = -\left(\frac{\partial A}{\partial T}\right)_l$$

La relation de Maxwell s'écrit

$$\frac{\partial}{\partial l}\left(\frac{\partial A}{\partial T}\right)_l = \frac{\partial}{\partial T}\left(\frac{\partial A}{\partial l}\right)_T \text{ et par conséquent } -\left(\frac{\partial S}{\partial l}\right)_T = \left(\frac{\partial f}{\partial T}\right)_l$$

Les variations $df$ et $dS$ s'écrivent alors,

$$\begin{cases} df = \frac{\partial f}{\partial l}\big|_T \cdot dl + \frac{\partial f}{\partial T}\big|_l \cdot dT \\ dS = \frac{\partial S}{\partial l}\big|_T \cdot dl + \frac{\partial S}{\partial T}\big|_l \cdot dT \end{cases}$$

On convertit ensuite ce système d'équations en grandeurs macroscopiques locales

$$\begin{cases} d\sigma = \frac{\partial \sigma}{\partial \varepsilon}\big|_T \cdot d\varepsilon + \frac{\partial \sigma}{\partial T}\big|_\varepsilon \cdot dT \\ ds = \frac{\partial s}{\partial \varepsilon}\big|_T \cdot d\varepsilon + \frac{\partial s}{\partial T}\big|_\varepsilon \cdot dT \end{cases}$$

avec $\sigma$ contrainte nominale, $\varepsilon$ déformation nominale, $\mathrm{E} = (\partial\sigma / \partial\varepsilon)_T$ est le module d'Young et $\frac{c}{T} = (\partial s / \partial T)_\varepsilon$ est la chaleur spécifique ($c$) divisée par la température ($T$). La relation de Maxwell implique alors

$$\beta = \left(\frac{\partial \sigma}{\partial T}\right)_\varepsilon = \frac{\partial}{\partial T}\left(\frac{\partial A}{\partial \varepsilon}\right)_T = \frac{\partial}{\partial \varepsilon}\left(\frac{\partial A}{\partial T}\right)_\varepsilon = -\left(\frac{\partial s}{\partial \varepsilon}\right)_T$$

$\beta = -\left(\frac{\partial s}{\partial \varepsilon}\right)_T$ est alors le coefficient élastocalorique[4], et $\beta = \left(\frac{\partial \sigma}{\partial T}\right)_\varepsilon$ est le facteur de Clausius-Clapeyron.

En remplaçant par les coefficients

$$\begin{cases} d\sigma = E \cdot d\varepsilon + \beta \cdot dT \\ ds = -\beta \cdot d\varepsilon + \dfrac{c}{T} \cdot dT \end{cases}$$

La variation de température adiabatique lors d'une augmentation de la déformation de 0 à une valeur maximum $\varepsilon$ est ensuite donnée par

$$\Delta T = -\frac{T_0}{c}\int_0^{\varepsilon}\left(\frac{\partial s}{\partial \varepsilon}\right)_T d\varepsilon = \frac{T_0}{c}\int_0^{\varepsilon}\left(\frac{\partial \sigma}{\partial T}\right)_{\varepsilon} d\varepsilon$$

Cette expression lie donc l'effet élastocalorique au coefficient thermomécanique (ou facteur de Clausius-Clapeyron). La détermination de ce coefficient par des mesures alternatives constitue la caractérisation indirecte. Dans l'hypothèse où le matériau se comporte de manière ergodique, les caractérisations directes et indirectes devraient être concordantes[149].

### 2.3 Caractérisation directe et indirecte de l'effet élastocalorique

**Caractérisation directe**

Le coefficient élastocalorique en déformation a été évalué par la mesure de la variation de température adiabatique. La variation $\Delta T$ est proportionnelle à la variation d'entropie isotherme $\Delta s$ en première approximation,

$$T_0 \times \Delta s\Big|_{T=T_0} = -c \times \Delta T\Big|_{s=s_0}$$

où $T_0 = 295K$ est la température à laquelle l'effet est mesuré, $s_0$ est l'entropie du matériau lors de la mesure adiabatique et $c = 1.8\times10^6 J\cdot K^{-1}\cdot m^{-3}$ est une valeur approximative de la chaleur spécifique du caoutchouc testé [144] (supposé indépendant de la déformation et de la température)

$$\Delta s = -\frac{c}{T_0}\Delta T$$

Ainsi, le coefficient élastocalorique est obtenu par une dérivation de la courbe température - déformation

$$\beta = \frac{c}{T_0}\cdot\frac{\partial T}{\partial \varepsilon}$$

Pour le matériau testé, le coefficient est fonction de la déformation et est tracé Fig.FR 17. On constate qu'il est maximum pour une déformation de 4,5, c'est-à-dire pour la déformation à laquelle la variation de la cristallisation en fonction de la déformation est maximale.

Il est aussi possible de définir un coefficient élastocalorique en contrainte par

$$\gamma = \frac{\partial T}{\partial \sigma_{stretching}}$$

Ce coefficient présente la même allure que le coefficient en déformation avec un maximum pour une déformation comprise entre 4 et 5.

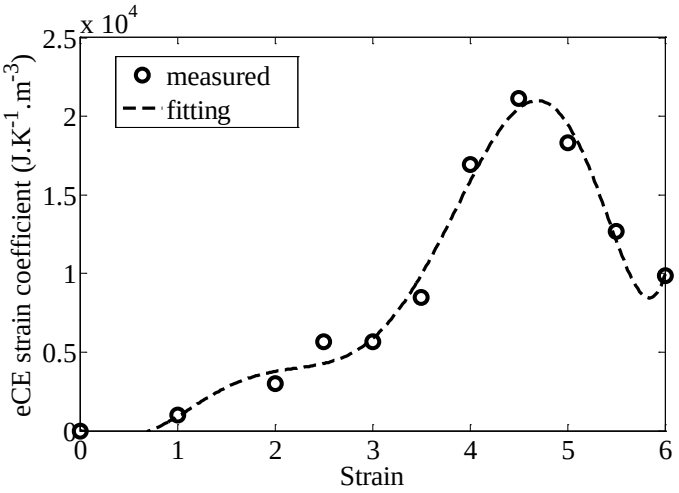


Fig.FR 17 Coefficient élastocalorique en déformation en fonction de celle-ci.

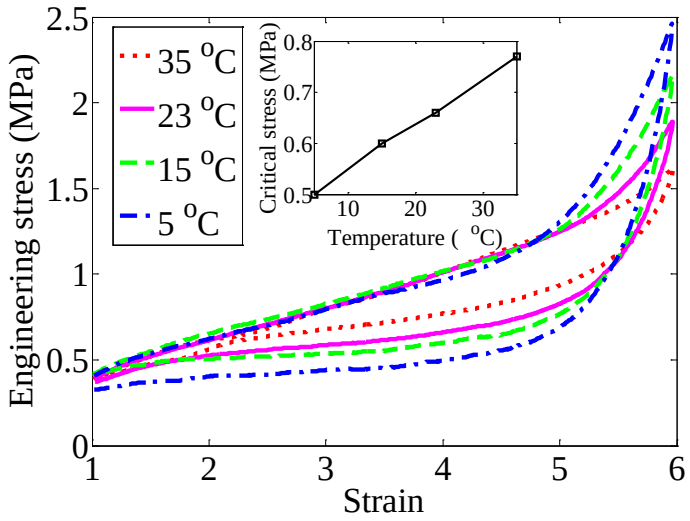


Fig.FR 18 Courbe contrainte-déformation mesurée avec une vitesse de déformation de 0.02 $s^{-1}$, pour 4 températures statiques différentes.

**Caractérisation indirecte**

L'utilisation de la relation de Maxwell peut permettre de remplacer des grandeurs difficiles à mesurer par d'autres plus accessibles. En effet, la caractérisation directe nécessite de contrôler précisément les conditions thermiques (adiabatique) tout en assurant une bonne précision de mesure. En revanche, la détermination du facteur de Clausius-Clapeyron peut se résumer à une condition isotherme, et une mesure purement mécanique, potentiellement bien plus précise que la mesure d'une grandeur thermique. Cela est employé largement dans le cas des alliages à mémoire de forme[13,19,151,152]. Dans cette partie, les mesures directes et indirectes sont comparées. Le facteur de Clausius-Clapeyron est déterminé de deux manières différentes.

1ère méthode :

Le comportement mécanique du matériau est déterminé pour différentes températures statiques. Le dispositif expérimental est alors modifié pour permettre de déporter l'échantillon sous étirement dans une étuve contrôlée en température.

Le résultat est donné Fig.FR 18. L'aspect remarquable de ce résultat est que lors de l'étirement, la contrainte semble indépendance de la température (toutes les courbes sont confondues), et pour des déformations dépassant 5, la contrainte maximale est obtenue pour les températures les plus froides. Cela est lié à l'effet durcissant de la cristallisation du caoutchouc, où, pour de plus hautes températures, l'effet est réduit en raison d'une plus faible cristallisation. En revanche, lors de la rétraction de l'échantillon, l'effet de relaxation devient prépondérant, et on constate alors que la contrainte la plus forte est obtenue pour la plus grande température. Partant de ce résultat, il devient difficile d'estimer le coefficient $(\partial\sigma/\partial T)_\varepsilon$ à partir de ces mesures. Si on considère l'étirement, le coefficient est soit nul, soit négatif, ce qui signifierait que l'échantillon devrait refroidir quand on l'étire, en contradiction avec la mesure directe. Si on considère la courbe de rétraction, le signe du coefficient devient positif, et on peut estimer la variation de température élastocalorique à $\Delta T = \frac{T_0}{c}\left(\frac{\partial\sigma}{\partial T}\right)_\varepsilon \Delta\varepsilon = 5.9K$, ce qui est inférieur à la mesure expérimentale. Le problème majeur de cette caractérisation semble donc être l'hystérésis de la contrainte. Pourtant, cette caractérisation fonctionne avec succès dans le cas des alliages à mémoire de forme, tel que montré dans différentes études[13,19,151,152]. Par contre, dans ce cas, un plateau beaucoup plus net est habituellement observé aussi bien pour l'étirement que pour la rétraction, et le coefficient $(\partial\sigma/\partial T)_\varepsilon$ est toujours positif. Le plateau de contrainte est attribué à la transformation de phase austénitique - martensitique[20]. Dans le cas du caoutchouc, l'absence de plateau en étirement rend la mesure indirecte imprécise. La nature de la transition est sans doute responsable d'un hystérésis dont la dépendance en température ne permet pas d'estimer de façon fiable le facteur de Clausius-Clapeyron.

2ème méthode :

Dans un second temps, afin de déterminer de façon plus directe ce coefficient, l'échantillon est d'abord étiré lentement à une valeur de déformation donnée puis gardé étiré le temps que la cristallisation soit stabilisée (150s) [153]. Puis la température est augmentée à déformation constante. On mesure alors la contrainte au cours de la variation de température. Dans ce cas, on observe toujours une augmentation de la contrainte, quelle que soit la déformation statique imposée (voir Fig.FR 19), ce qui implique que toujours $(\partial\sigma/\partial T)_\varepsilon > 0$.

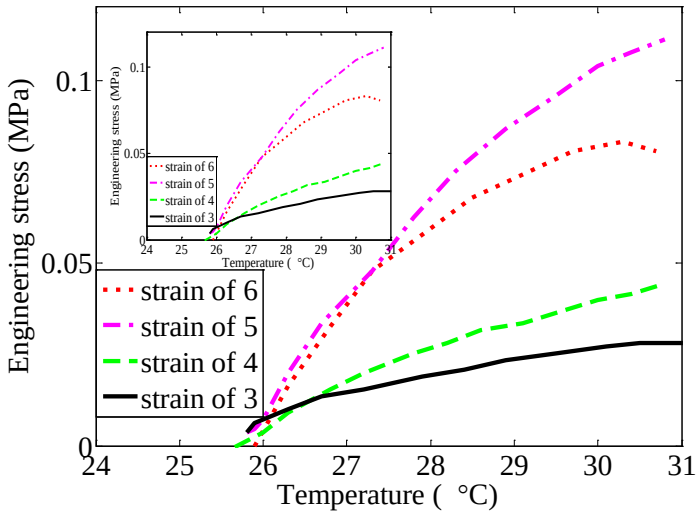


Fig.FR 19 Courbe d'évolution de la contrainte en fonction de la température pour différentes déformations statiques.

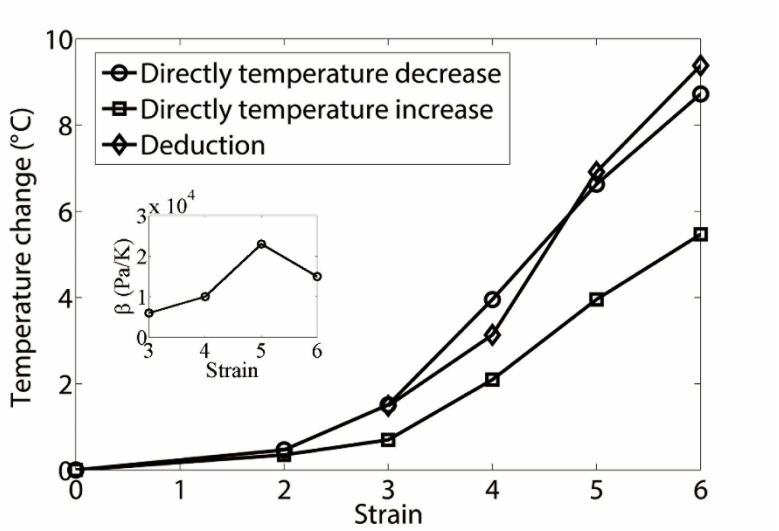


Fig.FR 20 Résultat de la caractérisation directe et indirecte de l'effet élastocalorique. La 2ème méthode indirecte est utilisée pour cette déduction.

A partir des valeurs du coefficient $(\partial\sigma/\partial T)_{\varepsilon}$ ainsi déterminées, la variation de température adiabatique est calculée et comparée à la mesure directe. Le résultat est donné Fig.FR 20. L'accord entre mesure indirecte et directe est alors excellent. Il est à noter que pour la mesure directe, il s'agit bien de la variation de température lors de la rétraction qu'il faut considérer ainsi qu'il a été établi dans l'analyse de la pertinence de la condition adiabatique et de la cinétique de transition.

En conclusion, il est possible d'utiliser une méthode indirecte de caractérisation, qui nécessite néanmoins de solliciter le couplage élastocalorique directement, c'est-à-dire mesurer une grandeur mécanique en appliquant une variation thermique.

### 2.4 Effet de la pré déformation sur le coefficient élastocalorique

Le coefficient élastocalorique montre une valeur maximale pour une déformation entre 4 et 5, montrant qu'il existe une zone de performance maximale. Dans un souci d'application de cet effet, on remarque qu'une très grande déformation imposée à l'échantillon rend la conception d'un échangeur thermique difficile si l'échantillon est étiré de plusieurs fois sa longueur. Dans cette partie, on cherche à déterminer un régime de fonctionnement permettant de travailler avec une pré déformation, pour éviter la zone initiale de faible effet couplé.

Une déformation relative est alors définie comme étant

$$\Delta\varepsilon_r = \frac{\Delta l}{l_{pre}} = \frac{\Delta l}{l_0 \cdot (1+\varepsilon_{pre})} = \frac{\Delta\varepsilon_m}{(1+\varepsilon_{pre})}$$

avec $\Delta l$ allongement supplémentaire à partir d'un allongement initial, $l_0$ longueur initiale sans pré déformation, $l_{pre}$ longueur à la pré déformation, $\varepsilon_{pre}$ pré déformation, et $\Delta\varepsilon_m$ variation de déformation dynamique.

La procédure expérimentale de caractérisation de l'effet élastocalorique est la même que pour les cas précédents, où seul le pic lors de la rétraction est considéré. La pré déformation est en revanche appliquée lentement pour que l'état pré déformé soit stabilisé avant la caractérisation de l'effet élastocalorique. Le résultat est donné Fig.FR 21. Il apparaît clairement que la pente température – déformation est augmentée par la pré déformation tel qu'on pouvait s'y attendre. On identifie alors une pré déformation optimale autour de 2 ou 3 permettant à la fois d'avoir un coefficient important, mais aussi une variation de température importante (3-4°), nécessaire pour envisager des applications[17].

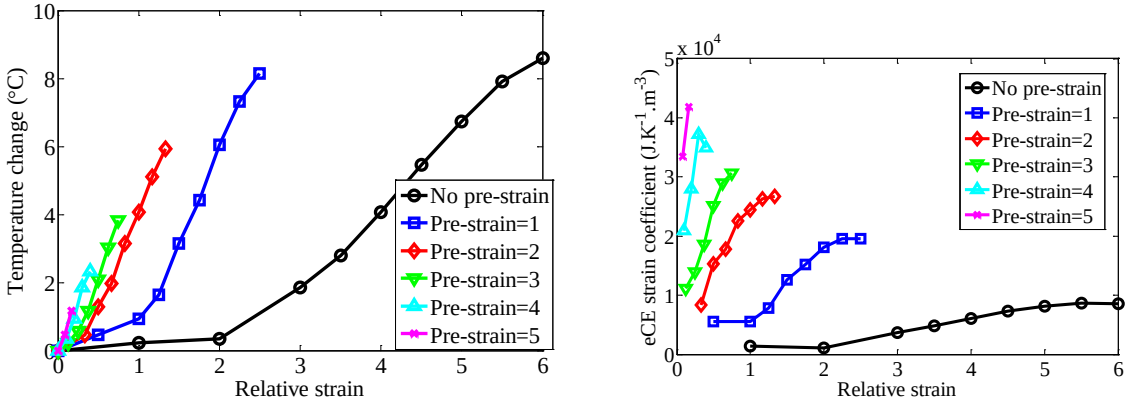


(a) (b)

Fig.FR 21 Effet élastocalorique en fonction de la déformation pour différentes pré déformations.

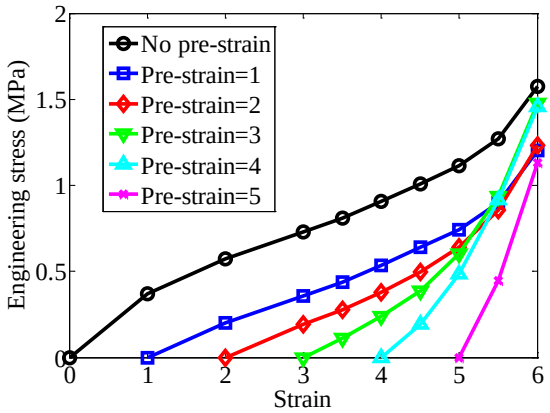


Fig.FR 22 Contrainte en fonction de la déformation pour différentes pré déformations. Contrairement à la figure précédente, l'abscisse correspond à la déformation totale et non relative pour faciliter la lecture de la courbe.

Pour les mêmes pré déformations, le coefficient élastocalorique en contrainte est aussi mesuré. Des valeurs optimales autour de 6 K/MPa sont alors obtenues pour une pré déformation de 2, et le coefficient élastocalorique en déformation est de $2.4 \times 10^4$ J.K$^{-1}$.m$^{-3}$.

Toutefois, on constate que suivant la pré déformation, la contrainte obtenue pour une déformation totale donnée varie, traduisant ainsi le fait que la contrainte dépend de l'histoire du matériau, alors que l'effet élastocalorique semble relativement indépendant. La dépendance de la contrainte avec la pré déformation est illustrée Fig.FR 22.

D'un point de vue du matériau, on constate néanmoins que le coefficient élastocalorique pour une pré déformation donnée est inférieur à celui obtenu sans pré déformation. Par exemple, la caractérisation directe donnait une variation de température de 6° quand la déformation passe de 3 à 6, alors qu'avec une pré déformation de 3 et une déformation dynamique de 3 donne une variation de température de seulement 4°. Pour une pré déformation donnée, compte-tenu du temps long pendant lequel l'échantillon est étiré, la cristallisation à cette déformation augmente dans le temps, et minimise donc le potentiel de cristallisation supplémentaire.

### 2.5 Conclusion

La caractérisation de l'effet élastocalorique a tout d'abord montré la forte variation de température (jusqu'à 8°), ainsi que les nécessaires précautions expérimentales. La définition de coefficients élastocaloriques a permis une quantification de l'effet qui pourra dans des travaux futurs

être utilisée pour la caractérisation d'autres matériaux. Ces mesures macroscopiques ont permis par ailleurs de confirmer de manière indirecte l'importance de la cristallisation dans l'effet élastocalorique.

La nature de la cristallisation entraîne un certain nombre de particularités dans le comportement du matériau, ce qui le différencie des alliages à mémoire de forme élastocaloriques. Notamment, la caractérisation indirecte est délicate car elle nécessite tout de même une mesure couplée. Toutefois, il a été montré que sous certaines conditions, la relation de Maxwell se vérifie.

Enfin, l'utilisation d'une pré déformation a été testée pour tenter de minimiser la déformation relative nécessaire pour obtenir un effet donné.

## 3 Modèle physique de l'effet élastocalorique du caoutchouc naturel

Dans ce chapitre, le modèle de la SIC (Strain induced cristallisation) de Flory est modifié pour prévoir le comportement de la contrainte à différentes températures ainsi que la variation de température élastocalorique à température ambiante.

### 3.1 Le modèle de Flory modifié

Dans le modèle de Flory, la SIC se produit complètement après étirement. *N* (densité de chaîne de réseau) et *n* (nombre de liens rigides entre les points de réticulation) sont maintenus constants en négligeant le réseau SIC dans le processus d'étirement. Ainsi, la SIC ne peut que contribuer à la relaxation de contrainte et ne permet pas de prévoir l'effet de durcissement de contrainte. La modification proposée ici consiste à considérer que *N* et *n* sont fonction de la déformation et de la température.

Un cristallite agissant comme un nouveau point de réticulation, la longue chaîne liée par des points de réticulation chimiques est séparée en chaînes courtes par les cristallites. Le nombre de chaînes courtes $N_c$ provoquée par les cristallites dans chaque chaîne est $N_c = 1 + \frac{\xi}{\psi}$, où $\xi$ est le nombre de liaisons cristallines par chaîne, $\psi$ est le nombre de liaisons dans une cristallite.

Ainsi, la densité de la chaîne de réseau totale $N_t$ après cristallisation est,

$$N_t = N_s \cdot N_c = N_s(1+\frac{\xi}{\psi}) = N_s(1+\frac{n_s \cdot C_e}{\psi}) \tag{3.1}$$

$N_s$ et $n_s$ sont la densité de réticulation chimique et le nombre de liaisons aléatoires équivalentes respectivement avant cristallisation; $C_e$ est la cristallinité à l'état équilibre.

Le nombre total de liens aléatoires équivalents après cristallisation est

$$n_t = \frac{n_s - \xi}{N_c} = \frac{\psi \cdot n_s \cdot (1-C_e)}{n_s \cdot C_e + \psi} \tag{3.2}$$

En remplaçant $N_t$ et $n_t$ dans le modèle de Flory, la contrainte $\sigma$ en fonction de l'élongation $\lambda$ s'écrit

$$\sigma = N_s(1+\frac{n_s \cdot C_e}{\psi}) \cdot \frac{kT}{1-\mathrm{C}_e}[(\lambda - 1/\lambda^2) - [\frac{6\psi \cdot n_s \cdot (1-C_e)}{\pi(n_s \cdot C_e + \psi)}]^{1/2}\,\mathrm{C}_e] \tag{3.3}$$

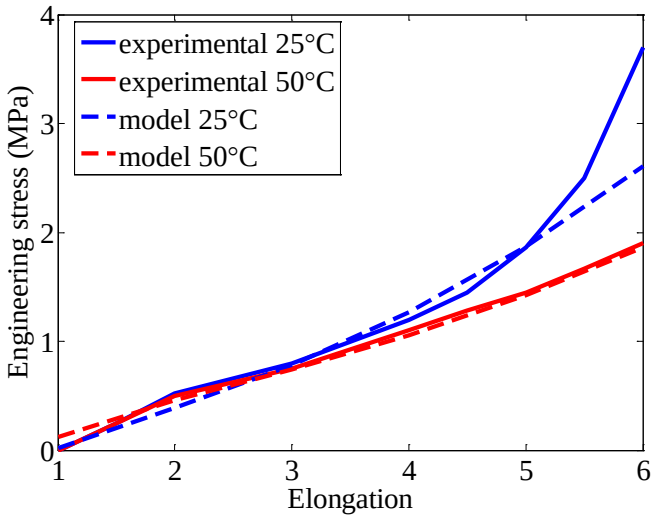


Fig.FR 23 La comparaison de la relation contrainte-déformation à des températures différentes avec le modèle. Les résultats ont été calculés à partir de Eq. (3.3) avec $N_s = 1.3\times10^{-4} mol\cdot cm^{-3}$, $n_s = 75$. Les données expérimentales a été prise à partir de Toki [87] pour la NR de même densité de chaîne de réseau.

L'équation (3.3) est utilisée pour calculer la contrainte en fonction de la déformation à des températures différentes. Le modèle est comparé avec le résultat expérimental sur la Fig.FR 23. Pour le résultat expérimental, il est montré que la contrainte la plus faible est obtenue pour la température plus élevée, en raison de l'effet de durcissement induit par la SIC moins important à haute température. Ainsi, la densité de chaîne de réseau induite par reticulation des cristallites est inférieure à une température plus élevée, ce qui entraîne la diminution de la contrainte. Dans la Fig.FR 23, lorsque l'allongement est inférieur à 5 ($\lambda < 5$), le modèle de Flory modifié correspond bien aux données expérimentales aux températures différentes, ce qui ne peut pas être prédite par la théorie standard de l'élasticité du caoutchouc (moins de stress pour la température plus basse). Lorsque $\lambda > 5$, le modèle s'écarte des données expérimentales à 25 ºC. Les chaînes du réseau SIC peuvent atteindre leur limite d''extensibilité. Ainsi, le modèle en utilisant la fonction de distribution Gaussienne ne peut pas prédire la contrainte pour un allongement supérieur à 5. Toutefois, pour 50 ºC, le modèle peut prédire le stress jusqu'à allongement de 6. Il est en raison de la moins cristallinité à 50 ºC et donc le moins de stress durcissement de SIC. Il prouve l'effet durcissement de contrainte provient principalement vient de la SIC.

### 3.2 Le changement de température déduite du modèle de Flory

Comme décrit dans le modèle de Flory, l'écart entre le modèle et les résultats expérimentaux devrait provenir de l'hypothèse de la Flory: la SIC se produit complètement après étirement. Ainsi, l'effet de durcissement de la contrainte induit par la SIC n'a pas été pris en compte et seule la relaxation de la contrainte induite par la SIC est considérée. Dans la partie suivante, une vérification expérimentale de l'hypothèse de Flory est proposée.

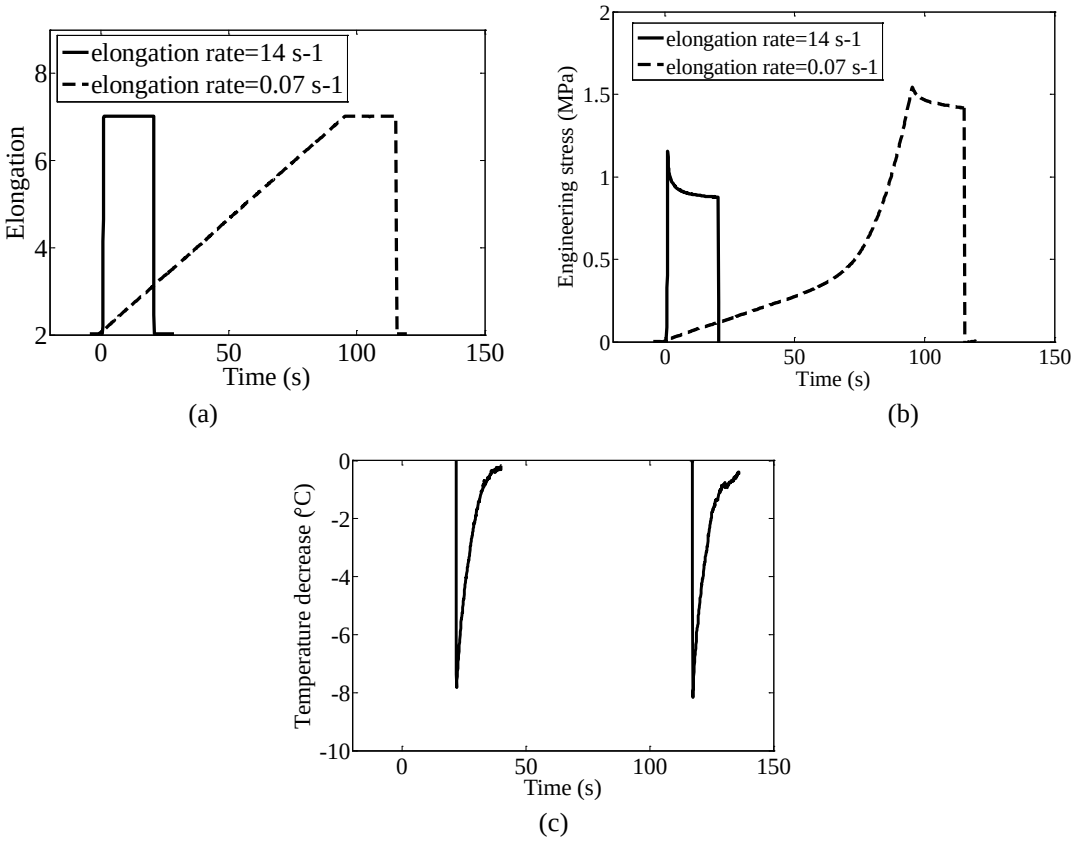


Fig.FR 24 Echantillon de caoutchouc étiré au taux d'allongement de 14 $s^{-1}$ et 0.07 $s^{-1}$ et rétracté à la même vitesse d'allongement rapide pour mesurer la diminution de la température adiabatique (effet élastocalorique): (a) allongement en fonction du temps; (b) contrainte en fonction du temps; (c) variation de température en fonction du temps.

Lors de l'étirement de la NR, une variation irréversible de l'entropie peut se produire en raison de la rupture des chaînes de réseau [155]. Dans ce travail, seule la diminution de la température dans le processus de rétraction a été présentée afin d'éviter que la détermination de l'entropie ne soit influencée par des ruptures de chaînes.

L'échantillon de caoutchouc a été étiré à différentes vitesses d'allongement (de 0.009 $s^{-1}$ à 70 $s^{-1}$) et rétractées au même taux d'allongement de 20 $s^{-1}$ pour l'enregistrement de la diminution de température adiabatique. La Fig.FR 24 montre la contrainte et la diminution de la température au taux d'allongement de 0.07 $s^{-1}$ et 14 $s^{-1}$.

Dans la Fig.FR 24, il est montré que le plus grand taux d'allongement conduit à la plus grand contrainte relaxation de la contrainte, mais aussi une plus petite contrainte lors de la rétraction, tandis que le plus petit taux d'allongement conduit à une plus faible relaxation de la contrainte, mais une plus grande contrainte lors de la rétraction.

La variation de température mesurée lors de la rétraction est liée principalement à la quantité de la SIC formée pendant l'étirement de l'échantillon, peu importe que l'effet soit un durcissement de la contrainte ou sa relaxation. Sur la Fig.FR 25 la contrainte lors de l'étirement est tracée en fonction du taux d'allongement (variant de 0.009 $s^{-1}$ à 70 $s^{-1}$) ; montrant une diminution de 1.7MPa à 1MPa. Néanmoins, la variation de température est quasiment constante pour tous les taux d'élongation. On en conclue que quel que soit le taux d'allongement, la quantité totale de SIC est quasiment la même. Toutefois, la SIC ayant besoin de temps pour s'établir, elle survient principalement pendant le plateau de déformation dans le cas d'un étirement rapide. A l'inverse, lors d'un processus d'étirement lent, la SIC se produit principalement pendant l'étirement, ce qui augmente l'effet de durcissement de la

contrainte. Ainsi, les effets de la SIC sur la contrainte dépendent de la cinétique de l'étirement, tandis que l'effet élastocalorique demeure indépendant. La variation de température $\Delta T$ est un indicateur de changement d'entropie $\Delta s = c \cdot \Delta T / T_0$. Ainsi, on montre expérimentalement que le changement d'entropie dépend uniquement de l'allongement avant rétraction (indépendamment de la rampe de montée), tandis que la contrainte est très sensible à l'histoire de chargement du caoutchouc.

Dans l'hypothèse de Flory, la SIC survient après l'étirement, ce qui peut être considéré comme le cas d'un étirement rapide où la SIC ne peut pas se produire pendant l'étirement trop rapide. Même si cette hypothèse ne permet pas de prévoir précisément la contrainte, elle permet néanmoins de donner une indication fiable sur le taux de cristallinité atteint après étirement. Ainsi, la variation de température est calculée à l'aide de la cristallinité calculée par le modèle de Flory. La contribution au changement de température élastocalorique $\Delta T_c$ de la SIC peut être écrit comme,

$$\Delta T_c = C_e \cdot \frac{h_f}{c} \tag{3. 4}$$

où $c = 1.8 \times 10^6 J \cdot K^{-1} \cdot m^{-3} = 2 J \cdot K^{-1} \cdot g^{-1}$ est une estimation de la chaleur spécifique du caoutchouc naturel[144], et $h_f = 64 J \cdot g^{-1}$ est la chaleur latente de fusion. $C_e$ est la cristallinité calculée à partir du modèle de Flory (voir Chapitre 3 pour plus de détails).

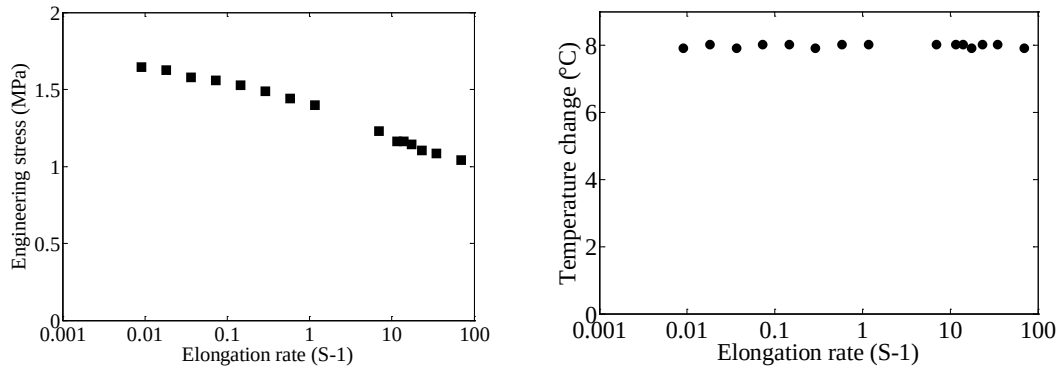


(a) (b)

Fig.FR 25 Contrainte (a) et variation de température élastocalorique (b) pour un même allongement de 6 en fonction du taux de montée de la déformation.

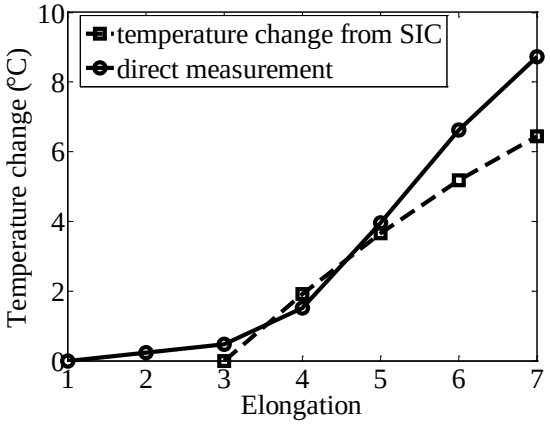


Fig.FR 26 La comparaison entre le changement de température mesurée directement et celle déduite de la contribution de SIC.

La comparaison entre la mesure élastocalorique directe et la variation calculée par l'équation (3.14) montre que la variation de température peut être principalement attribuée à la SIC. La différence entre les deux courbes peut être attribuée à la contribution de l'entropie élastique ou entropie d'un matériau élastomère.

En conclusion, même si le modèle de Flory rend difficilement compte de l'effet de durcissement de la SIC, il permet en revanche une bonne estimation de la quantité de SIC atteinte pour un étirement donné une fois l'équilibre atteint. Cette hypothèse correspond également à un étirement très rapide où la SIC ne peut pas se produire immédiatement dans le processus d'étirement. Cela prouve que la cristallinité ne dépend finalement pas de l'histoire de chargement. Cela indique en outre que la SIC contribuant à la relaxation de contrainte et la SIC contribuant à l'effet de durcissement de la contrainte contribue de la même façon à la variation de l'entropie.

## 4 Effets de la fatigue sur les propriétés élastocaloriques et mécaniques

Dans l'optique de concevoir un dispositif de refroidissement à base de matériau élastocalorique, il est primordial de s'assurer de la capacité du matériau à résister à un grand nombre de cycles d'excitation. Cette partie présente les essais en fatigue menés sur du caoutchouc naturel. Le matériau étudié est le même que celui caractérisé et présenté précédemment.

Pour l'application de l'effet élastocalorique, aussi bien la variation de température adiabatique que la contrainte sont des paramètres clés et sont donc mesurés ici. Dans un premier temps, des cycles de fatigue à très grande déformation (1-6) ont été testés. Dans un second temps, trois déformations intermédiaires ont été testées : cycles de déformation entre 0 et 3, cycles entre 2 et 5, et cycles entre 4 et 7.

Systématiquement, la caractérisation des propriétés élastocaloriques a été menée à l'aide d'échelon de déformation tel que présenté précédemment. A la suite d'une caractérisation élastocalorique, l'échantillon est "fatigué" par l'application de cycles sinusoïdaux à 2Hz et d'amplitude donnée.

La dégradation des propriétés est quantifiée par la définition d'indice de dégradation de l'effet élastocalorique $d_T = \frac{\Delta T_{before} - \Delta T_{fatigue}}{\Delta T_{before}}$ et d'un indice de dégradation de la contrainte $d_\sigma = \frac{\sigma_{before} - \sigma_{fatigue}}{\sigma_{before}}$ avec $\Delta T_{before}$, $\sigma_{before}$ variation de température et contrainte mesurées avant le cycle de fatigue, $\Delta T_{fatigue}$, $\sigma_{fatigue}$ mesurés après le cycle de fatigue.

### 4.1 Fatigue à grande déformation

Pour le test de fatigue à grande déformation, les cycles de fatigue à 2Hz sont des cycles de déformation variant de 1 à 6 (amplitude de 5). Après un certain nombre de cycles de fatigue, l'échantillon est alors caractérisé en échelon pour différentes amplitudes de déformation. Puis l'échantillon est à nouveau soumis à des cycles de fatigues de forte amplitude, etc. Suite à l'application de cycles de fatigue de grande amplitude (1-6), les propriétés élastocaloriques et mécaniques sont caractérisées régulièrement entre les cycles de fatigue. Les résultats sont tracés Fig.FR 27.

Entre le 1$^{er}$ cycle et le 10$^{ème}$ cycle, on constate une diminution importante de la contrainte (dégradation de 27%) et très peu de modification de l'activité élastocalorique. Entre le 10$^{ème}$ cycle et le 650$^{ème}$ cycle, on constate en revanche une dégradation aussi bien pour la contrainte que pour l'effet élastocalorique. Pour les propriétés mesurées à une déformation de 6, la dégradation est de 24% pour

l'effet élastocalorique et de 21 % pour la contrainte. Ceci est spécialement marqué à partir d'une déformation de 3 (correspondant au début de la SIC), ce qui signifie que la capacité du matériau à cristalliser subit un effet de fatigue.

Il est surprenant de constater qu'initialement, la contrainte présente des effets de fatigue mais que l'effet élastocalorique ne varie pas. Cela signifie que les variations d'entropie générées par la déformation restent identiques, mais que l'effet de cette dernière sur la contrainte diminue.

Après 800 cycles environ, des fissures apparaissent dans l'échantillon ce qui mène rapidement à sa rupture. Des points blancs sont observés dans l'échantillon et pourraient correspondre à de la cristallisation résiduelle ou à des défauts induits par la fatigue.

En exploitant le matériau entre une déformation de 1 et 6 permet de générer de très grandes variations de température (~8K), mais la faible durée de vie de l'échantillon rend le matériau inapplicable pour des systèmes de réfrigération. C'est pourquoi dans un second temps nous essayons de diminuer l'amplitude de la déformation pour augmenter la durée de vie de l'échantillon[8–10].

### 4.2 Fatigue à déformation moyenne

Le choix du régime de déformation doit être corrélé à l'apparition de la SIC. Lors de l'étirement du caoutchouc, la cristallisation débute pour une déformation de 3 tandis qu'à la rétraction, la fusion débute pour une déformation plus faible (environ 2) typique de l'hystérésis de la SIC[67]. La résistance à la fatigue peut être grandement améliorée par la SIC[88,107,108,163]. Le régime de déformation est choisi en conservant une amplitude dynamique toujours égale à 3, et la déformation minimale appliquée est de 0, 2 ou 4. Les régimes de déformation sont donc: zone amorphe (déformation 0-3), début de la SIC (déformation 2-5) et zone de forte SIC (déformation 4-7).

**<u>Test de fatigue pour le régime de déformation 0-3</u>**

Dans ces tests, les cycles sinusoïdaux sont appliqués à 2Hz et au régime de déformation 0-3. Contrairement aux caractérisations précédentes, l'effet élastocalorique et élastique ne sont déterminés que pour la même amplitude de déformation (pour éviter que la caractérisation ne soit responsable d'effets de fatigues supplémentaires).

La variation des propriétés électrocaloriques et élastiques sont tracés pour différents états de fatigue sur la Fig.FR 28. Il est remarquable de constater l'absence d'effet de fatigue sur l'effet élastocalorique, tandis que la contrainte diminue légèrement (dégradation de 10% au bout de 2200 cycles). En revanche, après 2200 cycles, des fissures de 1mm à 3mm apparaissent et mènent à la rupture de l'échantillon.

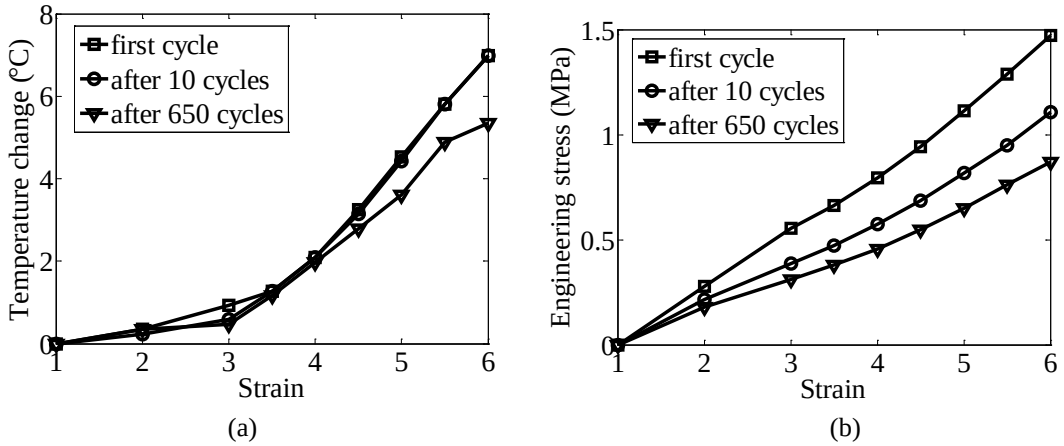


(a) (b)

Fig.FR 27 Dégradation des propriétés élastocaloriques et mécaniques en fonction de la déformation pour différents états de fatigue, après application de cycles répétés de déformation d'amplitude 1-6.

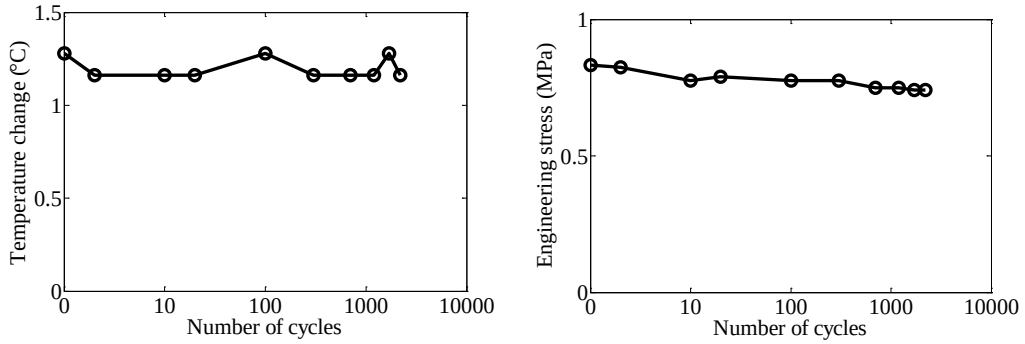


(a) (b)

Fig.FR 28 Dégradation des propriétés élastocaloriques et mécaniques en fonction de la déformation pour différents états de fatigue à un régime de déformation 0-3

**Test de fatigue pour le régime de déformation 2-5**

Dans un second temps, le même protocole a été appliqué sur un nouvel échantillon pour le régime de déformation 2-5. Dans ce cas, le matériau demeure intact après 3000 cycles, démontrant ainsi le mécanisme de protection de la SIC contre la rupture. La dégradation des propriétés est montrée Fig.FR 29. Au cours des 100 premiers cycles de fatigue, la variation de température élastocalorique passe de 4K à 3.3K (dégradation de 17%) tandis que la contrainte descend de 1.16MPa à 0.83MPa (dégradation de 28%). En revanche, la variation est ensuite stabilisée et varie peu jusqu'à 3000 cycles. Contrairement au régime de déformation 0-3, les propriétés élastocaloriques et élastiques se dégradent montrant ainsi un effet de la fatigue, mais dans le même temps, le matériau résiste à un plus grand nombre de cycles. La cristallisation semble donc être à la fois responsable de la fatigue observée et de la résistance à la rupture, conformément à d'autres études publiées[88,107].

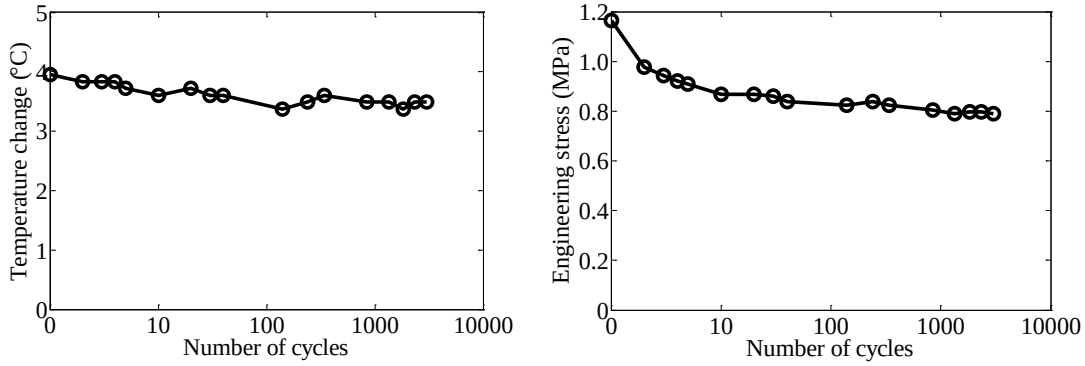


(a) (b)

Fig.FR 29 Dégradation des propriétés élastocaloriques et mécaniques en fonction de la déformation pour différents états de fatigue à un régime de déformation 2-5

**Test de fatigue pour le régime de déformation 4-7**

Pour ce régime de déformation, comme dans le cas précédent, il est possible d'atteindre 3000 cycles de déformation sans aucune rupture ou apparition de fissures. Entre le 1$^{er}$ cycle et de 500$^{ème}$ cycle, on constate une dégradation en température de 7% et en contrainte de 28%. Cette observation est comparable au cas de la déformation 2-5. Entre le 500$^{ème}$ cycle et 3000 cycles, la variation de température se stabilise tandis que la contrainte continue de se dégrader (Fig.FR 30).

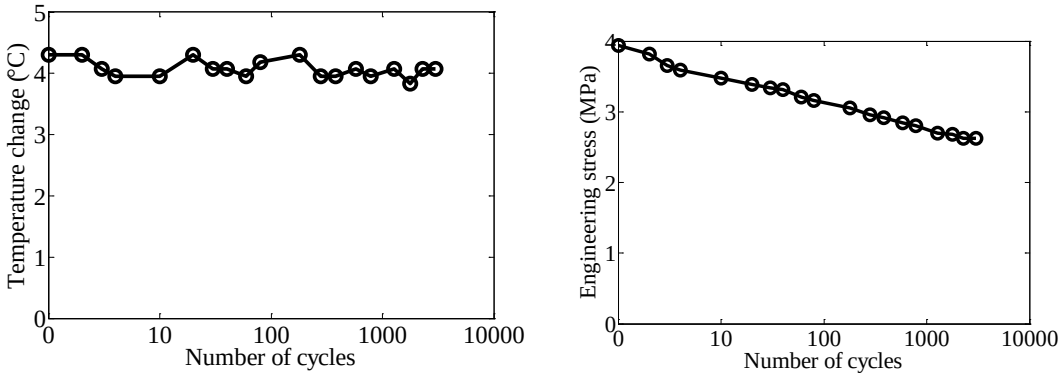


(a) (b)

Fig.FR 30 Dégradation des propriétés élastocaloriques et mécaniques en fonction de la déformation pour différents états de fatigue à un régime de déformation 4-7

**Comparaison entre les différents régimes de déformation**

Pour les régimes de déformation intermédiaire, il est important de noter tout d'abord que le régime de la plus basse déformation est non seulement associé à un faible effet élastocalorique, mais l'échantillon présente de plus une faible durée de vie en fatigue. De manière surprenante, c'est dans les régimes de plus grande déformation moyenne (2-5 et 4-7) que l'on observe aussi bien une forte activité élastocalorique qu'une bien meilleure résistance à la rupture.

Pour une même déformation dynamique de 3, la variation de température après un grand nombre de cycles pour les régimes de déformation 0-3, 2-5 et 4-7 est de 1.2 K, 3.5 K et 4.2 K, respectivement. Cela confirme l'importance de la SIC pour obtenir une forte activité élastocalorique. La dégradation des propriétés en fatigue sur la température reste modérée pour tous les régimes de déformation. La dégradation des propriétés en contrainte est en revanche plus importante dans les régimes de déformation de la SIC que dans le régime amorphe. Ce taux de dégradation de la contrainte est représenté Fig.FR 31. Entre les deux régimes de déformation de la SIC (2-5) et (4-7), on peut remarquer que la dégradation de la contrainte se poursuit pour le régime de plus grande déformation alors qu'il est stabilisé dans le cas de la plus faible déformation.

En outre, en comparant le coefficient élastocalorique en contrainte, il apparaît que le régime 2-5 présente un bien plus fort coefficient, dans la mesure où une variation de température comparable est obtenue pour une bien plus faible contrainte. Le coefficient déterminé expérimental est de $\gamma_{2-5} = 4.4K / MPa$ et $\gamma_{4-7} = 1.6K / MPa$.

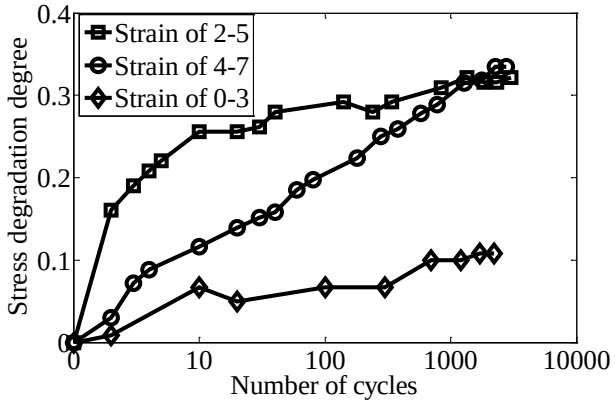


Fig.FR 31 Dégradation des propriétés mécaniques pour les trois régimes de déformation en fonction du nombre de cycles de fatigue.

### 4.3 Conclusions

Les effets de la fatigue sur les propriétés élastocaloriques et mécaniques ont été mesurées. Il est à noter que pour beaucoup d'autres effets caloriques, de tels essais n'ont pas encore été réalisés et publiés (notamment concernant l'effet électrocalorique dans les polymères).

Dans le cas du caoutchouc, il a été constaté qu'un régime de très grande déformation entraîne une rupture de l'échantillon pour un faible nombre de cycles. Pour des régimes de déformation intermédiaire (amplitude de 3), et en augmentant la déformation moyenne, il est possible d'obtenir à la fois un fort effet élastocalorique (à relier à la section 2 pour laquelle on a déjà montré l'intérêt d'une pré déformation), et une excellente résistance à la fatigue. En comparant le coefficient élastocalorique en contrainte, il s'avère que le régime de déformation 2- 5 est le plus adapté, avec une variation de température de presque 4K et une contrainte inférieure à 0,8MPa. Pour ce même régime de déformation, un banc de mesure plus adapté à un grand nombre de cycles a finalement été développé (moteur associé à une bielle – manivelle) a permis de s'assurer que l'échantillon ne rompt pas jusqu'à $3x10^5$ cycles, et que l'effet élastocalorique ne varie quasiment plus à partir de 10 000 cycles (variation de température de 3.8K après $3x10^5$ cycles).

D'autres études seront nécessaires pour établir l'influence de cycles combinés température – déformation tels que ceux rencontrés dans les machines thermiques, l'influence de la température sur les effets de fatigue, et d'établir une statistique de la rupture du caoutchouc pour différents régimes de déformation. Toutefois, les résultats préliminaires obtenus ici sont très encourageants pour l'applicabilité du caoutchouc naturel en tant que matériau calorique pour la réfrigération.

## 5 Modèle d'un système régénératif

Les matériaux caloriques, lorsqu'ils sont excités par la grandeur adaptée, sont le siège de variations de température cycliques dans le temps. Pour un système de réfrigération, il est nécessaire d'être capable de convertir cette variation temporelle en un gradient spatial, c'est à dire la capacité à générer une zone froide de l'espace, et une zone chaude. Une manière simple de réaliser cela a été introduite schématiquement Fig.FR 1 et consiste à déplacer le matériau actif entre les sources chaudes et froides de manière synchrone avec l'excitation calorique. Néanmoins, un tel système peut être complexe (mouvement mécanique à réaliser, contacts thermiques à assurer), et la différence de température entre les sources chaude et froide est limitée à la variation de température adiabatique générée par le matériau.

Les systèmes régénératifs permettent de résoudre simultanément le problème de la conversion temps – espace et de démultiplier la différence de température entre les sources chaude et froide. Dans le cas des matériaux magnétocaloriques, des systèmes dits AMR (active magnetic regenerator) ont été développé[16], et leur transposition au cas élastocalorique a été proposé par Tusek et al.[11].

Dans cette partie, nous proposons un modèle analytique de système régénératif. Il comprend un matériau actif calorique, et un matériau passif. Les matériaux sont en forme de plaques de dimensions latérales infinies, et un mouvement relatif entre les matériaux actif et passif est imposé de manière synchrone avec l'excitation calorique.

Dans les travaux exposés précédemment, nous avons mesuré les propriétés élastocaloriques, vérifié les effets de fatigue, et discuté des meilleurs régimes de déformation aussi bien pour les performances élastocaloriques que leur stabilité au cours de cycles de déformation. Toutefois, quelles sont les propriétés les plus importantes pour un dispositif de refroidissement ? C'est à travers la réflexion sur un système régénératif que les paramètres clés pourront être identifiés. Le modèle présenté ici utilise des hypothèses très restrictives mais permet néanmoins de donner des indications sur les propriétés importantes pour le refroidissement.

### 5.1 Présentation du modèle

Le modèle 2D est décomposé en deux modèles 1D pour en faciliter la résolution. La démarche de résolution est adaptée de travaux concernant des dispositifs thermoacoustiques[168–171].

Le système est illustré Fig.FR 32. Les plaques sont perpendiculaires à l'axe z tandis que le mouvement relatif est selon l'axe x. On suppose une dimension infinie suivant l'axe y (effet de bord négligés).

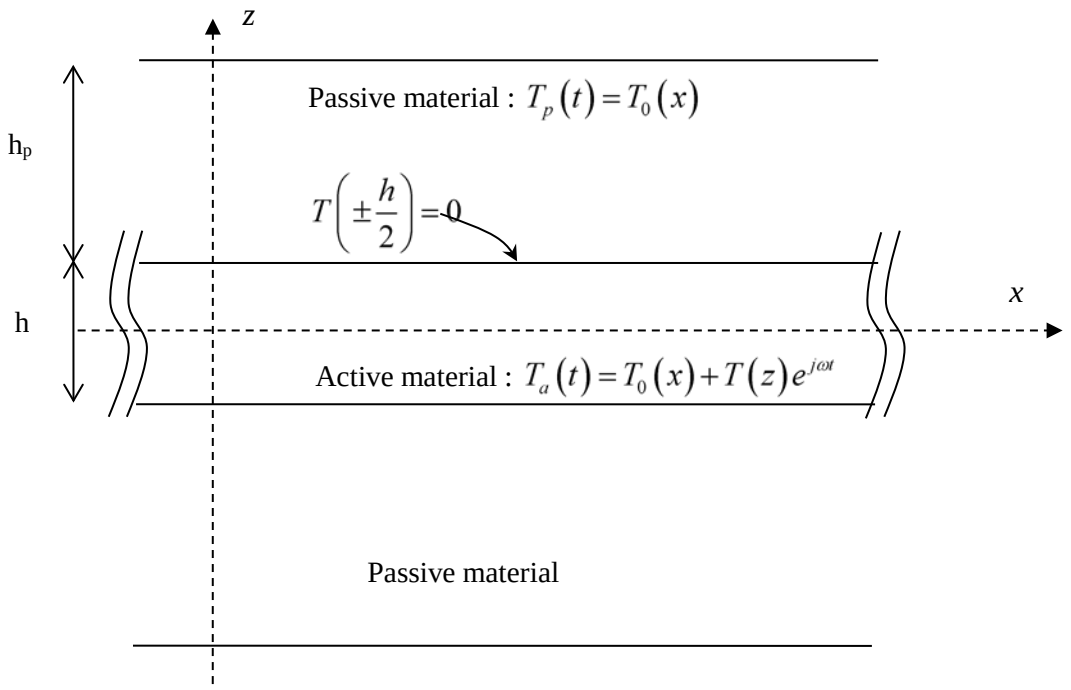


Fig.FR 32 Schéma du dispositif régénératif modélisé.

Le mouvement de la plaque active est écrit

$$\vec{v}(x,t) = v(x,t)\vec{u_x} = \underline{v_0}(x)e^{j\omega t}\vec{u_x} = v_0 e^{j\varphi}e^{j\omega t}\vec{u_x}$$

Le matériau actif se comporte comme une source de chaleur sinusoïdale donnée par $Q(t) = q_0 e^{j\omega t}$. Dans le cas d'un effet élastocalorique, $q_0 = T_0\beta\varepsilon_0$ avec $\varepsilon_0$ déformation dynamique appliquée, $\beta$ coefficient élastocalorique en déformation et $T_0$ température de travail. Le matériau passif joue à la fois le rôle de milieu de transfert thermique et de milieu de stockage de la chaleur. Dans ce modèle, nous supposons que le matériau passif est fixe (dans la mesure où seul le mouvement relatif entre les matériaux passifs et actifs compte).

L'hypothèse principale de ce modèle est que le matériau passif présente une conduction thermique et une chaleur spécifique très grandes devant celles du matériau actif, de sorte qu'on néglige les fluctuations temporelles de la température au sein du matériau passif. Les signaux de température au sein des différents matériaux peuvent alors s'écrire

$$T_p(t) = T_0(x)$$

$$T_a(t) = T_0(x) + T(z)e^{j\omega t} \text{ et } T\left(\pm\frac{h}{2}\right) = 0$$

L'équation générale de la chaleur est donnée par[172]*:*

$$T_a(\mathrm{x},t)\left(\frac{\partial S_a(\mathrm{x},t)}{\partial t}+\overrightarrow{v(\mathrm{x},t)}.\overrightarrow{grad}\left(S_a(\mathrm{x},t)\right)\right)=div\left(\lambda_a.\overrightarrow{grad}\left(T_a(\mathrm{x},t)\right)\right)$$

avec, $S_a$, $\lambda_a$ entropie et conductivité thermique.

La variation d'entropie est donnée par

$$T_a dS_a = dQ + c_a dT_a$$

En partant de l'expression de la température définie plus haut, et en ne conservant que les termes harmoniques, on obtient l'équation suivante

$$c_a\left(j\omega T+\underline{v_0}\frac{\partial T_0}{\partial x}\right)+j\omega q_0=\lambda_a\frac{\partial^2 T}{\partial z^2}$$

La solution générale de cette équation différentielle est

$$T=A\cos kz+B\sin kz+\frac{1}{k^2}\left(\frac{c_a}{\lambda_a}\underline{v_0}\frac{\partial T_0}{\partial x}+\frac{j\omega q_0}{\lambda_a}\right)$$

avec $k=\sqrt{-\frac{j\omega c_a}{\lambda_a}}=\pm\frac{1-j}{\delta}$ et $\delta=\sqrt{\frac{2\lambda_a}{\omega c_a}}$ est l'épaisseur de la couche limite thermique [168].

Par application des conditions limites $T\left(\pm\frac{h}{2}\right)=0$,

$$T=\left(j\frac{\underline{v_0}}{\omega}\frac{\partial T_0}{\partial x}-\frac{q_0}{c_a}\right)\left(1-\frac{\cos kz}{\cos\frac{kh}{2}}\right)$$

Dans un second temps, le flux thermique "actif" est calculé

$$\frac{dQ_a}{dt}(x,t)=T_0 S_a(x,t)v(x,t) \qquad (5.\ 22)$$

La moyenne temporelle de cette puissance intégrée sur la section de la plaque active donne alors après calculs une puissance par unité de surface:

$$P_{actif}=P_0-\lambda_{eq}\frac{\partial T_0}{\partial x}$$

$P_0=-\frac{q_0\delta_{eff}v_0}{2h}$ correspond au flux thermique actif généré à la fois par l'effet calorique et le mouvement imposé, et, $\lambda_{eq}=c_a\frac{\delta_{eff}}{h}\frac{{v_0}^2}{2\omega}$ correspond à une conductivité thermique supplémentaire due au mouvement.

Compte-tenu de ce résultat, on établit ensuite que le gradient thermique maximal est alors donné par

$$\left.\frac{\partial T_0}{\partial x}\right|_{MAX}=\frac{P_0}{\lambda_a+2\lambda_p\frac{h_p}{h}+\lambda_{eq}}$$

### 5.2 Résultats principaux de simulation

Dans l'exemple ci-dessous, le matériau actif est le caoutchouc dont les propriétés sont celles mesurées dans les chapitres précédents, et le matériau passif est de l'aluminium. Compte-tenu des valeurs numériques (rassemblées dans le Tableau 2), on obtient alors :

- Epaisseur de la couche limite thermique $\delta = 1.6\times10^{-4}$ m;
- Gradient thermique maximal $\left.\frac{\partial T_0}{\partial x}\right|_{MAX} = 0.5$ K/cm;
- Puissance de refroidissement maximale $P_0 = 8\times10^3$ W.m$^{-2}$, soit une puissance frigorifique de 0.4 W pour un système de section totale 7 mm x 1cm.

Tableau 2 : Paramètres de simulation

| **Couche active (caoutchouc)** | |
|---|---|
| **Epaisseur [mm]** | 5 |
| **Largeur [mm]** | 10 |
| **Chaleur spécifique [J.m$^{-3}$.K$^{-1}$]** | $1.8\times10^6$ |
| **Conductivité thermique [W.m$^{-1}$.K$^{-1}$]** | 0.18 |
| **Variation de température adiabatique [K]** | 4 |
| **Amplitude de la source de chaleur $q_0$** | $3.6\times10^6$ |
| **Déplacement selon l'axe x [mm]** | 20 |
| **Fréquence de travail [Hz]** | 1 |

| **Couche passive (aluminum)** | |
|---|---|
| **Epaisseur [mm]** | 1 |
| **Largeur [mm]** | 10 |
| **Chaleur spécifique [J.m$^{-3}$.K$^{-1}$]** | $2.5\times10^6$ |
| **Conductivité thermique [W.m$^{-1}$.K$^{-1}$]** | 200 |

L'effet de la fréquence est illustré dans Fig.FR 33.

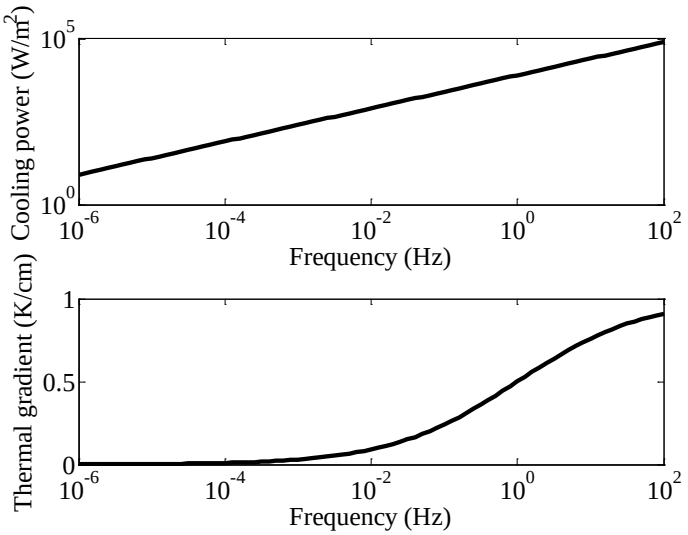


Fig.FR 33 :Effet de la fréquence sur les performances du système régénératif.

Par la suite, on cherche à établir l'effet des propriétés de chaleur spécifique, de l'effet élastocalorique et de la conductivité thermique du matériau actif. On montre alors que ces trois paramètres devraient être choisis les plus grand possibles pour maximiser les performances du système de refroidissement.

### 5.3 Conclusion

En comparaison à des modèles numériques, l'approche analytique permet des simulations rapides et l'établissement d'expressions simples mettant en jeu les paramètres du système (par exemple la puissance de réfrigération maximale ou le gradient thermique maximal). Le développement de ce modèle n'en est qu'à ses débuts, et des extensions futures sont prévues pour des systèmes multicouches, des mouvements non uniformes, et des hypothèses moins fortes sur les propriétés thermiques des différentes couches. Ces simulations devront par la suite être confrontées aussi bien à des résultats de simulations numériques que des expérimentations sur des systèmes réels.

## 6 Quelques autres essais de couplages caloriques

Durant la thèse, différents essais infructueux ont été menés à la recherche d'autres couplages caloriques. Pour ne donner qu'un seul exemple, de nombreux essais ont été effectués sur les fluides électrorhéologiques, qui ont montré l'absence de variation d'entropie lorsque le fluide se solidifie sous l'action d'un champ électrique. Soumis à l'action d'un champ électrique, les particules solides du fluide se rassemblent en structures compactes pouvant être assimilées à un réseau cristallin[174]. Nous cherchions alors à établir si cet assemblage s'associait à une chaleur de transition et permettrait de faire varier fortement l'entropie de l'ensemble. Bien que nous ayons fabriqué avec succès des fluides électrorhéologiques, nous avons établi par la suite que les variations entropiques resteront faibles étant donné la taille des particules mises en jeu, ce qui a été confirmé par une quantification simplifiée basée sur l'entropie de mélange entre les particules de fluide et les particules de solide.

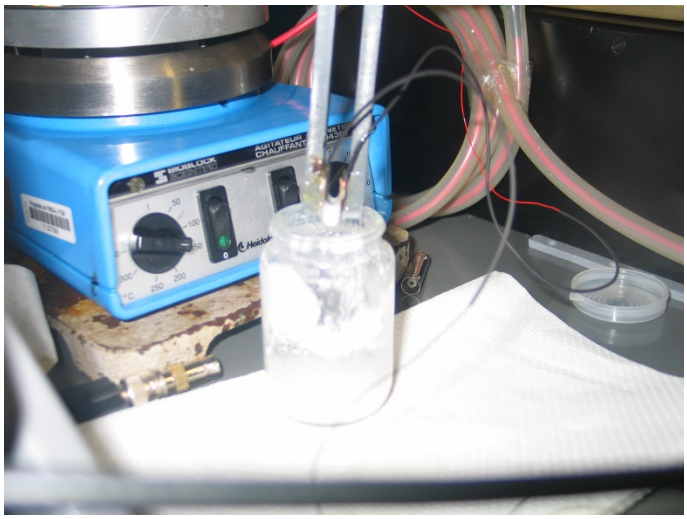

Fig.FR 34 Particules de zéolite basé à effet électrorhéologique.

## 7 A propos des équations constitutives

Si l'on parle de cycles de réfrigération à base de matériaux caloriques, nous avons besoin de connaître précisément le comportement du matériau soumis à deux sollicitations quasiment quelconques (déformation et température dans ce cas). Certaines caractérisations ont remis en cause la

nature de grandeur d'état de la contrainte, et l'équivalence de Maxwell a été invalidée par certaines caractérisations. Il est pourtant important de bien noter que dans ce cas, il existe un risque fort de violation du 1er principe de la thermodynamique.

Par exemple, regardons deux équations élastocaloriques fortement simplifiées (linéarisées autour d'un point de fonctionnement en déformation et en température)

$$\begin{cases} d\sigma = E \cdot d\varepsilon + \beta_1 \cdot dT \\ ds = -\beta_2 \cdot d\varepsilon + \frac{c}{T_0} \cdot dT \end{cases}$$

avec $E, \beta_1 > 0$, $\beta_2 > 0$ et $c$ indépendants de $\varepsilon$ et $T$ sur la plage de variation considérée.

| Etat | T (°C) | $\varepsilon$ | $\sigma$ | $s$ |
|---|---|---|---|---|
| A | $T_1$ | 0 | 0 | 0 |
| A→B | $W_1 = \frac{1}{2}(E + \beta_1 \cdot \frac{T_0\beta_2}{c})\varepsilon_B^2$ | | $Q_1 = 0$ | |
| B | $T_2$ | $\varepsilon_B = \frac{c(T_2 - T_1)}{T_0\beta_2}$ | $\sigma_B = (E + \beta_1 \cdot \frac{T_0\beta_2}{c})\varepsilon_B$ | 0 |
| B→C | $W_2 = \frac{1}{2}E(\varepsilon_C - \varepsilon_B)^2 + \sigma_B(\varepsilon_C - \varepsilon_B)$ | | $Q_2 = -\beta_2 T_2(\varepsilon_C - \varepsilon_B)$ | |
| C | $T_2$ | $\varepsilon_C$ | $\sigma_C = E \cdot (\varepsilon_C - \varepsilon_B) + \sigma_B$ | $s_C = -\beta_2(\varepsilon_C - \varepsilon_B)$ |
| C→D | $W_3 = -\frac{1}{2}(E + \frac{T_0\beta_1\beta_2}{c})(\varepsilon_D - \varepsilon_C)^2 + \sigma_D(\varepsilon_D - \varepsilon_C)$ | | $Q_3 = 0$ | |
| D | $T_1$ | $\varepsilon_D = \varepsilon_C - \varepsilon_B$ | $\sigma_D = \sigma_C - \sigma_B$ | $s_D = s_C$ |
| D→A | $W_4 = \frac{1}{2}E(\varepsilon_A^2 - \varepsilon_D^2) = -\frac{1}{2}E\varepsilon_D^2$ | | $Q_4 = \beta_2 T_1(\varepsilon_C - \varepsilon_B)$ | |

$\beta_1$ correspond au facteur de Clausius-Clapeyron et $\beta_2$ correspond au coefficient élastocalorique en déformation. Nous supposons dans un premier temps qu'ils puissent être différents. On calcule par la suite les variations d'entropie et de contrainte pour un cycle de Carnot appliqué à ce matériau. Un cycle de Carnot comprend 4 états (notés A, B, C D) avec un étirement adiabatique de A à B, un étirement isotherme à la température $T_2$ de la source chaude de B à C (de la chaleur est ainsi donnée à la source chaude de manière réversible), une rétraction adiabatique de C à D, puis une rétraction isotherme à la température $T_1$ de la source froide (la source froide donne de la chaleur à l'échantillon de manière réversible) de D à A.

Après calculs, on obtient les expressions de la contrainte et de l'entropie pour les différents états, ainsi que les échanges de chaleur et le travail mécanique.

On calcule ensuite la chaleur totale échangée avec la source chaude :

$$Q_h = Q_2 = -\beta_2 T_2(\varepsilon_C - \varepsilon_B)$$

Celle échangée avec la source froide

$$Q_c = Q_4 = \beta_2 T_1(\varepsilon_C - \varepsilon_B)$$

Et le travail mécanique fourni par l'actionneur mécanique

$$W = W_1 + W_2 + W_3 + W_4$$

$$= \frac{1}{2}(E + \beta_1 \cdot \frac{T_0 \beta_2}{c})\varepsilon_B^2 + \frac{1}{2}E(\varepsilon_C - \varepsilon_B)^2 + \sigma_B(\varepsilon_C - \varepsilon_B)$$

$$-\frac{1}{2}(E + \frac{T_0 \beta_1 \beta_2}{c})(\varepsilon_D - \varepsilon_C)^2 + \sigma_D(\varepsilon_D - \varepsilon_C) - \frac{1}{2}E\varepsilon_D^2$$

$$= \frac{1}{2}(E + \beta_1 \cdot \frac{T_0 \beta_2}{c})[\varepsilon_B^2 - (\varepsilon_D - \varepsilon_C)^2] + \frac{1}{2}E[(\varepsilon_C - \varepsilon_B)^2 - \varepsilon_D^2] + \sigma_B(\varepsilon_C - \varepsilon_B) + \sigma_D(\varepsilon_D - \varepsilon_C)$$

On applique ensuite le 1er principe de la thermodynamique (conservation de l'énergie), et après calculs, on obtient que

$$Q_h + Q_c + W = 0$$

Ou encore $-\beta_2 T_2(\varepsilon_C - \varepsilon_B) + \beta_2 T_1(\varepsilon_C - \varepsilon_B) + \beta_1(T_2 - T_1)(\varepsilon_C - \varepsilon_B) = 0$

$$(T_2 - T_1)(\varepsilon_C - \varepsilon_B)(\beta_1 - \beta_2) = 0$$

Par conséquent, on démontre alors que $\beta_1 = \beta_2$

En conclusion de ce calcul, on peut dire que quand, lors de la caractérisation indirecte, on observe deux coefficients différents (voir même un signe différent), il devient alors possible de violer le 1er principe par l'application d'un cycle de Carnot… Cela nous amène donc à réfléchir à ce qui est mesuré expérimentalement, et à s'assurer toujours de la possibilité de mesurer les propriétés à la fois de manière directe et indirecte pour être certains des valeurs mesurées.

# Conclusion générale

Dans le cadre du refroidissement à l'état solide, le potentiel de caoutchouc naturel en tant que matériau élastocalorique est étudié, et ces travaux montrent que ce matériau est un candidat prometteur par rapport aux autres matériaux caloriques. Bien que l'application du NR en tant que matériau actif d'un dispositif de refroidissement soit inhabituelle, certaines caractérisations importantes ont été menées dans cette thèse. En comparaison aux autres matériaux caloriques, comme les matériaux électrocaloriques ou magnétocaloriques, le caoutchouc présente de nombreux avantages: un grand effet calorique, une bonne résistance à la fatigue; un faible coût, et un faible impact environnemental.

L'effet élastocalorique dans le caoutchouc naturel est d'abord caractérisé directement par une mesure thermique et interprété en s'appuyant sur la notion de cristallisation induite par la déformation (Strain induced crystallization ou SIC). La dépendance en déformation de l'effet élastocalorique est déterminé à travers la définition d'un coefficient élastocalorique en déformation et d'un coefficient en contrainte $\beta = -\partial s / \partial \varepsilon$ et $\gamma = \partial T / \partial \sigma_{stretching}$ respectivement, avec $s$ l'entropie spécifique, $\varepsilon$ la déformation nominale, $T$ la température et $\sigma_{stretching}$ la contrainte obtenue lors de l'étirement. Les deux coefficients présentent des valeurs maximales à la déformation correspondant au maximum de la SIC (autour d'une déformation de 4,5). Cette propriété est attribuée au fait que le taux de cristallisation est maximal pour cette déformation. En raison de l'effet élastocalorique élevé pour cette déformation, une pré-déformation de 2 (début de la fusion de la SIC en rétraction) est le plus favorable d'un point de vue de l'application, parce que la déformation relative nécessaire pour obtenir un effet donné est plus faible d'une part, et les coefficients sont plus élevés d'autre part.

Les mesures directes et indirectes de l'effet élastocalorique sont ensuite comparées. La mesure indirecte est basée sur la relation de Maxwell $\left(\frac{\partial \sigma}{\partial T}\right)_{\varepsilon} = -\left(\frac{\partial s}{\partial \varepsilon}\right)_{T}$ et la variation de température adiabatique élastocalorique est donnée par $\Delta T = \frac{T_0}{c}\int_0^{\varepsilon}\left(\frac{\partial \sigma}{\partial T}\right)_{\varepsilon} d\varepsilon$, avec $\sigma$ la contrainte nominale, $T_0$ la température, et $c$ la chaleur spécifique. La mesure indirecte est réalisée par deux méthodes différentes. La première consiste à mesurer le comportement contrainte-déformation à différentes températures statiques. L'autre consiste à mesurer le comportement contrainte-température à déformation constante. Il se trouve que la déduction de la variation de température élastocalorique est sous-estimée ou même de signe opposé à celle mesurée directement dans le cas de la première méthode, tandis que la seconde méthode présente un bon accord quantitatif. Le comportement complexe de la contrainte souligne que celle-ci n'est pas une variable d'état, remettant ainsi en question le comportement ergodique du caoutchouc naturel. Il est proposé que ces comportements sont dus à la propriété inhomogène de la SIC; qui entraîne deux effets opposés sur la contrainte, suivant qu'il s'agisse de la nucléation des cristallites ou de leur croissance.

La contrainte et la variation de température élastocalorique sont deux quantités requises pour caractériser l'effet élastocalorique. Leur dépendance en température est une propriété importante pour l'application de l'effet élastocalorique. Le modèle de la SIC de Flory est modifié pour décrire à la fois la contrainte et la variation de température élastocalorique. Le modèle de la contrainte est en bon accord avec les résultats expérimentaux à différentes températures, et l'effet élastocalorique est correctement estimé. Pour valider davantage ce modèle de la SIC et le potentiel du caoutchouc en tant que matériau élastocalorique, il reste nécessaire de caractériser l'effet élastocalorique pour différentes températures. La SIC est principalement responsable du comportement thermomécanique du

caoutchouc, qui ne peut pas être décrit par la théorie standard de l'élasticité du caoutchouc. Enfin, le modèle devrait être développé en considérant à la fois le couplage multiphysique et la SIC.

Lorsque la variation de température élastocalorique est assez importante pour un cycle de refroidissement, l'effet de la fatigue constitue une propriété très importante pour des dispositifs de refroidissement. L'effet de la fatigue sur l'effet élastocalorique du caoutchouc naturel est caractérisé. Pour un régime de grande amplitude de déformation (1-6), le caoutchouc se fissure dès 800 cycles. Un aussi faible nombre de cycles est insuffisant pour un système de refroidissement. Pour réduire l'endommagement lié à la fatigue, l'amplitude de la déformation est diminuée. L'effet de la fatigue sur les performances élastocaloriques ont été mesurées et comparées pour trois régimes de déformation intermédiaires : déformation d'amplitude 0-3, 2-5 et 4-7. Le régime de déformation 0-3 est le régime de déformation amorphe et les régimes de déformation 2-5, 4-7 correspondent aux déformations auxquelles la SIC intervient. Il est montré que les propriétés élastocaloriques pour les régimes de déformation 2-5 et 4-7 sont non seulement plus élevées que pour le régime amorphe 0-3, mais présentent aussi une meilleure résistance à la fatigue (pas de fissure ou d'endommagement). On observe qu'une plus forte relaxation de la contrainte est associée à une stabilisation plus rapide des propriétés en fonction du nombre de cycles subis, en particulier pour le régime de déformation 2-5. Après 3000 cycles, les coefficients élastocaloriques en contrainte sont comparés pour les deux régimes de déformation 2-5 et 4-7, avec des valeurs de 4,4 K / MPa et 1,6 K / MPa respectivement. Ainsi, le régime de déformation 2-5, correspondant au début de la SIC est le régime le plus prometteur pour de futures applications. Ces résultats suggèrent qu'il est possible d'obtenir un effet élastocalorique stable et important jusqu'à 3000 cycles pour le régime de déformation 2-5, montrant qu'on peut améliorer l'effet de la fatigue par un choix judicieux du régime de déformation. Un test de fatigue pour un plus grand nombre de cycles est finalement mené au régime de déformation 2-5. Jusqu'à 1,7 $10^5$ cycles, aucune rupture ou fissure n'est observée, et la dégradation de l'effet élastocalorique est limitée à 12% comparée à sa valeur avant fatigue, l'effet devenant stable à partir de 3000 cycles. Ce travail constitue une étape importante pour l'application du caoutchouc dans des systèmes de réfrigération. Par la suite, il sera nécessaire d'établir des statistiques de rupture, ainsi que d'étudier l'influence de la température sur les effets de fatigue.

Enfin, compte tenu des performances du caoutchouc comme matériau élastocalorique, un modèle analytique simplifié d'un système de refroidissement régénératif est développé. Il peut évaluer la puissance de refroidissement et le gradient thermique atteignable. On montre alors que les performances du dispositif augmentent avec l'effet élastocalorique, la conductivité thermique et la capacité thermique. La suite de ces travaux serait de supprimer certaines hypothèses fortes du modèle, et de valider sa capacité de prédiction par des comparaisons avec des systèmes expérimentaux numériques.

Pour conclure ce travail, il a été expérimentalement établi que l'utilisation d'un caoutchouc naturel à un régime de déformation de 2-5 permet d'obtenir une activité élastocalorique optimale, avec une variation de température élastocalorique de 4K, et peu d'effets de fatigue jusqu'à $10^5$ cycles. Enfin, en se basant sur ces propriétés, un système de réfrigération régénératif permettrait d'obtenir un gradient de température allant jusqu'à 0.5K/cm et une puissance de refroidissement de 0.4W pour une section transversale de 50 $mm^2$. Certaines des caractéristiques les plus importantes du caoutchouc naturel ont été mises en évidence par une étude de ses propriétés et de l'application. D'autres travaux devraient être consacrés à des caractérisations plus complètes du caoutchouc naturel ainsi qu'au développement de systèmes de réfrigération de démonstration afin de valider ce concept. Les futures recherches sur les matériaux élastocaloriques devraient en outre s'appuyer sur la cristallisation induite par la déformation dans les élastomères. Pour leur caractérisation, la dépendance en température et les effets de fatigue doivent être caractérisés pour un grand nombre de cycles de déformation. A partir des simulations réalisées, des premiers dispositifs pourraient être réalisés.

## References


[1] J. Hansen, R. Ruedy, M. Sato, K. Lo, GLOBAL SURFACE TEMPERATURE CHANGE, Rev. Geophys. 48 (2010) RG4004. doi:10.1029/2010RG000345.

[2] X. Moya, S. Kar-Narayan, N.D. Mathur, Caloric materials near ferroic phase transitions., Nat. Mater. 13 (2014) 439–50. doi:10.1038/nmat3951.

[3] D. Guyomar, Y. Li, G. Sebald, P.J. Cottinet, B. Ducharne, J.F. Capsal, Elastocaloric modeling of natural rubber, Appl. Therm. Eng. 57 (2013) 33–38. doi:10.1016/j.applthermaleng.2013.03.032.

[4] Z. Xie, G. Sebald, D. Guyomar, Elastocaloric effect dependence on pre-elongation in natural rubber, Appl. Phys. Lett. 107 (2015) 081905. doi:10.1063/1.4929395.

[5] L.R.G. Treloar, The physics of rubber elasticity, Oxford university press, Oxford, 1975.

[6] S.L. Dart, R.L. Anthony, E. Guth, Rise of Temperature on Fast Stretching of Synthetics and Natural Rubbers, Ind. Eng. Chem. 34 (1942) 1340–1342. doi:10.1021/ie50395a020.

[7] J.C. Mitchell, D.J. Meier, Rapid Stress-Induced Crystallization in Natural Rubber, Rubber Chem. Technol. 42 (1969) 1420–1432. doi:10.5254/1.3539309.

[8] N. Saintier, G. Cailletaud, R. Piques, Multiaxial fatigue life prediction for a natural rubber, Int. J. Fatigue. 28 (2006) 530–539. doi:10.1016/j.ijfatigue.2005.05.011.

[9] N. Saintier, G. Cailletaud, R. Piques, Cyclic loadings and crystallization of natural rubber: An explanation of fatigue crack propagation reinforcement under a positive loading ratio, Mater. Sci. Eng. A. 528 (2011) 1078–1086. doi:10.1016/j.msea.2010.09.079.

[10] S.M. Cadwell, R. a. Merrill, C.M. Sloman, F.L. Yost, Dynamic Fatigue Life of Rubber, Rubber Chem. Technol. 13 (1940) 304–315. doi:10.5254/1.3539515.

[11] J. Tušek, K. Engelbrecht, R. Millán-Solsona, L. Mañosa, E. Vives, L.P. Mikkelsen, et al., The Elastocaloric Effect: A Way to Cool Efficiently, Adv. Energy Mater. 5 (2015) n/a–n/a. doi:10.1002/aenm.201500361.

[12] J. Diani, B. Fayolle, P. Gilormini, A review on the Mullins effect, Eur. Polym. J. 45 (2009) 601–612. doi:http://dx.doi.org/10.1016/j.eurpolymj.2008.11.017.

[13] L. Manosa, A. Planes, M. Acet, Advanced materials for solid-state refrigeration, J. Mater. Chem. A. 1 (2013) 4925–4936. doi:10.1039/C3TA01289A.

[14] K.A. Gschneidner, V.K. Pecharsky, Thirty years of near room temperature magnetic cooling: Where we are today and future prospects, Int. J. Refrig. 31 (2008) 945–961. doi:10.1016/j.ijrefrig.2008.01.004.

[15] V.K. Pecharsky, K. a. Gschneidner Jr, Magnetocaloric effect and magnetic refrigeration, J. Magn. Magn. Mater. 200 (1999) 44–56. doi:10.1016/S0304-8853(99)00397-2.

[16] B. Yu, M. Liu, P.W. Egolf, A. Kitanovski, A review of magnetic refrigerator and heat pump prototypes built before the year 2010, Int. J. Refrig. 33 (2010) 1029–1060. doi:10.1016/j.ijrefrig.2010.04.002.

[17] M. Valant, Electrocaloric materials for future solid-state refrigeration technologies, Prog. Mater. Sci. 57 (2012) 980–1009. doi:10.1016/j.pmatsci.2012.02.001.

[18] X. Yin, J.-F. Capsal, D. Guyomar, A comprehensive investigation of poly(vinylidene fluoride-trifluoroethylene-chlorofluoroethylene) terpolymer nanocomposites with carbon black for electrostrictive applications, Appl. Phys. Lett. 104 (2014) 052913. doi:10.1063/1.4864160.

[19] E. Bonnot, R. Romero, L. Mañosa, E. Vives, A. Planes, Elastocaloric effect associated with the martensitic transition in shape-memory alloys, Phys. Rev. Lett. 100 (2008). doi:10.1103/PhysRevLett.100.125901.

[20] J. Tušek, K. Engelbrecht, L.P. Mikkelsen, N. Pryds, Elastocaloric effect of Ni-Ti wire for application in a cooling device, J. Appl. Phys. 117 (2015) 124901. doi:10.1063/1.4913878.

[21] J. Cui, Y. Wu, J. Muehlbauer, Y. Hwang, R. Radermacher, S. Fackler, et al., Demonstration of high efficiency elastocaloric cooling with large ΔT using NiTi wires, Appl. Phys. Lett. 101 (2012) 073904. doi:http://dx.doi.org/10.1063/1.4746257.

[22] J. Cui, I. Takeuchi, M. Wuttig, Y. Wu, Reinhard, Radermacher, et al., Thermoelastic Cooling, 1 (2012). http://www.google.com/patents/US20120273158.

[23] S. Qian, A. Alabdulkarem, J. Ling, J. Muehlbauer, Y. Hwang, R. Radermacher, et al., Performance enhancement of a compressive thermoelastic cooling system using multi-

objective optimization and novel designs, Int. J. Refrig. 57 (2015) 62–76. doi:10.1016/j.ijrefrig.2015.04.012.
[24] S. Qian, J. Ling, Y. Hwang, R. Radermacher, I. Takeuchi, Thermodynamics cycle analysis and numerical modeling of thermoelastic cooling systems, Int. J. Refrig. 56 (2015) 65–80. doi:10.1016/j.ijrefrig.2015.04.001.
[25] M. Schmidt, A. Schütze, S. Seelecke, Scientific test setup for investigation of shape memory alloy based elastocaloric cooling processes, Int. J. Refrig. 54 (2015) 88–97. doi:10.1016/j.ijrefrig.2015.03.001.
[26] C.J. William Goetzler, Robert Zogg, Jim Young, Energy Savings Potential and RD & D Opportunities for Non- Vapor-Compression HVAC, Navig. Consult. Inc., Prep. US Dep. Energy. (2014).
[27] O. Gutfleisch, M. a. Willard, E. Brück, C.H. Chen, S.G. Sankar, J.P. Liu, Magnetic Materials and Devices for the 21st Century: Stronger, Lighter, and More Energy Efficient, Adv. Mater. 23 (2011) 821–842. doi:10.1002/adma.201002180.
[28] G. V. Brown, Magnetic heat pumping near room temperature, J. Appl. Phys. 47 (1976) 3673–3680. doi:10.1063/1.323176.
[29] W.A. Steyert, Stirling-cycle rotating magnetic refrigerators and heat engines for use near room temperature, J. Appl. Phys. 49 (1978).
[30] L. Shebanovs, K. Borman, W.N. Lawless, A. Kalvane, Electrocaloric Effect in Some Perovskite Ferroelectric Ceramics and Multilayer Capacitors, Ferroelectrics. 273 (2002) 137–142. doi:10.1080/00150190211761.
[31] R. Chukka, J.W. Cheah, Z. Chen, P. Yang, S. Shannigrahi, J. Wang, et al., Enhanced cooling capacities of ferroelectric materials at morphotropic phase boundaries, Appl. Phys. Lett. 98 (2011) 10–13. doi:10.1063/1.3595344.
[32] A.S. Mischenko, Q. Zhang, J.F. Scott, R.W. Whatmore, N.D. Mathur, Giant Electrocaloric Effect in Thin-Film PbZr0.95Ti0.05O3, Sci. . 311 (2006) 1270–1271. doi:10.1126/science.1123811.
[33] D. Saranya, A.R. Chaudhuri, J. Parui, S.B. Krupanidhi, Electrocaloric effect of PMN-PT thin films near morphotropic phase boundary, Bull. Mater. Sci. 32 (2009) 259–262. doi:10.1007/s12034-009-0039-3.
[34] B. Neese, B. Chu, S.-G. Lu, Y. Wang, E. Furman, Q.M. Zhang, Large Electrocaloric Effect in Ferroelectric Polymers Near Room Temperature, Sci. . 321 (2008) 821–823. doi:10.1126/science.1159655.
[35] P.F. Liu, J.L. Wang, X.J. Meng, J. Yang, B. Dkhil, J.H. Chu, Huge electrocaloric effect in Langmuir–Blodgett ferroelectric polymer thin films, New J. Phys. 12 (2010) 023035. doi:10.1088/1367-2630/12/2/023035.
[36] K. Alex Müller, F. Fauth, S. Fischer, M. Koch, A. Furrer, P. Lacorre, Cooling by adiabatic pressure application in Pr1−xLaxNiO3, Appl. Phys. Lett. 73 (1998).
[37] L. Manosa, D. Gonzalez Alonso, A. Planes, E. Bonnot, M. Barrio, J.L. Tamarit, et al., Giant solid-state barocaloric effect in the Ni-Mn-In magnetic shape-memory alloy, Nat Mater. 9 (2010) 478–481. http://dx.doi.org/10.1038/nmat2731.
[38] L. Mañosa, D. González-Alonso, A. Planes, M. Barrio, J.-L. Tamarit, I.S. Titov, et al., Inverse barocaloric effect in the giant magnetocaloric La–Fe–Si–Co compound, Nat Commun. 2 (2011) 595. http://dx.doi.org/10.1038/ncomms1606.
[39] S. Yuce, M. Barrio, B. Emre, E. Stern-Taulats, A. Planes, J.-L. Tamarit, et al., Barocaloric effect in the magnetocaloric prototype Gd5Si2Ge2, Appl. Phys. Lett. 101 (2012) 071906. doi:10.1063/1.4745920.
[40] C. Picornell, J. Pons, E. Cesari, Stress-Temperature Relationship in Compression Mode in Cu-Al-Ni Shape Memory Alloys, Mater. Trans. 45 (2004) 1679–1683. doi:10.2320/matertrans.45.1679.
[41] F. Xiao, T. Fukuda, T. Kakeshita, Significant elastocaloric effect in a Fe-31.2Pd (at. %) single crystal, Appl. Phys. Lett. 102 (2013) 161914. doi:10.1063/1.4803168.
[42] W.J. Buehler, J. V Gilfrich, R.C. Wiley, Effect of Low-Temperature Phase Changes on the Mechanical Properties of Alloys near Composition TiNi, J. Appl. Phys. 34 (1963).
[43] J. Cui, Y. Wu, J. Muehlbauer, Y. Hwang, R. Radermacher, S. Fackler, et al., Demonstration of

high efficiency elastocaloric cooling with large ??t using NiTi wires, Appl. Phys. Lett. 101 (2012) 25–28. doi:10.1063/1.4746257.
[44] C. Bechtold, C. Chluba, R. Lima de Miranda, E. Quandt, High cyclic stability of the elastocaloric effect in sputtered TiNiCu shape memory films, Appl. Phys. Lett. 101 (2012) 091903. doi:10.1063/1.4748307.
[45] A.N. Gent, Engineering with Rubber, 2012. doi:10.5254/1.3538214.
[46] A. Lendlein, R. Langer, Biodegradable, Elastic Shape-Memory Polymers for Potential Biomedical Applications, Sci. . 296 (2002) 1673–1676. doi:10.1126/science.1066102.
[47] B. Huneau, Strain-Induced Crystallization of Natural Rubber: a Review of X-Ray Diffraction Investigations, Rubber Chem. Technol. 84 (2011) 425–452. doi:10.5254/1.3601131.
[48] Y. Miyamoto, H. Yamao, K. Sekimoto, Crystallization and Melting of Polyisoprene Rubber under Uniaxial Deformation, Macromolecules. 36 (2003) 6462–6471. doi:10.1021/ma0342877.
[49] L. Mandelkern, Crystallization of Polymers Second Edition, 2002. doi:10.1017/CBO9780511541315.
[50] J.E. Mark, E. Burak, E. Mike Roland, The science and technology of rubber, Academic press, Oxford, 2013.
[51] M. Tosaka, S. Murakami, S. Poompradub, S. Kohjiya, Y. Ikeda, S. Toki, et al., Orientation and crystallization of natural rubber network as revealed by WAXD using synchrotron radiation, Macromolecules. 37 (2004) 3299–3309. doi:10.1021/ma0355608.
[52] J.R. Katz, Röntgenspektrographische Untersuchungen am gedehnten Kautschuk und ihre mögliche Bedeutung für das Problem der Dehnungseigenschaften dieser Substanz, Naturwissenschaften. 13 (1925) 410–416. doi:10.1007/BF01560952.
[53] L.A. Wood, N. Bekkedahl, Crystallization of Unvulcanized Rubber at Different Temperatures, J. Appl. Phys. 17 (1946).
[54] P.A. Albouy, J. Marchal, J. Rault, Chain orientation in natural rubber, Part I: The inverse yielding effect, Eur. Phys. J. E. 17 (2005) 247–259. doi:10.1140/epje/i2004-10145-6.
[55] N. Candau, L. Chazeau, J.-M. Chenal, C. Gauthier, J. Ferreira, E. Munch, et al., Strain induced crystallization and melting of natural rubber during dynamic cycles, Phys. Chem. Chem. Phys. 17 (2015) 15331–15338. doi:10.1039/C5CP00384A.
[56] J.M. Chenal, L. Chazeau, L. Guy, Y. Bomal, C. Gauthier, Molecular weight between physical entanglements in natural rubber: A critical parameter during strain-induced crystallization, Polymer (Guildf). 48 (2007) 1042–1046. doi:10.1016/j.polymer.2006.12.031.
[57] I.S. Choi, C.M. Roland, Strain-Crystallization of Guayule and Hevea Rubbers, Rubber Chem. Technol. 70 (1997) 202–210. doi:10.5254/1.3538425.
[58] K. Cui, L. Meng, Y. Ji, J. Li, S. Zhu, X. Li, et al., Extension-induced crystallization of poly(ethylene oxide) bidisperse blends: An entanglement network perspective, Macromolecules. 47 (2014) 677–686. doi:10.1021/ma402031m.
[59] Y. Ikeda, Y. Yasuda, K. Hijikata, M. Tosaka, S. Kohjiya, Comparative study on strain-induced crystallization behavior of peroxide cross-linked and sulfur cross-linked natural rubber, Macromolecules. 41 (2008) 5876–5884. doi:10.1021/ma800144u.
[60] J.B. Le Cam, J.R. Samaca Martinez, X. Balandraud, E. Toussaint, J. Caillard, Thermomechanical Analysis of the Singular Behavior of Rubber: Entropic Elasticity, Reinforcement by Fillers, Strain-Induced Crystallization and the Mullins Effect, Exp. Mech. (2014) 771–782. doi:10.1007/s11340-014-9908-9.
[61] W. Lin, M. Bian, G. Yang, Q. Chen, Strain-induced crystallization of natural rubber as studied by high-resolution solid-state 13C NMR spectroscopy, Polymer (Guildf). 45 (2004) 4939–4943. doi:10.1016/j.polymer.2004.04.064.
[62] Y. Nie, H. Gao, W. Hu, Variable trends of chain-folding in separate stages of strain-induced crystallization of bulk polymers, Polym. (United Kingdom). 55 (2014) 1267–1272. doi:10.1016/j.polymer.2014.01.034.
[63] L. Qu, G. Huang, Z. Liu, P. Zhang, G. Weng, Y. Nie, Remarkable reinforcement of natural rubber by deformation-induced crystallization in the presence of organophilic montmorillonite, Acta Mater. 57 (2009) 5053–5060. doi:10.1016/j.actamat.2009.07.007.
[64] S. Toki, I. Sics, S. Ran, L. Liu, B.S. Hsiao, Molecular orientation and structural development in vulcanized polyisoprene rubbers during uniaxial deformation by in situ synchrotron X-ray

diffraction, Polymer (Guildf). 44 (2003) 6003–6011. doi:10.1016/S0032-3861(03)00548-2.
[65] M. Tosaka, S. Kohjiya, Y. Ikeda, S. Toki, B.S. Hsiao, Molecular orientation and stress relaxation during strain-induced crystallization of vulcanized natural rubber, Polym. J. 42 (2010) 474–481. doi:10.1038/pj.2010.22.
[66] G.S.Y. Yeh, Strain-induced crystallization I. Limiting extents of strain-induced nuclei, Polym. Eng. Sci. 16 (1976) 138–144.
[67] N. Candau, R. Laghmach, L. Chazeau, J.-M. Chenal, C. Gauthier, T. Biben, et al., Strain-Induced Crystallization of Natural Rubber and Cross-Link Densities Heterogeneities, Macromolecules. 47 (2014) 5815–5824. doi:10.1021/ma5006843.
[68] R. Dargazany, V.N. Khiem, M. Itskov, A generalized network decomposition model for the quasi-static inelastic behavior of filled elastomers, Int. J. Plast. x (2014) xx. doi:10.1016/j.ijplas.2013.12.004.
[69] R. Dargazany, V.N. Khiêm, E. a. Poshtan, M. Itskov, Constitutive modeling of strain-induced crystallization in filled rubbers, Phys. Rev. E - Stat. Nonlinear, Soft Matter Phys. 89 (2014) 1–12. doi:10.1103/PhysRevE.89.022604.
[70] P.J. Flory, Thermodynamics of Crystallization in High Polymers. I. Crystallization Induced by Stretching, J. Chem. Phys. 15 (1947) 397–408. doi:10.1063/1.1746537.
[71] P.J. Flory, Thermodynamics of Crystallization in High Polymers. IV. A Theory of Crystalline States and Fusion in Polymers, Copolymers, and Their Mixtures with Diluents Paul J. Flory Thermodynamics of Crystallization in High Polymers. IV. A Theory of Crystalline State, J. Chem. Phys. 17 (1949) 223–240. doi:10.1063/1.1746537.
[72] R.J. Gaylord, A Theory of the Stress-Induced Crystallization of Crosslinked Polymeric Networks, J. Polym. Sci. Polym. Phys. Ed. 14 (1976) 1827–1837.
[73] R.J. Gaylord, D.J. Lohse, Morphological Changes During Oriented Polymer Crystallization., Am. Chem. Soc. Polym. Prepr. Div. Polym. Chem. 16 (1975) 331–336.
[74] a. N. Gent, Crystallization and the Relaxation of Stress in Stretched Natural-Rubber Vulcanizates, Rubber Chem. Technol. 28 (1955) 36–50. doi:10.5254/1.3542793.
[75] J. Guilié, T.-N. Le, P. Le Tallec, Micro-sphere model for strain-induced crystallisation and three-dimensional applications, J. Mech. Phys. Solids. 81 (2015) 58–74. doi:10.1016/j.jmps.2015.05.004.
[76] M. Kroon, A constitutive model for strain-crystallising Rubber-like materials, Mech. Mater. 42 (2010) 873–885. doi:10.1016/j.mechmat.2010.07.008.
[77] C. Miehe, A micro-macro approach to rubber-like materials?Part I: the non-affine micro-sphere model of rubber elasticity, J. Mech. Phys. Solids. 52 (2004) 2617–2660. doi:10.1016/j.jmps.2004.03.011.
[78] S.J. Mistry, S. Govindjee, A micro-mechanically based continuum model for strain-induced crystallization in natural rubber, Int. J. Solids Struct. 51 (2014) 530–539. doi:10.1016/j.ijsolstr.2013.10.027.
[79] E. a. Poshtan, R. Dargazany, M. Itskov, Influence of strain induced crystallization on the mechanical behavior of natural rubbers, Const. Model. Rubber VII. (2015) 215–219.
[80] K.J. Smith, Crystallization of Networks Under Stress., Am. Chem. Soc. Polym. Prepr. Div. Polym. Chem. 16 (1975) 337–338. doi:10.1002/pen.760160309.
[81] M. Avrami, Granulation, Phase Change, and Microstructure Kinetics of Phase Change. III, J. Chem. Phys. 9 (1941) 177. doi:10.1063/1.1750872.
[82] M. Avrami, Kinetics of Phase Change. I General Theory, J. Chem. Phys. 7 (1939) 1103. doi:10.1063/1.1750380.
[83] M. Avrami, Kinetics of Phase Change. II - Transformation-Time Relations for Random Distribution of Nuclei, J. Chem. Phys. 8 (1940) 212–224. doi:10.1063/1.1750631.
[84] M. Tosaka, Strain-Induced Crystallization of Crosslinked Natural Rubber As Revealed by X-ray Diffraction Using Synchrotron Radiation, Polymer (Guildf). 39 (2007) 1207–1220. doi:10.1295/polymj.PJ2007059.
[85] C.W. Bunn, Molecular Structure and Rubber-Like Elasticity. I. The Crystal Structures of $\beta $ Gutta-Percha, Rubber and Polychloroprene, Proc. R. Soc. London A Math. Phys. Eng. Sci. 180 (1942) 40–66. http://rspa.royalsocietypublishing.org/content/180/980/40.abstract.
[86] S. Toki, I. Sics, S. Ran, L. Liu, B.S. Hsiao, New Insights into Structural Development in

Natural Rubber during Uniaxial Deformation by In Situ Synchrotron X-ray Diffraction, Society. (2002) 6578–6584.
[87] S. Toki, J. Che, L. Rong, B.S. Hsiao, S. Amnuaypornsri, A. Nimpaiboon, et al., Entanglements and networks to strain-induced crystallization and stress-strain relations in natural rubber and synthetic polyisoprene at various temperatures, Macromolecules. 46 (2013) 5238–5248. doi:10.1021/ma400504k.
[88] S. Trabelsi, P.A. Albouy, J. Rault, Crystallization and melting processes in vulcanized stretched natural rubber, Macromolecules. 36 (2003) 7624–7639. doi:10.1021/ma030224c.
[89] P.J. Flory, Principles of Polymer Chemistry: Paul J. Flory, 1953.
[90] P.A. Albouy, G. Guillier, D. Petermann, A. Vieyres, O. Sanseau, P. Sotta, A stroboscopic X-ray apparatus for the study of the kinetics of strain-induced crystallization in natural rubber, Polymer (Guildf). 53 (2012) 3313–3324. doi:10.1016/j.polymer.2012.05.042.
[91] P.A. Albouy, A. Vieyres, R. Pérez-Aparicio, O. Sanséau, P. Sotta, The impact of strain-induced crystallization on strain during mechanical cycling of cross-linked natural rubber, Polymer (Guildf). 55 (2014) 4022–4031. doi:10.1016/j.polymer.2014.06.034.
[92] S. Toki, I. Sics, B.S. Hsiao, M. Tosaka, S. Poompradub, Y. Ikeda, et al., Probing the nature of strain-induced crystallization in polyisoprene rubber by combined thermomechanical and in situ X-ray diffraction techniques, Macromolecules. 38 (2005) 7064–7073. doi:10.1021/ma050465f.
[93] J. Che, C. Burger, S. Toki, L. Rong, B.S. Hsiao, S. Amnuaypornsri, et al., Crystal and Crystallites Structure of Natural Rubber and Synthetic cis-1,4-Polyisoprene by a New Two Dimensional Wide Angle X-ray Diffraction Simulation Method. I. Strain-Induced Crystallization, Macromolecules. 46 (2013) 4520–4528. doi:10.1021/ma400420k.
[94] J. Che, C. Burger, S. Toki, L. Rong, B.S. Hsiao, S. Amnuaypornsri, et al., Crystal and Crystallites Structure of Natural Rubber and Peroxide-Vulcanized Natural Rubber by a Two-Dimensional Wide-Angle X-ray Diffraction Simulation Method. II. Strain-Induced Crystallization versus Temperature-Induced Crystallization, Macromolecules. 46 (2013) 9712–9721. doi:10.1021/ma401812s.
[95] S. Toki, Strain-induced crystallization of natural rubber as detected real-time by wide-angle X-ray diffraction technique.pdf, Polymer (Guildf). (2000).
[96] J. Rault, J. Marchal, P. Judeinstein, P. a. Albouy, Chain orientation in natural rubber, Part II: 2H-NMR study, Eur. Phys. J. E. 21 (2006) 243–261. doi:10.1140/epje/i2006-10064-6.
[97] J. Rault, J. Marchal, P. Judeinstein, P. a. Albouy, Stress-induced crystallization and reinforcement in filled natural rubbers:2H NMR study, Macromolecules. 39 (2006) 8356–8368. doi:10.1021/ma0608424.
[98] S. Toki, T. Fujimaki, M. Okuyama, Strain-induced crystallisation of natural rubber as detected real-time bywide-angle X-Ray diffraction technique, Polymer (Guildf). 41 (2000) 5423–5429.
[99] S. Poompradub, M. Tosaka, S. Kohjiya, Y. Ikeda, S. Toki, I. Sics, et al., Mechanism of strain-induced crystallization in filled and unfilled natural rubber vulcanizates, J. Appl. Phys. 97 (2005). doi:10.1063/1.1900927.
[100] L.R.G. Treloar, The Physics of Rubber Elasticity, Oxford university press, 1975.
[101] A. Sakata, N. Suzuki, Y. Higashiura, T. Matsuo, T. Sato, Measurement of the mechanocaloric effect in rubber, J. Therm. Anal. Calorim. 113 (2013) 1555–1563. doi:10.1007/s10973-013-3066-7.
[102] J.R. Samaca Martinez, J.B. Le Cam, X. Balandraud, E. Toussaint, J. Caillard, Mechanisms of deformation in crystallizable natural rubber. Part 1: Thermal characterization, Polymer (Guildf). 54 (2013) 2717–2726. doi:10.1016/j.polymer.2013.03.011.
[103] J. Tušek, K. Engelbrecht, R. Millán-Solsona, L. Mañosa, E. Vives, L.P. Mikkelsen, et al., The Elastocaloric Effect: A Way to Cool Efficiently, Adv. Energy Mater. 5 (2015) 1500361. doi:10.1002/aenm.201500361.
[104] W. Mars, A. Fatemi, A literature survey on fatigue analysis approaches for rubber, Int. J. Fatigue. 24 (2002) 949–961. doi:10.1016/S0142-1123(02)00008-7.
[105] S. Trabelsi, P.A. Albouy, J. Rault, Stress-induced crystallization around a crack tip in natural rubber, Macromolecules. 35 (2002) 10054–10061. doi:10.1021/ma021106c.
[106] M. Tosaka, D. Kawakami, K. Senoo, S. Kohjiya, Y. Ikeda, S. Toki, et al., Crystallization and

stress relaxation in highly stretched samples of natural rubber and its synthetic analogue, Macromolecules. 39 (2006) 5100–5105. doi:10.1021/ma060407+.
[107] H.P. Zhang, J. Niemczura, G. Dennis, K. Ravi-Chandar, M. Marder, Toughening effect of strain-induced crystallites in natural rubber, Phys. Rev. Lett. 102 (2009) 4–7. doi:10.1103/PhysRevLett.102.245503.
[108] S. Beurrot-Borgarino, B. Huneau, E. Verron, P. Rublon, Strain-induced crystallization of carbon black-filled natural rubber during fatigue measured by in situ synchrotron X-ray diffraction, Int. J. Fatigue. 47 (2013) 1–7. doi:10.1016/j.ijfatigue.2012.07.001.
[109] K. Brüning, K. Schneider, S. V. Roth, G. Heinrich, Strain-induced crystallization around a crack tip in natural rubber under dynamic load, Polym. (United Kingdom). 54 (2013) 6200–6205. doi:10.1016/j.polymer.2013.08.045.
[110] J.B. Le Cam, E. Toussaint, The mechanism of fatigue crack growth in rubbers under severe loading: The effect of stress-induced crystallization, Macromolecules. 43 (2010) 4708–4714. doi:10.1021/ma100042n.
[111] P. Rublon, B. Huneau, N. Saintier, S. Beurrot, A. Leygue, E. Verron, et al., In situ synchrotron wide-angle X-ray diffraction investigation of fatigue cracks in natural rubber, J. Synchrotron Radiat. 20 (2013) 105–109. doi:10.1107/S0909049512044457.
[112] P. Rublon, B. Huneau, E. Verron, N. Saintier, S. Beurrot, A. Leygue, et al., Multiaxial deformation and strain-induced crystallization around a fatigue crack in natural rubber, Eng. Fract. Mech. 123 (2014) 59–69. doi:10.1016/j.engfracmech.2014.04.003.
[113] N. Of, Factors That Affect the Fatigue Life of Rubber, History. 77 (2004) 419–423.
[114] N. Saintier, G. Cailletaud, R. Piques, Crack initiation and propagation under multiaxial fatigue in a natural rubber, Int. J. Fatigue. 28 (2006) 61–72. doi:10.1016/j.ijfatigue.2005.03.006.
[115] A.F. MARS, W. V., A. Fatemi, Fatigue crack nucleation and growth in filled natural rubber, …and Fract. Eng. Mater. …. (2003) 779–789. doi:10.1046/j.1460-2695.2003.00678.x.
[116] L. Munoz, L. Vanel, O. Sanseau, P. Sotta, D. Long, L. Odoni, et al., Fatigue crack growth dynamics in filled natural rubber, Plast. Rubber Compos. 41 (2012) 273–276. doi:10.1179/1743289812Y.0000000013.
[117] J.H. Fielding, Flex Life and Crystallization of Synthetic Rubber, Ind. Eng. Chem. 35 (1943) 1259–1261. doi:10.1021/ie50408a008.
[118] P.B. Lindley, Relation between hysteresis and the dynamic crack growth resistance of natural rubber, Int. J. Fract. 9 (1973) 449–462. doi:10.1007/BF00036325.
[119] P.B. Lindley, Non-Relaxing Crack Growth and Fatigue in a Non-Crystallizing Rubber, Rubber Chem. Technol. 47 (1974) 1253–1264. doi:10.5254/1.3540497.
[120] M. Tosaka, K. Senoo, K. Sato, M. Noda, N. Ohta, Detection of fast and slow crystallization processes in instantaneously-strained samples of cis-1,4-polyisoprene, Polymer (Guildf). 53 (2012) 864–872. doi:10.1016/j.polymer.2011.12.035.
[121] K. Brüning, K. Schneider, S. V. Roth, G. Heinrich, Kinetics of strain-induced crystallization in natural rubber studied by WAXD: Dynamic and impact tensile experiments, Macromolecules. 45 (2012) 7914–7919. doi:10.1021/ma3011476.
[122] N. Candau, L. Chazeau, J.M. Chenal, C. Gauthier, J. Ferreira, E. Munch, et al., Characteristic time of strain induced crystallization of crosslinked natural rubber, Polymer (Guildf). 53 (2012) 2540–2543. doi:10.1016/j.polymer.2012.04.027.
[123] N. Candau, R. Laghmach, L. Chazeau, J.-M. Chenal, C. Gauthier, T. Biben, et al., Influence of strain rate and temperature on the onset of strain induced crystallization in natural rubber, Eur. Polym. J. 64 (2015) 244–252. doi:10.1016/j.eurpolymj.2015.01.008.
[124] Y. Akagi, T. Katashima, Y. Katsumoto, K. Fujii, T. Matsunaga, U. Chung, et al., Examination of the Theories of Rubber Elasticity Using an Ideal Polymer Network, Macromolecules. 44 (2011) 5817–5821. doi:10.1021/ma201088r.
[125] S. Amnuaypornsri, S. Toki, B.S. Hsiao, J. Sakdapipanich, The effects of endlinking network and entanglement to stress-strain relation and strain-induced crystallization of un-vulcanized and vulcanized natural rubber, Polym. (United Kingdom). 53 (2012) 3325–3330. doi:10.1016/j.polymer.2012.05.020.
[126] J.M. Chenal, C. Gauthier, L. Chazeau, L. Guy, Y. Bomal, Parameters governing strain induced crystallization in filled natural rubber, Polymer (Guildf). 48 (2007) 6893–6901.

doi:10.1016/j.polymer.2007.09.023.
[127] J. a. C. Harwood, L. Mullins, a. R. Payne, Stress Softening in Natural Rubber Vulcanizates. Part II. Stress Softening Effects in Pure Gum and Filler Loaded Rubbers, Rubber Chem. Technol. 39 (1966) 814–822. doi:10.5254/1.3547145.
[128] C. Chluba, W. Ge, R. Lima de Miranda, J. Strobel, L. Kienle, E. Quandt, et al., Ultralow-fatigue shape memory alloy films, Sci. . 348 (2015) 1004–1007. doi:10.1126/science.1261164.
[129] S. Crossley, N.D. Mathur, X. Moya, New developments in caloric materials for cooling applications, AIP Adv. 5 (2015) 067153. doi:10.1063/1.4922871.
[130] J.B. Le Cam, J.R. Samaca Martinez, X. Balandraud, E. Toussaint, J. Caillard, Thermomechanical Analysis of the Singular Behavior of Rubber: Entropic Elasticity, Reinforcement by Fillers, Strain-Induced Crystallization and the Mullins Effect, Exp. Mech. (2014). doi:10.1007/s11340-014-9908-9.
[131] X. Balandraud, J.-B. Le Cam, Some specific features and consequences of the thermal response of rubber under cyclic mechanical loading, Arch. Appl. Mech. 84 (2014) 773–788. doi:10.1007/s00419-014-0832-3.
[132] J.R. Samaca Martinez, J.B. Le Cam, X. Balandraud, E. Toussaint, J. Caillard, New elements concerning the Mullins effect: A thermomechanical analysis, Eur. Polym. J. 55 (2014) 98–107. doi:10.1016/j.eurpolymj.2014.03.014.
[133] J.R. Samaca Martinez, E. Toussaint, X. Balandraud, J.-B. Le Cam, D. Berghezan, Heat and strain measurements at the crack tip of filled rubber under cyclic loadings using full-field techniques, Mech. Mater. 81 (2015) 62–71. doi:10.1016/j.mechmat.2014.09.011.
[134] J.R. Samaca Martinez, J.B. Le Cam, X. Balandraud, E. Toussaint, J. Caillard, Mechanisms of deformation in crystallizable natural rubber. Part 2: Quantitative calorimetric analysis, Polym. (United Kingdom). 54 (2013) 2727–2736. doi:10.1016/j.polymer.2013.03.012.
[135] C.M. Roland, Mechanical Behavior of Rubber at High Strain Rates, Rubber Chem. Technol. 79 (2006) 429–459. doi:10.5254/1.3547945.
[136] A.N. Gent, L.-Q. Zhang, Strain-induced crystallization and strength of elastomers. I. cis-1,4-polybutadiene, J. Polym. Sci. Part B Polym. Phys. 39 (2001) 811–817. doi:10.1002/1099-0488(20010401)39:7<811::AID-POLB1055>3.0.CO;2-C.
[137] E.H. Andrews, Resistance to Ozone Cracking in Elastomer Blends, Rubber Chem. Technol. 40 (1967) 635–649. doi:10.5254/1.3539078.
[138] B.C. Edwards, P.J. Phillips, High-pressure Phases in Polymers . II. Spherulitic Growth Morphology in cis-Polyisoprene, J. Polym. Sci. Polym. Phys. Ed. 13 (1975) 2117. doi:10.1002/pol.1975.180131105.
[139] S. Toki, T. Fujimaki, M. Okuyama, Strain-induced crystallization of natural rubber as detected real-time by wide-angle X-ray diffraction technique, Polymer (Guildf). 41 (2000) 5423–5429. doi:10.1016/S0032-3861(99)00724-7.
[140] G. Sebald, L. Seveyrat, J.F. Capsal, P.J. Cottinet, D. Guyomar, Differential scanning calorimeter and infrared imaging for electrocaloric characterization of poly(vinylidene fluoride-trifluoroethylene- chlorofluoroethylene) terpolymer, Appl. Phys. Lett. 101 (2012) 2010–2013. doi:10.1063/1.4734924.
[141] T.R. Emery, J.M. Dulieu-Barton, Thermoelastic stress analysis of damage mechanisms in composite materials, Compos. Part A. 41 (2010) 1729–1742. doi:10.1016/j.compositesa.2009.08.015.
[142] S. Quinn, R.K. Fruehmann, J.M. Dulieu-Barton, Development of thermoelastic stress analysis as a non-destructive evaluation tool, (2009).
[143] S. Murakami, K. Senoo, S. Toki, S. Kohjiya, Structural development of natural rubber during uniaxial stretching by in situ wide angle X-ray diffraction using a synchrotron radiation, 43 (2002) 2117–2120.
[144] P. Ortiz-Serna, R. Díaz-Calleja, M.J. Sanchis, Evaluation of natural rubber specific heat capacity at high pressures from DSC experimental data at atmospheric pressure, J. Appl. Polym. Sci. (2012) 2269–2272. doi:10.1002/app.38118.
[145] G. Natta, P. Corradini, General considerations on the structure of crystalline polyhydrocarbons, Nuovo Cim. Ser. 10. 15 (1960) 9–39. doi:10.1007/BF02731858.
[146] C.W. Bunn, Molecular Structure and Rubberlike Elasticity. III. Molecular Movements in

Rubberlike Polymers, Rubber Chem. Technol. 15 (1942) 742–755. doi:10.5254/1.3543160.
[147] P.G. De Gennes, Coil-stretch transition of dilute flexible polymers under ultrahigh velocity gradients, J. Chem. Phys. 60 (1974) 5030–5042. doi:10.1063/1.1681018.
[148] S. Toki, B.S. Hsiao, S. Amnuaypornsri, J. Sakdapipanich, New insights into the relationship between network structure and strain-induced crystallization in un-vulcanized and vulcanized natural rubber by synchrotron X-ray diffraction, Polymer (Guildf). 50 (2009) 2142–2148. doi:10.1016/j.polymer.2009.03.001.
[149] S.G. Lu, B. Rožič, Q.M. Zhang, Z. Kutnjak, R. Pirc, M. Lin, et al., Comparison of directly and indirectly measured electrocaloric effect in relaxor ferroelectric polymers, Appl. Phys. Lett. 97 (2010) 202901. doi:http://dx.doi.org/10.1063/1.3514255.
[150] B. Lu, J. Liu, Mechanocaloric materials for solid-state cooling, Sci. Bull. 60 (2015) 1638–1643. doi:10.1007/s11434-015-0898-5.
[151] L. Mañosa, S. Jarque-Farnos, E. Vives, A. Planes, Large temperature span and giant refrigerant capacity in elastocaloric Cu-Zn-Al shape memory alloys, Appl. Phys. Lett. 103 (2013) 211904. doi:10.1063/1.4832339.
[152] G.J. Pataky, E. Ertekin, H. Sehitoglu, Elastocaloric cooling potential of NiTi, Ni2FeGa, and CoNiAl, Acta Mater. 96 (2015) 420–427. doi:http://dx.doi.org/10.1016/j.actamat.2015.06.011.
[153] N. Candau, R. Laghmach, L. Chazeau, J.-M. Chenal, C. Gauthier, T. Biben, et al., Strain-Induced Crystallization of Natural Rubber and Cross-Link Densities Heterogeneities, Macromolecules. 47 (2014) 5815–5824. doi:10.1021/ma5006843.
[154] D.E. Hanson, Numerical simulations of rubber networks at moderate to high tensile strains using a purely enthalpic force extension curve for individual chains, J. Chem. Phys. 131 (2009). doi:10.1063/1.3270166.
[155] L.R.G. Treloar, The photo-elastic properties of rubber II. Double refraction and crystallisation in stretched vulcanised rubber, Trans. Faraday Soc. 43 (1947) 284–293. doi:10.1039/TF9474300284.
[156] L. Mullins, Determination of degree of crosslinking in natural rubber vulcanizates. Part IV. Stress-strain behavior at large extensions, J. Appl. Polym. Sci. 2 (1959) 257–263. doi:10.1002/app.1959.070020601.
[157] L. Mullins, Determination of degree of crosslinking in natural rubber vulcanizates. Part I, J. Polym. Sci. 19 (1956) 225–236. doi:10.1002/pol.1956.120199201.
[158] J.A.C. Harwood, L. Mullins, A.R. Payne, Stress softening in natural rubber vulcanizates. Part II. Stress softening effects in pure gum and filler loaded rubbers, J. Appl. Polym. Sci. 9 (1965) 3011–3021. doi:10.1002/app.1965.070090907.
[159] C. Miehe, S. Goktepe, F. Lulei, A micro-macro approach to rubber-like materials — Part I : the non-a ne micro-sphere model of rubber elasticity, 52 (2004) 2617–2660. doi:10.1016/j.jmps.2004.03.011.
[160] M.C. Boyce, E.M. Arruda, Constitutive Models of Rubber Elasticity: A Review, Rubber Chem. Technol. 73 (2000) 504–523. doi:10.5254/1.3547602.
[161] C.M. Roland, J.W. Sobieski, Anomalous Fatigue Behavior in Polyisoprene, Rubber Chem. Technol. 62 (1989) 683–697. doi:10.5254/1.3536268.
[162] N. Candau, L. Chazeau, J.-M. Chenal, C. Gauthier, J. Ferreira, E. Munch, et al., Strain induced crystallization and melting of natural rubber during dynamic cycles, Phys. Chem. Chem. Phys. (2015). doi:10.1039/C5CP00384A.
[163] Strain induced crystallization and melting of natural rubber during dynamic cycles.pdf, (n.d.).
[164] K.K. Nielsen, J. Tusek, K. Engelbrecht, S. Schopfer, a. Kitanovski, C.R.H. Bahl, et al., Review on numerical modeling of active magnetic regenerators for room temperature applications, Int. J. Refrig. 34 (2011) 603–616. doi:10.1016/j.ijrefrig.2010.12.026.
[165] H. Bouchekara, a. Kedous-Lebouc, C. Dupuis, F. Allab, Prediction and optimisation of geometrical properties of the refrigerant bed in an AMRR cycle, Int. J. Refrig. 31 (2008) 1224–1230. doi:10.1016/j.ijrefrig.2008.02.007.
[166] M. Liu, B. Yu, Numerical investigations on internal temperature distribution and refrigeration performance of reciprocating active magnetic regenerator of room temperature magnetic refrigeration, Int. J. Refrig. 34 (2011) 617–627. doi:http://dx.doi.org/10.1016/j.ijrefrig.2010.12.003.

[167] J. Bouchard, H. Nesreddine, N. Galanis, Model of a porous regenerator used for magnetic refrigeration at room temperature, Int. J. Heat Mass Transf. 52 (2009) 1223–1229. doi:10.1016/j.ijheatmasstransfer.2008.08.031.
[168] G. Poignand, Réfrigérateur thermoacoustique: Étude du systeme compact et du comportement transitoire, (2006).
[169] M.E.H. Tijani, S. Spoelstra, G. Poignand, Study of a thermoacoustic-Stirling engine, J. Acoust. Soc. Am. 123 (2008) 3541. doi:10.1121/1.2934525.
[170] G. Poignand, B. Lihoreau, P. Lotton, E. Gaviot, M. Bruneau, V. Gusev, Optimal acoustic fields in compact thermoacoustic refrigerators, Appl. Acoust. 68 (2007) 642–659. doi:10.1016/j.apacoust.2006.03.009.
[171] P. Lotton, P. Blanc-Benon, M. Bruneau, V. Gusev, S. Duffourd, M. Mironov, et al., Transient temperature profile inside thermoacoustic refrigerators, Int. J. Heat Mass Transf. 52 (2009) 4986–4996. doi:10.1016/j.ijheatmasstransfer.2009.03.075.
[172] L.D. Landau, E.M. Lifshitz, Fluid mechanics, Elsevier, 1987.
[173] U. Legait, F. Guillou, A. Kedous-Lebouc, V. Hardy, M. Almanza, An experimental comparison of four magnetocaloric regenerators using three different materials, Int. J. Refrig. 37 (2014) 147–155. doi:10.1016/j.ijrefrig.2013.07.006.
[174] H. Ma, W. Wen, W.Y. Tam, P. Sheng, Frequency dependent electrorheological properties: origin and bounds, Phys. Rev. Lett. 77 (1996) 2499.
[175] M.S. Cho, H.J. Choi, I. Chin, W. Ahn, Electrorheological characterization of zeolite suspensions, 32 (1999) 233–239.
[176] Y. Tian, Y. Meng, S. Wen, ER fluid based on zeolite and silicone oil with high strength, (2001) 120–123.
[177] Y. Tian, M. Zhang, J. Jiang, N. Pesika, H. Zeng, J. Israelachvili, et al., Reversible shear thickening at low shear rates of electrorheological fluids under electric fields, Phys. Rev. E. 83 (2011) 11401. http://link.aps.org/doi/10.1103/PhysRevE.83.011401.
[178] B. Neese, B. Chu, S.-G. Lu, Y. Wang, E. Furman, Q.M. Zhang, Large Electrocaloric Effect in Ferroelectric Polymers Near Room Temperature, Science (80-. ). 321 (2008) 821–823. doi:10.1126/science.1159655.

## Own publications related to the PhD

[1] Z. Xie, G. Sebald, D. Guyomar, Elastocaloric effect dependence on pre-elongation in natural rubber, Appl. Phys. Lett. 107 (2015) 081905. doi:10.1063/1.4929395.

**Abstract**

In the context of solid-state-cooling, the elastocaloric effect offers a very large controlled entropy change based in low-cost polymers, especially natural rubber which is environmentally friendly. However, large elastocaloric activity requires large elongation (>5), which makes this material impractical for cooling systems due to the large change in sample's area. By performing a pre-

elongation, area change is limited, and $\beta = -\partial\gamma / \partial\lambda$ (where $\gamma$ is the specific entropy and $\lambda$ is the elongation) is larger. The highest $\beta$ value is obtained when pre-elongation is right before (at the "eve") the onset of the strain-induced crystallization (SIC), which is also interpreted in the view of molecular conformation. Experimental results obtained on a natural rubber sample showed an adiabatic temperature change of 4.3°C for pre-elongation of 4 with further elongation of 4 (true strain change of 69%). Furthermore, the entropy exhibits a quasi-linear dependence on elongation and the $\beta$ value is found to be 6400 $J.K^{-1}.m^{-3}$.

[2] Z. Xie, G. Sebald, D. Guyomar, Comparison of direct and indirect measurement of the elastocaloric effect in natural rubber, Appl. Phys. Lett. (in press).

**Abstract**

The directly measured temperature change $\Delta T$ upon deformation (elastocaloric effect) of natural rubber (NR) was compared with indirect method, which is deduced from the Clausius-Clapeyron factor $(\partial\sigma / \partial T)_\varepsilon$, where $\sigma$ is the stress, $\varepsilon$ is the strain. The factor $(\partial\sigma / \partial T)_\varepsilon$ can be measured by two different methods. One is to measure the stress vs. strain behavior at different static temperatures. It is found that the $\Delta T$ deduction is underestimated or even of opposite sign compared to the directly measured one. These behaviors are different from elastocaloric effect of shape memory alloys. An interpretation based on strain-induced crystallite is proposed. The other characterization is to measure the stress vs. temperature at constant strain. It results in a prediction, which is in good quantitative agreement with the directly measured one. The stress appears then to be a non-state variable, thus questioning the ergodicity of the material.

[3] Z. Xie, G. Sebald, D. Guyomar, Elastocaloric effect in natural rubber: fatigue effects, poster presentation at the Royal Society of London, Discussion Meeting entitled "Taking the temperature of phase transitions in cool materials", 8-9 Feb, 2016, London.

Invited paper to be submitted to the Philosophical Transactions of the Royal Society A: Mathematical, Physical & Engineering Science.

**Abstract**

Natural rubber (NR) is a promising elastocaloric (eC) material thanks to its large adiabatic temperature change upon deformation, while being environment friendly and low cost. Its fatigue life and the degradation of its properties for repetitive deformation cycles is a key issue for further applications, and is the object of the present work. Applying a strain regime from 1 to 6, cracks appeared rapidly (around 800 cycles). The strain amplitude was therefore decreased for improving fatigue life. With the same strain amplitude of 3, fatigue properties were investigated at three different strain regimes, before onset strain of strain-induced crystallization (SIC) (strain regime of 0-3), onset strain of SIC (strain regime of 2-5) and high strain of SIC (strain regime of 4-7). At strain of 0-3, many cracks appeared after 2000 cycles while the eC adiabatic temperature change is only 1.2 K. At strain of 2-5 and 4-7, there was no crack after 3000 cycles. The eC adiabatic temperature changes stabilized at 3.5 K and 4.2 K respectively, confirming that SIC is responsible for a large eC effect and an excellent crack growth resistance. A high-cycle fatigue was finally applied successfully at the strain of 2-5 (most promising strain regime) up to $1.7\times10^5$ cycles, where eC temperature change exhibited a slight degradation degree of 12% before stabilization.

# FOLIO ADMINISTRATIF

## THESE DE L'UNIVERSITE DE LYON OPEREE AU SEIN DE L'INSA LYON

NOM : XIE
(avec précision du nom de jeune fille, le cas échéant)

DATE de SOUTENANCE : 25/03/2016

Prénoms : Zhong jian

TITRE : Effet élastocalorique dans le caoutchouc naturel

NATURE : Doctorat

Numéro d'ordre : 2016LYSEI025

Ecole doctorale : Electronique, Electrotechnique, Automatique

Spécialité : Génie Electrique

RESUME :
Les effets caloriques représentent la capacité d'un matériau à voir son entropie varier sous l'effet d'une sollicitation externe et peuvent être utilisés pour des systèmes de refroidissement à l'état solide en remplacement (ou complément) des dispositifs traditionnels à base de fluides frigorifiques. Dans cette thèse, nous avons cherché à étudier l'effet élastocalorique du caoutchouc naturel. Après une présentation des différents matériaux caloriques et du caoutchouc naturel, le chapitre 2 détaille la caractérisation élastocalorique du caoutchouc naturel, et les résultats sont interprétés à partir de la notion de cristallisation induite par la déformation. Le changement de température adiabatique élastocalorique et la variation d'entropie associée atteignent 9K et 50kJ.m-3.K-1, ce qui est très important comparé aux autres matériaux caloriques. L'effet élastocalorique étant maximum pour une déformation voisine de 4,5, une pré-déformation peut être appliquée pour éviter la zone moindre activité élastocalorique. La mesure directe de l'effet élastocalorique est ensuite comparée à une méthode indirecte déduite du facteur de Clapeyron, et les divergences sont discutées. Dans le chapitre 3, la contrainte et la température élastocalorique sont simulées par un modèle de Flory modifié sur la base de la cristallisation. Il est possible de prédire le comportement contrainte-déformation à différentes températures, ainsi que les variations de température élastocaloriques à température ambiante. Dans le chapitre 4, les effets de la fatigue sur l'effet élastocalorique du caoutchouc naturel sont ensuite étudiés. La résistance à la fatigue pour de grandes amplitudes de déformation est très faible (<800 cycles). Trois régimes de déformation intermédiaire sont ensuite testés : 0-3, 2-5, et 4-7, et permet d'établir que le régime 2-5 est le plus performant (jusqu'à 100 000 cycles). Dans le dernier chapitre, un modèle de système régénératif de refroidissement à base de matériaux caloriques est développé afin d'établir des lignes directrices pour le choix des matériaux élastocaloriques.

MOTS-CLÉS :

Laboratoire (s) de recherche : Laboratoire de Génie Electrique et de Ferroélectricité (LGEF, EA682)

Directeur de thèse: Pr Daniel Guyomar, Dr Gael Sebald

Président de jury :

Composition du jury : M. Jean-Marc Chenal, M. Bertrand Garnier, M. Daniel Guyomar, Mme Afef Lebouc, M. Denis Remiens, M. Gael Sebald.